# Polynomial Chaos Approaches to Parameter Estimation and Control Design for Mechanical Systems with Uncertain Parameters

Emmanuel D. Blanchard

Dissertation submitted to the faculty of the
Virginia Polytechnic Institute and State University
in partial fulfillment of the requirements for the degree of

Doctor of Philosophy
in
Mechanical Engineering

Adrian Sandu, Chair
Corina Sandu, Co-Chair
Mehdi Ahmadian
Jeffrey T. Borggaard
Donald J. Leo

March 26, 2010
Blacksburg, Virginia

Keywords: Parametric Uncertainty, Polynomial Chaos, Collocation, Parameter Estimation, Extended Kalman Filter (EKF), Bayesian Estimation, Vehicle Dynamics, Control Design, Robust Control, LQR

# Polynomial Chaos Approaches to Parameter Estimation and Control Design for Mechanical Systems with Uncertain Parameters

Emmanuel D. Blanchard

## ABSTRACT

Mechanical systems operate under parametric and external excitation uncertainties. The polynomial chaos approach has been shown to be more efficient than Monte Carlo approaches for quantifying the effects of such uncertainties on the system response. This work uses the polynomial chaos framework to develop new methodologies for the simulation, parameter estimation, and control of mechanical systems with uncertainty.

This study has led to new computational approaches for parameter estimation in nonlinear mechanical systems. The first approach is a polynomial-chaos based Bayesian approach in which maximum likelihood estimates are obtained by minimizing a cost function derived from the Bayesian theorem. The second approach is based on the Extended Kalman Filter (EKF). The error covariances needed for the EKF approach are computed from polynomial chaos expansions, and the EKF is used to update the polynomial chaos representation of the uncertain states and the uncertain parameters. The advantages and drawbacks of each method have been investigated.

This study has demonstrated the effectiveness of the polynomial chaos approach for control systems analysis. For control system design the study has focused on the LQR problem when dealing with parametric uncertainties. The LQR problem was written as an optimality problem using Lagrange multipliers in an extended form associated with the polynomial chaos framework. The solution to the $H_\infty$ problem as well as the $H_2$ problem can be seen as extensions of the LQR problem. This method might therefore have the potential of being a first step towards the development of computationally efficient numerical methods for $H_\infty$ design with parametric uncertainties.

I would like to gratefully acknowledge the support provided for this work under NASA Grant NNL05AA18A.

# Acknowledgements

I would like to thank my advisor Dr. Adrian Sandu and my co-advisor, Dr. Corina Sandu, for their guidance and support throughout my time as a Ph.D. student, as well as for their encouragement. I truly believe that the main reason my Ph.D. studies have been more successful than I ever hoped for is the fact that I was able to learn so much from them. I was very lucky to work with them, and I was very lucky to be part of the Computational Science Laboratory (CSL), the Advanced Vehicle Dynamics Laboratory (AVDL) and the Center for Vehicle Systems and Safety (CVeSS). I would also like to thank Dr. Ahmadian, Dr. Leo and Dr. Borggaard for serving on my graduate committee. I am grateful to Dr. Mehdi Ahmadian, Dr. Steve Southward, Dr. John Ferris, Dr. Pushkin Kachroo, Dr. Sean Kenny, Dr. Luis Crespo, Dr. Daniel Giesy, and Mr. Carvel Holton for many fruitful discussions on different topics related to this work. I would also like to thank all my labmates at CSL and at CVeSS for their companionship and for their help. In particular, I would like to thank Brendan Chan, who was not working on a very similar project but still helped me many times by expanding my knowledge on different subjects and gave me many ideas during the time he was my roommate, Brian Templeton for many fruitful discussions very relevant to this project, Haiyan Cheng for her help with the polynomial chaos theory, as well as Kumaresh Singh and Mihai Alexe for their help with coding issues. Many other labmates also contributed to this research project by attending my presentations and asking questions which opened my mind to different ideas. I am truly grateful for their assistance. I am also grateful for everyone's assistance in the Computer Science Department and in the Mechanical Engineering Department of Virginia Tech. In particular, I would like to thank Cathy Hill and Sue Teel for having answered my questions so many times.

I would also like to thank my family and friends for their support, especially my parents, Denis and Christine. Their love, care, help and financial support for so many years has made this achievement possible. I know it is not easy to have a son dreaming of going even farther away. I want to thank them for being so supportive over the years despite my choices in life. I would also like to thank my girlfriend, Alaleh, for being so supportive and for valuing my work so much. Life is strange sometimes: the day I officially took the first step towards leaving the U.S. for Australia and therefore started thinking there was no point looking for a relationship until

finishing my Ph.D. was also the exact same day I met the nicest person I have ever met. I thought my last two years here would only consist of finishing my work at Virginia Tech, but they turned out to be much more than that, thanks to her. I feel very lucky to share my life with someone who has such a great character.

I would also like to make a very impersonal acknowledgment, but one that also means the world to me. Even though it is not related to this research in any way, I would like to thank the Australian government for granting me Permanent Residency in Australia, and my migration agent, Noel Hewitt. After spending so many years constantly worrying about immigration issues, it feels fantastic to know that I finally have a place to call home waiting for me. It made it much easier for me to focus on my studies, and I am now happier than ever before. I would also like to thank the government of Canada for granting me an immigrant visa while I was starting my Ph.D. (and for letting me live and work in Canada before I could start my Master's at Virginia Tech in 2001).

Finally, I would like to gratefully acknowledge the support provided for this work under NASA Grant NNL05AA18A.

# Contents

# List of Figures

# List of Tables

# 1 Introduction

This chapter introduces the reader to the research conducted throughout the course of this study. First, a brief overview of the polynomial chaos theory, parameter estimation, and robust control is provided. Then, the motivation for the work is presented. The research objectives and the research methodology are then discussed. Finally, an outline of the remaining chapters is provided.

## 1.1 Motivation

Mechanical systems operate under parametric and external excitation uncertainties. The polynomial chaos approach has been shown to be more efficient than Monte Carlo approaches for quantifying the effects of such uncertainties on the system response. Applying it to computationally expensive problems such as parameter estimation is a valuable approach. Parameter estimation is an important problem, because in many applications parameters cannot be directly measured with sufficient accuracy; this is the case, for example, in real time applications. Rather, parameter values must be inferred from available measurements of different aspects of the system response. Information about them is obtained via parameter estimation techniques. Parameter estimation is especially difficult for large systems, where a considerable computational effort is needed. Estimating a large number of parameters often proves to be computationally intractable. Different methodologies to estimate parameters in a Bayesian framework are possible. To the best of my knowledge, the polynomial chaos theory had not been previously applied to Bayesian estimation. The idea of combining the polynomial chaos theory and the Extended Kalman Filter theory has been mentioned in the literature in about the same time as the publication of our first papers; to my knowledge this work provides the most rigorous and complete treatment of the problem.

Coupling the polynomial chaos theory with different control approaches is also a judicious idea. Many simple control problems with parametric uncertainties, such as the Linear Quadratic Regulator (LQR) with parametric uncertainties, do not have a known closed-form solution. The

polynomial chaos framework yields a new problem with a new framework where a finite polynomial chaos coefficients need to be calculated in order to approximate a solution. The polynomial chaos theory also has the potential of making well-known control methods computationally much less expensive and therefore more attractive. This is especially attractive with robust control methods since they are methods designed in order to deal with uncertainties. Advanced robust control methods such as $H_\infty$ methods and μ-synthesis focus on stability robustness and/or performance robustness in the presence of uncertainties. One of the main problems associated with $H_\infty$ based methods is that they focus on optimizing the worst-case performance, without providing information on the probability cases yielding results close to the worst-case performance do occur, which leads to very conservative designs. Working in a probabilistic framework in order to address that problem would include valuable information. The polynomial chaos theory has the potential of making these approaches useful in practice since this can be a computationally expensive problem.

## 1.2 Research Objectives

This dissertation work has two primary objectives. The first objective is to develop new computational approaches for parameter estimation based on the polynomial chaos theory. Two computational methods have been proposed. The first approach is a polynomial-chaos based Bayesian approach in which maximum likelihood estimates are obtained by minimizing a cost function derived from the Bayesian theorem. The second approach is based on the Extended Kalman Filter (EKF). The error covariances needed are computed from polynomial chaos expansions, and the EKF is used to update the polynomial chaos representation of the uncertain states and the uncertain parameters.

The second objective of this work is to develop control methods based on the polynomial chaos theory. This second objective consists of two parts: controller analysis, which consists of studying the performance of a given controller, and controller synthesis, which consists of designing a controller best suited for a given application or at least meeting certain stability and performance requirements. The first part consisted of finding which control analysis problems were suited for the polynomial chaos theory. It has been found that the Polynomial Chaos theory is not very well adapted to controller design with control methods based on pole placement

because it needs to be applied to variables which are $C^1$ (i.e., have continuous derivatives) with respect to the uncertain parameters in order to work. The synthesis part therefore focused on state-space methods. The goal of the second part was to couple the polynomial chaos theory with the LQR problem with parametric uncertainties. The ultimate goal of the research direction would be to couple the $H_\infty$ theory with the polynomial chaos theory in order to design better $H_\infty$ controllers, which would be a difficult problem and therefore an ambitious task. Since the solution to the $H_\infty$ problem as well as the $H_2$ problem are based on solutions of Riccati equations and can therefore be seen as extensions of the LQR problem, it was decided to try deriving a closed-form solution for the LQR problem with parametric uncertainties. Such a solution does not exist yet to the best of our knowledge in a general framework. The objective was to find a solution that would depend on the number of terms $S$ in the polynomial chaos expansions and that would numerically converge to the solution of the problem as $S \to \infty$.

## 1.3 Research Approach

The first step in accomplishing the parameter estimation objectives of this research was to develop algorithms for numerical methods for parameter estimation based on the polynomial chaos theory. After working on a theoretical framework for two different approaches (a Bayesian approach, and an EKF approach), the next step was to write the Matlab codes with the help of Mathematica when needed and apply them to simple systems in order to test the feasibility of the methods and have a basic understanding of how the quality of their results can be affected by simple issues such as noise in measurements, undersampling, non-identifiability of the system, and choice of excitation signals. The next step was to choose a more complex dynamic system with uncertain parameters and apply the two parameter estimation methods for different excitation signals and noise levels in order to compare the results obtained with the two different approaches. Then, regularization techniques were applied to the Bayesian approach when dealing with non-identifiable systems. After realizing that the quality of the estimations obtained with the EKF approach yielded deteriorated with increasing the sampling rate, a rigorous error analysis was performed in order to explain this counter-intuitive behavior, and a new version of the EKF approach was developed to alleviate this problem. The final step was to draw conclusion on the advantages and drawbacks of each method.

The first step in accomplishing the control objectives of this research was to apply the polynomial chaos theory to several well-known control problems in order to find which problems would fit the polynomial chaos framework. A bicycle model with a $H_2$ controller designed to prevent 'spinout', or uncontrolled yawing was used in order to apply the polynomial chaos theory to controller analysis. The polynomial chaos could be used to obtain PDFs of Bode diagrams and stability margins, but was not adapted to problems related to the location of open-loop and closed loop poles. This is due to the fact that the polynomial chaos theory needs to be applied to variables which are $C^1$ (i.e., have continuous derivatives) with respect to the uncertain parameters. Therefore, this controller analysis part showed that the polynomial chaos theory cannot be used for very general applications based on pole placement methods; many well-known classical methods for controller design, such as the root locus, cannot be applied in the general case. A second example, an active suspension, was used to illustrate that the polynomial chaos theory can also be applied to the analysis of transfer functions obtained using state –space controllers.

The second part of this study on control methods has focused on LQR design in the presence of parametric uncertainties. The objective was to find a solution that would depend on the number of terms $S$ in the polynomial chaos expansions and that would numerically converge to the solution of the problem as $S \to \infty$. This proved to be extremely difficult, if not impossible. However, this led to new polynomial-chaos based numerical method based on the fundamental approach to solving the LQR problem. The LQR problem was written as an optimality problem using Lagrange multipliers in an extended form associated with the polynomial chaos framework, and an iterative algorithm converges to the optimal answer. The LQR controller is not very well adapted to robust design, and the optimal controller does not guarantee a minimum performance or even stability for the worst case scenario. Stability robustness and performance robustness in the presence of uncertainties are therefore not guaranteed. However, this is a first step aimed at designing more judicious controllers if combined with other techniques in the future. The solution to the $H_\infty$ problem as well as the $H_2$ problem can be seen as extensions of the LQR problem. This method developed under VIPER might therefore have the potential of being a first step towards the development of computationally efficient numerical methods for $H_\infty$ design with parametric uncertainties.

## 1.4 Main Contributions of this Research

The main contributions of this study on parameter estimation are the development two new computational approaches for parameter estimation based on the polynomial chaos theory. The first approach is a polynomial-chaos based Bayesian approach in which maximum likelihood estimates are obtained by minimizing a cost function derived from the Bayesian theorem. One of the advantages of the Bayesian approach is that it is not tailored to any specific distribution. To the best of our knowledge, it is the first time the polynomial chaos theory has been applied to Bayesian estimation. The second one uses polynomial chaoses to propagate uncertainties and estimate error covariances in the EKF framework in order to obtain aposteriori probability densities of the estimated parameters. The advantages and drawbacks of each method are illustrated using numerical simulations with a roll plane vehicle model. Finally, rigorous analyses explaining potential problems for both approaches are included, as well as possible solutions alleviating the potential problems: regularization techniques for the Bayesian approach and alternate formulation for the EKF approach.

The main contribution of this study on control methods is the development of an efficient polynomial chaos based numerical method providing an optimal controller for the linear-quadratic regulator (LQR) problem when the parameters in the formulation are uncertain, i.e., a controller minimizing the mean value of the LQR cost function obtained for a certain distribution of the uncertainties which is assumed to be known. This method has the potential of being a first step aimed at designing more judicious controllers if combined with other techniques in the future. The ultimate objective would be to extend this method to $H_\infty$ problems. Another contribution of this study on control methods consists of several examples showing the efficiency of the polynomial chaos theory for certain controller analysis problems.

## 1.5 Outline of the Dissertation

Chapter 2 provides the necessary background information to understand the polynomial chaos theory, parameter estimation, and stochastic control theory. It also contains a literature review related to these three subjects. The work of Chapters 3, 4 and 5 follows the work in Blanchard *et al.* [1-6]. In Chapter 3, the polynomial chaos theory is applied to parameter estimation problems

using a Bayesian approach. First, the theory developed for estimating the maximum likelihood of selected parameter system parameters or initial values by minimizing a cost function is explained. Then, the applicability of the methodology developed is illustrated on very simple mechanical systems, which are used as a support to discuss how the cost function is affected by undersampling, non-identifiability of the system, non-observability, noise level in the measurements, and relevance of excitation signal on the estimation capability. Finally, the Bayesian approach is applied to a nonlinear four degree of freedom roll plane model of a vehicle, in which an uncertain mass with an uncertain position is added on the roll bar. In Chapter 4, the Extended Kalman Filter (EKF) approach is introduced and applied to the same four degree of freedom roll plane model of a vehicle used in Chapter 3. Then, Chapter 5 compares the results obtained with the EKF approach to the results of the Bayesian approach, summarizes the important findings, and discusses the advantages and disadvantages of each method.

In Chapter 6, the polynomial chaos theory is applied to controller analysis. A bicycle model is used to explain why it can be applied to some control problems (Bode diagrams and stability margins in this example) and not others (location of open-loop and closed loop poles): the polynomial chaos theory needs to be applied to variables which are $C^1$ (i.e., have continuous derivatives) with respect to the uncertain parameters. A second example, an active suspension model, is used in Chapter 6 to illustrate that the polynomial chaos theory can also be applied to the analysis of transfer functions obtained using state –space controllers. Since Chapter 6 showed that the polynomial chaos theory cannot be used for very general applications related to pole placement methods, Chapter 7 focuses on state-space methods.

In Chapter 7, the polynomial chaos theory is applied to controller synthesis. Specifically, Chapter 7 focuses on LQR design when dealing with parametric uncertainties. The LQR problem is written as an optimality problem using Lagrange multipliers in an extended form associated with the polynomial chaos framework, and an iterative algorithm converges to the optimal answer. The Linear-Quadratic Regulator controller is not very well adapted to robust design, and the optimal controller does not guarantee a minimum performance or even stability for the worst case scenario. Stability robustness and performance robustness in the presence of uncertainties are therefore not guaranteed. However, this is a first step aimed at designing more judicious controllers if combined with other techniques in the future. The solution to the $H_\infty$ problem as well as the $H_2$ problem are based on solutions of Riccati equations and can therefore be seen as

extensions of the LQR problem. This new method might therefore have the potential of being a first step towards the development of computationally efficient numerical methods for $H_\infty$ design with parametric uncertainties.

Finally, Chapter 8 discusses the contribution of this work and recommendations for future research.

# 2 Background

The purpose of this chapter is to provide the background for the research conducted in this study. The first part of this chapter will present an overview of the polynomial chaos theory and explain how to obtain the Probability Density Functions (PDF) of the stochastic variable of interest. The second part of this chapter will introduce the background necessary to understand how to specifically apply the polynomial chaos theory to systems of Ordinary differential Equations (ODEs), which are used in the polynomial chaos based methods presented in Chapters 3-5. The chapter will conclude with a literature search on past research done in areas relating to this work: the polynomial chaos theory, parameter estimation, and robust control and its application to vehicle suspensions, and the LQR problem with uncertain parameters in the formulation .

## 2.1 Overview of the Polynomial Chaos Theory

This section presenting an overview of the Polynomial Chaos theory (Section 2.1) is adapted from [7]. The fundamental idea of polynomial chaos approach is that random processes of interest can be approximated by sums of orthogonal polynomial chaoses of random independent variables. In this context, any uncertain parameter can be viewed as a second order random process (processes with finite variance; from a physical point of view they have finite energy). Thus, a second order random process $Z(\vartheta)$, viewed as a function of the random event $\vartheta$, can be expanded in terms of orthogonal polynomial chaos [8] as:

$$Z(\vartheta) = \sum_{j=1}^{\infty} c^j \psi^j(\xi(\vartheta)) \tag{2.1}$$

Here $\psi^j(\xi_1 \cdots \xi_n)$ are generalized Wiener-Askey polynomial chaoses [9, 10], in terms of the multi-dimensional random variable $\xi = (\xi_1 \cdots \xi_n) \in \Omega \subseteq \Re^n$, where is $\Omega$ is the space of possible value for the unknown variables. The Wiener-Askey polynomial chaoses form a basis with respect to the joint probability density $\rho(\xi_1 \cdots \xi_n)$ in the ensemble inner product $\langle \psi, \varphi \rangle = \int_{\Omega} \psi(\xi)\varphi(\xi)\rho(\xi)\, d\xi$

The basis functions are selected depending on the type of random variable functions. For Gaussian random variables the basis functions are Hermite polynomials, for uniformly distributed random variables the basis functions are Legendre polynomials, for Beta distributed random variables the basis functions are Jacobi polynomials, and for gamma distributed random variables the basis functions are Laguerre polynomials [11, 12].

This study will generally use Beta distributed random variables with parameters $a$ = 1, $b$ = 1, i.e. Beta (2, 2) distributions, for which the basis functions are Jacobi (1, 1) polynomials. The Beta PDF is defined as follows:

$$\rho(\xi) = \frac{\Gamma(a+b+2)}{2^{a+b+1}\,\Gamma(a+1)\,\Gamma(b+1)} \cdot (1-\xi)^a\,(1-\xi)^b \text{ , where } \Gamma(x) = \int_0^\infty t^{x-1}\,e^{-t}\,dt \qquad (2.2)$$

Figure 2.1(a) shows the PDF of uniform random variables. The PDF of a Beta function with parameters $a$ = 1, $b$ = 1 is shown in Figure 2.1(b). The comparison of a Beta PDF with parameters $a$ = 4, $b$ = 4 (solid) and Gaussian distribution (dashed) is shown in Figure 2.1(c).

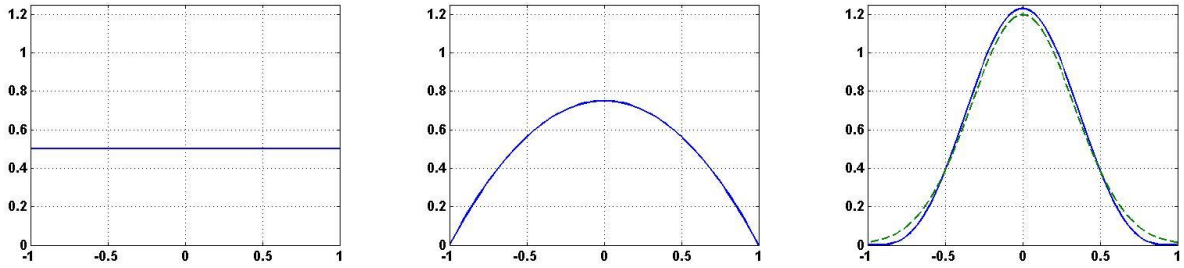


(a) (b) (c)

Figure 2.1: Probability Densities for Uniform, Gaussian and Beta Distributions: (a) Uniform Distribution ($a$ = 0, $b$ = 0); (b) Beta (2, 2) Distribution ($a$ = 1, $b$ = 1); (c) Gaussian Distribution (dashed) and Beta (5, 5) Distribution (solid) ($a$ = 4, $b$ = 4) (adapted from [7])

In practice, a truncated expansion of Equation (2.1) is used,

$$Z = \sum_{j=1}^{S} c^j \psi^j(\xi) \qquad (2.3)$$

For independent random variables $\xi_1 \cdots \xi_n$, the multi-dimensional basis functions are tensor products of 1-dimensional polynomial basis:

$$\psi^j(\xi_1 \cdots \xi_n) = \prod_{k=1}^{n} (\text{P1d})_k^{l_k}(\xi_k), \;\; j = 1, 2, \cdots, S; \; l_k = 1, 2, \cdots, p \tag{2.4}$$

where $S = \dfrac{(n+p)!}{n!\,p!}$, (P1d) is a 1-dimensional polynomial, $n$ is the number of random variables, and $p$ is the maximum order of the polynomial basis. The total number of terms $S$ increases rapidly with $n$ and $p$.

To illustrate the use of polynomial chaos method, consider the deterministic model:

$$y' = f(y), \quad t^0 \le t \le T, \;\; y(t^0) = y^0 \tag{2.5}$$

with each state a vector of length $m$. Assume, without loss of generality, that the initial state is uncertain. To express the resulting uncertainty in the state vector $y$, we expand the state vector along the polynomial chaos basis $\psi^1(\xi_1, \ldots, \xi_n), \ldots, \psi^S(\xi_1, \ldots, \xi_n)$:

$$y = \sum_{j=1}^{S} y^j \psi^j(\xi) \tag{2.6}$$

and insert it into the deterministic system (2.5) to obtain:

$$\sum_{j=1}^{S} (y^j)' \psi^j(\xi) = f\left( \sum_{j=1}^{S} y^j \psi^j(\xi) \right) \tag{2.7}$$

Using the polynomial chaos expansion, the original ODE is replaced by an ODE for the polynomial chaos coefficients, and the uncertainty information is embedded in these coefficients. The evolution equation for the stochastic coefficients can be obtained by either Galerkin or collocation approaches as explained below.

In the Galerkin polynomial chaos approach, we project the system (2.7) on the space spanned by the orthogonal polynomials, i.e., we take the inner product of (2.7) with $\psi^j(\xi)$ and divide $\left\langle \psi^j(\xi), \psi^j(\xi) \right\rangle$ at both sides to obtain:

$$(y^j) = \frac{1}{\left\langle \psi^j, \psi^j \right\rangle} \left\langle \psi^j(\xi), \; f\left( \sum_{j=1}^{S} y^j \psi^j(\xi) \right) \right\rangle, \;\; 1 \le j \le S \tag{2.8}$$

This system has $m \times S$ components and their evolution is coupled (each of the $m$ variables in (2.5) is represented by $S$ polynomial chaos coefficients).

The Galerkin approach requires the modification (expansion) of the deterministic system to a stochastic system, and the entire stochastic system needs to be evolved in time. Although only one system integration is needed, the computation time is significantly increased. At the end of integration, solving the linear system coefficients causes a computational cost increasing from $O(m^3)$ in the deterministic case to $O(m^3S^3)$ for the stochastic case. The $S^3$-fold increase can make the computation prohibitive [13], especially for large-scale simulation models.

The collocation approach imposes the system (2.7) to be satisfied at a given set of points $\mu^i \ (1 \le i \le Q)$:

$$\sum_{j=1}^{S} (y^j)' \psi^j(\mu^i) = f\left( \sum_{j=1}^{S} y^j \psi^j(\mu^i) \right), \ 1 \le i \le Q \tag{2.9}$$

With matrix $A$ defined using the basis function values at the collocation points

$$A = \left( A_{i,j} \right), \ A_{i,j} = \psi^j(\mu^i), \ 1 \le j \le S, \ 1 \le i \le Q \tag{2.10}$$

the collocation points in the system state space are:

$$Y^i(t) = \sum_{j=1}^{S} y^j(t) \, \psi^j(\mu^i) = \sum_{j=1}^{S} A_{i,j} y^j(t), \ 1 \le i \le Q \tag{2.11}$$

With this notation, Equation (2.9) becomes:

$$(Y^i(t))' = f(Y^i(t)), \ \ t^0 \le t \le T, \ 1 \le i \le Q \tag{2.12}$$

These are $Q$ independent integrations of the deterministic system (2.5) starting from the initial conditions

$$Y^i(t^0) == \sum_{j=1}^{S} A_{i,j} y^j(t^0), \ 1 \le i \le Q \tag{2.13}$$

After integration, we recover the stochastic solution coefficients at the final time $T$ by solving the linear system of equations for $y^j$:

$$y^j(t) = \sum_{i=1}^{Q} \left(A^{\#}\right)_{j,i} Y^i(t), \quad 1 \le j \le S \tag{2.14}$$

where $A^{\#}$ is the pseudo-inverse ( $A^{\#} = A^{-1}$ if $Q = S$ and $A$ is invertible).

The criterion for choosing the collocation points is that the system matrix $A$ (Equation 2.10) is not singular or near singular. Several options have been explored in [13], such as the random data sets, the Hammersley/Halton data sets [14, 15], and the sparse grid Smolyak data set [16-18]. In lower dimensions (small $n$), Hammersley/Halton and Smolyak data sets generate more accurate results than a randomly generated data set. However, in higher dimensional stochastic spaces (large $n$), both the Hammersley/Halton and Smolyak data sets have their data points aligned, causing the system matrix A to become singular or near singular. In this case, a randomly generated data set that leads to a non-singular system matrix should be used. The transformation from the collocation points for a uniform distribution to the points for another distribution is achieved by applying the inverse Cumulative Distribution Function of the new distribution. For instance, the transformation from the collocation points for a uniform distribution to the points for a Beta (2, 2) distribution, is achieved by applying the inverse Cumulative Distribution Function of the Beta (2, 2) distribution, as shown in Figure 2.2 for 30 collocation points generated with the Halton algorithm for two uncertain parameters.

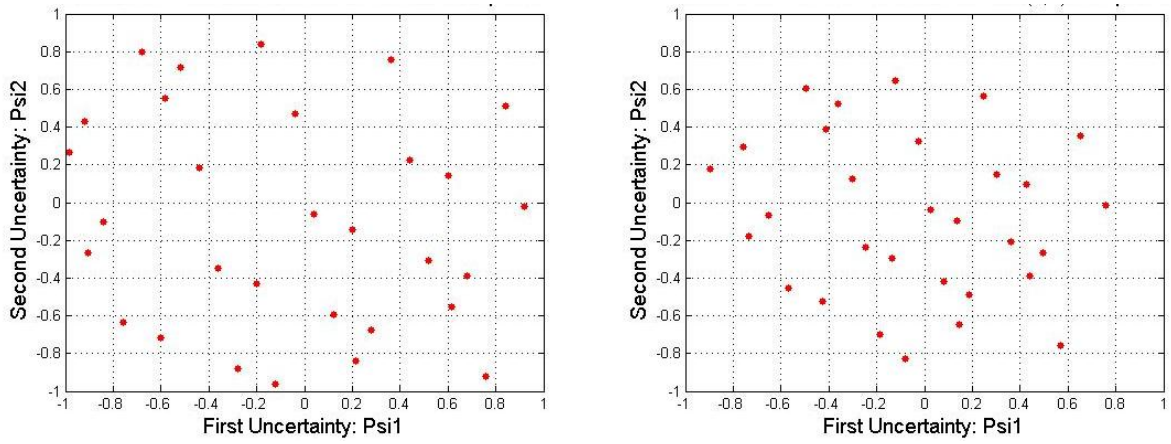


(a) (b)

Figure 2.2: Halton Collocation Points (2 dimensions, 30 points): (a) for Uniform Distribution; (b) for Beta (2, 2) Distribution

The comparison of the Galerkin PC approach and the collocation PC approach against the traditional Monte Carlo method for uncertainty quantification purpose is made in [13]. Obviously, without the requirement to modify the deterministic model, the non-intrusive collocation approach provides an easier implementation with similar accurate result compared with the Galerkin approach.

In general, the implementation of the PC collocation method includes the following steps:

1. Model the sources of uncertainty by random variables with appropriate PDFs
2. Build the *S* orthogonal polynomials (expansion basis)
3. Generate the polynomial chaos expansion of the uncertain parameters (or uncertain initial conditions)
4. Select $Q \geq S$ collocation points and generate the system matrix *A*.
5. Run *Q* deterministic system simulations with the expansion obtained from (2.7).
6. Recover the polynomial chaos coefficients of the results by formulating and solving the linear equation systems.
7. Extract the mean and the standard deviation of the final solution, and generate the PDFs.

In this procedure, the majority of the computation time will be spent on step (5) for repeated deterministic system runs. After the coefficients are recovered, the system solution can be represented by a linear combination of stochastic coefficients multiplied by basis functions:

After the coefficients are recovered, the system solution can be represented by a linear combination of stochastic coefficients multiplied by basis functions:

$$y(t) = y^0(t) + y^1(t)\,\psi^1(\xi) + y^2(t)\,\psi^2(\xi) + \ldots + y^n(t)\,\psi^n(\xi) + H.O.T. \qquad (2.15)$$

In the above representation, the superscripts for the system coefficients represent the stochastic modes $\psi^1(\xi), \ldots, \psi^n(\xi)$ are linear polynomials in variables $\xi_1, \ldots, \xi_n$ respectively. The H.O.T. represents the terms of orders 2 and up.

From the PC representation we can derive the statistics of the output uncertainty. The mean value is given by the $0^{th}$ order term in the stochastic representation (2.15)

$$\langle y_l(t)\rangle = y_l^0(t),\ 1 \le l \le m \tag{2.16}$$

The variance is computed as:

$$s_l^2(t) = \langle y_l(t) - \langle y_l(t)\rangle, y_l(t) - \langle y_l(t)\rangle\rangle = \sum_{j=1}^{S} y_l^j(t)\ y_l^j(t),\ 1 \le l \le m \tag{2.17}$$

The standard deviation is thus $s_l(t)$.

The covariance matrix of the model state at any time is computed by:

$$R_{k,l}(t) = \langle y_k(t),\ y_l(t)\rangle = \sum_{j=1}^{S} y_l^j(t)\ y_l^j(t)\ \langle\ \psi^{\,j},\ \psi^{\,j}\rangle \tag{2.18}$$

Using these measures, the model output can be visualized with an "error bar" representation for the uncertainty. In order to generate the PDF at any time, random samples with an appropriate distribution need to be drawn and plugged into the PC representation of the time-dependent state. With the known coefficients and the random numbers, an ensemble of states can be generated and represented by a PDF. In PC approach, as long as the PC coefficients and basis are known, a large state ensemble can easily be generated to form a smooth PDF curve. However, in Monte Carlo approach, each member of the ensemble states requires a full system run.

The impact of enforcing dynamics at these few collocation points is discussed in [19]. In practice, using collocation with judicious algorithms such as using the Hammersley/Halton points yields very similar results to what is obtained with Galerkin, when using enough collocation points. Practically, what needs to be done is checking that adding more terms and more collocation points does not significantly improve the results. Even though the number of points needed in order to obtain satisfactory results is quite dependent on the example used, a satisfactory number of points will typically result in a much faster computation time than any Monte-Carlo based simulation.

Finally, let's conclude with the fact that in order to work properly, the polynomial chaos theory needs to be applied to variables which are $C^1$ with respect to the uncertain parameters (i.e., their derivatives are continuous), which will be illustrated in Chapter 6.

## 2.2 Polynomial Chaos Theory Applied to System of ODEs

The purpose of this section is to show how to apply the polynomial chaos theory to a system of ODEs with uncertain parameters, which will be the framework of the work presented in Chapters 3-5.

In the deterministic case, a second order system can be described by the following Ordinary Differential Equation (ODE):

$$\begin{cases} \dot{x}(t) = v \\ \dot{v}(t) = F\left(t, x(t), v(t), \theta\right) \\ x(t_0) = x_0 \\ v(t_0) = v_0 \end{cases} \tag{2.19}$$

In the stochastic framework developed in this study, the displacement $x(t)$, the velocity $v(t)$, and the set of parameters $\theta \in \Re^{n_P}$ (the set of $n_p$ parameters being possibly uncertain) of a second order system can be expanded using Equation (2.3) as:

$$x_m(t,\xi) = \sum_{i=1}^{S} x_m^i(t)\,\psi^i(\xi), \quad v_m(t,\xi) = \sum_{i=1}^{S} v_m^i(t)\,\psi^i(\xi), \quad \theta_l(\xi) = \sum_{i=1}^{S} \theta_l^i\,\psi^i(\xi), \quad 1 \le m \le n_S, \quad 1 \le l \le n_p \tag{2.20}$$

We use subscripts to index system components and superscripts to index stochastic modes. Inserting Equation (2.20) in the deterministic system of equations leads to:

$$\begin{cases} \dot{x}_m^j(t) = v_m^j(t), 1 \le m \le n_S, 1 \le j \le S, \; t_0 \le t \le t_F \\ \sum_{j=1}^{S} \dot{v}_m^j(t)\,\psi^j(\xi) = F_m\left(t, \sum_{k=1}^{S} x^k\psi^k(\xi), \sum_{k=1}^{S} v^k\psi^k(\xi); \sum_{k=1}^{S} \theta^k\psi^k(\xi)\right) \\ x_m(t_0) = x_{m,0} \end{cases} \tag{2.21}$$

where $m$ is a state index and $n_S$ is the dimension of the state vector.

To derive evolution equations for the stochastic coefficients $x_m^i(t)$ we impose that Equation (2.21) holds at a given set of collocation points $\mu^1, \ldots, \mu^Q$. This leads to:

$$\dot{x}_m^i = v_m^i, \sum_{j=1}^{S} A_{i,j}\,\dot{v}_m^j = F\left(t, \sum_{k=1}^{S} A_{i,k}\,x^k, \sum_{k=1}^{S} A_{i,k}\,v^k; \sum_{k=1}^{S} A_{i,k}\,\theta^k\right), 1 \le i \le Q \tag{2.22}$$

where $A$ represents the matrix of basis function values at the collocation points:

$$A = \left( A_{i,j} \right),\ A_{i,j} = \psi^{j}(\mu^{i}),\ 1 \le i \le Q,\ 1 \le j \le S \tag{2.23}$$

The collocation points have to be chosen such that $Q \ge S$ and $A$ is nonsingular. Let $A^{\#}$ be the Moore-Penrose pseudo-inverse of $A$. With $X^{i} = \sum_{k=1}^{S} A_{i,k} x^{k},\ V^{i} = \sum_{k=1}^{S} A_{i,k} v^{k}, \Theta^{i} = \sum_{k=1}^{S} A_{i,k} \theta^{k}$, the collocation system can be written as:

$$\dot{X}^{i} = V^{i},\ \dot{V}^{i} = F\left(t, X^{i}, V^{i}, \Theta^{i}\right),\ 1 \le i \le Q \tag{2.24}$$

After integration, the stochastic solution coefficients are recovered using:

$$x^{i}(t) = \sum_{j=1}^{S} \left(A^{\#}\right)_{i,j} X^{j}(t),\ v^{i}(t) = \sum_{j=1}^{S} \left(A^{\#}\right)_{i,j} V^{j}(t)\ , 1 \le i \le S \tag{2.25}$$

Assuming that $\psi^{1}$ is the constant (order zero) term in the polynomial expansion, the mean values of $x(t)$ and $v(t)$ are $\bar{x}(t) = x^{1}(t)\,\psi^{1}$ and $\bar{v}(t) = v^{1}(t)\,\psi^{1}$, respectively. The standard deviations of $x(t)$ and $v(t)$ are given by:

$$\sqrt{\int_{\Omega} \left( \sum_{i=2}^{S} x^{i}(t) \psi^{i}(\xi) \right)^{2} \rho(\xi)\, d\xi}\ ,\ \sqrt{\int_{\Omega} \left( \sum_{i=2}^{S} v^{i}(t) \psi^{i}(\xi) \right)^{2} \rho(\xi)\, d\xi} \tag{2.26}$$

When the basis functions are orthogonal polynomials, the standard deviations of $x(t)$ and $v(t)$ are given by:

$$\sqrt{\sum_{i=2}^{S} \left( x^{i}(t) \right)^{2} \left\langle \psi^{i}, \psi^{i} \right\rangle}\ ,\ \sqrt{\sum_{i=2}^{S} \left( v^{i}(t) \right)^{2} \left\langle \psi^{i}, \psi^{i} \right\rangle} \tag{2.27}$$

When the bases are orthonormal, the standard deviations of $x(t)$ and $v(t)$ are given by:

$$\sqrt{\sum_{i=2}^{S} \left( x^{i}(t) \right)^{2}}\ ,\ \sqrt{\sum_{i=2}^{S} \left( v^{i}(t) \right)^{2}} \tag{2.28}$$

Similarly, the covariance of two variables can be computed from the polynomial chaos expansion. For example the covariance of uncertainties in state component *m* and in parameter *p* is:

$$\operatorname{cov}\left(x_m(t),\theta_p\right)=\sum_{i=2}^{S}x_m^i(t)\;\theta_p^i\int_\Omega\left\langle\psi^i(\xi),\psi^i(\xi)\right\rangle d\xi \tag{2.29}$$

The Probability Density Functions (PDF) of $x(t)$ and $v(t)$ are obtained by drawing histograms of their values using a Monte Carlo simulation and normalizing the area under the curves obtained. In order to generate the PDF at any time, random samples with an appropriate distribution need to be drawn and plugged into the polynomial chaos representation of the time-dependent state. With the known coefficients and the random numbers, an ensemble of states can be generated and represented by a PDF. With the polynomial chaos approach, as long as the polynomial chaos coefficients and basis are known, a large state ensemble can easily be generated to form a smooth PDF curve. However, in a Monte Carlo approach, each member of the ensemble states requires a full system run. Therefore, generating a PDF with the polynomial chaos approach is not computationally expensive, since the Monte Carlo simulation is run on the final result – we have repeated evaluations of polynomial values but not repeated ODE simulations. To be specific, the number of ODE runs equals the number of collocation points, which is typically much lower than the number of runs used in a Monte Carlo simulation.

## 2.3 Literature Review

### 2.3.1 Parameter Estimation

Parameter estimation is an important problem, because in many instances parameters cannot be physically measured, or cannot be measured with sufficient accuracy in real time applications. Rather, parameter values must be inferred from available measurements of different aspects of the system response. The theoretical foundations of parameter estimation can be found in [20-22]. Parameter estimation finds applications in many fields, including mechanical engineering [23], material science [24], aerospace [25], geosciences [26], chemical engineering [27], etc. A literature review specific to the online estimation of on-road vehicles' mass can be found in [28], in which an algorithm providing conservative error estimates is also proposed.

Various approaches to parameter estimation are discussed in the literature. These include energy methods [29], frequency domain methods [30], and set inversion via interval analysis (SIVIA) with Taylor expansions [31]. A rigorous framework for parameter estimation is the

Bayesian approach, where probability densities functions are being considered representations of uncertainty. The Bayesian approach has been widely used [32-35]. The Bayesian approach consists of estimating aposteriori probabilities of the parameters and therefore transforming a parameter estimation problem into the problem of finding maximum likelihood values of the parameters.

Different methodologies to estimate parameters in a Bayesian framework are possible. Maximum likelihood parameter estimation can be formulated as an optimization problem (typically large and nonconvex, therefore challenging). It can be numerically solved by gradient methods [36] or by global optimization methods [37-41]. Another approach to solving the global continuous optimization problem is the use of Evolutionary Algorithms (EAs) which are inspired by biological evolution [42]. Differential Evolution (DE) techniques are EA techniques that have been used successfully and Estimation of Distribution Algorithms (EDAs) are a promising new class of EAs [43]. Sun *et al.* [44] proposed a DE/EDA hybrid approach. Another hybrid approach called estimation of distribution algorithm with local search (EDA/L) has been developed by Zhang *et al.* [45]. Zhang *et al.* [46] also proposed an evolutionary algorithm with guided mutation (EA/G).

Another Bayesian parameter estimation method is the Kalman Filter [47], which is optimal for linear systems with Gaussian noise. The Extended Kalman Filter (EKF) allows for nonlinear models and observations by assuming that the error propagation is linear [48, 49]. The Ensemble Kalman Filter (EnKF) is a Monte Carlo approximation of the Kalman filter suitable for large problems [50]. In the context of stochastic optimization, propagation of uncertainties can be represented using Probability Density Functions (PDFs). The Kalman Filter and its approximations estimate the states and their uncertainties at the same time through covariance matrices. In order to approximate PDFs propagated through the system, linearization using the EKF [2] and Monte Carlo techniques using the EnKF [51] are common approaches. The EKF has the advantage of taking nonlinear dynamic effects into account and therefore dealing with non-Gaussian probabilities, but the EnKF is more practical when dealing with large state space systems for which the covariance matrix becomes too large. Particle filters are ensemble-based assimilation methods which can also take nonlinear dynamic effects into account and deal with non-Gaussian probabilities, but are not adapted to high-dimensional systems [52].

Parameter estimation is well recognized as a theoretically difficult problem; moreover, estimating a large number of parameters is often computationally very expensive. This has led to the development of techniques determining which parameters affect the system's dynamics the most, in order to choose the parameters that are important to estimate [53]. Sohns *et al.* [53] proposed the use of activity analysis as an alternative to sensitivity-based and principal component-based techniques. Their approach combines the advantages of the sensitivity-based techniques (i.e., efficiency for large models) and of the component-based techniques (i.e., using parameters that can be physically interpreted). Zhang and Lu [54] combined the Karhunen–Loeve decomposition and perturbation methods with polynomial expansions in order to evaluate higher-order moments for saturated flow in randomly heterogeneous porous media.

### 2.3.2 Polynomial Chaos Theory and Applications to Parameter Estimation

The polynomial chaos method started to gain attention after Ghanem and Spanos [8, 55-57] applied it successfully to the study of uncertainties in structural mechanics and vibration using Wiener-Hermite polynomials. Xiu extended the approach to general formulations based on the Wiener-Askey polynomials family [11], and applied it to fluid mechanics [12, 58, 59]. Sandu *et al.* applied for the first time the polynomial chaos method to multibody dynamic systems [19, 60-62], terramechanics [63, 64], and parameter estimation in the time domain for fixed parameters [1, 2].

In their groundbreaking work, Soize and Ghanem [65] described mathematical settings for characterizing problems for which random uncertainties have arbitrary probability densities. Desceliers *et al.* [66] used a polynomial chaos representation of a random field to be identified, developed a method to estimate the coefficients of that representation, and extended it to apply it to experimental vibration tests using frequency response functions [67]. Saad *et al.* [51] coupled the polynomial chaos theory with the Ensemble Kalman Filter (EnKF) to indentify unknown variables in a non-parametric stochastic representation of the non-linearities in a shear building model. Their identification method proved to be an effective way of accurately detecting changes in the behavior of a system affected by both measurement noise and modeling noise. Li and Xiu [68] also developed a methodology combining the polynomial chaos theory with the EnKF, in which they sampled the polynomial chaos expression of the stochastic solution in order to reduce

the sampling errors. The benefits and drawbacks of the EnKF are discussed in [69] and [70]. Smith *et al.* [71] designed a polynomial chaos observer for indirect measurements which provides a full probability density function from the polynomial chaos coefficients, and which is computationally less expensive than using a regular EKF. Their approach is designed to compensate for the modeling noise but needs to be tuned (e.g. with a Kalman approach) to take observation noise into account. Finally, let us mention that long-time integration errors are a major problem with the polynomial chaos theory, which has been addressed by Wan and Karniadakis [72] who developed a multi-element generalized polynomial chaos (ME-gPC) method.

The generalized polynomial chaos theory developed by Xiu and Karniadakis [11] is also explained in [19] in which direct stochastic collocation is proposed as a less expensive alternative to the traditional Galerkin approach. The relation between collocation and Galerkin methods is explained in [19]. Cheng and Sandu [73, 74] further discuss the computational cost of using the polynomial chaos theory with both Galerkin and collocation methods. One of the major drawbacks of the polynomial chaos theory is the fact that long-time integration errors are a major problem, which has been addressed by Wan and Karniadakis [72] who developed a multi-element generalized polynomial chaos (ME-gPC) method.

The polynomial chaos theory has been shown to be consistently more efficient than Monte Carlo simulations in order to assess uncertainties in mechanical systems [19, 62, 73, 74] and coupling it with the Bayesian approach and with the Extended Kalman Filter has the potential of making these two parameter estimation methods computationally much less expensive and therefore more attractive, especially for real-time applications. This study extends the polynomial chaos theory to the problem of parameter estimation. In Chapter 3, a maximum likelihood parameter estimation approach in a Bayesian framework is developed. In Chapter 4, a new computational approach for parameter estimation based on the Extended Kalman Filter (EKF) and the polynomial chaos theory for parameter estimation is proposed. The error covariances needed by the EKF are computed from polynomial chaos expansions, and the EKF is used to update the polynomial chaos representation of the uncertain states and the uncertain parameters. Aposteriori PDFs are obtained using the polynomial chaos theory for propagating uncertainties through system dynamics. The proposed methods will be illustrated on a nonlinear four degree of freedom roll plane vehicle model, in which an uncertain mass and its uncertain

position are estimated. The methods have the advantage of being able to deal with large parametric uncertainties, non-Gaussian probability densities, and nonlinear system dynamics.

### 2.3.3 Robust Control and Applications to Vehicle Suspensions

Robust control methods consist of designing controllers able to deal with uncertain parameters in the formulation. Robust control methods can focus on stability robustness and performance robustness in the presence of uncertainties, and the following terms are found extensively in the literature [75]

- **Nominal stability (NS).** The system is stable with no model uncertainty.
- **Nominal performance (NP).** The system satisfies the performance specifications with no model uncertainty.
- **Robust stability (RS).** The system is stable for all perturbed plants about the nominal model up to the worst-case model uncertainty
- **Robust performance (RP).** The system satisfies the performance specifications for all perturbed plants about the nominal model up to the worst-case model uncertainty.

Some of the early robust control methods were developed by Bode in the 1930's. He introduced quantities such as gain margin, phase margin, system sensitivity and root sensitivity which can be used as measures of stability robustness. Dorf and Bishop [76] describe methods for robust design that include root locus, frequency response and ITAE (Integral of Time Multipled by Absolute Error) methods for a robust PID controller. In classical control, another way to measure the stability of a system is the Nyquist stability criterion: the distance from the point (-1, 0) can be used as a measure of the stability robustness of a system. One of the advantages of the classical control theory is that parameter uncertainty can easily be expressed in terms of transfer function [77]. The main disadvantage of these frequency domain methods is that they are too difficult to implement on systems with too many inputs and outputs [77].

The state-space methods, which describe systems in the time domain using differential equations, appeared in the 1960's. They provide a convenient and efficient way to analyze

MIMO (multiple-input and multiple-output) systems, but they were usually found to lack robustness mainly because they have problems capturing uncertainties. Robustness is indeed not part of their formulation and must be checked after design [77]. Doyle [78] showed that the linear-quadratic-Gaussian (LQG) controller, which combines the Kalman Filter, which is a Linear-Quadratic Estimator (LQE) with a Linear-Quadratic Regulator (LQR), was not adapted for robust design. However, Doyle et *al.* [79] showed that the $H_\infty$ problem consisting of designing controllers resulting in closed-loop systems in the presence of uncertainties could be seen as a state-space problem similar to LQG problems. Since then, the $H_\infty$ theory has been widely used for developing robust control methods achieving robust performance or stabilization.

The early development of the $H_\infty$ theory can be attributed to Doyle and Stein [80] and Zames [81], and is well explained in [82-84]. The $H_\infty$ -synthesis methods, which consist of finding a controller minimizing the $H_\infty$ -norm of a linear fractional transformation, are usually solved using the solutions of two Riccati equations. A drawback associated with the $H_\infty$ methodology is that it often leads to conservative results [85], which led to the development of μ-analysis methods. With the $H_\infty$ loop-shaping theory, classical loop-shaping concepts can be applied to the frequency responses of multiple variables. The $H_\infty$ loop-shaping method has the advantage of addressing robust performance and then robust stabilization by weighting the plant transfer function in the frequency domain, typically without affecting the performance robustness at low and high frequencies. A good example illustrating the $H_\infty$ loop-shaping method is the work of Safonov et *al.* [86] on the NASA HiMAT aircraft model, which is used as an example in the Matlab Robust Control Toolbox™. The structured singular value (μ) theory was developed to study linear fractional perturbations, which are used to model many types of uncertainty in linear systems [87]. The conservative results associated with the $H_\infty$ methodology led to the development of μ-analysis methods, which can relate to the classical control theory robustness measures and be applied to multivariable systems. The μ-synthesis methodology uses $H_\infty$ design methods and the structured singular value in order to synthesize robust controllers. Balas [85] showed that the μ-synthesis design methodology has the ability to incorporate performance and robustness specifications into the control design process by applying it to the problem of vibration control in flexible structures.

Since the value of μ cannot be computed in the general case, D-K iterations have become popular methods for designing controllers achieving robust controller, and are available in the Matlab Robust Control Toolbox™. The D-K iteration procedure is explained in [84]. It is an approximation to μ-synthesis, which consists of alternatively finding a scaling matrix D while fixing the controller K and then solving for the controller K with the matrix D being fixed. However, Stein and Doyle [88] showed that the D-K iteration is not guaranteed to converge to an optimal controller. Also, the D-K iteration yields a conservative controller design, as illustrated by VanAntwerp et *al.* [89], who developed a computational approach that resulted controllers 50% less conservative than controllers designed via DK-iteration for a mass-spring benchmark problem. Their approach was based on optimization with bilinear matrix inequality (BMI) constraints and was robust to nonlinear time-varying perturbations in the plant. Linear Matrix Inequality (LMI) techniques have applications in many control problems, including Lyapunov based methods and quadratic optimal problems [90], and also $H_\infty$ robust control [91].

$H_\infty$ methods have been applied successfully to vehicle suspensions. $H_\infty$ methods can be applied to passive suspensions. In this case, the controller is simply the chosen value for the dampers. A review of the past research on $H_\infty$ and $H_2$ optimization problems of the Voigt type dynamic vibration absorber (DVA) can be found in [92], where a series solution for the $H_\infty$ problem when damping is present between the primary system and the exciting force (i.e. the unsprung mass and the road in the case of a vehicle suspension) is proposed. $H_\infty$ optimization techniques have also been applied to semiactive suspensions, for which the values of the dampers can be tuned. Sammier et *al.* [93] used a quarter car model to show that the $H_\infty$ control methodology is more efficient than the skyhook control policy for semiactive suspensions. Du *et al.* [94] studied the efficiency of an $H_\infty$ semiactive controller measuring the suspension deflection and the velocity of the sprung mass. Robust control methods have also been used on active suspensions, where a force can be generated across the suspensions using an actuator. Du and Zhang [95] presented a time-delay dependent $H_\infty$ design method for robust performance for active suspensions with bounded time delay. Their approach was based on the solution of delay-dependent matrix inequalities to synthesize an $H_\infty$ controller. Du et *al*. [96] designed $H_\infty$ controllers for active suspensions based on the solvability of linear matrix inequalities (LMI) and genetic algorithms.

### 2.3.4 LQR Problem with Uncertain Parameters in the Formulation

The solution to the $H_\infty$ problem as well as the $H_2$ problem are based on solutions of Riccati equations and can therefore be seen as extensions of the LQR problem [83]. Therefore, developing a new computationally efficient numerical method in order to solve the LQR problem in a framework taking parametric uncertainties into account might have the potential of leading to other computationally efficient methods solving $H_2$ and $H_\infty$ problems with parametric uncertainties. Fisher and Bhattacharya [97] presented a framework for LQR design with uncertain parameters in the formulation, using the polynomial chaos theory. However, their work yields a system of equations with no known answer for the specific problem described in this dissertation. Templeton [98] used the same framework than Fisher and Bhattacharya [97], which consists of extended matrices in a polynomial chaos framework, and developed a gradient descent optimization method finding optimal gains for $H_2$ and LQR design with parametric uncertainties.

We are not aware of any study trying to use the polynomial chaos framework to find a closed form solution for the LQR problem in this framework, i.e., a solution that would depend on the number of terms $S$ in the polynomial chaos expansions and that would numerically converge to the solution of the problem as $S \to \infty$. Also, gradient methods would be difficult to extend to the $H_\infty$ problem, while a method going to the root of the solution of the LQR problem, which is derived using Lagrange multipliers in the deterministic case [99] and leads to the well-known algebraic Riccati equations, might have the potential of being a first steps towards a new method for $H_\infty$ problems with uncertainties in the formulation.

# 3 Polynomial Chaos Based Bayesian Approach for Parameter Estimation

This chapter extends the polynomial chaos theory, which has been shown to be consistently more efficient than Monte Carlo simulations in order to assess uncertainties in mechanical systems [19, 62], to the problem of parameter estimation in the Bayesian framework. Aposteriori PDFs are obtained using the polynomial chaos theory for propagating uncertainties through system dynamics. The new method has the advantage of being able to deal with large parametric uncertainties, non-Gaussian probability densities, and nonlinear dynamics. The maximum likelihood estimates are obtained by minimizing a cost function derived from the Bayesian theorem. Direct stochastic collocation is used as a less computationally expensive alternative to the traditional Galerkin approach to propagate the uncertainties through the system in the polynomial chaos framework.

The new approach is explained and is applied to very simple mechanical systems in order to illustrate how the Bayesian cost function can be affected by the noise level in the measurements, by undersampling, non-identifiability of the system, non-observability, and by excitation signals that are not rich enough. When the system is non-identifiable and an apriori knowledge of the parameter uncertainties is available, regularization techniques can still yield most likely values among the possible combinations of uncertain parameters resulting in the same time responses than the ones observed.

The new parameter estimation method is then illustrated on a nonlinear four-degree-of-freedom roll plane model of a vehicle in which an uncertain mass with an uncertain position is added on the roll bar. The value of the mass and its position are estimated from periodic observations of the displacements and velocities across the suspensions, generated with synthetic measurements obtained from a reference simulation with the reference values of the uncertain parameters and with added noise. When using appropriate excitations, the results obtained with this approach are close to the actual values of the parameters.

## 3.1 Formulation of the Bayesian Approach

Optimal parameter estimation combines information from three different sources: the physical laws of evolution (encapsulated in the model), the reality (as captured by the observations), and the current best estimate of the parameters. The information from each source is imperfect and has associated errors. Consider the mechanical system model (2.21) in Chapter 2, which advances the state in time represented in a simpler notation:

$$y_k = \begin{bmatrix} x_k \\ v_k \\ \theta_k \end{bmatrix}, \quad y_k = \mathbf{M}\left(t_{k-1}, y_{k-1}\right), \quad y_0 = y\left(t_0\right), \quad k = 1, 2, \ldots, N \tag{3.1}$$

The state of the model $y_k \in \Re^{n_S}$ at time moment $t_k$ depends implicitly on the set of parameters $\theta \in \Re^{n_P}$, possibly uncertain (the model has $n_S$ states and $n_P$ parameters). $\mathbf{M}$ is the model solution operator which integrates the model equations forward in time (starting from state $y_{k-1}$ at time $t_{k-1}$ to state $y_k$ at time $t_k$). $N$ is the number of time points at which measurements are available.

For parameter estimation it is convenient to formally extend the model state to include the model parameters and extend the model with trivial equations for parameters (such that parameters do not change during the model evolution)

$$\theta_k = \theta_{k-1} \tag{3.2}$$

The optimal estimation of the uncertain parameters is thus reduced to the problem of optimal state estimation. We assume that observations of quantities that depend on system state are available at discrete times $t_k$

$$z_k = h\left(y_k\right) + \eta_k \approx H_k y_k + \eta_k, \quad \overline{\eta_k} = 0, \quad \overline{\left(\eta_k\right)\left(\eta_k\right)^T} = R_k \tag{3.3}$$

where $z_k \in \Re^{n_O}$ is the observation vector at $t_k$, $h$ is the (model equivalent) observation operator, $H_k$ is the linearization of $h$ about the solution $y_k$, and $\eta_k$ is the measurement noise at time index $k$. Note that there are $n_O$ observations for the $n_S$–dimensional state vector, and that typically $n_O < n_S$. Each observation is corrupted by observational (measurement and

representativeness) errors [100]. We denote by $\left(\overline{\cdot}\right)$ the ensemble average over the uncertainty space. The observational error $\eta_k$ is the experimental uncertainty associated with the measurements and is usually considered to have a Gaussian distribution with zero mean and a known covariance matrix $R_k$.

Using polynomial chaoses the uncertain parameters are modeled explicitly as functions of a set of random variables $\xi \in \Omega \subset \Re^p$ with a joint probability density function $\rho(\xi)$. The explicit dependency of the system state on the random variables is obtained via a collocation approach:

$$\theta(\xi) = \sum_{i=1}^{S} \theta^i \psi^i(\xi), \quad y_k(\xi,t) = \sum_{i=1}^{S} (y_k(t))^i \psi^i(\xi) \tag{3.4}$$

We adopt the point of view that the "state of knowledge" about the uncertain parameters can be described by probability densities. From Bayes' rule the probability density of the parameter distribution conditioned by all observations is

$$P\left[y_N \middle| z_N \ldots z_0\right] = \frac{P[z_N | y_N] \cdot P[y_N | z_{N-1} \ldots z_0]}{\int P[z_N | y] \cdot P[y | z_{N-1} \ldots z_0]\, dy} \tag{3.5}$$

where $P[z_N \mid y_N]$ is the Probability Density Function (PDF) of the latest observational error (taken at time $t_N$), $P[y_N | z_{N-1} \ldots z_0]$ is the "model forecast PDF" conditioned by all previous observations (taken at times $t_0$ to $t_{N-1}$), and $P[y_N | z_N \ldots z_0]$ is the "assimilated PDF". The assimilated PDF represents the aposteriori probability of the parameters after all the observations have been taken into account.

For simplicity denote by $y$ the current state of the system (the best estimation obtained using all previous observations $z_{N-1} \ldots z_0$) and by $z = z_N$ the latest, yet-to-be-used set of observations. Moreover, consider that the observational error has a Gaussian distribution with covariance $R_k$ and that the observations at different times are independent. Then Bayes' formula becomes

$$P\left[y \middle| z\right] = \frac{P[z | y] \cdot P[y]}{\int_{\Re^n} P[z | y] \cdot P[y]\, dy} = \frac{e^{-\frac{1}{2}\sum_{k=0}^{N} (z_k - H y_k)^T R_k^{-1} (z_k - H y_k)} \cdot P[y]}{\int_{\Re^n} e^{-\frac{1}{2}\sum_{k=0}^{N} (z_k - H y_k)^T R_k^{-1} (z_k - H y_k)} \cdot P[y]\, dy} \tag{3.6}$$

The unconditional probability density $P[y]$ is the PDF of the current system state, and is implicitly represented by the polynomial chaos expansion of the state $y = y(\xi)$. Moreover, integration against this probability density can be evaluated by integration in the independent random variables

$$\int_{\Re^n} f(y) \cdot P[y] \cdot dy = \int_{\Omega} f\big(y(\xi)\big) \cdot \rho(\xi) \cdot d\xi \quad \text{for any } f(\cdot) \tag{3.7}$$

The denominator can be evaluated by a multidimensional integration. However, in our approach, there is no need to evaluate this scaling factor, since its omission does not change the estimation procedure. (The omission of this scaling factor is equivalent to adding a constant to the function we minimize, and this does not change the result of the minimization procedure).

The mean of the best state estimate that uses the new observations *z* is obtained from Bayes formula as

$$\begin{aligned} \bar{y} = \int_{\Re^n} y \cdot P[y \mid z] \cdot dy &= \frac{1}{\text{den}} \int_{\Re^n} y \cdot e^{-\frac{1}{2}\sum_{k=0}^{N} (z_k - H y_k)^T R_k^{-1} (z_k - H y_k)} \cdot P[y] \cdot dy \\ &= \frac{1}{\text{den}} \int_{\Omega} y(\xi) \cdot e^{-\frac{1}{2}\sum_{k=0}^{N} (z_k - H y_k)^T R_k^{-1} (z_k - H y_k)} \cdot \rho(\xi) \cdot d\xi \end{aligned} \tag{3.8}$$

For the parameter estimation the Bayes' formula specializes to:

$$P\big[\theta \mid z\big] = \frac{P[z|\theta] \cdot P[\theta]}{\text{den}} = \frac{e^{-\frac{1}{2}\sum_{k=0}^{N} (z_k - H y_k(\theta))^T R_k^{-1} (z_k - H y_k(\theta))} \cdot P[\theta]}{\int_{\Re^m} e^{-\frac{1}{2}\sum_{k=0}^{N} (z_k - H y_k(\theta))^T R_k^{-1} (z_k - H y_k(\theta))} \cdot P[\theta]\, d\theta} \tag{3.9}$$

Note that the aposteriori probability defined by Bayes formula can be written (in principle) as a function of the independent random variables $\xi$

$$\hat{\rho}(\xi) = P\big[\xi \mid z\big] = \frac{e^{-\frac{1}{2}\sum_{k=0}^{N} (z_k - H y_k(\xi))^T R_k^{-1} (z_k - H y_k(\xi))} \cdot \rho(\xi)}{\int_{\Omega} e^{-\frac{1}{2}\sum_{k=0}^{N} (z_k - H y_k(\xi))^T R_k^{-1} (z_k - H y_k(\xi))} \cdot \rho(\xi)\, d\xi} \tag{3.10}$$

In this setting polynomial chaos is used to model the *a priori* pdf of the parameters; the Bayes formula is employed to obtain the *a posteriori* pdf (i.e., the pdf conditioned by the observations).

The maximum likelihood estimate is given by that realization of the parameters (that value of $\xi$) which maximizes the *aposteriori* probability $P[\theta \mid z]$, or, equivalently, minimizes $-\log(P[\theta \mid z])$:

$$\min_{\xi \in \Omega} J = \tfrac{1}{2} \sum_{k=0}^{N} (z_k - H y_k(\xi))^T R_k^{-1} (z_k - H y_k(\xi)) - \log(\rho(\xi)) \tag{3.11}$$

Note that for $\xi \notin \Omega$ we have $\rho(\xi) = 0$ and cost the function $J$ becomes infinite. This cost function is composed of two parts:

$$J_{\text{total}}(\xi) = \underbrace{\tfrac{1}{2} \sum_{k=0}^{N} (z_k - H y_k(\xi))^T R_k^{-1} (z_k - H y_k(\xi))}_{J_{\text{mismatch}}} + \underbrace{(-\log(\rho(\xi)))}_{J_{\text{apriori}}} \tag{3.12}$$

where $J_{\text{mismatch}}$ comes only from the differences between the available measurements and the model response, while $J_{\text{apriori}}$ encapsulates the apriori knowledge of the parameter uncertainty. The value $\hat{\xi} = \arg\min J$ minimizing the cost function (3.12) gives the most likely values of our uncertain parameters as $\hat{\theta} = \theta(\hat{\xi})$.

## 3.2 Insight into the Bayesian Approach Using Simple Mechanical Systems

We now illustrate the proposed Bayesian approach for the estimation of parameters of several simple mechanical systems. We discuss how the cost function and the estimate can be affected by low sampling rates (i.e., below the Nyquist frequency), by measurement noise, and by non-identifiability issues.

The state of the model $y_k \in \Re^{n_S}$ at time moment $t_k$ depends implicitly on the set of uncertain parameters $\theta \in \Re^{n_P}$, and therefore on the set of independent random variables $\xi$. This dependency is explicitly represented in the polynomial chaos framework, specifically, at each time moment $t_k$ the state is given as a polynomial of the random variables $y_k = y_k(\xi)$. The probability density of the state can also be obtained from this relation. $H$ is simply a matrix converting the states of the model $y(\xi)$ to the observable parameters of the system (i.e., the

quantities which can be measured), which are contained in $z$. $R_k$ is the covariance matrix of the uncertainty associated with the measurements, i.e., of the measurement noise.

$J_{apriori} = -\log(\rho(\xi))$ comes from the apriori knowledge of the uncertain parameters. Using polynomial chaoses the uncertain parameters can be modeled explicitly as functions of a set of random variables $\xi \in \Omega \subset \Re^p$ with a joint probability density function $\rho(\xi)$.

$J_{mismatch}$ is usually the most important component of the cost function, but $J_{apriori}$ is useful when $J_{mismatch}$ does not contain enough information in order to find a clear minimum value for our cost function. This is illustrated in the next section of this chapter.

### 3.2.1. Mass-Spring System with Uncertain Initial Velocity

This section applies the Bayesian approach to the simple mass-spring system shown in Figure 3.1.

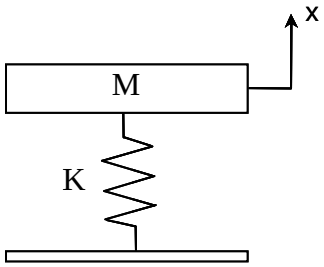


Figure 3.1: Mass–Spring System

The parameters $K$ (the stiffness of the spring) and $M$ (the mass of the body) are known. The system has a zero initial displacement $x_0 = 0$ but a nonzero initial velocity $v_0$ (e.g., created by hitting the mass from below with a hammer at $t = 0$, which will produce $v_0 > 0$). We want to estimate the uncertain initial condition $v_0$ based on measurements of the displacement $x(t)$ at later times.

The equation of motion of the system is

$$\mathrm{M}\ \ddot{x}(t) + K\ x(t) = 0 \tag{3.13}$$

and admits the general solution [101]:

$$x(t) = \sqrt{\frac{v_0^{\,2} + (x_0\,\omega_n)^2}{\omega_n^{\,2}}}\,\sin\!\left(\omega_n t + \tan^{-1}\!\left(\frac{x_0\,\omega_n}{v_0}\right)\right)\ ,\ \omega_n = \sqrt{\frac{K}{M}} \tag{3.14}$$

The values chosen for the numerical experiments are $\mathrm{K} = 0.1\times(2\pi)^2 \approx 3.9478$ N/m, $\mathrm{M} = 0.1$ kg and therefore $\omega_n = 2\pi$ rad/s $= 1$ Hz. For these values, and with $x_0 = 0$, the solution (3.14) becomes:

$$x(t) = \frac{v_0}{2\pi}\sin(2\pi t), \quad v(t) = v_0\cos(2\pi t). \tag{3.15}$$

The amplitude of $x(t)$ and the amplitude of $v(t)$ are both proportional to the uncertain parameter $v_0$, as illustrated in Figure 3.2. A *single* measurement of the displacement at a time $t_1 \neq m/2$ (with $m$ integer) allows estimating the initial velocity as $v_0 = 2\pi x(t_1)/\sin(2\pi t_1)$. Note that $\sin(2\pi t_1) \neq 0$. A single measurement of both the velocity and the displacement at any time $t_2$ is sufficient to retrieve the initial velocity, since for any $t_2$ at least one of the variables is nonzero, $\sin(2\pi t_2) \neq 0$ or $\cos(2\pi t_2) \neq 0$.

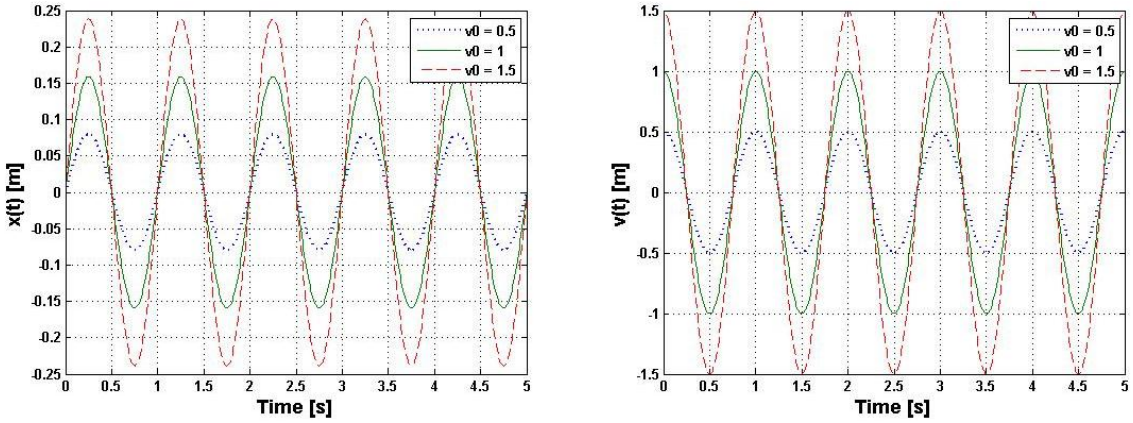


Figure 3.2: Displacements and Velocities of the Mass–Spring System

We now consider the case where measurements of the displacement only are taken at multiple time moments $t_1, t_2, \cdots, t_N$. This will give insight on how the two parts of the Bayesian cost

function can be affected by low sampling rates (i.e., below the Nyquist frequency) and by measurement noise.

We assume some prior knowledge of the initial velocity, which represents how hard different people can hit the mass with the hammer. The range of possible initial velocities is between $0.5\,\text{m/s}$ and $1.5\,\text{m/s}$, with a most likely value of $v_0 = 1\,\text{m/s}$. We model this prior knowledge as shown in Figure 3.3. Let $\xi$ be a random variable with a Beta (2, 2) probability distribution $\rho(\xi)$ in the range $\xi \in [-1,1]$. The random initial velocity is then

$$v(\xi,0) = v_{0\,nom}\left(1 + 0.5\,\xi\right) \quad [m/s] \tag{3.16}$$

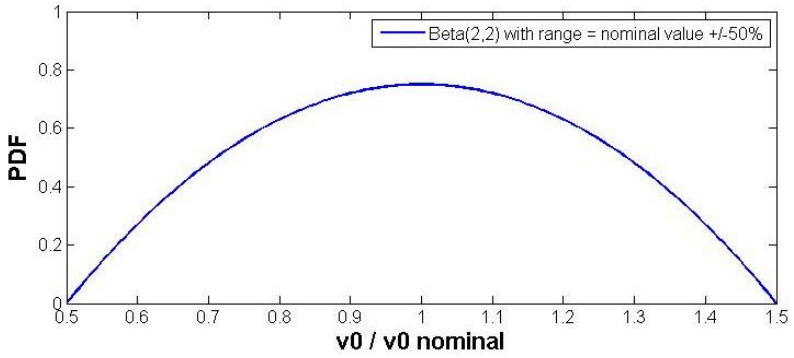


Figure 3.3: Beta (2, 2) Distribution for $v_0$

The state of the system at future times depends on the random initial velocity and can be represented by $y(\xi,t) = \left[x(\xi,t)^T \;\; v(\xi,t)^T \;\; \theta(\xi,t)^T\right]^T$. Synthetic measurements are obtained from a reference simulation with the reference value of the uncertain parameter $\xi^{ref} = 0.23$. If we assume that only the displacement can be measured we have that $H = \begin{bmatrix}1 & 0 & 0\end{bmatrix}$ and the measurements yield

$$z_k = H \cdot y^{\text{ref}}(t_k) + \eta_k = x^{\text{ref}}(t_k) + \eta_k, \quad \eta_k \in \mathbf{N}(0, R_k). \tag{3.17}$$

The measurement noise $\eta_k$ is assumed to be Gaussian with a zero mean and a variance 1% (or 0.01% or 10% when indicated) of the value of $x(t)$ plus the maximum measured value of $x(t)$ divided by 1000. Therefore, the covariance of the uncertainty associated with the measurements

is $R_k = \max\left\{10^{-12}, \left(0.01\ z_k + 0.001\ \max_t(z_k)\right)^2\right\}[m^2]$. This value is always greater than zero and $R_k^{-1}$ can always be computed. Measurement errors at different times are independent random variables.

The maximum likelihood estimate is obtained by minimizing the Bayesian cost function

$$J_{\text{total}}(\xi) = \underbrace{\tfrac{1}{2}\sum_{k=1}^{N}\left(z_k - H\ y(\xi,t_k)\right)^T R_k^{-1}\left(z_k - H\ y(\xi,t_k)\right)}_{J_{\text{mismatch}}} + \underbrace{\left(-\log\left(\rho(\xi)\right)\right)}_{J_{\text{apriori}}} \tag{3.18}$$

The random system output $y(\xi,t)$ is discretized using 6 terms in the polynomial chaos expansions, and 12 collocation points will be used to derive the polynomial chaos coefficients. The collocation points used in this study are obtained using an algorithm based on the Halton algorithm [15], which is similar to the Hammersley algorithm [14].

The frequency of the output signal $x(t,\xi)$ is 1 Hz for any value of $\xi$. If $x(t)$ is measured every $0.5\,\text{s}$ from $t = 0.5\,\text{s}$ to $t = 5\,\text{s}$, then $x(t_k,\xi) = 0$ for any value of $\xi$ and $z_k = \eta_k$ mismatch part gives no extra information, as shown in Figure 3.4, in which the plot for $x(t)$ was obtained with $\xi = 0.23$.

$$J_{\text{mismatch}}(\xi) = \tfrac{1}{2}\sum_{k=1}^{N}(\eta_k)^T R_k^{-1}(\eta_k) \tag{3.19}$$

For clarity we will illustrate this detailing the step by step procedure using analytical formulas for this particular example.

The explicit dependency of $x(t,\xi)$ is obtained via a collocation approach. It can be represented as

$$x(t,\xi) = \sum_{i=1}^{S=6} x^i(t)\,\psi^i(\xi) \tag{3.20}$$

The equation of motion of the system illustrated in Figure 3.1 is given by Equation (3.13). As shown earlier, the solution for this equation for $\omega_n = \sqrt{K/M} = 2\pi$ rad/s $= 1$ Hz and for a zero initial displacement is given by Equation (3.15).

In a polynomial chaos framework, the equation of motion of the system yields six equations for $S = 6$:

$$M\ \ddot{x}^i(t) + K\ x^i(t) = 0, \quad i = 1, 2, \ldots, S = 6 \tag{3.21}$$

Solving the six different equations of motions separately yields

$$x^i(t) = \frac{v_0^i}{2\pi} \sin(2\pi\ t_k), \quad i = 1,\ 2,\ \ldots,\ S = 6 \tag{3.22}$$

and the polynomial expression of the displacement is

$$x(t,\xi) = \sum_{i=1}^{S=6} \frac{v_0^i}{2\pi} \sin(2\pi\ t_k) \psi^i(\xi) \tag{3.23}$$

Let's note that, in the general case, there is no need to know the closed form solution of the equations of motion. The approach presented in this chapter still works when using the states variables obtained with numerical techniques to solve ODE's at the chosen collocation points.

The coefficients $v_0^i$ are obtained using

$$v(\xi,0) = v_{0\,nom} + 0.5\, v_{0\,nom}\, \xi = v_0^1\, \psi^1(\xi) + v_0^2\, \psi^2(\xi) + v_0^3\, \psi^3(\xi) + v_0^4\, \psi^4(\xi) + v_0^5\, \psi^5(\xi) + v_0^6\, \psi^6(\xi) \tag{3.24}$$

For Beta (2, 2) distributed random variables the basis are Jacobi (1, 1) polynomials. With one random variable and for the range $\xi \in [-1,1]$, the normalized Jacobi (1,1) polynomials are:

$$\begin{cases} \psi^1(\xi) = 1/2 \\ \psi^2(\xi) = (3/28)\,(-1 + 2\,\xi) \\ \psi^3(\xi) = (1/106)\,(1 - 5\,\xi + 5\,\xi^2) \\ \psi^4(\xi) = (5/8344)\,(-1 + 9\,\xi - 21\,\xi^2 + 14\,\xi^3) \\ \psi^5(\xi) = (3/92822)\,(1 - 14\,\xi + 56\,\xi^2 - 84\,\xi^3 + 42\,\xi^4) \\ \psi^6(\xi) = (7/4455028)\,(-1 + 20\,\xi - 120\,\xi^2 + 300\,\xi^3 - 330\,\xi^4 + 132\,\xi^5) \end{cases} \tag{3.25}$$

Therefore, the coefficients $v_0^i$ are

$$v_0^1 = \frac{5\,v_{0\,nom}}{2},\ v_0^2 = \frac{7\,v_{0\,nom}}{3},\ v_0^3 = 0,\ v_0^4 = 0,\ v_0^5 = 0,\ v_0^6 = 0 \tag{3.26}$$

The cost function from Equation (3.18) can be written as

$$J(\xi)=\frac{1}{2}\sum_{k=1}^{N}\frac{1}{R_k}\left[z^k-\left(\sum_{i=1}^{S=6}\frac{v_0^i}{2\pi}\sin\left(2\pi\, t_k\right)\,\psi^i(\xi)\right)\right]^2-\log\left(\rho(\xi)\right),\quad \rho(\xi)=\frac{3}{4}\left(1-\xi^2\right) \tag{3.27}$$

Using the fact that only $v_0^1$ and $v_0^2$ are nonzero and replacing $v_0^1$ by $(5/2)\,v_{0\,nom}$ and $v_0^2$ by $(7/3)\,v_{0\,nom}$, it yields

$$\begin{aligned}J(\xi)&=-\log\left(\frac{3}{4}\left(1-\xi^2\right)\right)\\&+\frac{1}{2}\sum_{k=1}^{N}\frac{1}{R_k}\left(z^k-\frac{(5/2)\,v_{0\,nom}}{2\pi}\sin\left(2\pi\, t_k\right)\left(\frac{1}{2}\right)-\frac{(7/3)\,v_{0\,nom}}{2\pi}\sin\left(2\pi\, t_k\right)\;(3/28)\,(-1+2\,\xi)\right)^2\end{aligned} \tag{3.28}$$

which can be simplified as

$$J(\xi)=\frac{1}{2}\sum_{k=1}^{N}\frac{1}{R_k}\left(z^k-\frac{v_{0\,nom}}{2\pi}\sin\left(2\pi\, t_k\right)-\frac{(v_{0\,nom}/4)}{2\pi}\sin\left(2\pi\, t_k\right)\;(2\,\xi)\right)^2-\log\left(\frac{3}{4}\left(1-\xi^2\right)\right) \tag{3.29}$$

which is also equal to

$$\begin{aligned}J(\xi)=&\frac{1}{2}\sum_{k=1}^{N}\frac{1}{R_k}\left(z^k-\frac{v_{0\,nom}}{2\pi}\sin\left(2\pi\, t_k\right)\right)^2\\&-\sum_{k=1}^{N}\frac{1}{R_k}\left(z^k-\frac{v_{0\,nom}}{2\pi}\sin\left(2\pi\, t_k\right)\right)\frac{(v_{0\,nom}/4)}{2\pi}\sin\left(2\pi\, t_k\right)\;2\xi\\&+\frac{1}{2}\sum_{k=1}^{N}\frac{1}{R_k}\left(\frac{(v_{0\,nom}/4)}{2\pi}\sin\left(2\pi\, t_k\right)\right)^2(2\xi)^2-\log\left(\frac{3}{4}\left(1-\xi^2\right)\right)\end{aligned} \tag{3.30}$$

The closed form solution of the value minimizing the total cost function is a long expression that is not written here. The mismatch part of the cost function is

$$\begin{aligned}J_{mismatch}(\xi)=&\frac{1}{2}\sum_{k=1}^{N}\frac{1}{R_k}\left(z^k-\frac{v_0}{2\pi}\sin\left(2\pi\, t_k\right)\right)^2\\&-\sum_{k=1}^{N}\frac{1}{R_k}\left(z^k-\frac{v_0}{2\pi}\sin\left(2\pi\, t_k\right)\right)^2\frac{v_0^2}{2\pi}\sin\left(2\pi\, t_k\right)\;2\xi\\&+\frac{1}{2}\sum_{k=1}^{N}\frac{1}{R_k}\left(\frac{(v_0/4)}{2\pi}\sin\left(2\pi\, t_k\right)\right)^2(2\xi)^2\end{aligned} \tag{3.31}$$

The value $\hat{\xi}_{mismatch} = \arg\min J_{mismatch}$ minimizing mismatch part the cost function

$$\hat{\xi}_{mismatch} = \frac{\sum_{k=1}^{N} \frac{1}{R_k}\left(z^k - \frac{v_0}{2\pi}\sin(2\pi t_k)\right)^2 \frac{v_0^2}{2\pi}\sin(2\pi t_k)}{2\sum_{k=1}^{N} \frac{1}{R_k}\left(\frac{(v_0/4)}{2\pi}\sin(2\pi t_k)\right)^2} \tag{3.32}$$

If $x(t)$ is measured every 0.5 s from $t = 0.5$ to $t = 1.5$, then $x(t_k, \xi) = 0$ for any value of $\xi$ and $z_k = \eta_k$

$$J_{mismatch}(\xi) = \frac{1}{2}\sum_{k=1}^{N} \frac{(\eta_k)^2}{R_k} \tag{3.33}$$

which is the formula that was already obtained in Equation (3.19)

In this case, the denominator of Equation (3.32) is not defined and $\hat{\xi}_{mismatch}$ is not defined, because the mismatch part does not depend on $\xi$ and yields an estimation where all possible values of $v_0(\xi) = v_0(1 + 0.5\xi)$ are equally likely. Therefore, the value $\hat{\xi} = \arg\min J_{total}$ minimizing the total cost function is also the value minimizing the apriori part of the cost function, i.e., $\hat{\xi} = 0$.

### 3.2.2. Possible Impact of Undersampling

Increasing the number of measurements generally yields a better estimation, and as a general rule, sampling above the Nyquist frequency rate should always be done when possible. This section studies the possible impact of undersampling for two reasons. Measurements might not be available at a rate above the Nyquist frequency rate when this frequency is very high, for instance. It will also be shown that in some cases, it is possible to know that the estimation is already quite accurate when using only a very few measurements points instead of all of them. This can be useful when computational time is an issue and an answer is needed quickly, which does not prevent one from continuing to process the extra information later on if needed, knowing that the extra measurements will generally yield more precision.

The mismatch part of the cost function is driven by the observational errors. The summed contribution of errors makes $J_{mismatch}$ a random variable with a $\chi^2$ distribution with *n* degrees of freedom. For a relatively large number of measurements this distribution behaves like a normal one with mean *n* and variance *n*. The mismatch part does not depend on $\xi$ and yields an estimation where all possible values of $v_0$ are equally likely. This is illustrated in Figure 3.4 where the mismatch part of the cost function is constant. The mismatch part does not depend on the noise level in this case since $R_k^{-1}$ is inversely proportional to $(\eta_k)^T(\eta_k)$. In Figure 3.4, as well as in consequent figures, we identify with the "o" sign the points where measurements were available (i.e., the points for which we collected measurements).

In this case the estimation relies entirely on the apriori part of the cost function, i.e. $-\log(\rho(\xi))$. The estimate coincides with the best initial guess, i.e., $\hat{\xi} = 0$. This is really the worst-case scenario: the frequency of sampling the output is below the Nyquist frequency rate, and the sampling points are exactly those time moments when the displacement is zero and the observations contain no information.

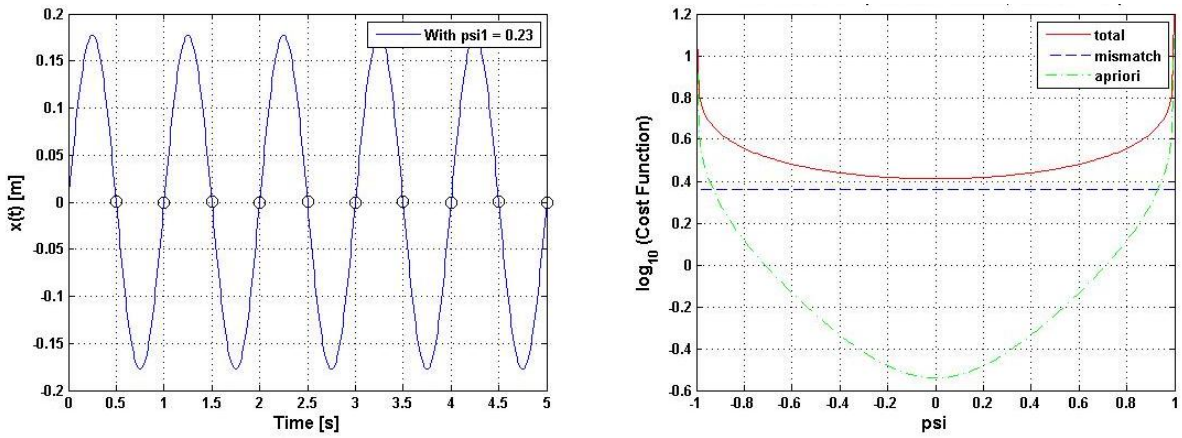


(a) (b) Estimate = 0

Figure 3.4: Bayesian Estimation with 10 Time Points: (a) Displacement when no Noise Added; (b) Estimation with Noise = 1%

If we measure $x(t)$ at any other additional time point then the Bayesian approach yields an accurate estimation result (for any reasonable amount of measurement noise). We can interpret this fact as follows. If the output sampling is not done at least at the Nyquist frequency, one cannot guarantee that all the relevant information in the output signal is captured, i.e. one cannot guarantee that the mismatch part of the cost function will bring extra information. We still have a PDF of the possible values of the uncertain parameter, but in the worst case scenario, it will be no better than the apriori PDF.

In most practical situations, however, it is very likely that the Bayesian approach will provide an accurate estimate even when the output is sampled below the Nyquist frequency. In the example above a single measurement point is sufficient, provided that the measurement time is not one for which the displacement is zero. This is where the Parameter Estimation and Signal Reconstruction differ. In the above setting of parameter estimation one samples outputs of the system. If the outputs were arbitrary signals then their full reconstruction would require a sufficient sampling frequency. But the outputs are constrained by the input and by the system dynamics, and only a small set of all the possible reconstructed signals are consistent with both the known input and with the equations of motion. The reconstruction of signals in this small family requires less information than the reconstruction of arbitrary signals. In our example all possible system outputs form a one-parameter family of signals (frequency of 1 Hz, phase equal to zero, and variable amplitude). Consequently a single measurement of the output is almost always sufficient to estimate the single uncertain parameter.

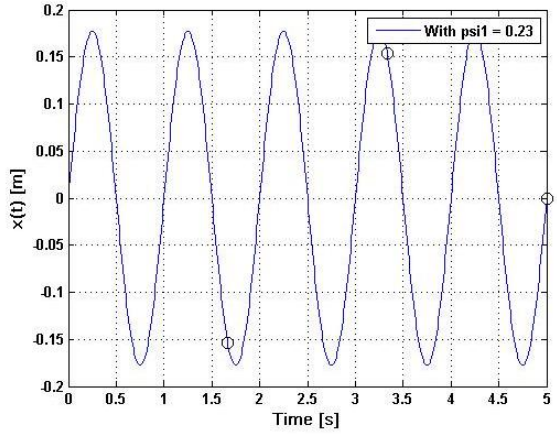


(a)

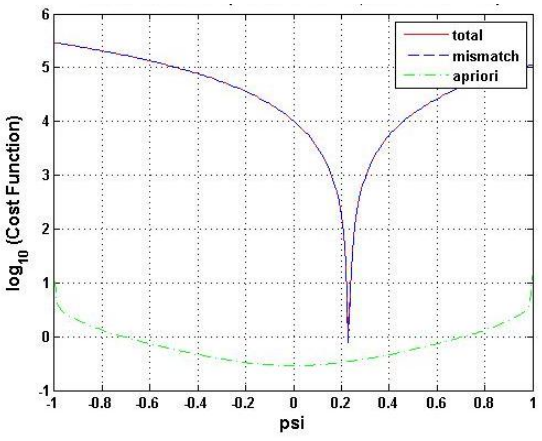


(b) Estimate = 0.23

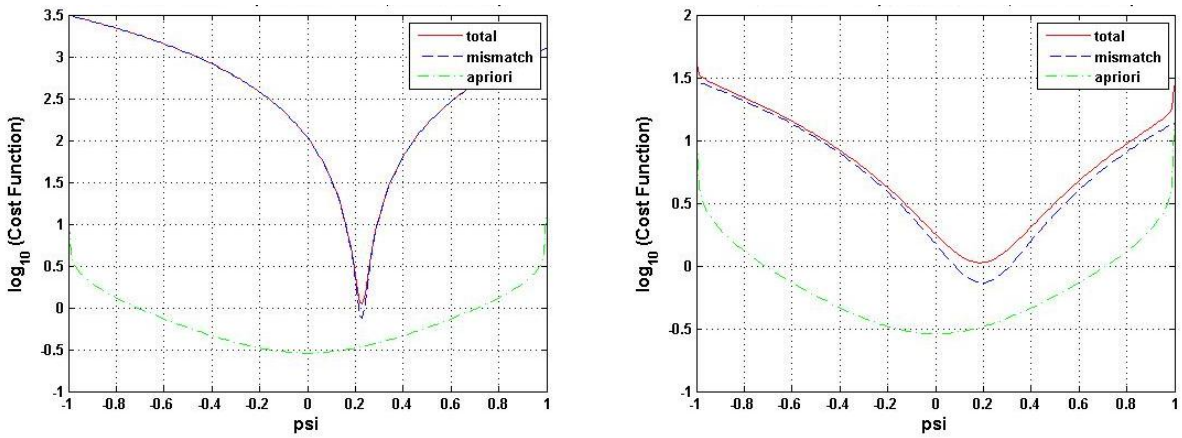


(c) Estimate = 0.23 (d) Estimate = 0.19

Figure 3.5: Bayesian Estimation with 3 Time Points: (a) Displacement when no Noise Added; (b) Estimation with Noise = 0.01%; (c) Estimation with Noise = 1%; (d) Estimation with Noise = 10%

The practical question is now how to decide whether the sampling of the output is sufficient. The answer is given by the shape of the Bayesian cost function which indicates whether there is enough information to obtain a good estimate or not. The second derivative of the cost function at the minimum approximates the inverse of the covariance of the uncertainty in the estimate. Loosely speaking, the sharper the minimum of the cost function the more trustworthy the estimate is; and the wider the minimum the larger the estimation error can be.

The role of the shape of the cost function is illustrated in Figure 3.5, in which only three measurements points for $t > 0$ are used. Different levels of measurement errors lead to different shapes of the cost function, and to different estimation accuracies. For noise levels of 0.01% and 0.1% the total cost function is almost equal to its mismatch part for all values of $\xi$, it has a sharp minimum, and the Bayesian approach yields an accurate estimate. For very noisy measurements (10%) the relative weight of the information coming from measurements is smaller, and the relative weight of the apriori information is higher. Consequently the apriori part of the cost function is more significant and the minimum of the total cost function is wider. In this scenario the output sampling is done below the Nyquist frequency, but we know that the estimates are accurate for noise levels of 0.01% and 1% because the cost functions have clear minima.

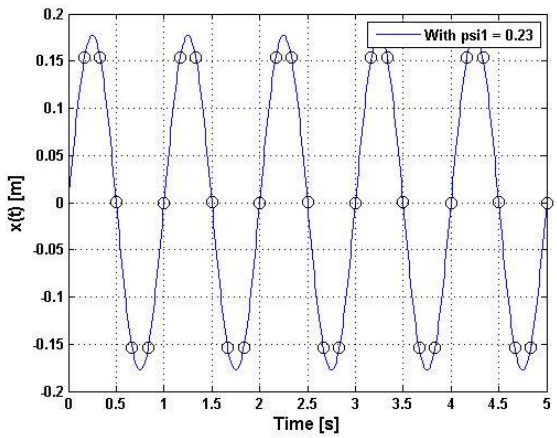


(a)

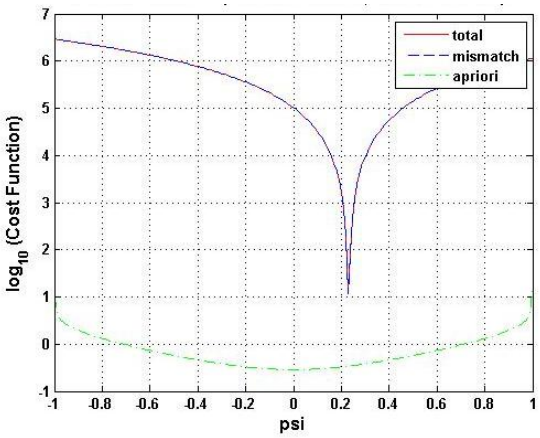


(b) Estimate = 0.23

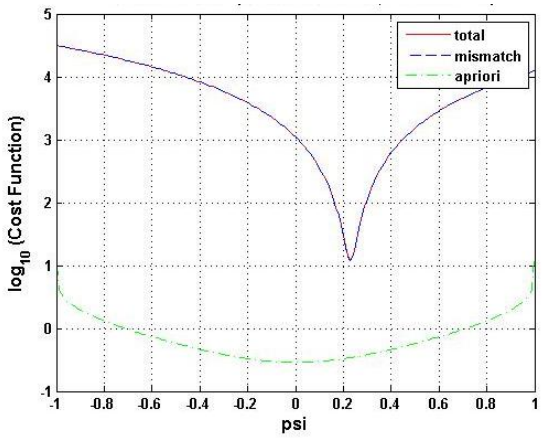


(c) Estimate = 0.23

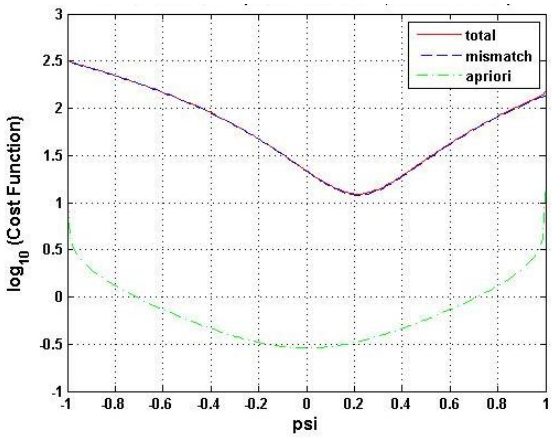


(d) Estimate = 0.22

Figure 3.6: Bayesian Estimation with 30 Time Points: (a) Displacement when no Noise added; (b) Estimation with Noise = 0.01%; (c) Estimation with Noise = 1%; (d) Estimation with Noise = 10%

One very accurate output sample would be enough for a perfect estimation. Taking more sample points leads to a better estimation for noisy measurements because the effect of the noise averages out as we take more samples. Figure 3.6 illustrates the cost function when 30 measurements are used. The relative weight of the mismatch part increases and we get a better estimation when the noise is 10%.

When the extra samples do not bring additional information to the estimation process the cost function changes as shown in Figure 3.7. The net result of the additional measurements is to add a constant to the mismatch part (which corresponds to the effect of measurement noise). The shape of the cost function does not change, in particular the minimum is not more pronounced, and the quality of the estimate is not improved.

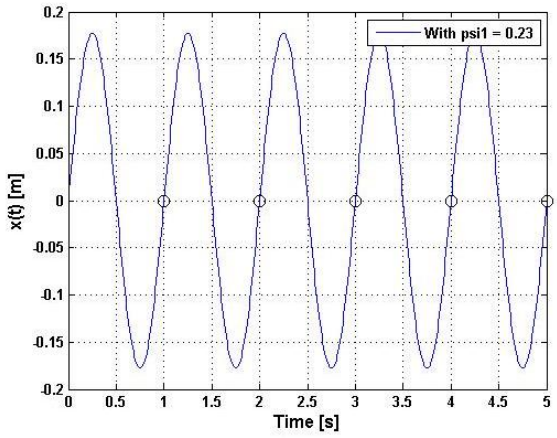


(a)

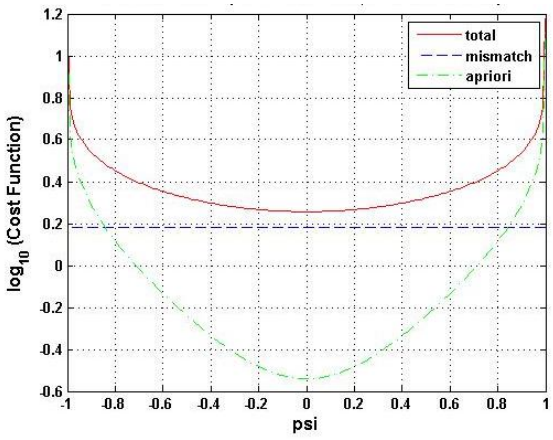


(b) Estimate = 0

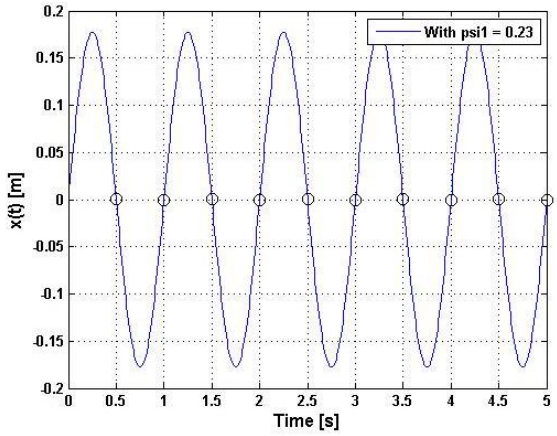


(c)

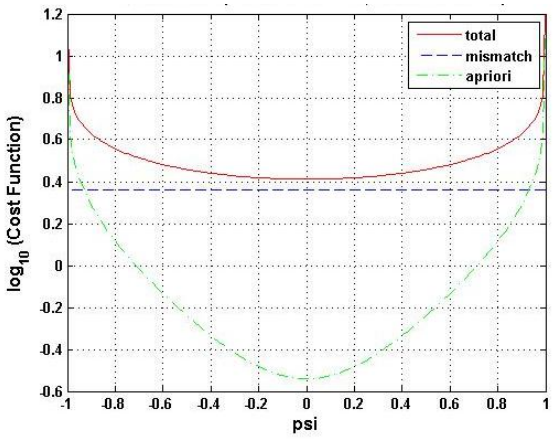


(d) Estimate = 0

Figure 3.7: Effect of Adding Sample Points Containing no Useful Information: (a) Displacement when no Noise Added with 5 Time Points; (b) Estimation with 5 Time Points and Noise = 0.01%; (c) Displacement when no Noise Added with 10 Time Points; (d) Estimation with 10 Time Points and Noise = 0.01%

Next we consider the situation where both $x(t)$ and $v(t)$ are measured at times $t_k > 0$. The observation operator is

$$H = \begin{bmatrix} 1 & 0 & 0 \\ 0 & 1 & 0 \end{bmatrix} \tag{3.34}$$

and the measured values are

$$z_k = H\, y(\xi, t_k) + \eta_k = \begin{bmatrix} x(\xi, t_k) \\ v(\xi, t_k) \end{bmatrix} + \begin{bmatrix} \eta_k^x \\ \eta_k^v \end{bmatrix} \tag{3.35}$$

The measurement noise is assumed Gaussian with zero mean and covariance matrix

$$R_k = \begin{bmatrix} \max\left\{10^{-12}, \left(0.01\ x(t_k) + 0.001\ \max_t\left(x(t)\right)\right)^2\right\} & 0 \\ 0 & \max\left\{10^{-12}, \left(0.01\ v(t_k) + 0.001\ \max_t\left(v(t)\right)\right)^2\right\} \end{bmatrix} \tag{3.36}$$

The inverse $R_k^{-1}$ can always be computed.

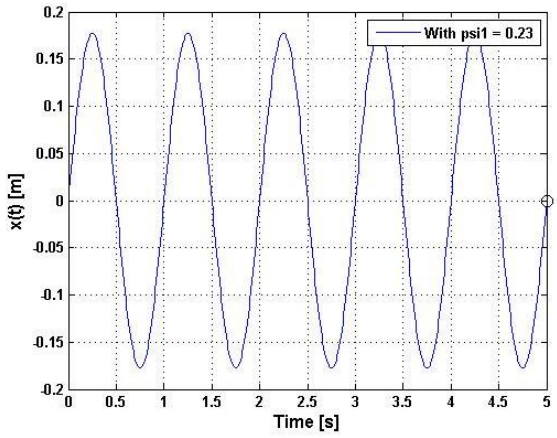


(a)

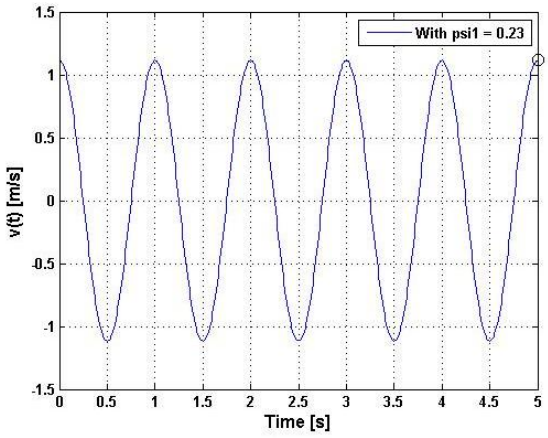


(b)

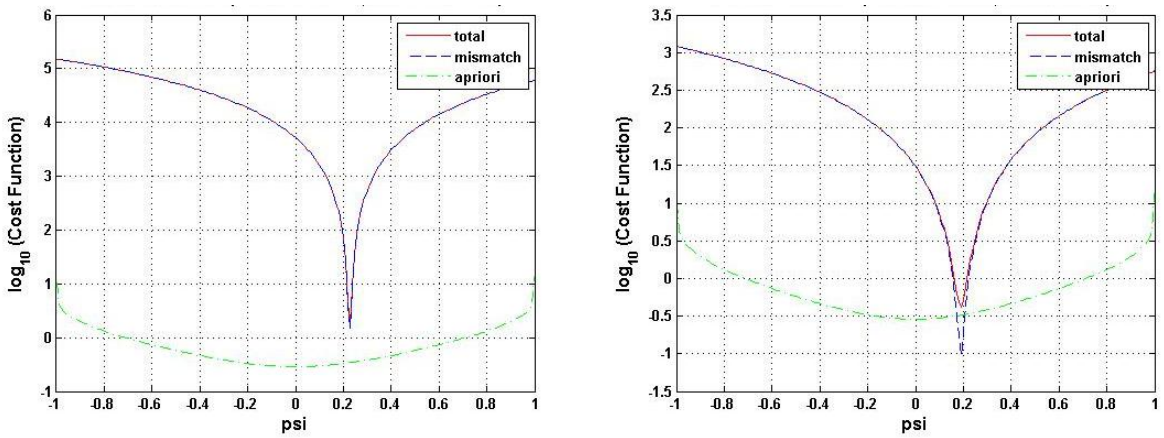


(c) Estimate = 0.23 (d) Estimate = 0.19

Figure 3.8: Bayesian Estimation with 1 Time Point when Velocity Measurements are Available: (a) Displacement when no Noise Added; (b) Velocity when no Noise Added; (c) Estimation with Noise = 0.01%; (d) Estimation with Noise = 1%

One data point at any $t > 0$ is sufficient to estimate our unknown parameter $v_0$ for low noise levels, as shown in Figure 3.8. In the general case, however, measurements of the full state vector do not guarantee that they contain useful information when the sampling rate is below the Nyquist frequency.

### 3.2.3. Mass-Spring System with Sinusoidal Forcing Function

This section applies the parameter estimation Bayesian approach developed in this study to the simple mass-spring system with sinusoidal forcing function shown in Figure 3.9.

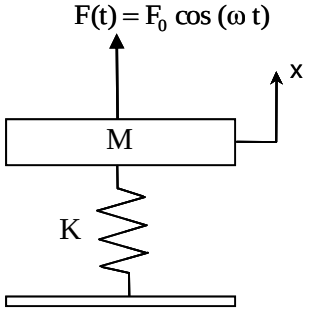


Figure 3.9: Mass –Spring System with Sinusoidal Forcing Function

The parameters $K$ (the stiffness of the spring), $M$ (the value of the mass) are known. The system is initially at equilibrium, i.e., it has zero initial displacement $x_0 = 0$ and velocity $v_0 = 0$. The problem is to estimate the uncertain amplitude of the forcing function $F_0$.

We assume the following apriori information. $F_0$ has a Beta (2, 2) distribution in the range $[500\,N,\ 1500\,N]$ with the most likely value $F_0 = 1{,}000\ \mathrm{N}$. With $\xi \in [-1, 1]$ a Beta (2, 2) distributed variable the apriori distribution of $F_0$ is

$$F_0 = 1{,}000\ \mathrm{N} + \xi \cdot 500\ \mathrm{N} \tag{3.37}$$

The reference value of the force amplitude is $F_0^{\mathrm{ref}} = 1{,}115\ \mathrm{N}$, or $\xi^{\mathrm{ref}} = 0.23$. This reference value is used to generate artificial observations and is not available to the estimation procedure. The numerical values of the other parameters are as follows: $K = 200 \times (1.5 \times 2\pi)^2 \approx 17{,}765\ \mathrm{N/m}$, $\mathrm{M} = 200\,\mathrm{kg}$, $x_0 = 0$, $v_0 = 0$, and $\omega = \pi\ \mathrm{rad/s} = 0.5\ \mathrm{Hz}$. Note that $\omega_n = \sqrt{K/M} = 1.5 \times 2\pi\ \mathrm{rad/s}$, i.e. $\omega_n = 1.5\ \mathrm{Hz}$.

The equation of motion of the system is:

$$\mathrm{M}\ \ddot{x}(t) + K\ x(t) = F_0\ \cos(\omega t) \tag{3.38}$$

The solution is sought in the time interval from $t$ = 0 to $t$ =5. Since $x_0 = 0$ and $v_0 = 0$, the analytical solution of this equation of motion is [101]:

$$x(t) = \frac{2\,(F_0 / M)}{\omega_n{}^2 - \omega^2}\ \sin\left(\frac{\omega_n - \omega}{2} t\right)\ \sin\left(\frac{\omega_n + \omega}{2}\ t\right) \tag{3.39}$$

With our numerical values, the displacement of the mass can be written as:

$$x(t) \approx 1.2665 \times 10^{-4}\ F_0\ \ \sin(\pi t)\ \sin(2\pi t) \tag{3.40}$$

It can be seen that the amplitude of $x(t)$ and the amplitude of $v(t)$ are both proportional to the uncertain parameter $F_0$, as shown in Figure 3.10. Therefore, the estimation of $F_0$ can be in principle based on a single measurement of the output.

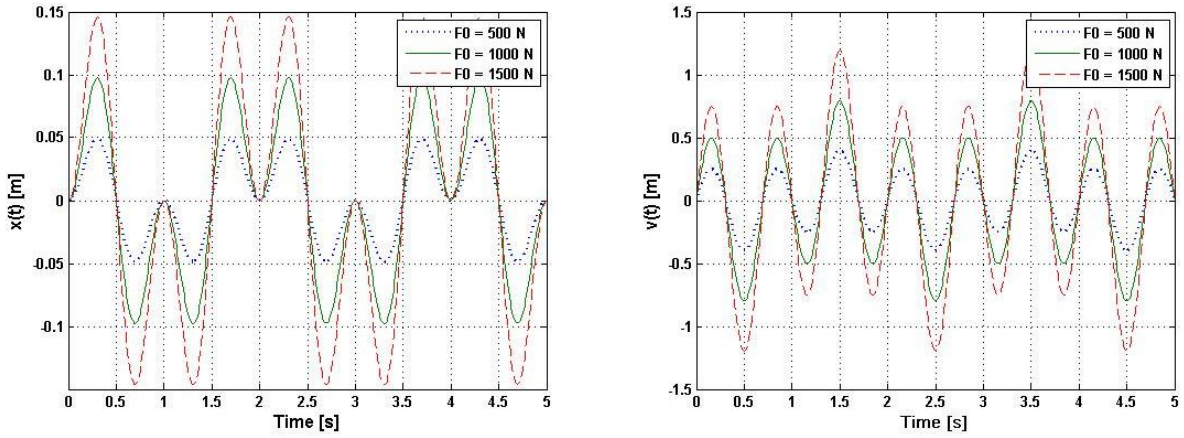


(a) (b)

Figure 3.10: Displacement and Velocities of the Mass – Spring System with Sinusoidal Forcing Function: (a) Displacement; (b) Velocities

Figure 3.11 illustrates the effect of measurements of both $x(t)$ and $v(t)$ at five time points. This sampling provides no information on the uncertain parameter, and in this worst-case scenario the estimate is based solely on apriori information. A sampling of the output below the Nyquist frequency does not guarantee that we get sufficient information from the output signal about the uncertain parameter. The mismatch part does not depend on the noise level in this case since $R_k^{-1}$ is inversely proportional to $(\eta_k)^T(\eta_k)$, as shown in Equation (3.19).

However, we can see in Figure 3.12 that three time measurements yield an accurate estimation for a low noise level, even though the sampling is well below the Nyquist frequency. Once again, the shape of the cost function indicates that for low noise levels we have enough information to accurately estimate our uncertain parameter. While there are many signals with a maximum frequency of 1.5 Hz which fit the observations at the chosen three measurement times, only one of them is consistent with the input signal and with equation of motion.

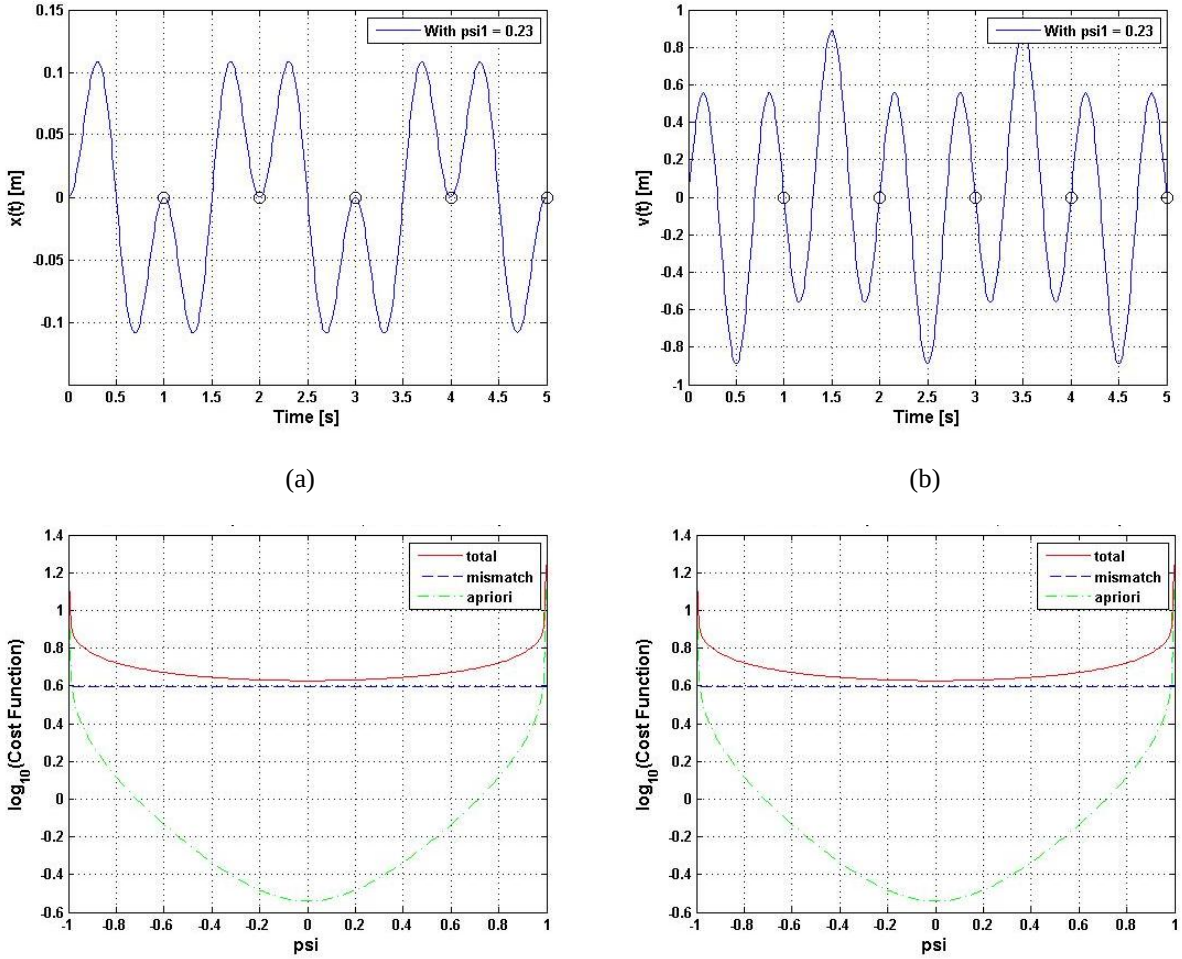


(a) (b)

(c) Estimate = 0 (d) Estimate = 0.23

Figure 3.11: Bayesian Estimation with 5 Time Points when Velocity Measurements are Available: (a) Displacement when no Noise Added; (b) Velocity when no Noise Added; (c) Estimation with Noise = 0.01%; (d) Estimation with Noise = 10%

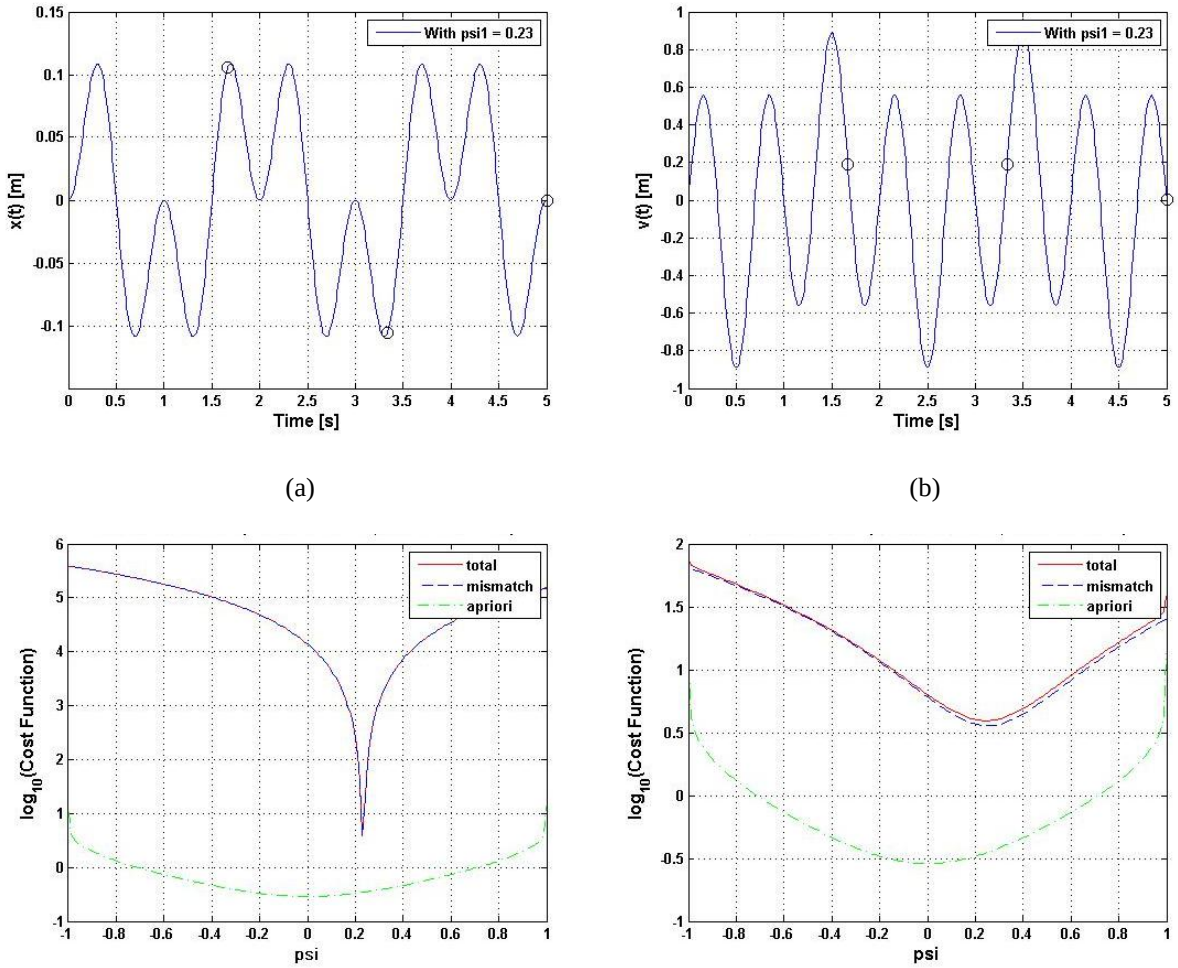


(a) (b)

(c) Estimate = 0.23 (d) Estimate = 0.25

Figure 3.12: Bayesian Estimation with 3 Time Points when Velocity Measurements are Available: (a) Displacement when no Noise Added; (b) Velocity when no Noise Added; (c) Estimation with Noise = 0.01%; (d) Estimation with Noise = 10%

### 3.2.4. Regularization Techniques Applied to a Mass-Spring System with Uncertain Stiffness and Uncertain Mass

This example addresses the issue of non-identifiability. The Bayesian approach is applied to the simple mass-spring system shown in Figure 3.1. The difference between the example in this section and the one from Section 3.1 is that the uncertain parameters are different: they are the

stiffness of the spring ($K$) and the value of the mass ($M$). Our apriori information about the uncertain parameters is expressed in terms of probability densities as follows. The mass has a normal distribution with mean $M_0 = 200\,\text{kg}$ and a standard deviation $\sigma_M = 6.667\,\text{kg}$. The stiffness has also a normal distribution with mean $K_0 = 200\times(2\pi)^2\ \text{N/m} \approx 7{,}895.68\ \text{N/m}$ and standard deviation $\sigma_K = 1{,}052.8\ \text{N/m}$. We represent the uncertain parameters as functions of a random vector of two independent normal random variables $\xi = (\xi_1, \xi_2)$ as follows

$$M(\xi) = M_0 + \sigma_M \cdot \xi_1, \quad K(\xi) = K_0 + \sigma_K \cdot \xi_2, \quad \xi_1, \xi_2 \in \mathrm{N}(0,1). \tag{3.41}$$

We consider the "true" values of the parameters to be $M^{\text{ref}} = 201.533\ \text{kg}$ and $K^{\text{ref}} = 7495.62\ \text{N/m}$, which correspond to the reference values of the random variables $\xi^{\text{ref}} = (\xi_1^{\text{ref}}, \xi_2^{\text{ref}}) = (0.23, -0.38)$. These values are not available to the estimation process, but are used in a reference simulation to generate synthetic observations.

We measure the values of the oscillation frequency $\omega_{\text{obs}}$ (along the reference solution) and use it to derive information about $K$ and $M$. The measurement errors are assumed to have a normal distribution with zero mean (unbiased) and a standard deviation equal to $\sigma_{meas} = 0.01\sqrt{K_0/M_0} = 0.3938\,\text{rad/s}$.

This example allows an analytical solution to the Bayesian approach and provides insight into the role of the mismatch and the a priori parts of the cost function in the estimation. The position of the mass is given by:

$$x(t) = \sqrt{\frac{v_0^{\,2} + (x_0\,\omega_n)^2}{\omega_n^{\,2}}}\,\sin\left(\omega_n\,t + \tan^{-1}\left(\frac{x_0\,\omega_n}{v_0}\right)\right), \tag{3.42}$$

and clearly it depends only on $\omega_n = \sqrt{K^{\text{ref}}/M^{\text{ref}}}$.

The Bayesian cost function is defined in this case as:

$$\begin{aligned} J(\xi) &= \frac{1}{2}\,\frac{(M(\xi) - M_0)^2}{\sigma_M^{\,2}} + \frac{1}{2}\,\frac{(K(\xi) - K_0)^2}{\sigma_K^{\,2}} + \frac{1}{2}\,\frac{\left(\sqrt{K(\xi)/M(\xi)} - \omega_{\text{obs}}\right)^2}{\sigma_{meas}^{\,2}} \\ &= \frac{1}{2}\xi_1^2 + \frac{1}{2}\xi_2^2 + \frac{1}{2}\,\frac{\left(\sqrt{(K_0 + \sigma_K\,\xi_2)/(M_0 + \sigma_M\,\xi_1)} - \omega_{\text{obs}}\right)^2}{\sigma_{meas}^{\,2}} \end{aligned} \tag{3.43}$$

The maximum likelihood value of the parameters is the argument that minimizes this cost function, $\hat{\xi} = \arg\min J(\xi)$. The contour plots shown in Figure 3.13 represent the mismatch part of the cost function, its apriori part, and the total value of the cost function in the space of random variables.

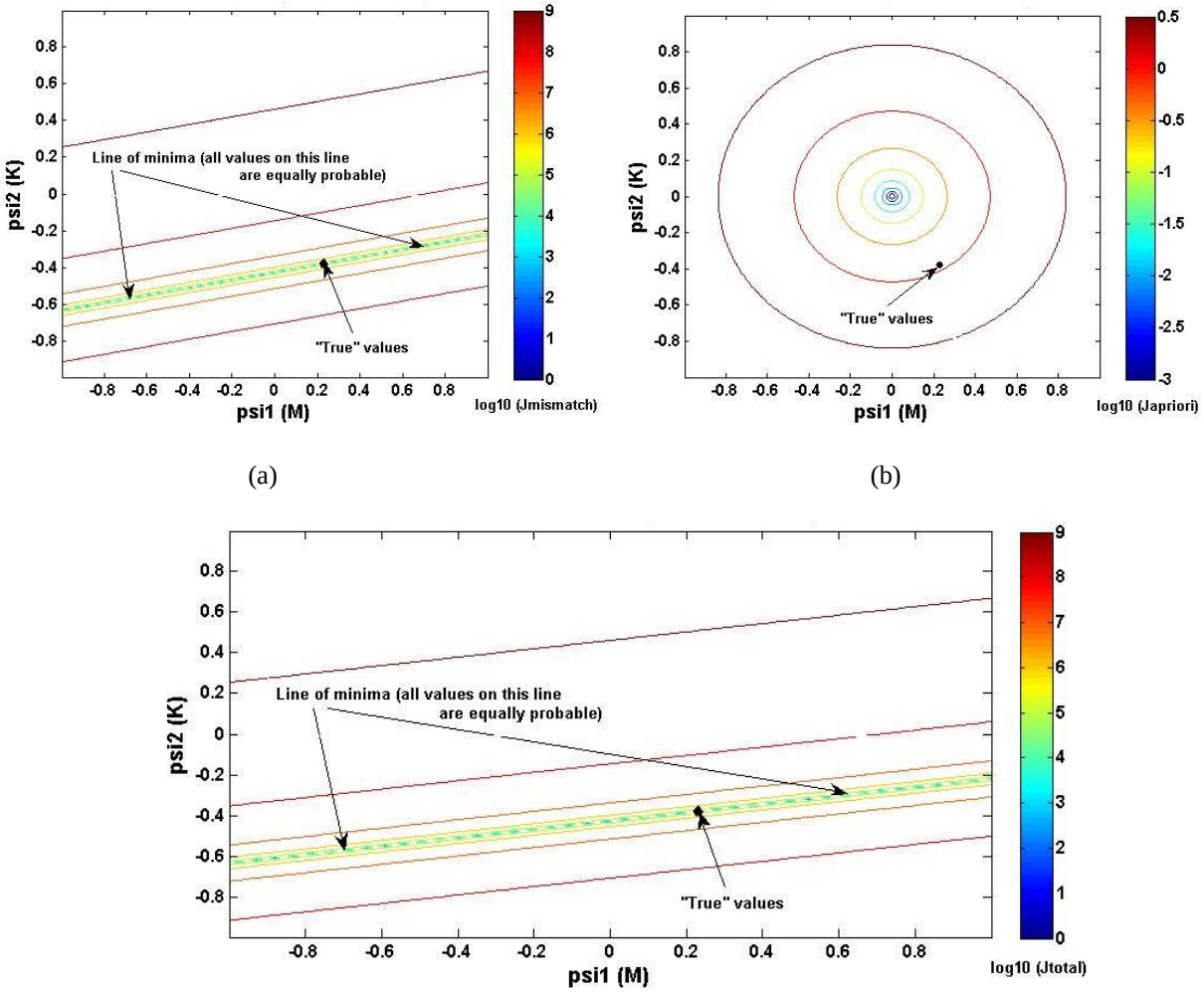


(a) (b)

(c)

Figure 3.13: Contours of the Cost Function: (a) Mismatch Part; (b) Apriori Part; (c) Total Cost Function

The magnitude of the apriori part is relatively small and the total cost function is roughly equal to its mismatch part. As expected, the mismatch part yields a line of possible minima, because

the measured ratio $\omega_n = \sqrt{K/M}$ does not contain information about the individual values of $K$ and $M$. The point $\xi^{\text{ref}}$ is plotted in Figure 3.13 and it lies on the line of minima. The *Bayesian interpretation is the following: all the pairs* $(K,M)$ *along the line are equally likely to produce the value of the measured oscillation frequency. We say that the (individual values of the) parameters K and M are non-identifiable.*

When multiple combinations of uncertain parameter values result in the same observed behavior of the system (same measurements) a regularization approach [22] can be used in estimation. In order to find the most likely parameter values one increases the relative importance of the apriori knowledge of the system. This is done by multiplying the apriori part by a "regularization coefficient" large enough so that the new total cost function has a clear minimum value along the possible values.

$$J^{\text{regularized}}(\xi,\alpha) = \alpha^2 \cdot \left( \frac{1}{2} \frac{(M(\xi)-M_0)^2}{\sigma_M{}^2} + \frac{1}{2} \frac{(K(\xi)-K_0)^2}{\sigma_K{}^2} \right) + \frac{1}{2} \frac{\left(\sqrt{K(\xi)/M(\xi)} - \omega_{\text{obs}}\right)^2}{\sigma_{meas}{}^2} \quad (3.44)$$

The net effect of regularization in this example is to reduce the standard deviations in the apriori distributions (to $\sigma_M/\alpha$ and $\sigma_K/\alpha$ respectively), therefore to increase the trust in the apriori information. The contour plots of the regularized cost functions are shown in Figure 3.14 for different regularization coefficients.

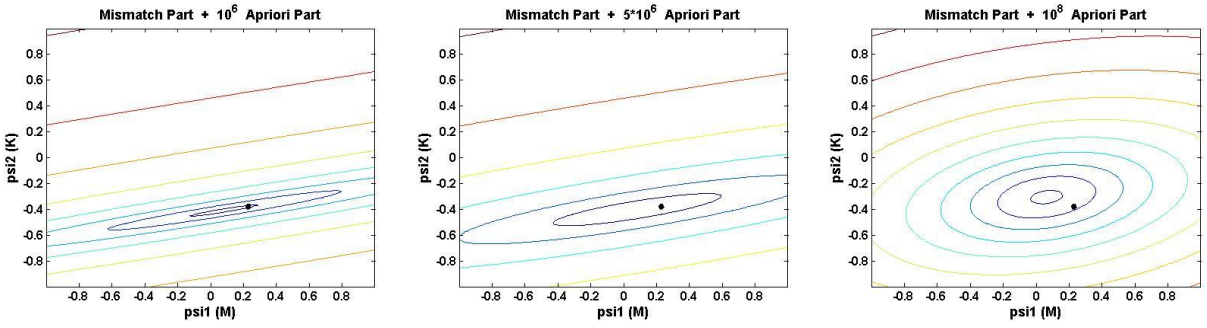


Figure 3.14: Contour Plots of the Cost Function after Regularization for Different Coefficients

The cost function looks like its mismatch part when the regularization coefficient is very low and looks like its apriori part when the regularization coefficient is very high. As the

regularization coefficient gets larger, the line of possible minima becomes an ellipse, and starts moving away from the location of the original line of minima and toward (0, 0), the apriori most likely value. When the line becomes an ellipse with a well defined center, the regularization coefficient is large enough; it should not be further increased as this leads to an increase of the bias in the estimate. In our example $\alpha^2 = 5\times10^6$ seems to be a good value for the regularization coefficient and it results in the estimated values $(\xi_1, \xi_2) = (0.09, -0.40)$. *The choice of the regularization coefficient is problem-dependent and requires a careful analysis of the resulting estimates. Regularization leads to biased estimates, as stronger assumptions are being artificially imposed.*

### 3.2.5. Non-observability

We now discuss the effect of observability on parameter identifiability. Consider a linear system whose evolution depends linearly on a parameter $\theta$. We add a trivial equation for the evolution of the parameter and represent the system as follows:

$$\begin{cases} \dot{x}_1 = -2\,x_1 + x_2 + \theta + u_1 \\ \dot{x}_2 = x_1 - 2\,x_2 + \theta + u_2 \\ \dot{\theta} = 0 \end{cases} \quad \text{with the observed variable} \quad y = x_1 - x_2 . \tag{3.45}$$

The system is asymptotically stable in $x_1, x_2$, and neutrally stable in $\theta$. The two states $x_1, x_2$ can be excited independently. Our goal is to estimate the uncertain parameter $\theta$ based on measurements of the output $y(t)$.

The observability matrix of the system is $\begin{bmatrix} 1 & -1 & 0 \\ -3 & 3 & 0 \\ 9 & -9 & 0 \end{bmatrix}$, and has rank 1 and zeros in the $\theta$ column.

This system is non-observable and this leads to the non-identifiability of $\theta$. Specifically, it can be seen that the output rate of change $\dot{y} = \dot{x}_1 - \dot{x}_2 = -3\,(x_1 - x_2) + u_1 - u_2$ does not depend on $\theta$, and therefore the information provided by the measurements cannot distinguish between different values of the parameter. The effect on the cost function is that the mismatch part is

constant since $y(t,\xi) - y_{\text{ref}}(t)$ does not depend on $\xi$. As far as the measurements are concerned all real values of $\theta$ are equally likely! Therefore, the result of the Bayesian estimation is based entirely on the apriori knowledge, and equals the most likely apriori value of the parameter. *In this case the non-identifiability problem can be addressed by including measurements of additional states in the estimation procedure.*

### 3.2.6. Choice of Excitation

Non-identifiability can also be the result of the choice of the inputs $u_1$ and $u_2$. The input signal may not be "rich enough" to excite all the relevant dynamics and the output values are similar for different possible parameter values.

As an example consider the two degree of freedom roll plane model in Figure 3.15. Let $L$ be the length of the bar of mass $M$ and inertia $I$. The two springs have equal stiffnesses $K_1 = K_2 = K$. We want to estimate the values of the uncertain parameters $M$ and $I$ from measurements of the left and right displacements $x_1(t)$ and $x_2(t)$.

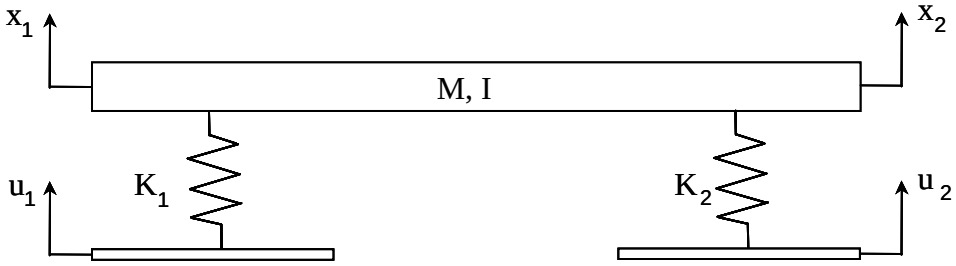


Figure 3.15: Two Degree of Freedom Roll Plane Model

For small angles (i.e., for $(\ddot{x}_2 - \ddot{x}_1)/L$ small) the equations of motion are:

$$\begin{cases} M\left(\dfrac{\ddot{x}_1 + \ddot{x}_2}{2}\right) + K_1\,(x_1 - u_1) + K_2\,(x_2 - u_2) = 0 \\ I\left(\dfrac{\ddot{x}_2 - \ddot{x}_1}{L}\right) + K_1\,(x_1 - u_1) - K_2\,(x_2 - u_2) = 0 \end{cases} \tag{3.46}$$

For the same excitations on the left and on the right, i.e. $u_1(t) = u_2(t) = u(t)$ the equations of motion become

$$\begin{cases} \frac{M}{2}\ (\ddot{x}_1 + \ddot{x}_2) + K\ (x_1 + x_2 - 2\,u) = 0 \\ \frac{I}{L}\ (\ddot{x}_2 - \ddot{x}_1) + K\ (x_1 - x_2) = 0 \end{cases} \tag{3.47}$$

If $u_1(t) = u_2(t) = u(t)$, $x_1(0) = x_2(0)$, and $\dot{x}_1(0) = \dot{x}_2(0)$, then $x_1(t) = x_2(t)$ for all future times. The second equation of motion is trivially satisfied and the system output does not depend on $I$ (the system has the same evolution for any value of $I$). This means that the parameter $I$ is non-identifiable. An excitation that is different on the left and on the right would easily lead to outputs that depend on the inertia, and would allow the estimation of this parameter. *In summary an input signal that is not rich enough can lead to non –identifiability. In this case the problem can be addressed by changing the kind of excitations applied to the system.*

### 3.2.7. Discussion of the Bayesian Approach

The quality of the maximum likelihood estimate is related to the shape of the Bayesian cost function, with a sharp minimum indicating an accurate estimate. Inaccurate estimates can be caused by different factors, including a sampling rate below the Nyquist frequency, non-identifiability, non-observability, and an excitation signal that is not rich enough.

The parameters are non-identifiable when different parameter values lead to identical system outputs. In this case the Bayesian cost function has an entire region of minima (e.g., a valley), with each parameter value in the region being equally likely. A regularization approach based on increasing the weight of the apriori information can be used to select reasonable estimates.

For identifiable and observable systems accurate estimates can be obtained in most cases even if the output signal is sampled below the Nyquist rate. In the worst case, however, sampling below the Nyquist rate cannot guarantee that sufficient information is extracted from the output. In this worst case the apriori information becomes important and the estimate is biased toward the apriori most likely value.

## 3.3 Application to a More Complex Mechanical System

### 3.3.1. Roll Plane Modeling of a Vehicle

The model used to apply the theory presented in this chapter is based on the four degree of freedom roll plane model of a vehicle used in [102] with the addition of a mass on the roll bar, as shown in Figure 3.16. The difference is that the suspension dampers and the suspension springs used in this study are nonlinear and that a mass is added on the roll bar, which represents the driver, the passenger, and other objects in the vehicle. The added mass $M$ and its position $d_{CG}$ away from the left end of the roll bar are assumed to be uncertain. It is assumed that there is a passenger, and apriori distribution of the added mass will therefore be centered in the middle of the bar. This added mass will be represented as a point mass for the sake of simplicity. Measuring the position of the C.G. of the added mass physically is not straightforward. However, if a well defined road input can be used and sensors are available, these two parameters can be estimated based on the observed displacements and velocities across the suspensions.

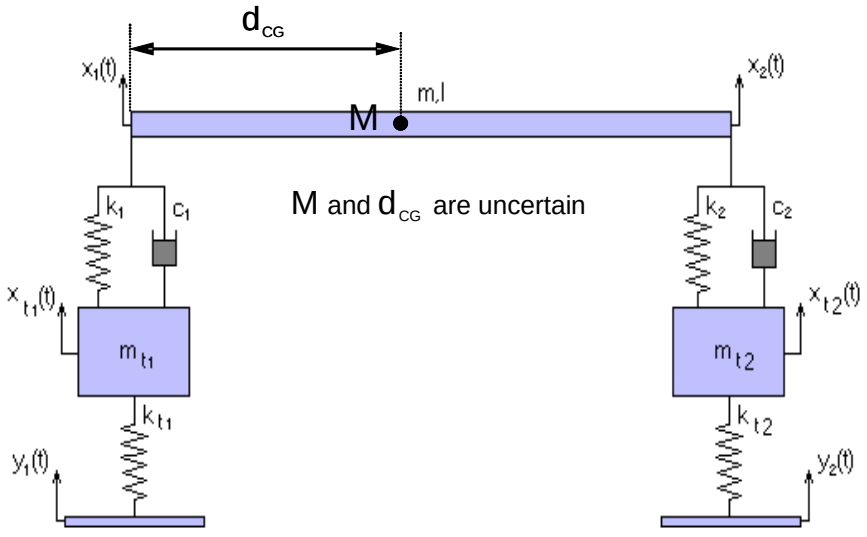


Figure 3.16: Four Degree of Freedom Roll Plane Model (adapted from the model used in [102])

The body of the vehicle is represented as a bar of mass $m$ (sprung mass) and length $l$ that has a moment of inertia $I$. The unsprung masses, i.e., the masses of each tire/axle combination, are represented by $m_{t1}$ and $m_{t2}$. A mass is added on the roll bar, which represents the driver and other objects in the vehicle. That added mass is represented as a point mass of value $M$ situated at a distance $d_{CG}$ from the left extremity of the roll bar.

The motion variables $x_1$ and $x_2$ correspond to the vertical position of each side of the vehicle body, while the motion variables $x_{t1}$ and $x_{t2}$ correspond to the position of the tires.

The inputs to this system are $y_1$ and $y_2$, which represent the road profile under each wheel.

If *x* is the relative displacement across the suspension spring with a stiffness $k_i$ ($i$ = 1, 2), the force across the suspension spring is given by:

$$F_{K_i}(x) = k_i x + k_{i,3} x^3, \quad i = 1, 2 \tag{3.48}$$

If *v* is the relative velocity across the damper with a damping coefficient $c_i$ ($i$ = 1, 2), the force across the damper is given by:

$$F_{C_i}(v) = c_i (0.2 \tanh(10v)) \tag{3.49}$$

For small angles, i.e. for $\frac{x_2 - x_1}{L}$ small, the equations of motion of the system are

$$\left(\frac{m+M}{2}\right)\left(\ddot{x}_2 + \ddot{x}_1 + (\ddot{x}_2 - \ddot{x}_1)\frac{M}{(m+M)}\left(2(d_{CG}/L) - 1\right)\right) +$$
$$F_{K_1}(x_1 - x_{t1}) + F_{K_2}(x_2 - x_{t2}) + F_{C_1}(\dot{x}_1 - \dot{x}_{t1}) + F_{C_2}(\dot{x}_2 - \dot{x}_{t2}) = 0 \tag{3.50}$$

$$\cos\left(\left(\frac{x_2-x_1}{L}\right)+\left(\frac{x_2-x_1}{L}\right)_{STATIC}\right)\times$$

$$\left[D\left(F_{K_1}\left(x_1-x_{t1}\right)+F_{C_1}\left(\dot{x}_1-\dot{x}_{t1}\right)\right)-\left(L-D\right)\left(F_{K_2}\left(x_2-x_{t2}\right)+F_{C_2}\left(\dot{x}_2-\dot{x}_{t2}\right)\right)+g\left(M\left(D-d_{CG}\right)-m\left(\frac{L}{2}-D\right)\right)\right]$$

$$+\left(I+m\left(\frac{L}{2}-D\right)^2+M\left(D-d_{CG}\right)^2\right)\left(\frac{\ddot{x}_2+\ddot{x}_1}{L}\right)=0 \quad with \quad D=\frac{M\ d_{CG}+m\ (L/2)}{M+m} \tag{3.51}$$

$$m_{t1}\ddot{x}_{t1}+F_{K_1}\left(x_{t1}-x_1\right)+F_{C_1}\left(\dot{x}_{t1}-\dot{x}_1\right)=k_{t1}\left(y_1-x_{t1}\right) \tag{3.52}$$

$$m_{t2}\ddot{x}_{t2}+F_{K2}\left(x_{t2}-x_2\right)+F_{C_2}\left(\dot{x}_{t2}-\dot{x}_2\right)=k_{t2}\left(y_2-x_{t2}\right) \tag{3.53}$$

where $F_{K_1}$, $F_{K_2}$, $F_{C_1}$, and $F_{C_2}$ are defined in equations (3.48) and (3.49).

In these equations, the variables are expressed versus their position at equilibrium (If the added mass *M* is not in the middle, we have static deflections). $\left(\frac{x_2-x_1}{L}\right)_{STATIC}$ is relative to the position of the ground, which is fixed. It has to be estimated numerically because of the nonlinearities in the system.

The parameters used in this study are shown in Table 3.1. They are the parameters used in [102], with the addition of nonlinearities and uncertainties for $M$ and $d_{CG}$. For the parameters shown in Table 3.1, the minimum static angle (i.e., the angle of the roll bar with respect to a fixed reference on the ground) is -1.21 degrees and the maximum static angle is 1.21 degrees, which corresponds to $x_2-x_1=0.032\,\text{m}$. These values are obtained for $(\xi_1,\xi_2)=(1,1)$ and $(\xi_1,\xi_2)=(1,-1)$, i.e., for the maximum possible value of $M$ with the added mass as far as possible from the center of the bar.

The uncertainties of 50% and 25% on the values of $M$ and $d_{CG}$ can be represented as:

$$M=M_{nom}(1+0.50\,\xi_1),\quad \xi_1\in[-1,\ 1] \tag{3.54}$$

$$d_{CG}=d_{CG,nom}(1+0.25\,\xi_2),\quad \xi_2\in[-1,\ 1] \tag{3.55}$$

where $M_{nom}$ and $d_{CG,nom}$ are the nominal values of the added mass and of the distance between the center of gravity of the mass and the left extremity of the roll bar ($M_{nom} = 200$ kg and $d_{CG,nom} = 0.7620$ m) and where $\xi_1$ and $\xi_2$ are stochastic variables with a Beta (2, 2) distribution.

Table 3.1: Vehicle Parameters

| Parameter | Description | Value |
|---|---|---|
| $m$ | Mass of the roll bar | 580 kg |
| $m_{t1}$, $m_{t2}$ | Mass of the tire/axle | 36.26 kg |
| $c_1$, $c_2$ | Damping coefficients | 710.70 N s m$^{-1}$ |
| $k_1$, $k_2$ | Spring constants – linear component | 19,357.2 N m$^{-1}$ |
| $k_{1,3}$, $k_{2,3}$ | Spring constants – cubic component | 100,000 N m$^{-3}$ |
| $l$ | Length of the roll bar | 1.524 m |
| $I$ | Inertia of the roll bar | 63.3316 kg m$^2$ |
| $k_{t1}$, $k_{t2}$ | Tires vertical stiffnesses | 96,319.76 N m$^{-1}$ |
| $M$ | Added mass | 200 kg +/-50%, with Beta (2, 2) distribution |
| $d_{CG}$ | Distance between the C.G. of the mass and the left extremity of the roll bar | 0.7620 m +/-25%, with Beta (2, 2) distribution |

It is assumed that the probability density functions of the values of $M$ and $d_{CG}$ can be represented with Beta (2, 2) distributions, with uncertainties of +/- 50% and +/- 25%,

respectively. A Beta (2, 2) distribution is similar to a Gaussian distribution in the sense that the probability density decreases as the values of the uncertain parameters move away from their nominal values, and it has the advantage of being bounded, which is more realistic. This work could be done with any other distribution. The most significant difference would be observed for the regularization techniques presented later in Section 3.3.6: in that case, the mismatch part of the cost function would not change since it does not depend on the distribution, but the apriori part of the cost function would be different since it depends entirely on the distribution. A Beta (2, 2) is also a judicious choice of bounded support distribution to work with the EKF approach presented in Chapter 4. As mentioned after Equation (4.19), the Kalman filter formula is optimal for the linear Gaussian case. For non-Gaussian uncertainties the Kalman filter formula is sub-optimal, but is still expected to work. The distributions of the uncertainties related to the values of $M$ and $d_{CG}$, defined on the interval $[-1,\ 1]$, are represented in Figure 3.17. They have the following Probability Density Functions (PDFs):

$$w(\xi_i) = \frac{3}{4}\left(1-\xi_i^{\,2}\right), \quad i = 1, 2 \tag{3.56}$$

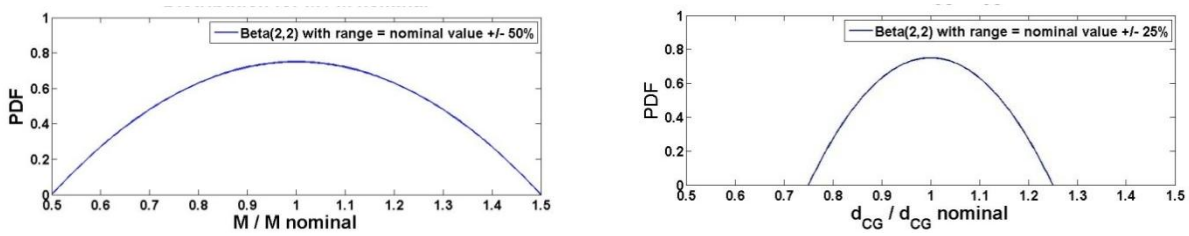


(a) (b)

Figure 3.17: Beta (2, 2) Distribution: (a) for Value of the Mass; (b) for Value of the Position of the C.G. of the Mass

### 3.3.2. Collocation Points

The generalized polynomial chaos theory is explained in [19], in which direct stochastic collocation is proposed as a less expensive alternative to the traditional Galerkin approach. The collocation approach consists of imposing that the equations system holds at a given set of

collocation points. If the polynomial chaos expansions contain 15 terms for instance, then at least 15 collocation points are needed in order to have at least 15 equations for 15 unknown polynomial chaos coefficients. It is desirable to have more collocation points than polynomial coefficients to solve for. In that case a least-squares algorithm is used to solve the system with more equations than unknowns.

Unless otherwise specified, in this study, the polynomial chaos expansions of $M$ and $d_{CG}$ will use 15 terms. All the other variables affected by the uncertainties on $M$ and $d_{CG}$ will be modeled by a polynomial chaos expansion using 15 terms as well. The collocation approach is the one used in this study. It requires at least 15 collocation points to derive the coefficients associated to each of the 15 terms of the different polynomial chaos expansions. Unless otherwise specified, 30 collocation points will be used in this study to derive the coefficients associated to each of the 15 terms of the different polynomial chaos expansions. The collocation points used in this study are obtained using an algorithm based on the Halton algorithm [15], which is similar to the Hammersley algorithm [14]. These collocation points for a uniform distribution were shown in Figure 2.2(a).

One of the advantages of the Hammersley/Halton points used in this study is that when the number of points is increased, the new set of points still contains all the old points. We therefore know that more points should result in a better approximation. The collocation points for a Beta (2, 2) distribution, which is used in this study, were shown in Figure 2.2(b). Let's note that there is no collocation point at the boundary, i.e., no point associated with an uncertainty equal to -1 or 1, which is needed in order to avoid having a cost function equal to infinity.

### 3.3.3. Experimental Setting and Results for a Speed Bump Input

In order to assess the efficiency of the polynomial chaos theory for parameter estimation, $M$ and $d_{CG}$ will be estimated using observations of four motion variables obtained for a given road input: the displacements across the suspensions ($x_1 - x_{t1}$ and $x_2 - x_{t2}$), and their corresponding velocities ($\dot{x}_1 - \dot{x}_{t1}$ and $\dot{x}_2 - \dot{x}_{t2}$). The road profile is shown in Figure 3.18, and the road input is obtained assuming the vehicle has a constant speed of 16 km/h (10 mph). The road profile can be

seen as a long speed bump. The first tire is subjected to a ramp at $t = 0$, and reaches a height of 10 cm (4") for a horizontal displacement of 1m, then stays at the same height for 1m after a total horizontal displacement of 3 m, and goes back down to its initial height. The second tire is subjected to the same kind of input, but with a time delay of 20% of the time it takes to cover 3 m (i.e., the bump starts 0.6 m later for the right tire), and it reaches a maximum height of only 8 cm.

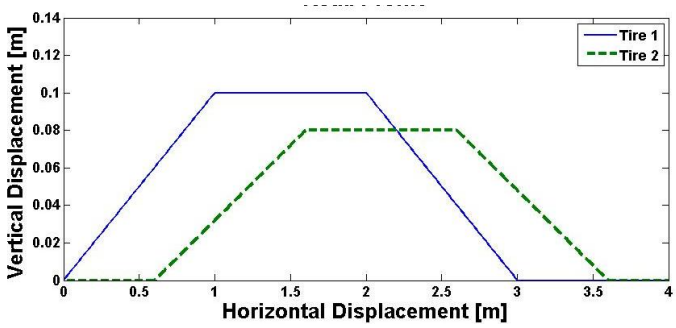


Figure 3.18: Road Profile – Speed Bump

The four motion variables are plotted from $t = 0$ to $t = 3\,\text{seconds}$ using $M^{ref} = 223.26$ kg and $d_{CG}{}^{ref} = 0.6882\,\text{m}$ (i.e., $\xi_1{}^{ref} = 0.2326$ and $\xi_2{}^{ref} = -0.3875$) and assuming these values can only be measured with a sampling rate of $0.3\,\text{s}$.

However, for the proof of concept of the parameter estimation method presented in this chapter, we pretend we do not know the values of $M$ and $d_{CG}$, the objective being to estimate those values based on the plot of the four motion variables shown in Figure 3.19. Let's note that 3 seconds of data correspond to a horizontal displacement of 13.33 meters. The end of the speed bump occurs at $t = 0.675\,\text{s}$. The end of the speed bump occurs at $t = 0.81\,\text{s}$, which corresponds to a total horizontal displacement of 3.6 m.

The excitation signal is supposed to be perfectly known. In other words, the road profile shown in Figure 3.18 is supposed to be exactly known and the speed of the vehicle is supposed to be exactly 16 km/h at all time, which enables us to use any desired sampling rate for the input signal. However, only 10 measurement points are used for the output displacements and

velocities (not counting the measurements at $t = 0$, which give no useful information in order to estimate the unknown parameter). It is always better to take a number of measurement points as large as possible when computational time is not an issue and precision is very important. However, using a lower number of measurements can be useful when an answer is needed quickly, which does not prevent from continuing to process the extra information later on if needed, knowing that the extra measurements will generally yields more precision. Adding more measurement points does not usually add much precision to the estimations, as will be shown later in this chapter.

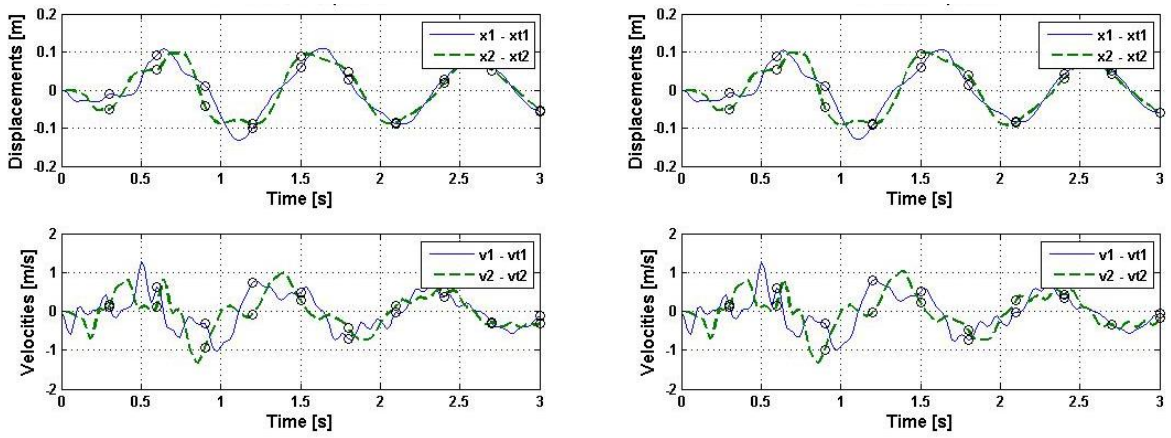


(a) (b)

Figure 3.19: Observed States - Displacements and Velocities: (a) Measured; (b) for Nominal Values ($\xi_1 = 0$, $\xi_2 = 0$)

As explained in Section 3.2.7, the quality of the maximum likelihood estimate is related to the shape of the Bayesian cost function, with a sharp minimum indicating an accurate estimate. Inaccurate estimates can be caused by different factors, including a sampling rate below the Nyquist frequency, non-identifiability, non-observability, and an excitation signal that is not rich enough.

The parameters are non-identifiable when different parameter values lead to identical system outputs. In this case the Bayesian cost function has an entire region of minima (e.g., a valley),

with each parameter value in the region being equally likely. A regularization approach based on increasing the weight of the apriori information can be used to select reasonable estimates.

For identifiable and observable systems accurate estimates can be obtained in most cases even if the output signal is sampled below the Nyquist rate. In the worst case, however, sampling below the Nyquist rate cannot guarantee that sufficient information is extracted from the output. In this worst case the apriori information becomes important and the estimate is biased toward the apriori most likely value.

The measurements shown in Figure 3.19(a) are synthetic measurements obtained from a reference simulation with the reference value of the uncertain parameter $\xi_1^{ref} = 0.2326$ and $\xi_2^{ref} = -0.3875$. Parameters estimation is performed using the Bayesian approach. In order to work with a realistic set of measurements, a Gaussian measurement noise with zero mean and 1% variance is added to the observations shown in Figure 3.19 (for the relative displacements and velocities) before performing parameter estimation.

The state of the system at future times depends on the random initial velocity and can be represented by

$$y(\xi,t) = \left[ x_1(\xi,t) \quad x_2(\xi,t) \quad x_{t1}(\xi,t) \quad x_{t2}(\xi,t) \quad \frac{dx_1(\xi,t)}{dt} \quad \frac{dx_2(\xi,t)}{dt} \quad \frac{dx_{t1}(\xi,t)}{dt} \quad \frac{dx_{t2}(\xi,t)}{dt} \quad \theta_1(\xi,t) \;\; \theta_2(\xi,t) \right]^T \tag{3.57}$$

where $\theta_1(\xi,t)$ and $\theta_2(\xi,t)$ represent the uncertain parameters $M$ and $d_{CG}$.

If we assume that only the displacements across the suspensions ( $x_1 - x_{t1}$ and $x_2 - x_{t2}$ ), and their corresponding velocities ( $\dot{x}_1 - \dot{x}_{t1}$ and $\dot{x}_2 - \dot{x}_{t2}$ ) can be measured, then

$$H = \begin{bmatrix} 1 & 0 & -1 & 0 & 0 & 0 & 0 & 0 & 0 & 0 \\ 0 & 0 & 0 & 0 & 1 & 0 & -1 & 0 & 0 & 0 \\ 0 & 1 & 0 & -1 & 0 & 0 & 0 & 0 & 0 & 0 \\ 0 & 0 & 0 & 0 & 0 & 1 & 0 & -1 & 0 & 0 \end{bmatrix} \tag{3.58}$$

and the measurements yield

$$z_k = H \cdot y^{\text{ref}}(t_k) + \eta_k = x^{\text{ref}}(t_k) + \eta_k, \quad \eta_k \in \mathrm{N}(0, R_k) \tag{3.59}$$

Measurement errors at different times are independent random variables. The measurement noise $\eta_k$ is assumed to be Gaussian with a zero mean and a variance 1% (or 0.01% when indicated) of the value of $x(t)$. The diagonal elements of the covariance matrix of the uncertainty associated with the measurements will still be set to at least $10^{-12}$ when necessary so that $R_k^{-1}$ can always be computed. Therefore, the covariance of the uncertainty associated with the measurements is

$$R_k = \begin{bmatrix} R_{k1} & 0 & 0 & 0 \\ 0 & R_{k2} & 0 & 0 \\ 0 & 0 & R_{k3} & 0 \\ 0 & 0 & 0 & R_{k4} \end{bmatrix} \tag{3.60}$$

where

$$R_{k1} = \max\left\{10^{-12}, (0.01\ z_{k1})^2\right\} \tag{3.61}$$

$$R_{k2} = \max\left\{10^{-12}, (0.01\ z_{k2})^2\right\} \tag{3.62}$$

$$R_{k3} = \max\left\{10^{-12}, (0.01\ z_{k3})^2\right\} \tag{3.63}$$

$$R_{k4} = \max\left\{10^{-12}, (0.01\ z_{k4})^2\right\} \tag{3.64}$$

As explained in Section 3.1, the maximum likelihood estimate is obtained by minimizing the Bayesian cost function

$$J_{\text{total}}(\xi) = \underbrace{\tfrac{1}{2}\sum_{k=1}^{N}\left(z_k - H\ y(\xi, t_k)\right)^T R_k^{-1}\left(z_k - H\ y(\xi, t_k)\right)}_{J_{\text{mismatch}}} + \underbrace{\left(-\log\left(\rho(\xi)\right)\right)}_{J_{\text{apriori}}} \tag{3.65}$$

For this particular example, the joint probability density function $\rho(\xi)$ is

$$\rho(\xi) = \frac{3}{4}\left(1 - \xi_i^{\,2}\right) \times \frac{3}{4}\left(1 - \xi_2^{\,2}\right) \tag{3.66}$$

The value of the cost function can be visualized, as shown in Figure 3.20. A simple Matlab code can estimate the values of $\xi_1$ and $\xi_2$ (and thus the values of $M$ and $d_{CG}$) corresponding to the minimum value of the cost function.

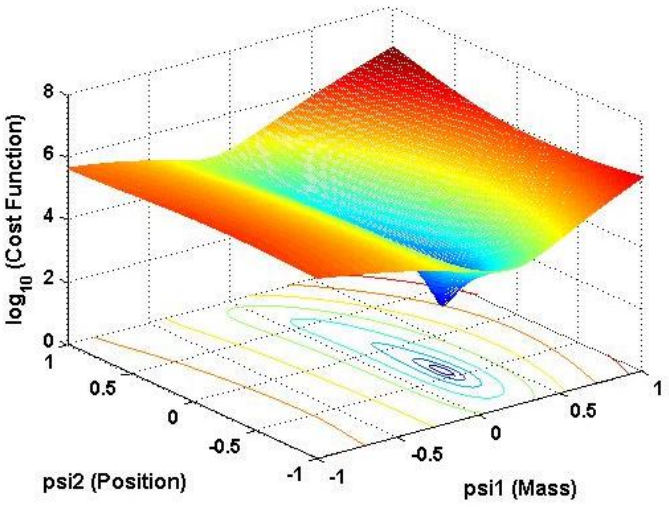


Figure 3.20: Cost Function Using the Bayesian Approach – 10 Time Points (Noise = 1%)

The estimated values of $\xi_1$ and $\xi_2$ obtained using the Bayesian approach are $\xi_1{}^{est} = 0.2236$ and $\xi_2{}^{est} = -0.4024$, i.e., $M^{est}\,222.36\,\text{kg}$ and $d_{CG}{}^{est} = 0.6853\,\text{m}$. The actual values were $\xi_1{}^{ref} = 0.2326$ and $\xi_2{}^{ref} = -0.3875$, i.e., $M^{ref} = 223.26$ kg and $d_{CG}{}^{ref} = 0.6882\,\text{m}$. It seems to be a good estimation since there is noise associated to the measurements. With a Gaussian measurement noise with zero mean and 0.01% variance the results would be $\xi_1{}^{est} = 0.2237$ and $\xi_2{}^{est} = -0.3992$, i.e., $M^{est} = 222.37$ kg and $d_{CG}{}^{est} = 0.6860\,\text{m}$. It shows that the effects of a Gaussian measurement noise with zero mean and 1% variance cannot be completely neglected.

Figure 3.21 shows the cost function that would be obtained if the motion variables could be measured with a sampling rate of 0.03 s, for a noise level of 1%. It can be observed that the extra measurement point do not change the shape of the cost function by much. The fact that the cost function had a well defined minimum value with 10 measurement points told us that we had enough information in order to obtain a precise estimation that can be trusted. Using 100 measurement points will add more accuracy, but not so much considering that the computing time will be 10 times greater.

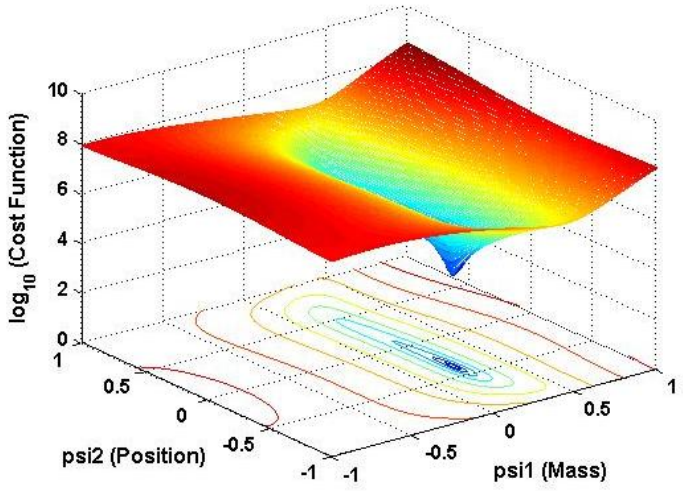


Figure 3.21: Cost Function Using the Bayesian Approach – 100 Time Points (Noise = 1%)

With 100 sample points and a noise level of 1%, which corresponds to the cost function shown in Figure 3.21, the estimated values of $\xi_1$ and $\xi_2$ obtained using the Bayesian approach are ${\xi_1}^{est} = 0.2339$ and ${\xi_2}^{est} = -0.3662$, i.e., ${M}^{est} = 223.39$ kg and ${d_{CG}}^{est} = 0.6922\,\text{m}$. The estimation of $\xi_1$ (i.e., of the added mass) is more accurate than with 10 measurement points, but the estimation of $\xi_2$ is not more accurate in this case. With a Gaussian measurement noise of 0.01% variance, the results would be ${\xi_1}^{est} = 0.2341$ and ${\xi_2}^{est} = -0.3736$, i.e., ${M}^{est} = 223.41$ kg and ${d_{CG}}^{est} = 0.6908\,\text{m}$, which also yields a more accurate estimation of the added mass when compared with the results obtained with 10 measurement points. As a conclusion, adding more measurements points adds accuracy. However, the shape of the cost function indicated that the estimation using only 10 measurement points was already quite accurate. Adding more measurement points is not the only thing that affects the results. Table 3.2 shows that the results of the estimation process are also affected by the number of terms used in the polynomial chaos approximation and by the number of collocation points. Adding more measurement points is desirable if the computational cost is not already high, which also depends on the complexity of the system. If the computational time is an issue and the cost function yields a clear minimum, not adding more measurements might be a good idea then.

Table 3.2 shows that the estimations obtained with 15 terms become similar to the observations obtained with 21 terms as the number of collocation points gets larger. Therefore, working with 15 terms in the polynomial chaos expansions and with 30 collocation points seems to be a good comprise. Adding more terms and more collocation points would increase the precision of the estimation, but the extra precision would eventually become small compared with the effect of the noise, and would come at a great computational cost.

Table 3.2: Effect of the Polynomial Chaos Approximation for the Bayesian Approach (with 10 Time Points and a Gaussian Measurement Noise with Zero Mean and 1% Variance)

| Number of Collocation Points | 10 terms | 15 terms | 21 terms |
|---|---|---|---|
| 10 | 0.2305, -0.3864 | | |
| 15 | 0.2249, -0.3793 | 0.2307, -0.3790 | |
| 21 | 0.2218, -0.3918 | 0.2307, -0.3885 | 0.2239, -0.5036 |
| 30 | 0.2224, -0.3869 | **0.2236, -0.4024** | 0.2279, -0.4012 |
| 40 | | | 0.2275, -0.4004 |
| 45 | | 0.2257, -0.4006 | |
| 60 | | | 0.2270, -0.3972 |
| Actual Values | 0.2326, -0.3875 | 0.2326, -0.3875 | 0.2326, -0.3875 |

It can be noticed that when using the minimum number of collocation points required to perform the estimation, i.e., a number of collocation points equal to the number of terms, increasing the number of terms results in poorer estimations. This is something that has been observed on other test cases. For this case, it becomes very noticeable when using 21 terms and 21 collocation points. This makes sense since solving a system with more unknowns is more complicated, and adding extra information into a least squares algorithm becomes more valuable as the system becomes more complex.

The fact that the estimation performed with 10 collocations for 10 terms seems to be due to a very favorable random choice of the collocation points. Using 10 terms in the polynomial chaos expressions results in approximations. Using only 10 collocation points also results in less precision. However, many approximations can still lead to an accurate result when they cancel out each other by chance.

### 3.3.4. Results for a Chirp Input

In this section, linear swept-frequency sine input signals are used from $t = 0$ to $t = 3\,\text{seconds}$ with frequencies ranging from 0 Hz at $t = 0$ to 2 Hz at $t = 3\,\text{seconds}$, as shown in Figure 3.22. The amplitude of the input signals is 5 cm. The highest frequency of the chirp input used in this study was selected to be 2 Hz because this is the frequency when the dampers enter the saturation mode for a very significant percentage of the time due to higher velocities, which will be shown later. When the dampers saturate, there is no one-to-one relationship between the relative velocities across the dampers and the force they produce, which can lead to non-identifiability.

The inputs signals are:

$$y_1 = 0.05\ \sin\left(t\frac{2\pi}{3}t\right), \quad i.e.\ y_1 = 0.05\ \sin\left(\omega(t)\times t\right)\ \text{with}\ \omega(t) = \frac{2\pi}{3}t \tag{3.67}$$

$$y_2 = -0.05\ \sin\left(t\frac{2\pi}{3}t\right), \quad i.e.\ y_2 = -0.05\ \sin\left(\omega(t)\times t\right)\ \text{with}\ \omega(t) = \frac{2\pi}{3}t \tag{3.68}$$

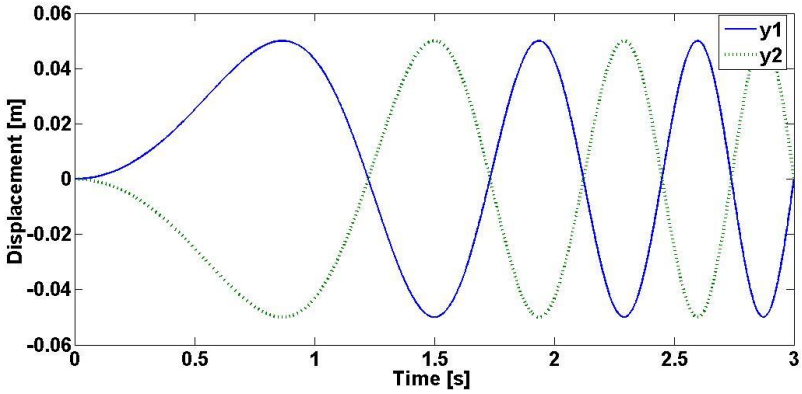


Figure 3.22: Chirp Input Going from DC to 2 Hz in 3 seconds

Parameters estimation is performed using the Bayesian approach. In order to work with a realistic set of measurements, a Gaussian measurement noise with zero mean and 1% variance is

added to the observed relative displacements and velocities before performing parameter estimation. Figure 3.23 shows the cost function obtained with a sampling rate of 0.1 s, for a noise level of 1%. Since the maximum frequency in the chirp input is 2 Hz, using 30 measurement points is enough in order to respect the Nyquist criterion.

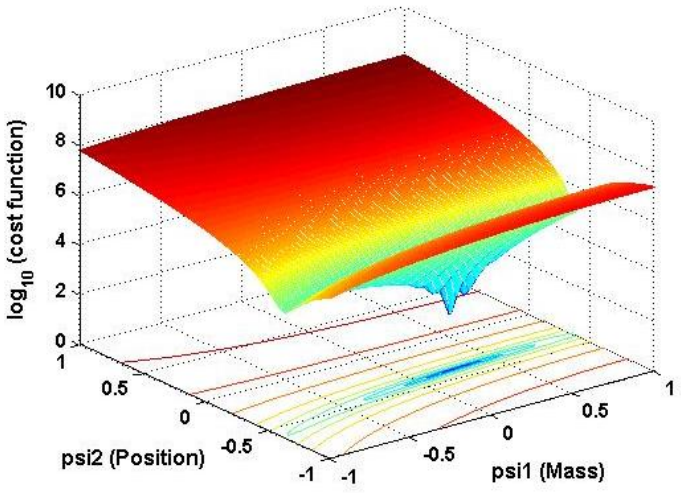


Figure 3.23: Cost Function for the Chirp Input with 30 Time Points and 1% Measurement Noise

The estimated values of $\xi_1$ and $\xi_2$ obtained using the Bayesian approach are $\xi_1^{\,est} = 0.2381$ and $\xi_2^{\,est} = -0.3868$, i.e., $M^{est} = 223.81\,\text{kg}$ and $d_{CG}^{\,est} = 0.6883\,\text{m}$. The actual values were $\xi_1^{\,ref} = 0.2326$ and $\xi_2^{\,ref} = -0.3875$, i.e., $M^{ref} = 223.26$ kg and $d_{CG}^{\,ref} = 0.6882\,\text{m}$. Using a chirp signal is therefore a good way to estimate the value of the mass and its position, as long as it doesn't contain frequencies where the dampers are in saturation mode most of the time. The cost function has a clear minimum, but it can be seen that this minima is in a region of low values along the line. Adding higher frequency content in the input signal would start preventing us from obtaining a clear minimum along this line. This is illustrated in the next section.

### 3.3.5. Relationship Between Quality of Estimation and the Frequency of the Input Signal

In order to assess the efficiency of the polynomial chaos theory for parameter estimation, $M$ and $d_{CG}$ will be estimated using a plot of four motion variables: the displacements across the suspensions ($x_1 - x_{t1}$ and $x_2 - x_{t2}$), and their corresponding velocities ($\dot{x}_1 - \dot{x}_{t1}$ and $\dot{x}_2 - \dot{x}_{t2}$). The estimations will be performed for different harmonic inputs, ranging from 0.33 Hz to 25 Hz, with amplitudes of +/- 0.05 m for $y_1$ and $y_2$. The input signals are still supposed to be exactly known. Figure 3.24 shows the harmonic inputs that will be used at 1 Hz.

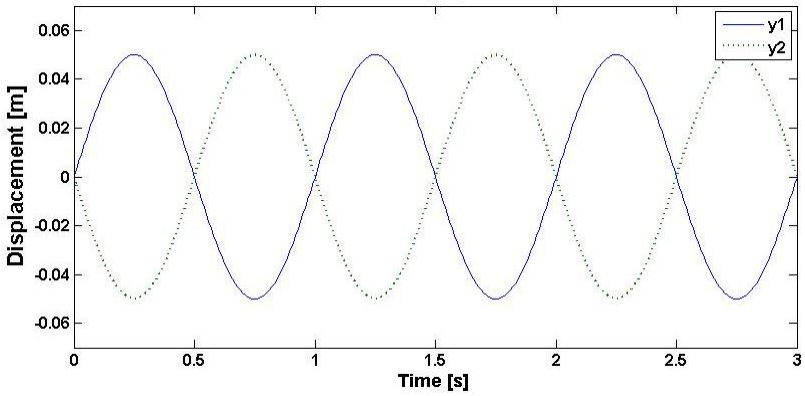


Figure 3.24: Road Input at 1 Hz

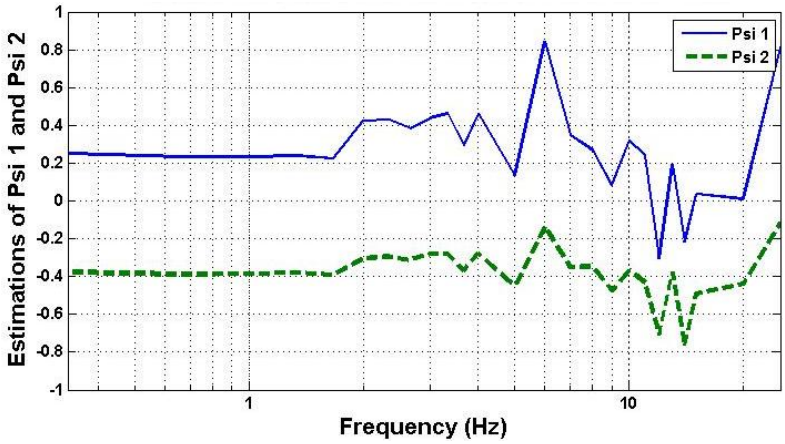


Figure 3.25: Bayesian Estimation of the Added Mass and the Position of the Mass at Different Frequencies Using 10 Time Points and a 1% Noise

The estimations are performed using 15 terms in the polynomial chaos expansions and 30 collocation points. Figure 3.25 shows the estimated values of $M$ and $d_{CG}$, obtained using the Bayesian approach for harmonic inputs with frequencies ranging from 0.33 Hz to 25 Hz. It is still assumed that measurements can only be obtained at a sampling rate of 0.3 s and that the Gaussian measurement noise has a zero mean and 1% variance. It can be observed that good estimations are obtained for frequencies lower than or equal to 1.33 Hz, but the quality of the estimations is clearly poorer for frequencies higher than or equal to 1.66 Hz.

One might wonder if increasing the sampling rate of the measurement and being able to work with an extremely low measurement noise level would improve the results. Figure 3.26 shows the estimated values of $M$ and $d_{CG}$ obtained with a sampling rate of 0.3 s (i.e., 10 time points) for the Bayesian approach when the Gaussian measurement noise has a 0.01% variance instead of a 1%. It can be observed that even though the estimations can be different, the same problems remain for estimating $M$ (i.e. $\xi_1$) at frequencies higher than or equal to 2 Hz estimated values of However, the estimation of $d_{CG}$ (i.e. $\xi_2$) yields much better results at frequencies higher than or equal to 2 Hz.

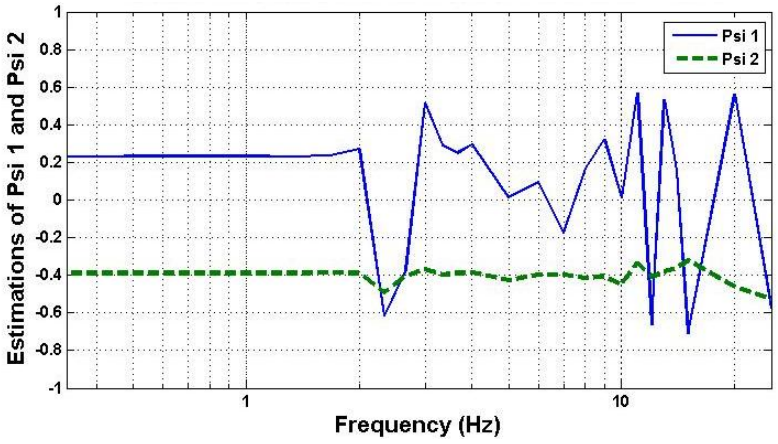


Figure 3.26: Bayesian Estimation of the Added Mass and the Position of the Mass at Different Frequencies Using 10 Time Points and a 0.01% Noise

One might wonder if being able to increase the sampling rate of the measurement instead of being able to work with an extremely low measurement noise level would improve the results. Figure 3.27 shows the estimated values of $M$ and $d_{CG}$ obtained with a sampling rate of 0.02 s (i.e., 150 time points) for the Bayesian approach when the Gaussian measurement noise has a 1% variance. It can be observed that the results are very similar than the results obtained with 10 time points and a 0.01% noise. Being able to increase the sampling rate and being to lower the noise level both have the same effect on the quality of the estimations. The same problems remain for estimating $M$ (i.e. $\xi_1$) at frequencies higher than or equal to 2 Hz.

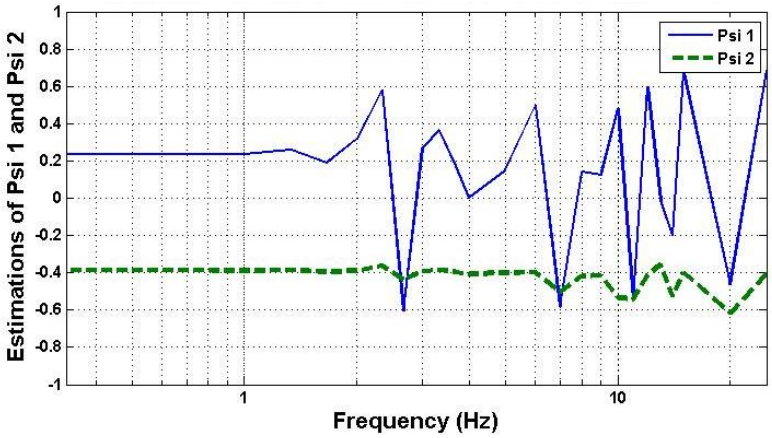


Figure 3.27: Bayesian Estimation of the Added Mass and the Position of the Mass at Different Frequencies Using 150 Time Points and a 1% Noise

One might wonder if increasing the sampling rate of the measurement while still being able to work with an extremely low measurement noise level would improve the results. Figure 3.28 shows the estimated values of $M$ and $d_{CG}$ obtained with a sampling rate of 0.02 s (i.e., 150 time points) for the Bayesian approach when the Gaussian measurement noise has a 0.01%. It can be observed that even though the estimations can be different, the same problem remains for frequencies higher than or equal to 2 Hz. It can be observed that the results are still very similar than for the previous two configurations and that the same problems remain for estimating $M$ (i.e. $\xi_1$) at frequencies higher than or equal to 2 Hz. When the noise level is extremely low, adding extra measurement points does not yield better results.

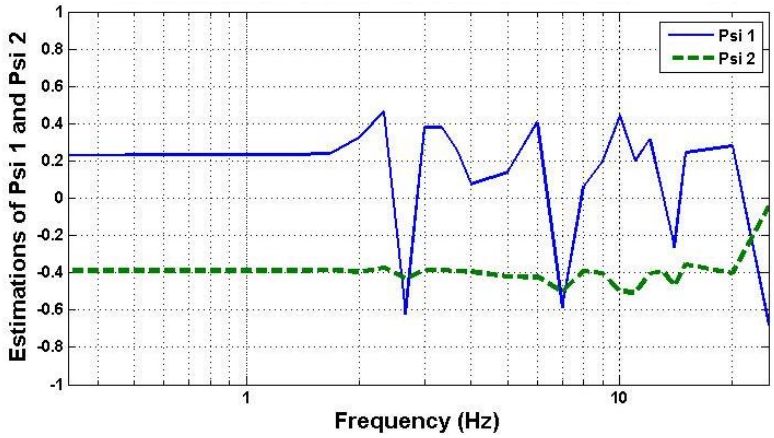


Figure 3.28: Bayesian Estimation of the Added Mass and the Position of the Mass at Different Frequencies Using 150 Time Points and a 0.01% Noise

Therefore, the mass cannot be estimated when using inputs at frequency higher than or equal to 2 Hz even with measurements of very good quality. The reason the estimations are not accurate for input frequencies of 2 Hz and above is a problem of non-identifiability: different values of $M$ and $d_{CG}$ can result in the same time response for the displacements and velocities across the suspensions. For instance, if we look at the cost function at 1 Hz with 10 time points and a 0.01% measurement noise added to the observations, as shown in Figure 3.29, we can see that the cost function has a clear minimum. If we look at the cost function at 2 Hz, as shown in Figure 3.30, we can see that the cost function has minima along a curve. Those minima correspond to several combinations ($M$ , $d_{CG}$) yielding the same time response for the 2 Hz input. The estimated values ($\xi_1^{\,est} = 0.2707$ and $\xi_2^{\,est} = -0.3890$) and the actual values ( $\xi_1^{\,ref} = 0.2326$ and $\xi_2^{\,ref} = -0.3875$) are both on this curve containing the minima. Figure 3.31 shows he cost function at 3 Hz, which yields no clear minimum as well.

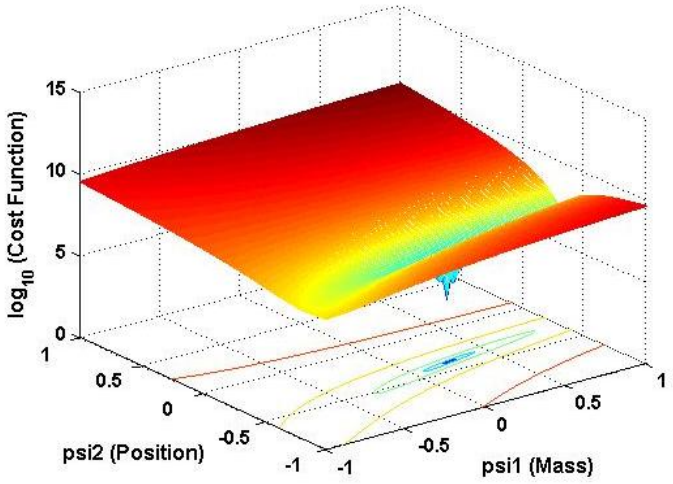


Figure 3.29: Cost Function at 1 Hz with 10 Time Points and 0.01% Measurement Noise

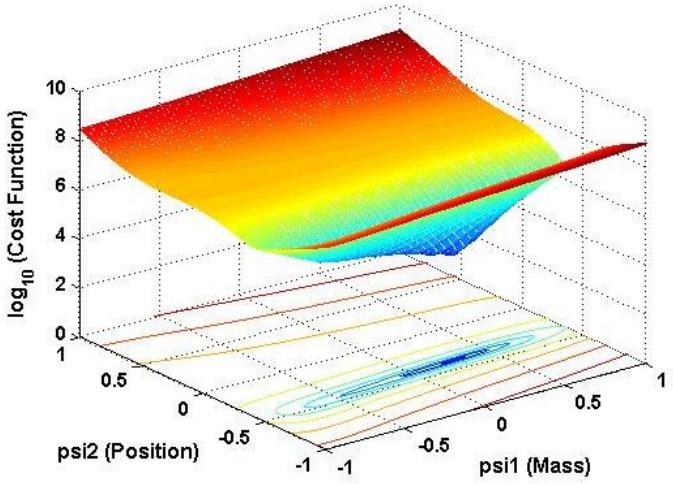


Figure 3.30: Cost function at 2 Hz with 10 time points and 0.01% measurement noise

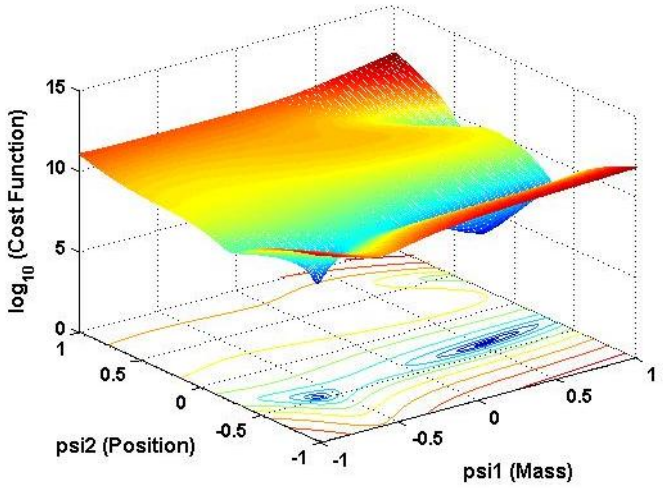


Figure 3.31: Cost Function at 3 Hz with 10 Time Points and 0.01% Measurement Noise

Figure 3.32 shows the time responses at 1 Hz for the nominal values $(\xi_1, \xi_2) = (0, 0)$ and for values that were used $(\xi_1, \xi_2) = (0.2326, -0.3875)$, which were estimated very well by the Bayesian approach . It can be noticed that the curves are quite distinct.

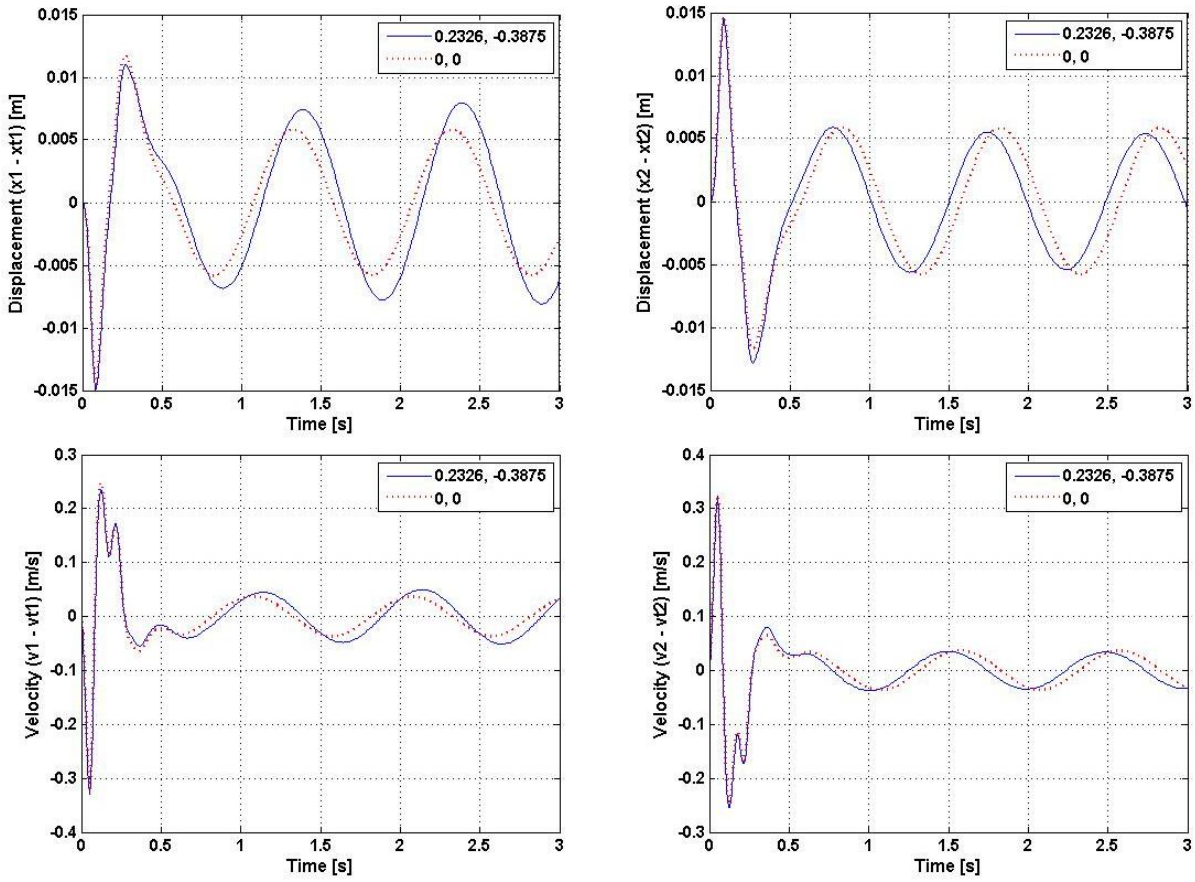


Figure 3.32: Time Responses at 1 Hz

Figure 3.33 shows the time responses at 2 Hz for the nominal values $(\xi_1, \xi_2) = (0, 0)$, for the values that were used $(\xi_1, \xi_2) = (0.2326, -0.3875)$, and for the estimated values $(\xi_1, \xi_2) = (0.2707, -0.3890)$. It shows that the estimated values yield the same time response than the actual values at 2Hz, which is why no estimation technique can work. Also, the observed time response is more similar to the nominal time response than it was at 1 Hz, which is why estimating uncertainties gets more difficult in a more general sense.

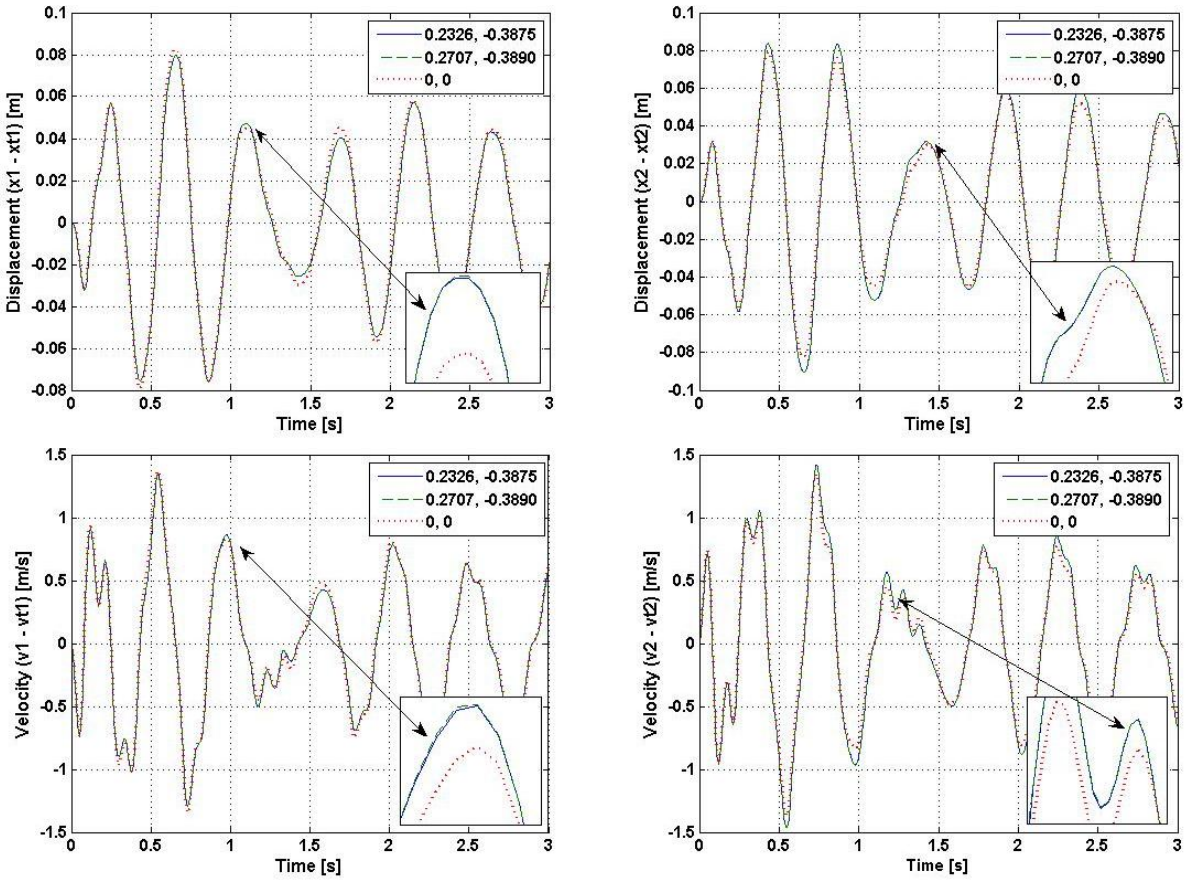


Figure 3.33: Time Responses at 2 Hz

Figure 3.34 shows the time responses at 3 Hz for the nominal values $(\xi_1, \xi_2) = (0, 0)$, for the values that were used $(\xi_1, \xi_2) = (0.2326, -0.3875)$, and for the estimated values $(\xi_1, \xi_2) = (0.5188, -0.3690)$. It shows that the estimated values yield the same time response than the actual values at 3Hz, which is why no estimation technique can work. Also, the observed time response and the nominal time response are getting even more similar. At frequency higher than 3 Hz, which are not shown in the time plots, the relative velocities across the suspension start decreasing as the frequency is increased: 3 Hz is close a resonance across the suspensions.

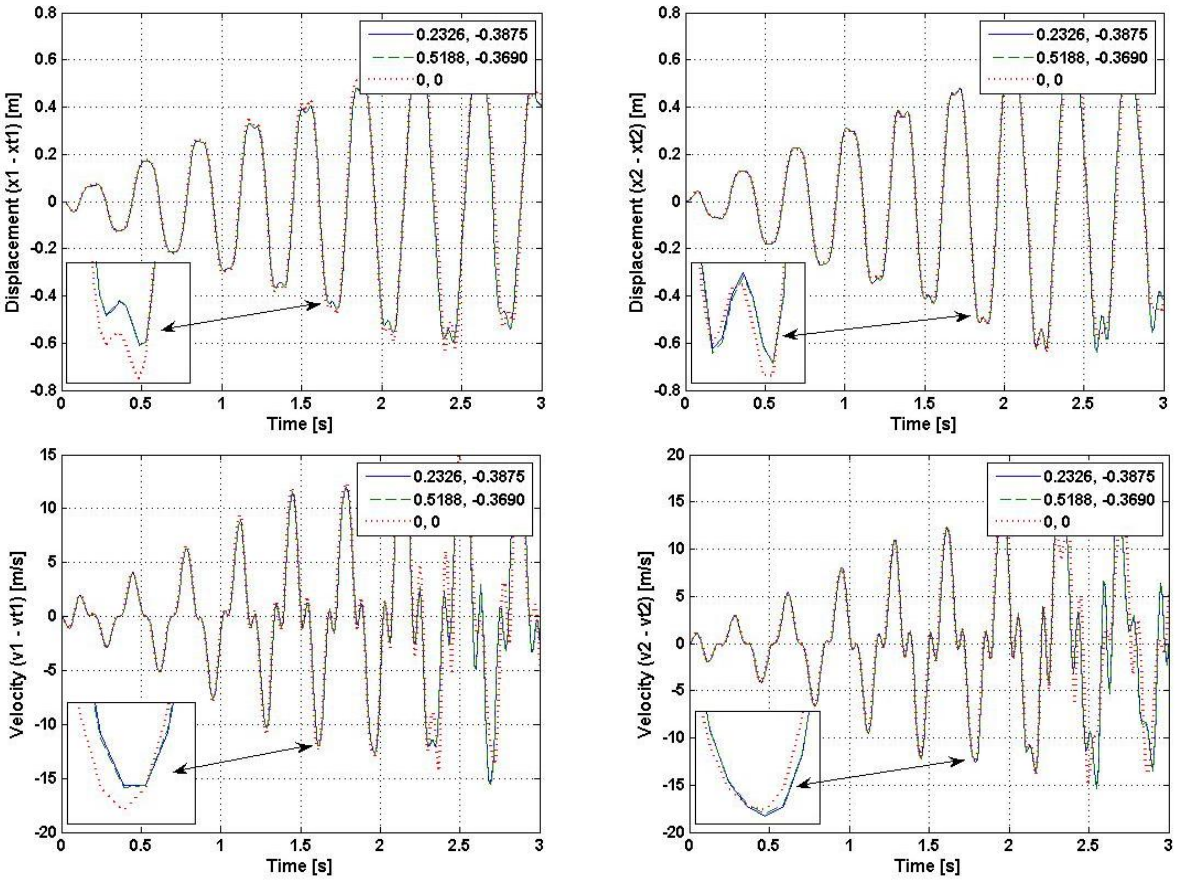


Figure 3.34: Time responses at 3 Hz

Let us recall that if $v$ is the relative velocity across the damper with a damping coefficient $c_i$ ($i = 1, 2$), the force across the damper is given by: $F_{C_i}(v) = c_i\left(0.2\tanh(10v)\right)$. The dampers can therefore be considered to be saturating at speeds higher than 0.2 m $s^{-1}$. At high frequency, the velocities get higher and the dampers are in saturation regime more often. When the dampers saturate, different velocities can yield the same force across the damper, which makes the system is non-identifiable at high frequencies.

For a linearized system, i.e., with $F_{C_i}(v) = c_i v$ for the dampers and $k_{i,3} = 0$ for the suspension springs ($i$ = 1, 2), the system become identifiable for all frequencies from 0.33 Hz to 25 Hz, as shown in Figure 3.35. The estimation is still sensitive to numerical approximations (e.g., in running the ODE's) and the polynomial chaos approximation, which explains why the estimation of the added mass is not always perfect.

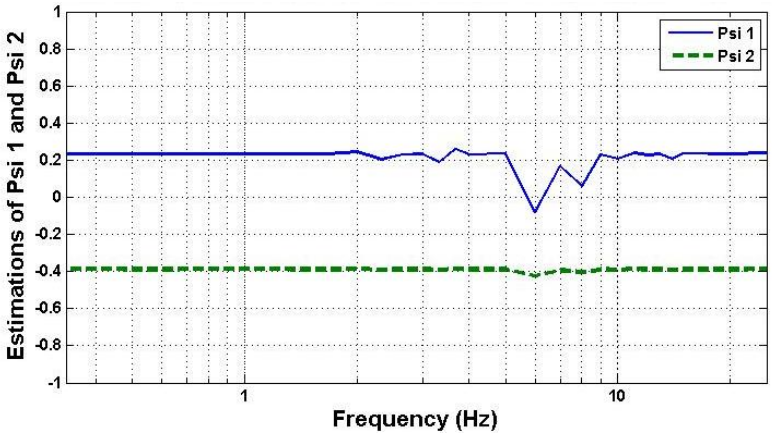


Figure 3.35: Bayesian Estimation for the Linearized System Using 150 Time Points and a 0.01% Noise

### 3.3.6. Regularization

When several combinations of values for the uncertain parameters result in the same behavior of the system, regularization techniques [22] can be used in order to find the most likely values among the values resulting in a minimum, based on our apriori knowledge of the system. It consists of multiplying the apriori part by a coefficient so that the new total cost function has a

clear minimum value along the possible values. This is illustrated in Figure 3.36, where the cost function at 2 Hz is shown for different regularization coefficients.

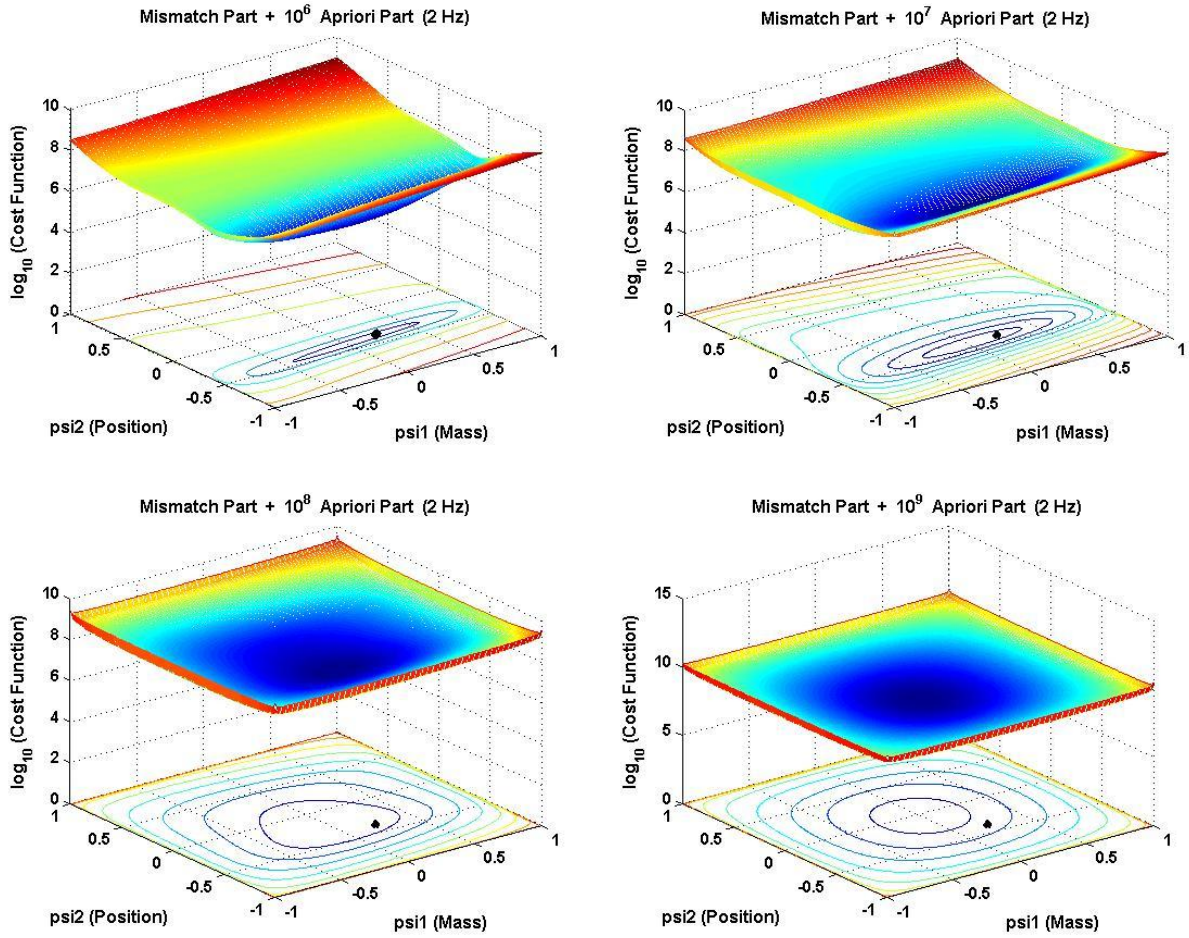


Figure 3.36: Regularization at 2 Hz

The cost function will look like its mismatch part when the regularization coefficient is very low and it will look like its apriori part when the regularization coefficient is very high. As the regularization coefficient gets larger, the line of possible minima becomes an ellipse, which starts moving away from the location of the original line of minima while becoming more and more like a circle. Eventually, it becomes a circle centered at (0, 0), like the apriori part of the cost function. When the line becomes an ellipse with a well defined center, the regularization coefficient is large enough and it is not desirable to continue to increase its value since the ellipse

will start moving away from its original location while becoming a center. In this case, $10^7$ seems to be a good regularization coefficient and it results in the following estimation: $(\xi_1, \xi_2) = (0.05, -0.39)$

When the cost function has a region of possible minimum values that cannot be differentiated, e.g. when dealing with a non-identifiability issue, using regularization techniques will yield better results on average. However, there is no guarantee that it will yield a value closer to the actual values of the uncertain parameters for any given problem. For instance, 2 Hz is not a very relevant example, because the "plain" cost function almost finds the right result. I would need to recomputed everything at a higher frequency where the results is way off, but it will take time

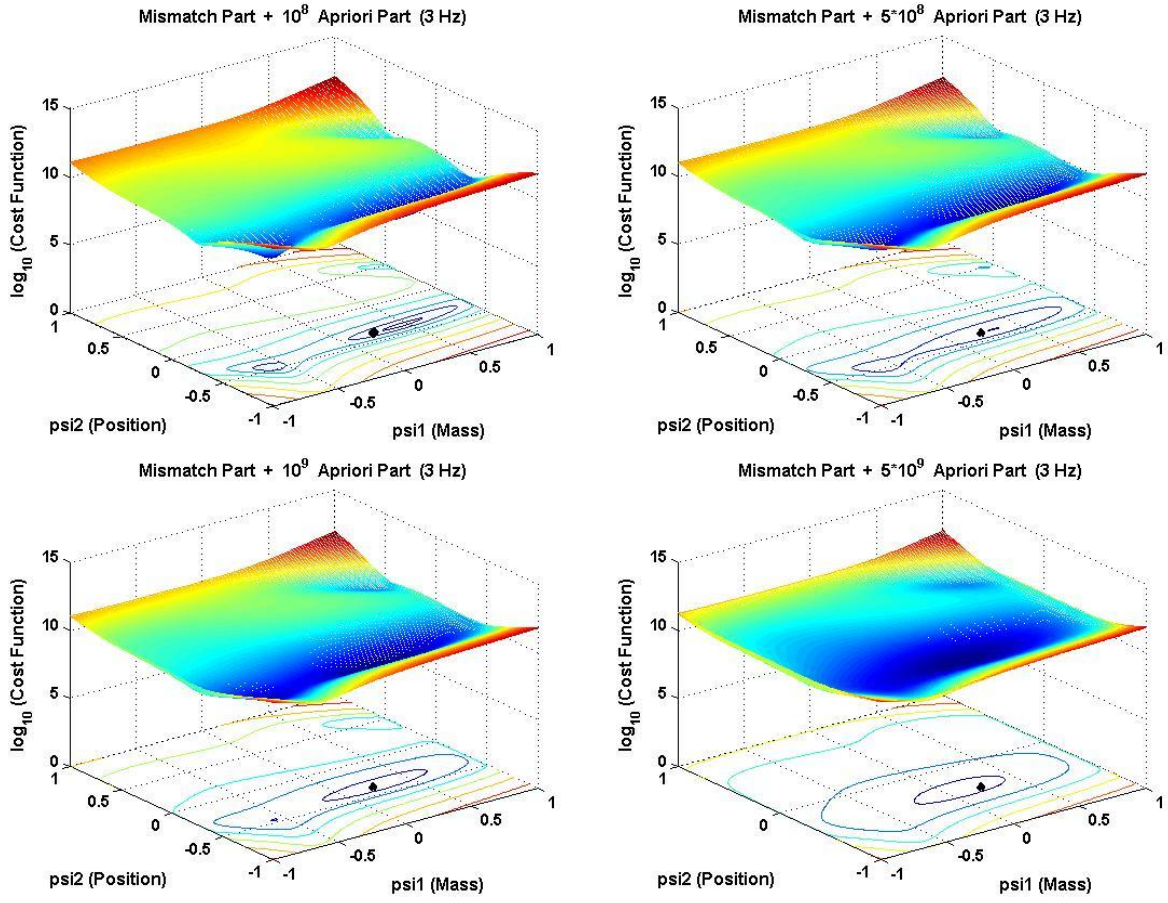


Figure 3.37: Regularization at 3 Hz

Figure 3.37 shows the cost function at 3 Hz for different regularization coefficients. In this case, $10^9$ seems to be a good regularization coefficient and it results in the following estimation: $(\xi_1, \xi_2) = (0.26, -0.37)$. Regularization techniques are more valuable at 3 Hz than at 2 Hz since the estimation was still working approximately at 2 Hz, but was not accurate at all anymore at 3 Hz for estimating $M$ (i.e., $\xi_1$).

## 3.4 Summary and Conclusions

In this chapter, the polynomial chaos theory is applied to the problem of parameter estimation in the Bayesian framework, using direct stochastic collocation. The maximum likelihood estimates are obtained by minimizing a cost function derived from the Bayesian theorem. This approach was first applied to very simple mechanical systems in order to illustrate how the cost function can be affected by undersampling, non-identifiability of the system, non-observability, and by excitation signals that are not rich enough. Inaccurate estimates can be caused by those different factors. It has been shown that the quality of the maximum likelihood estimate is related to the shape of the Bayesian cost function, with a sharp minimum indicating an accurate estimate. The parameters are non-identifiable when different parameter values lead to identical system outputs. In this case the Bayesian cost function has an entire region of minima (e.g., a valley), with each parameter value in the region being equally likely. Regularization techniques can still yield most likely values among the possible combinations of uncertain parameters resulting in the same time responses than the ones observed. This was illustrated using a simple spring-mass system. For identifiable and observable systems accurate estimates can be obtained in most cases even if the output signal is sampled below the Nyquist frequency. In the worst case, however, sampling below the Nyquist rate cannot guarantee that sufficient information is extracted from the output. In this worst case the apriori information becomes important and the estimate is biased toward the apriori most likely value. The proposed method has several advantages. Simulations using Polynomial Chaos methods are much faster than Monte Carlo simulations. Another advantage of this method is that it is optimal; it can treat non-Gaussian uncertainties since the Bayesian approach is not tailored to any specific distribution.

To further analyze the capabilities of the new parameter estimation method and to aid in interpreting results for more complex systems, the Polynomial-Chaos based Bayesian approach was illustrated on a nonlinear four-degree-of-freedom roll plane model of a vehicle in which the parameters of interest to be estimated are an uncertain mass and its uncertain position at which the mass is added on the roll bar. Uncertainties on the values of the added mass and its position are assumed to have a Beta (2, 2) distribution. The value of the mass and its position are estimated from periodic observations of the displacements and velocities across the suspensions. Appropriate excitations are needed in order to obtain accurate results. For some excitations, different combinations of uncertain parameters lead to essentially the same time responses, and no estimation method can work without additional information. Regularization techniques can still yield most likely values among the possible combinations of uncertain parameters resulting in the same time responses than the ones observed. When using appropriate excitations, the results obtained with this approach are close to the actual values of the parameters. The proposed estimation procedure can work with noisy measurements.

# 4 Polynomial Chaos Based Extended Kalman Filter Approach for Parameter Estimation

In this chapter, a new computational approach for parameter estimation based on the Extended Kalman Filter (EKF) and the polynomial chaos theory for parameter estimation is proposed. The error covariances needed by EKF are computed from polynomial chaos expansions, and the EKF is used to update the polynomial chaos representation of the uncertain states and the uncertain parameters. The proposed method is applied to a nonlinear four degree of freedom roll plane model of a vehicle, in which an uncertain mass with an uncertain position is added on the roll bar. The main advantages of this method are an accurate representation of uncertainties via polynomial chaoses, a computationally efficient update formula based on EKF, and the ability to provide aposteriori probability densities of the estimated parameters. The method is able to deal with non-Gaussian parametric uncertainties. A possible weakness of the EKF with approximate covariances is identified, and theoretically explained in Appendix: numerical errors due to the truncation in the polynomial chaos expansions can accumulate quickly when measurements are taken at a fast sampling rate. To prevent filter divergence, it is proposed to lower the sampling rate, and to take a smoother approach where a set of time-distributed observations are all processed at once.

## 4.1 Formulation of the EKF Approach

Optimal parameter estimation combines information from three different sources: the physical laws of evolution (encapsulated in the model), the reality (as captured by the observations), and the current best estimate of the parameters. The information from each source is imperfect and has associated errors. Consider the mechanical system model (2.21) in Chapter 2, which advances the state in time represented in a simpler notation:

$$y_k = \begin{bmatrix} x_k \\ v_k \end{bmatrix},\ y_k = \mathbf{M}(t_{k-1}, y_{k-1}, \theta),\ y_0 = y(t_0),\ k = 1,2,\ldots,N \tag{4.1}$$

The state of the model $y_k \in \Re^{n_S}$ at time moment $t_k$ depends implicitly on the set of parameters $\theta \in \Re^{n_P}$, possibly uncertain (the model has $n_S$ states and $n_P$ parameters). $\mathbf{M}$ is the model solution operator which integrates the model equations forward in time (starting from state $y_{k-1}$ at time $t_{k-1}$ to state $y_k$ at time $t_k$). $N$ is the number of time points at which measurements are available.

For parameter estimation it is convenient to formally extend the model state to include the model parameters and extend the model with trivial equations for parameters (such that parameters do not change during the model evolution)

$$\theta_k = \theta_{k-1} \tag{4.2}$$

The optimal estimation of the uncertain parameters is thus reduced to the problem of optimal state estimation. We assume that observations of quantities that depend on the system state are available at discrete times $t_k$

$$z_k = h(y_k) + \eta_k \approx H_k\, y_k + \eta_k,\ \ \eta_k \in \mathbf{N}(0, R_k) \tag{4.3}$$

where $z_k \in \Re^{n_O}$ is the observation vector at $t_k$, $h$ is the (model equivalent) observation operator and $H_k$ is the linearization of $h$ about the solution $y_k$. Note that there are $n_O$ observations for the $n_S$-dimensional state vector, and that typically $n_O < n_S$. Each observation is corrupted by observational (measurement and representativeness) errors [100]. The observational error $\eta_k$ is the experimental uncertainty associated with the measurements and is usually considered to have a Gaussian distribution with zero mean and a known covariance matrix $R_k$.

The Kalman filter [47-49, 103] assumes that the model (4.1) is linear, and the model state at previous time $t_{k-1}$ is normally distributed with mean $y^a_{k-1}$ and covariance matrix $P^a_{k-1}$. The Extended Kalman Filter (EKF) allows for nonlinear models and observations by assuming that the error propagation is linear. The nonlinear observation operators are also linearized.

The state is propagated from $t_{k-1}$ to $t_k$ using model equations (4.1), and the covariance matrix is explicitly propagated using the tangent linear model operator $\mathbf{M}'$ and its adjoint $\mathbf{M}'^*$,

$$P_k^f = \mathbf{M}' \, P_{k-1}^a \, \mathbf{M}'^* + Q \tag{4.4}$$

where the superscripts $f$ and $a$ stand for "forecast" and "analysis", respectively. $Q$ represents the covariance of the model errors.

Under linear, Gaussian assumptions, the PDFs of the forecast and assimilated fields are also Gaussian, and completely described by the mean state and the covariance matrix. The assimilated state $y_k^a$ and its covariance matrix $P_k^a$ are computed from the model forecast $y_k^f$, the current observations $z_k$, and from their covariances using:

$$\begin{aligned} y_k^a &= y_k^f + P_k^f H_k^T \left( R_k + H_k P_k^f H_k^T \right)^{-1} \left( z_k - H_k y_k^f \right), \\ P_k^a &= P_k^f - P_k^f H_k^T \left( R_k + H_k P_k^f H_k^T \right)^{-1} H_k P_k^f . \end{aligned} \tag{4.5}$$

One step of the extended Kalman filter can be represented as:

$$y_{k-1}^a \text{ and } P_{k-1}^a \xrightarrow{\text{Model\&TangentLinearModel}} y_k^f \text{ and } P_k^f \xrightarrow[z_k \text{ and } R_k]{\text{Filter}} y_k^a \text{ and } P_k^a \tag{4.6}$$

For parameter estimation, we extend the model state to formally include the model parameters:

$$\begin{bmatrix} y_k^f \\ \theta_k^f \end{bmatrix} = \begin{bmatrix} \mathbf{M}\left(t_{k-1}, y_{k-1}^a, \theta_{k-1}^a\right) \\ \theta_{k-1}^a \end{bmatrix} \tag{4.7}$$

The covariance matrix of the extended state vector can be estimated from the polynomial chaos expansions of $y(\xi)$ and $\theta(\xi)$.

$$P_k^f = \operatorname{cov}\left( \begin{bmatrix} y_k^f(\xi) \\ \theta_k^f(\xi) \end{bmatrix} \right) = \begin{bmatrix} \operatorname{cov}\left(y_k^f\right) & \operatorname{cov}\left(\left[y_k^f, \theta_k^f\right]\right) \\ \operatorname{cov}\left(\left[\theta_k^f, y_k^f\right]\right) & \operatorname{cov}\left(\theta_k^f\right) \end{bmatrix} \tag{4.8}$$

Using this covariance matrix compute the Kalman gain matrix using the formula:

$$K_k = P_k^f H_k^T \left( R_k + H_k P_k^f H_k^T \right)^{-1} \tag{4.9}$$

The Kalman filter formula computes the assimilated state and parameter vector as:

$$\begin{bmatrix} y_k^a \\ \theta_k^a \end{bmatrix} = \begin{bmatrix} y_k^f \\ \theta_k^f \end{bmatrix} + K_k \left( z_k - H_k \begin{bmatrix} y_k^f \\ \theta_k^f \end{bmatrix} \right) = \left( I - K_k H_k \right) \begin{bmatrix} y_k^f \\ \theta_k^f \end{bmatrix} + K_k z_k \tag{4.10}$$

Assuming that no direct observations are made on the parameters, and only the state is observed, we obtain:

$$\begin{bmatrix} y_k^a \\ \theta_k^a \end{bmatrix} = \begin{bmatrix} y_k^f \\ \theta_k^f \end{bmatrix} + K_k \left( z_k - H_k y_k^f \right) = \left( I - K_k H_k \right) y_k^f + K_k z_k \tag{4.11}$$

Using the polynomial chaos expansions of the forecast state and the parameters:

$$\begin{bmatrix} y_k^f(\xi) \\ \theta_k^f(\xi) \end{bmatrix} = \begin{bmatrix} \sum_{i=1}^{S} \left( y_k^f \right)^i \psi^i(\xi) \\ \sum_{i=1}^{S} \left( \theta_k^f \right)^i \psi^i(\xi) \end{bmatrix} \tag{4.12}$$

the Kalman filter formula is used to determine the polynomial chaos expansion of the assimilated model and parameters. For this, first insert the polynomial chaos expansions into the filter formula:

$$\begin{bmatrix} \sum_{i=1}^{S} \left( y_k^a \right)^i \psi^i(\xi) \\ \sum_{i=1}^{S} \left( \theta_k^a \right)^i \psi^i(\xi) \end{bmatrix} = \left( I - K_k H_k \right) \begin{bmatrix} \sum_{i=1}^{S} \left( y_k^f \right)^i \psi^i(\xi) \\ \sum_{i=1}^{S} \left( \theta_k^f \right)^i \psi^i(\xi) \end{bmatrix} + K_k z_k \psi^1(\xi) \tag{4.13}$$

Note that the term with the observations does not depend on the random variables and is therefore associated with only the first (constant) basis function. By a Galerkin projection we see that the polynomial chaos coefficients of the assimilated state and parameters are:

$$\begin{bmatrix} \left( y_k^a \right)^i \\ \left( \theta_k^a \right)^i \end{bmatrix} = \left( I - K_k H_k \right) \begin{bmatrix} \left( y_k^f \right)^i \\ \left( \theta_k^f \right)^i \end{bmatrix} + K_k z_k \delta_{i-1}, \quad i = 1, \cdots, S \tag{4.14}$$

If all the observations are made only on the state of the system we have that:

$$\begin{bmatrix} \left( y_k^a \right)^i \\ \left( \theta_k^a \right)^i \end{bmatrix} = \left( I - K_k H_k \right) \left( y_k^f \right)^i + K_k z_k \delta_{i-1}, \quad i = 1, \cdots, S \tag{4.15}$$

The covariance of the extended state vector is:

$$P_k = \mathrm{cov}\left(\begin{bmatrix} y_k \\ \theta_k \end{bmatrix}\right) = \begin{bmatrix} \mathrm{cov}(y_k) & \mathrm{cov}([y_k, \theta_k]) \\ \mathrm{cov}([\theta_k, y_k]) & \mathrm{cov}(\theta_k) \end{bmatrix} = \begin{bmatrix} P_{yy}^k & P_{y\theta}^k \\ P_{\theta y}^k & P_{\theta\theta}^k \end{bmatrix},$$
$$\begin{bmatrix} H_k & 0 \end{bmatrix} P_k \begin{bmatrix} H_k^T \\ 0 \end{bmatrix} = H_k P_{yy} H_k^T \tag{4.16}$$

The Kalman gain reads:

$$K_k = P_k \begin{bmatrix} H_k^T \\ 0 \end{bmatrix} \left(R_k + H_k P_{yy}^k H_k^T\right)^{-1} = \begin{bmatrix} P_{yy}^k H_k^T \\ P_{\theta y}^k H_k^T \end{bmatrix} \left(R_k + H_k P_{yy}^k H_k^T\right)^{-1} \tag{4.17}$$

The parameter estimate is then:

$$\theta_k^a = \theta_k + P_{\theta y}^k H_k^T \left(R_k + H_k P_{yy}^k H_k^T\right)^{-1} \left(z_k - H_k y_k\right) \tag{4.18}$$

In the polynomial chaos framework the covariance matrices $P_{yy}$ and $P_{\theta y}$ can be estimated from the polynomial chaos expansion of the solution and the parameters. Then the polynomial chaos coefficients of the parameters are adjusted as:

$$\left(\theta_k^a\right)^i = \left(\theta_k\right)^i + P_{\theta y}^k H_k^T \left(R_k + H_k P_{yy}^k H_k^T\right)^{-1} \left(z_k \cdot \delta_{i-1} - H_k y_k^{\,i}\right),\ i = 1, \cdots, S \tag{4.19}$$

Let's note that the Kalman filter formula is optimal for the linear Gaussian case. For non-Gaussian uncertainties the Kalman filter formula is sub-optimal, but is still expected to work.

Another possible approach is to apply the filter formula only once, on a vector containing all the observations from $t_1$ to $t_k$:

$$\left(\theta^a\right)^i = \left(\theta_0\right)^i + P_{\theta y} H^T \left(R + H P_{yy} H^T\right)^{-1} \left(z \cdot \delta_{i-1} - H y^i\right),\ i = 1, \cdots, S \tag{4.20}$$

where

$$z = \left[(z_1)^T \quad \ldots \quad (z_k)^T \quad \ldots \quad (z_N)^T\right]^T \tag{4.21}$$

$$H = \mathrm{diag}\left(H_1, \cdots, H_N\right) \tag{4.22}$$

$$R = \mathrm{diag}\left(R_1, \cdots, R_N\right) \tag{4.23}$$

$$P_{\theta y} = \mathrm{cov}([\theta_0, y]),\ P_{yy} = \mathrm{cov}(y) \ \text{ with } \ y = \left[(y_1)^T \quad \ldots \quad (y_k)^T \quad \ldots \quad (y_N)^T\right]^T \tag{4.24}$$

The original approach will be called the one-time-step-at-a-time EKF approach, and this alternative approach will be called the whole-set-of-data-at-once EKF approach. The two approaches are equivalent only for linear systems with Gaussian assumptions. Even in that case, they might not always be equivalent in practice, due to numerical issues.

The polynomial chaos theory allows for nonlinear propagation of the covariance matrix, which is likely to lead to improvements over the traditional EKF. The traditional EKF performs a linear propagation of the covariance through linearized dynamic systems. For example, consider the system $y' = 1 - y^2$, which has a solution $y_{ref}(t) = \tanh(t)$. Let us go through one step of filtering from $t_0 = -1$ to $t_f = 1$ assuming an initial guess $y_0 = -0.7$ with a standard deviation $y_{std} = 0.1$ and a Beta (2, 2) distribution, which would be based on previous filtering steps. The reference solution at $t_0 = -1$ is actually $y_{ref}(t_0) = \tanh(-1) = -0.7616$. The observation at $t_f = 1$ will be $y_{ref}(t_f) = \tanh(1) = 0.7616$, with an added measurement noise assumed to be Gaussian with a zero mean and a variance 1% of the value of the observation. Using 1000 runs in order to account for the noise, the average estimate obtained at $t_f = 1$ using the polynomial chaos based EKF estimation method with five terms in the polynomial chaos expansions and 10 collocation points is 0.8124, while the average estimate obtained with the traditional EKF using linear propagation is 0.8623. In other words, the polynomial chaos based EKF yields an average error of 0.0508 while the traditional EKF with linear propagation yields an average error of 0.1007. The collocation approach is explained in Section 2.1.

Figure 4.1(a) shows the distribution of the forecast state $y_f$ obtained with traditional EKF using linear propagation with 1000 runs. Figure 4.1(b) shows the distribution of the forecast state $y_f$ obtained with the polynomial chaos based EKF with 1000 runs. With the polynomial chaos based EKF estimation method, the skewness of the forecast state $y_f$ can be represented, while using the traditional EKF with linear propagation results in a Gaussian distribution of the forecast state $y_f$. As a consequence, the polynomial chaos based EKF approach leads to a better estimate, which is obtained using the assimilated state $y_a$, as shown in Figs. 4.1(c) and 4.1(d). For this example, the error obtained using the polynomial chaos based EKF approach is about half the error obtained using the traditional EKF approach.

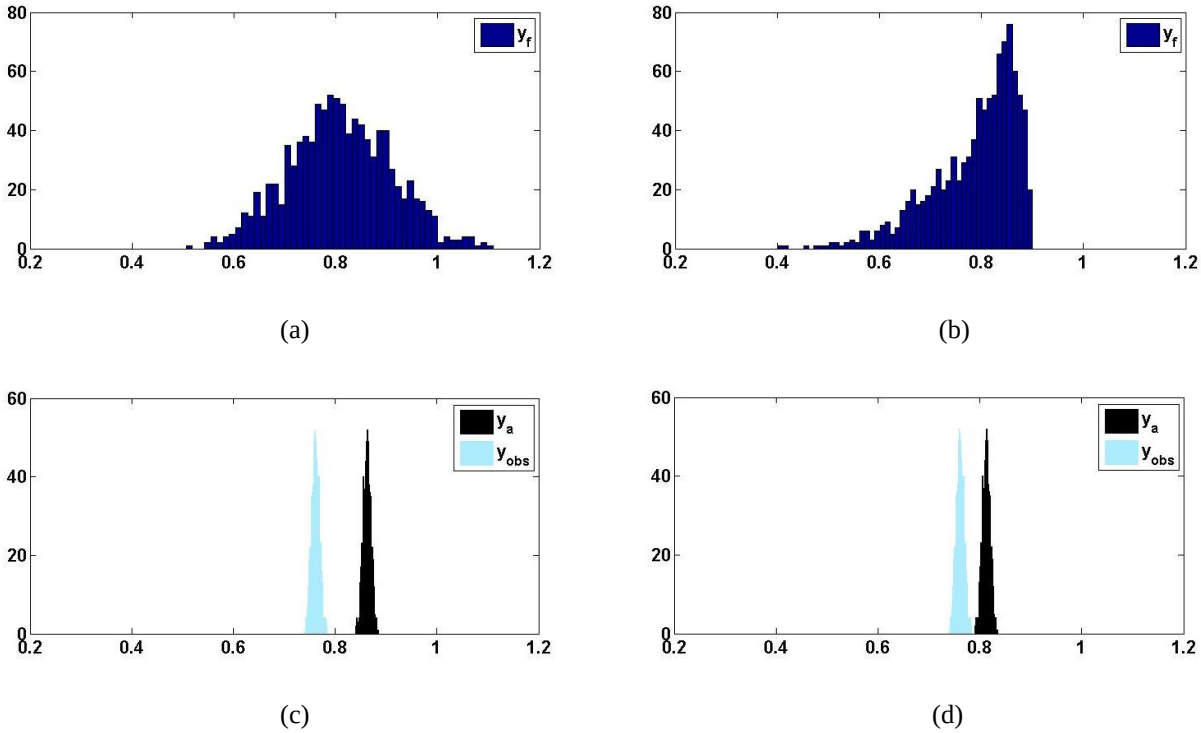


Figure 4.1: Polynomial Chaos Based EKF vs. Traditional EKF Using Linear Propagation Histograms: (a) Forecast State for EKF with Linear Propagation; (b) Forecast State for Polynomial Chaos Based EKF; (c) Assimilated State for EKF with Linear Propagation; (d) Assimilated State for Polynomial Chaos Based EKF

## 4.2 Insight into the EKF Approach Using the Roll Plane Model

The model used to apply the theory presented in this chapter is the same roll plane model of a vehicle used in Chapter 3. It is based on the same four degree of freedom roll plane model of a vehicle used in [102] with the addition of a mass on the roll bar, as shown in Figure 3.16. The parameters still have the same values than in Chapter 3, and their values can be found in Table 3.1. The uncertain parameters are still the value of the added mass $M$, and the distance $d_{CG}$ between its center of gravity and the roll bar. It is still assumed that the probability density functions of the values of $M$ and $d_{CG}$ can be represented with Beta (2, 2) distributions, with uncertainties of +/- 50% and +/- 25%, respectively, as shown in Figure 3.17. The polynomial

chaos expansions of all the variables affected by the uncertainties on $M$ and $d_{CG}$ are still modeled by polynomials chaos expansions using 15 terms, and 30 collocation points will be used to derive the coefficients associated to each of the 15 terms of the different polynomial chaos expansions. The set of collocation points is still the same one that was used in Chapter 3, which is shown in Figure 2.2(b)

The impact of enforcing dynamics at these few collocation points is discussed in [19]. In practice, using collocation with judicious algorithms such as using the Hammersley/Halton points yields very similar results to what is obtained with Galerkin, when using enough collocation points. Practically, what needs to be done is checking that adding more terms and more collocation points does not significantly improve the results. Even though the number of points needed in order to obtain satisfactory results is quite dependent on the example used for parameter estimation, a satisfactory number of points will typically result in a much faster computation time than any Monte-Carlo based simulation. An example comparing the computational efficiency of a simulation using the polynomial chaos theory with collocation points and a Monte Carlo based simulation yielding the exact same accuracy can be found in Table 3 in [73].

### 4.2.1. Results for a Speed Bump Input

The road profile referred to as the speed bump is the same one than in Chapter 3, which was shown in Figure 3.18. It is still assumed that the vehicle has a constant speed of 16 km/h (10 mph). For the proof of concept of the parameter estimation method presented in this chapter, we still pretend we do not know the values of $M$ and $d_{CG}$, the objective being to estimate those values based on the plot of the four motion variables shown in Figure 3.19(a).The measurements shown in Figure 3.19(a) are synthetic measurements obtained from a reference simulation with the reference value of the uncertain parameter $M^{ref} = 223.26 \text{ kg}$ and $d_{CG}{}^{ref} = 0.6882 \text{ m}$ (i.e., $\xi_1{}^{ref} = 0.2326$ and $\xi_2{}^{ref} = -0.3875$). Parameters estimation is performed using the EKF approach. In order to work with a realistic set of measurements, a Gaussian measurement noise with zero mean and 1% variance is added to the observations shown in Figure 3.19 (for the relative displacements and velocities) before performing parameter estimation. Let's remind that

the EKF filter formulas in the polynomial chaos framework are defined by equations (4.19-4.23), and that in this case, the matrices $H_k$'s are all equal to the matrix which was defined in Equation (3.58), the measurements $z_k$'s are still the same ones that were shown in Equation (3.59). Finally, $\theta$ and $\theta_0$ are defined by:

$$\theta = \begin{bmatrix} M & d_{CG} \end{bmatrix}^T, \quad \theta_0 = \begin{bmatrix} 200 & 0.7620 \end{bmatrix}^T \tag{4.25}$$

The estimated values of $\xi_1$ and $\xi_2$ obtained using the one-time-step-at-a-time EKF approach with 10 sample points (i.e., with time steps of 0.3 s), which are given by the first terms of the corresponding polynomial chaos expansions, are ${\xi_1}^{est} = 0.2240$ and ${\xi_2}^{est} = -0.4415$, i.e., $M^{est} = 222.40$ kg and ${d_{CG}}^{est} = 0.6779\,\text{m}$, which seems to be a good estimation considering that only 10 measurement points were used and that there is noise associated to the measurements. The actual values were ${\xi_1}^{ref} = 0.2326$ and ${\xi_2}^{ref} = -0.3875$, i.e., $M^{ref} = 223.26$ kg and ${d_{CG}}^{ref} = 0.6882\,\text{m}$. The EKF estimations come in the form of PDFs, as shown in Figure 4.2(a) for $M$, and Figure 4.2(b) for $d_{CG}$. The estimated values and the corresponding standard deviations at each time step are plotted in Figure 4.2(c) for $M$, and Figure 4.2(d) for $d_{CG}$. The standard deviations are computed using Equation (2.27).

With 100 sample points (i.e., with time steps of 0.03 s instead of 0.3 s) and a noise level of 1%, the estimated values of $\xi_1$ and $\xi_2$ obtained using the one-time-step-at-a-time EKF approach are ${\xi_1}^{est} = 0.3988$ and ${\xi_2}^{est} = -0.0834$, i.e., $M^{est} = 239.88$ kg and ${d_{CG}}^{est} = 0.7461\,\text{m}$. This is illustrated in Figure 4.3, which shows that the one-time-step-at-a-time EKF approach does not work anymore when using a time step of 0.03 s instead of 0.3 s.

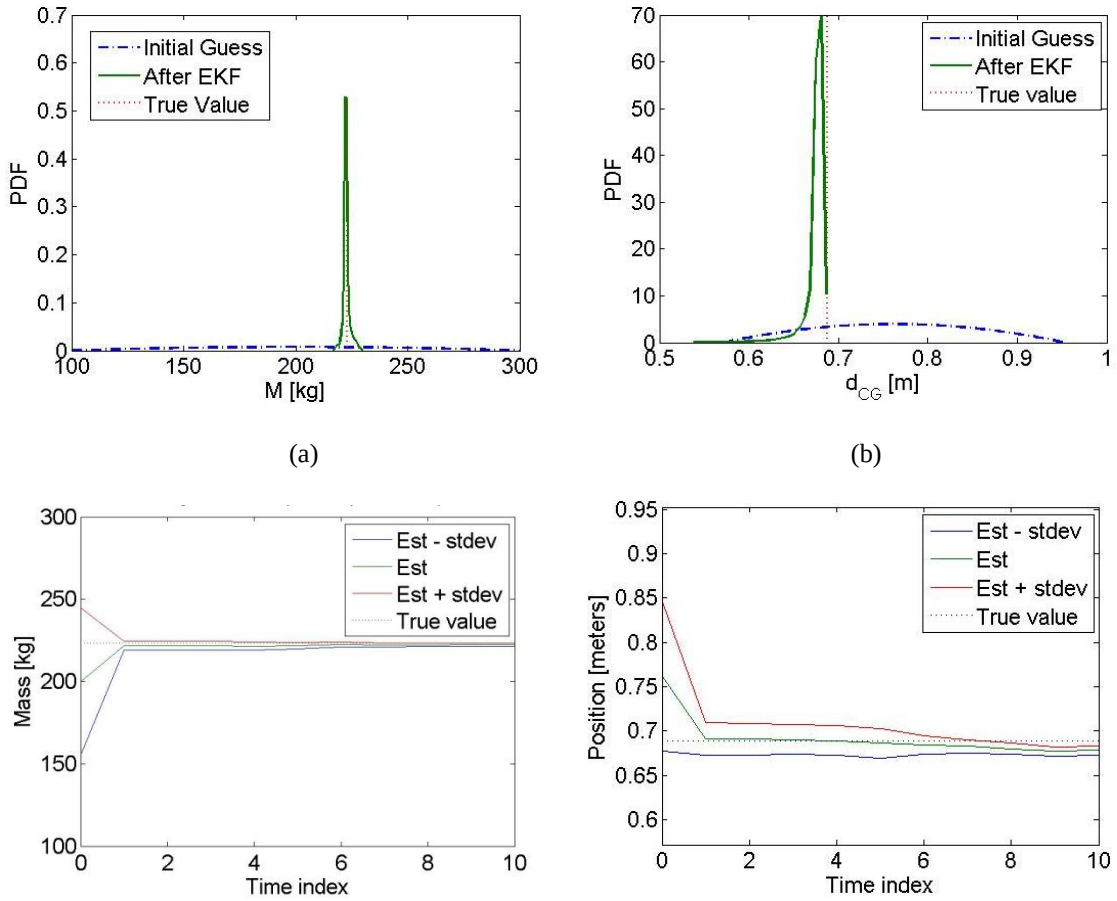


Figure 4.2: EKF Estimation (One-Time-Step-at-a-Time) for Speed Bump Input with 10 Time Points (Noise = 1%): (a) Mass in the Form of PDF; (b) Distance in the Form of PDF; (c) Mass for Each Term Index; (d) Distance for Each Term Index

Figure 4.4 shows the absolute error for our two estimated parameters, i.e., $\left| \xi_{1,est} - \xi_{1,ref} \right|$ and $\left| \xi_{2,est} - \xi_{2,ref} \right|$, with respect to the number of time points, and equivalently, the length of the time step, which is inversely proportional to the number of time points. It can be observed that a long time step is not really desirable, which one would expect since less information is available for longer time steps. However, a short time step is even less desirable. This seems to be counterintuitive since one would expect that more information would yield more accurate results.

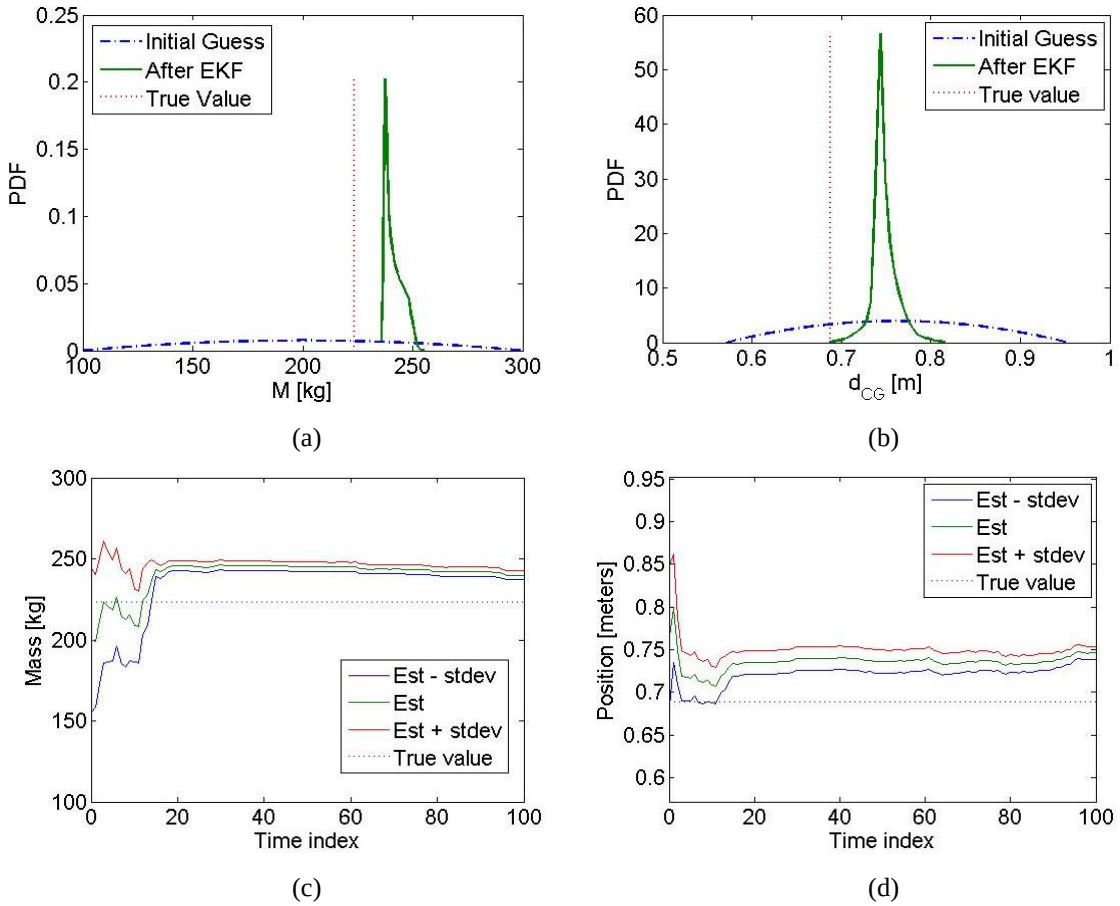


Figure 4.3: EKF Estimation (One-Time-Step-at-a-Time) for Speed Bump Input with 100 Time Points (Noise = 1%): (a) Mass in the Form of PDF; (b) Distance in the Form of PDF; (c) Mass for Each Term Index; (d) Distance for Each Term Index

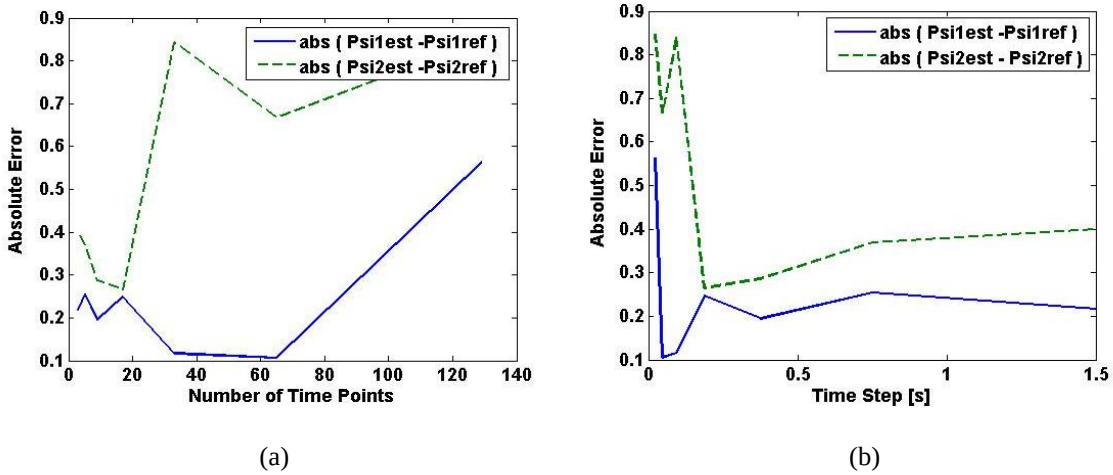


Figure 4.4: Absolute Error for the Estimated Parameters $\xi_1$ and $\xi_2$ with the Nonlinear Half-Car Model for the Speed Bump with Respect to: (a) the Number of Time Points; (b) the Length of the Time Step

The problem is that the EKF can diverge when using a high sampling frequency. When applying the polynomial chaos theory to the Extended Kalman Filter (EKF), numerical errors can accumulate even faster than in the general case due to the truncation in the polynomial chaos expansions. It is shown in Appendix that for the simple scalar system $y' = a\,y$ with $a < 0$ (where $a$ is known), the truncations in the polynomial chaos expansions can prevent the convergence of the covariance of the assimilated state $y_a$. It is also shown in Appendix that the covariance of the error after assimilation $E_k^a = y_k^a - y_{tk}^{true}$ decreases with the time step $\Delta t$ when there is no model error (which is the case for this study), meaning that using means a larger $\Delta t$ results in a smaller error (unless the covariance of $y_a$ has not converged yet, which can happen when $\Delta t$ is too large). Figures 4.3(c) and 4.3(d), which plotted the estimated values of the two parameters +/- their standard deviations, showed that the results with a time step of 0.03 s could not be trusted, because the EKF was diverging. Indeed, the range of values spanned by the estimated values +/- their standard deviations at time index $k$ does not always include the range of values spanned by the estimated values +/- their standard deviations at time index $k+1$. The curves representing the estimated values +/- the standard deviations of the estimations can decrease and suddenly increase with new observations or vice versa, unlike what was observed in Figures 4.2(c) and 4.2(d), where the curves representing the estimated values +/- their standard deviations smoothly decrease/increase. Therefore, it is judicious to look at the estimated values and their standard deviations at each time step. When the estimated values +/- their standard deviations display non-monotonous behaviors, it is a sign that the sampling frequency should be decreased. Sampling below the Nyquist frequency is usually a necessity in order to prevent the EKF from diverging. In most cases, sampling below the Nyquist frequency does not result in non-identifiability issues, but it can in a few rare cases, as illustrated in Chapter 3.

Another possible approach is to apply the filter formula only once, on a vector containing all the observations from $t_1$ to $t_k$. Using this alternative approach, we get better results with a Gaussian measurement noise with zero mean and 1% variance, for both 10 time points (Figure 4.5) and 100 time points (Figure 4.6). Applying the EKF formula on the whole set of data at once with 10 time points yields $\xi_1^{\,est} = 0.2321$ and $\xi_2^{\,est} = -0.3969$, i.e., $M^{est} = 223.21$ kg and

$d_{CG}{}^{est} = 0.6864\,\text{m}$. Applying the EKF formula on the whole set of data at once with 100 time points yields $\xi_1{}^{est} = 0.2305$ and $\xi_2{}^{est} = -0.3773$, i.e., $M^{est} = 223.05$ kg and $d_{CG}{}^{est} = 0.6901\,\text{m}$. For this particular road input, applying the filter formula only once, on a vector containing all the observations clearly yields better results, and this whole-set-of-data-at-once EKF approach still works with a sampling rate of 0.03 s, while the one-time-step-at-a-time EKF approach was clearly not working.

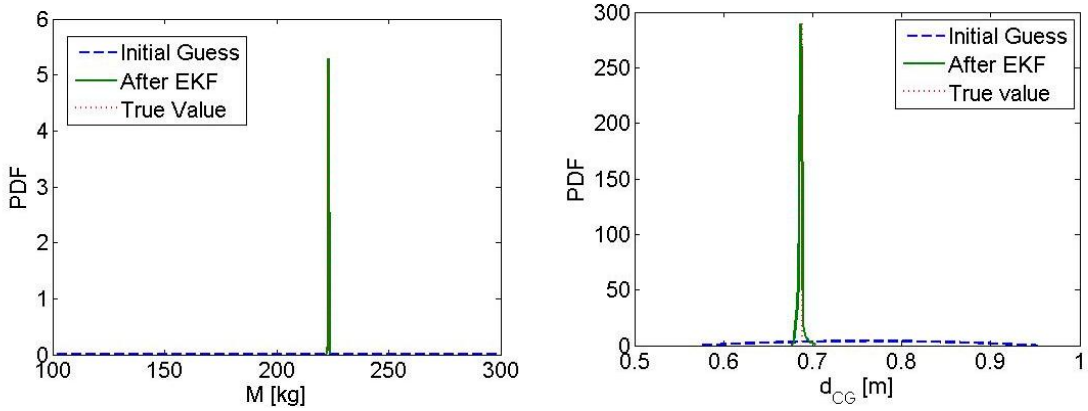


(a) (b)

Figure 4.5: EKF Estimation (Whole-Set-of-Data-at-Once) for Speed Bump Input with 10 Time Points (Noise = 1%): (a) Mass in the Form of PDF; (b) Distance in the Form of PDF

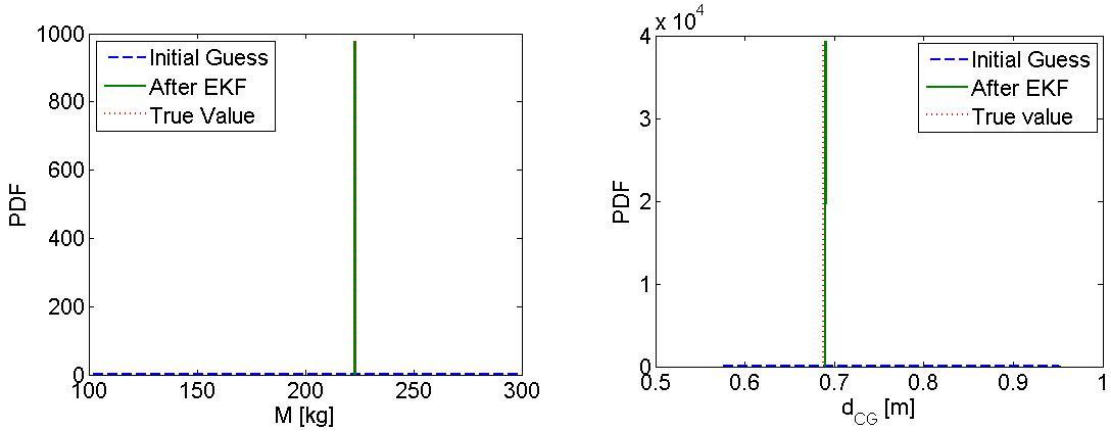


(a) (b)

Figure 4.6: EKF Estimation (Whole-Set-of-Data-at-Once) for Speed Bump Input with 100 Time Points (Noise = 1%): (a) Mass in the Form of PDF; (b) Distance in the Form of PDF

### 4.2.2. Relationship Between Quality of Estimation and the Frequency of the Input Signal

In order to continue assessing the efficiency of the polynomial chaos theory for parameter estimation, the estimations will now be performed for different harmonic inputs, ranging from 0.33 Hz to 25 Hz, with, with amplitudes of +/- 0.05 m for $y_1$ and $y_2$. The input signal is supposed to be exactly known, which enables us to use any desired sampling rate for the input signal. A Gaussian measurement noise with zero mean and 1% variance is still added to the observations.

Figure 4.7 shows the results obtained when using the one-time-step-at-a-time EKF approach with 10 time points, i.e., with a sampling rate of 0.3 s. Figure 4.7(c) shows that the estimation of the mass should actually not be trusted for the reasons explained previously. It can also be observed in Figure 4.7(a): the PDF contains values above 300 kg, i.e., outside the range of the Beta (2, 2) distribution, which means the filter has convergence problems.

Figure 4.8 shows the results obtained when using the whole-set-of-data-at-once EKF approach with the same 10 time points. It yields better results for the estimation of the distance, but not for the estimation of the added mass. This shows that this alternative approach does not necessarily work better for every problem, even though it often yields better results, as it clearly did with the speed bump.

Figure 4.9 shows the results obtained when using the one-time-step-at-a-time EKF approach with 100 time points, i.e., with a sampling rate of 0.03 s. The filter clearly diverges and the estimations cannot be trusted, which is especially evident for the estimation of the mass.

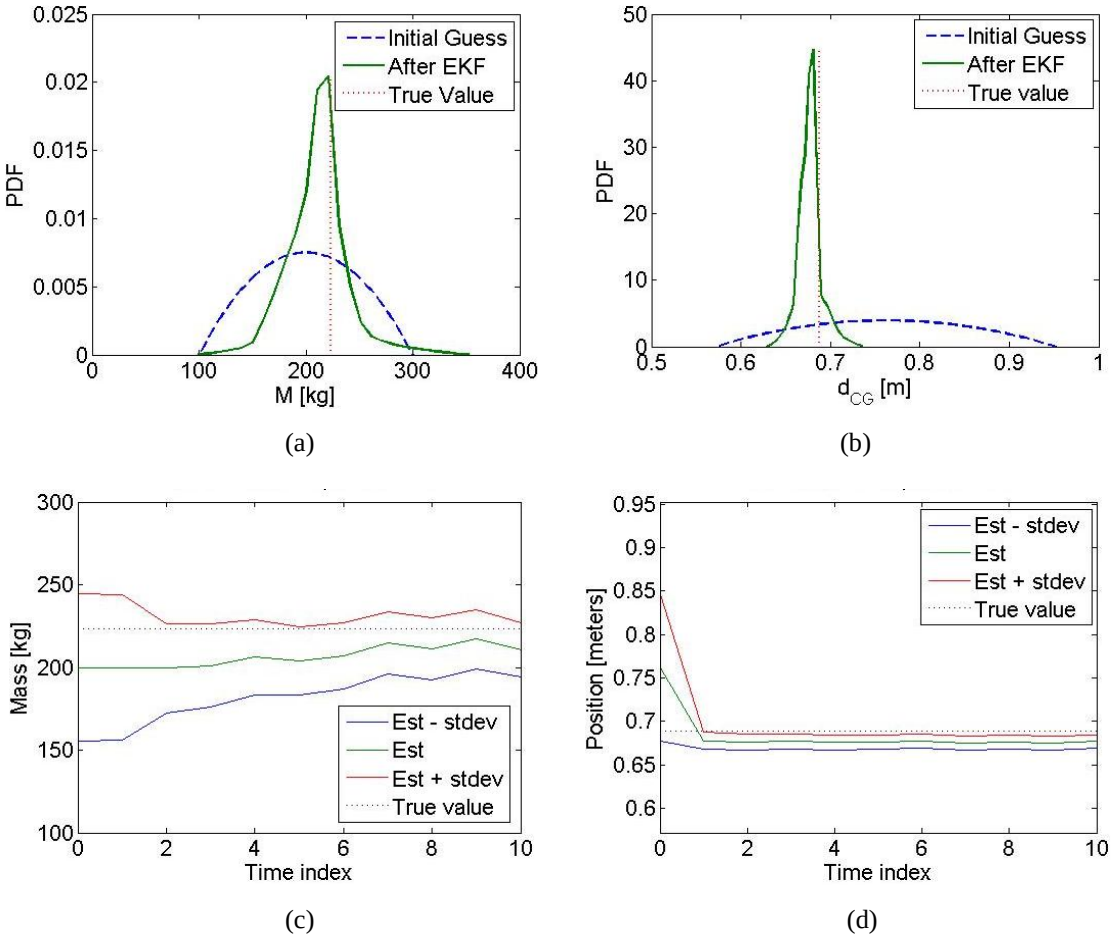


(a) (b)

(c) (d)

Figure 4.7: EKF Estimation (One-Time-Step-at-a-Time) at 1 Hz with 10 Time Points (Noise= 1%): (a) Mass in the Form of PDF; (b) Distance in the Form of PDF; (c) Mass at Each Time Index; (d) Distance at Each Time Index

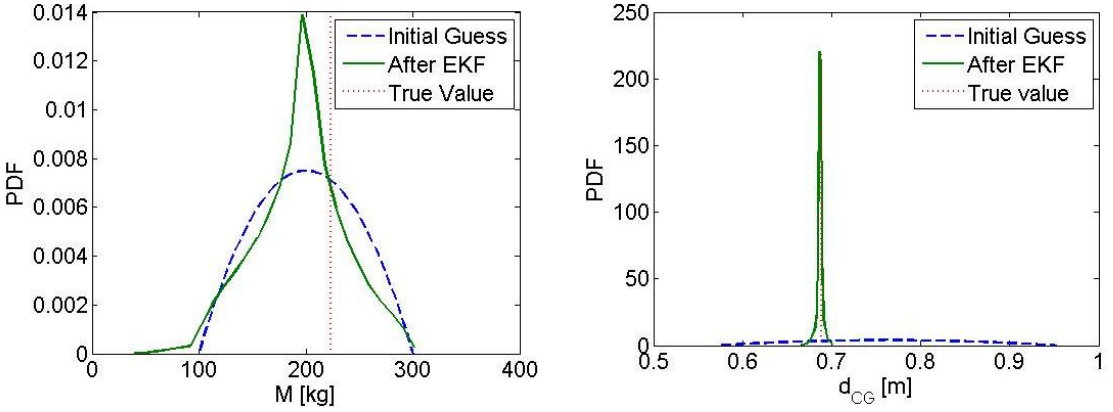


(a) (b)

Figure 4.8: EKF Estimation (Whole-Set-of-Data-at-Once) at 1 Hz with 10 Time Points (Noise= 1%): (a) Mass in the Form of PDF; (b) Distance in the Form of PDF

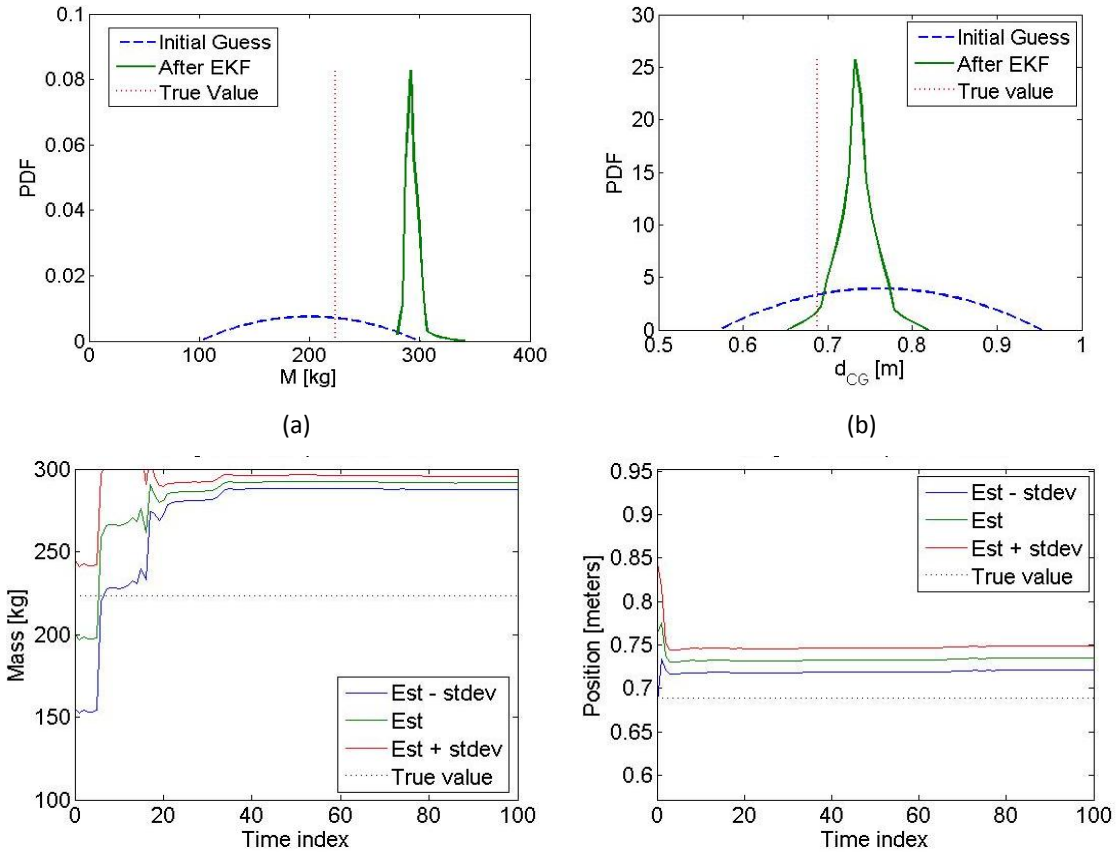


Figure 4.9: EKF Estimation (One-Time-Step-at-a-Time) at 1 Hz with 100 Time Points (Noise= 1%): (a) Mass in the Form of PDF; (b) Distance in the Form of PDF; (c) Mass at Each Time Index; (d) Distance at Each Time Index

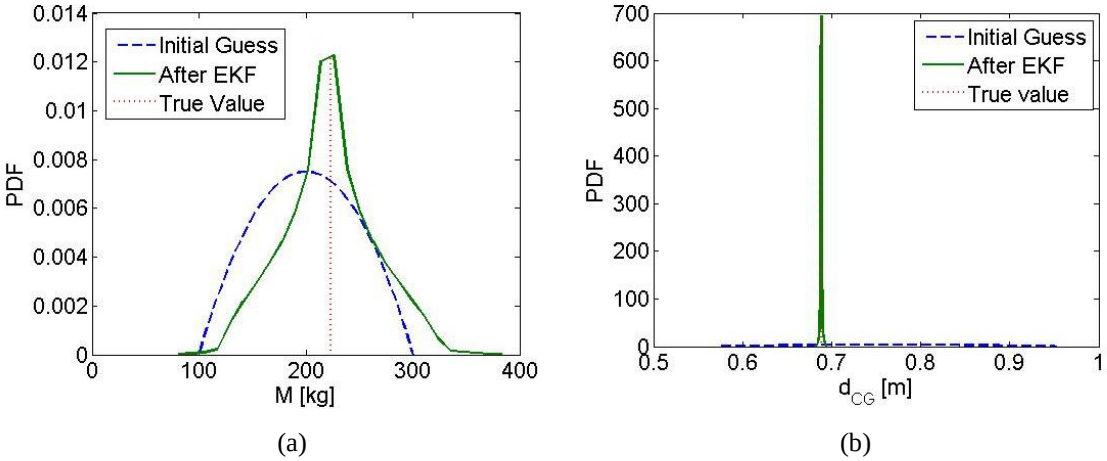


Figure 4.10: EKF Estimation (Whole-Set-of-Data-at-Once) at 1 Hz with 100 Time Points (Noise = 1%): (a) Mass in the Form of PDF; (b) Distance in the Form of PDF

Figure 4.10 shows the results obtained when using the whole-set-of-data-at-once EKF approach with the same 100 time points. The estimation of the mass comes with a large standard deviation, but this approach actually yields an acceptable estimation for the mass: $M^{est} = 221.12$ kg ($\xi_1^{est} = 0.2112$). In this case, the whole-set-of-data-at-once EKF approach yields better results with 100 time points than with 10 time points. However, the whole-set-of-data-at-once approach still does not solve all the drawbacks associated with the use of an EKF. It can be observed that the PDF contains values outside the range of the Beta (2, 2) distribution, i.e., below 100 kg or above 300 kg, so the convergence problems also appear to affect the whole-set-of-data-at-once approach. When the whole-set-of-data-at-once approach yields a PDF with a large range of possible values, it is not clear how much it can be trusted. As a conclusion, the EKF estimation obtained when applying the filter formula only once on the whole set of data can sometimes yield much better results, but not always, so comparing the results to a different approach (e.g., a Bayesian approach) is strongly recommended. Parameter estimation has also been performed for the same system using linear springs and dampers and it was observed that the PDFs obtained for the linear case and the nonlinear case were quite similar, which indicates that the problems we encountered do not seem to come from the nonlinearities in the springs and dampers.

## 4.3 Summary and Conclusions

In this chapter, a new computational approach for parameter estimation based on the Extended Kalman Filter (EKF) and the polynomial chaos theory is proposed. The error covariances needed by the EKF are computed from polynomial chaos expansions, and the EKF is used to update the polynomial chaos representation of the uncertain states and the uncertain parameters. The proposed method has several advantages. It benefits from the computational efficiency of the polynomial chaos approach in the simulation of systems with a small number of uncertain parameters. The filter formula based on the EKF is also computationally inexpensive. Polynomial chaoses offer an accurate representation of uncertainties and can accommodate non-Gaussian probability distributions. The approach gives more information about the parameters of

interest than a single value: the estimation comes in the form of a polynomial chaos expansion from which the aposteriori probability density of the estimated parameters can be retrieved.

For illustration we consider a nonlinear four degree of freedom roll plane model of a vehicle, and we estimate the uncertain mass and the uncertain position of a body added on the roll bar. The apriori uncertainties on the values of the added mass and its position were assumed to have a Beta (2, 2) distribution. Synthetic observations of the displacements and velocities across the suspensions are obtained by adding "measurement noise" to the reference simulation results. Two different inputs were used: a speed bump and a 1-Hz sinusoidal roll.

Two variations of the approach are discussed: the one-time-step-at-a-time EKF approach, in which the Kalman filter formula is used at each time step in order to update the polynomial chaos expressions of the uncertain states and the uncertain parameters, and the whole-set-of-data-at-once EKF approach, which consists of applying the filter formula once, on a vector containing all the observations. For linear systems with Gaussian distribution of uncertainty the two approaches are theoretically equivalent. For the test problem under consideration the one-time-step-at-a-time EKF approach yields good estimations for lower sampling rates, but the quality of these estimations deteriorates with increasing the sampling rate. We explain this counter-intuitive behavior via a rigorous error analysis carried out in Appendix. The polynomial chaos truncation errors affect the solution at each filter step; more filter steps mean more information but also more errors. The truncation errors can accumulate at a fast rate, and over-ride the benefits of the additional information coming from more measurements. To alleviate this effect we discuss a version of the filter that uses all the information in a single batch. In most cases, the whole-set-of-data-at-once EKF approach yields more accurate results than the ones obtained with the one-time-step-at-a-time EKF approach. For a few of the input excitations and sampling frequencies, however, the results are not very accurate; therefore it is recommended to repeat the estimation with different sampling rates in order to verify the coherence of the results.

# 5 Bayesian Approach vs. EKF Approach

The objective of this chapter is to compare the results obtained with the Bayesian approach presented in Chapter 3 and the results obtained with the whole-set-of-data-at-once EKF approach presented in Chapter 4, which yielded better results than the original one-time-step-at-a-time EKF approach. After a quick overview of the parameter estimation methods, important results will be analyzed and compared in order to draw conclusions on the advantages and drawbacks of each method.

## 5.1 Overview of the Two Polynomial-Chaos Based Estimation Methods

### 5.1.1 Bayesian approach

Chapter 3 introduced the Bayesian approach for parameter estimation. Using polynomial chaoses the uncertain parameters were modeled explicitly as functions of a set of random variables. The values minimizing the cost function (3.12) gives the most likely values of our uncertain parameters. The applicability of the methodology developed was first illustrated on a simple mass-spring system with uncertain initial velocity, which was used as a support to discuss how the cost function is affected by undersampling, non-identifiability of the system, non-observability, and relevance of excitation signal on the estimation capability. It was showed that the accuracy of their estimation depends on several factors. A sharp minimum in the shape of the Bayesian cost function has been used as a direct indication of the gravity of the maximum likelihood estimation. The parameters are non-identifiable when different parameter values lead to identical system outputs. In this case the Bayesian cost function has an entire region of minima (e.g., a valley), with each parameter value in the region being equally likely. Regularization techniques can still yield most likely values among the possible combinations of uncertain parameters resulting in the same time responses than the ones observed. This was illustrated using a simple spring-mass system. For identifiable and observable systems accurate estimates can be obtained in most cases even if the output signal is sampled below the Nyquist

frequency. In the worst case, however, sampling below the Nyquist rate cannot guarantee that sufficient information is extracted from the output. In this worst case the apriori information becomes important and the estimate is biased toward the apriori most likely value. When the cost function has no clear minimum but of region of minima, we know whether it is a non-identifiability issue or an issue related to sampling below the Nyquist frequency by plotting the outputs of the ODE's for different values of the uncertain parameter belonging to the region of minima. If the different values yield different time plot, it is sampling frequency issue. If they yield identical time plots, it is a non-identifiability issue. In Section 3.3, the Bayesian approach was applied to a more complex system: nonlinear four degree of freedom roll plane model of a vehicle, in which an uncertain mass with an uncertain position is added on the roll bar. In the next section, these results will be compared with the results obtained with the same roll plane model using the EKF approach

### 5.1.2 EKF Approach

Chapter 4 introduced the EKF approach. The first version of this approach was called the one-time-step-at-a-time EKF approach. For the nonlinear four degree of freedom roll plane model of a vehicle example under consideration in this study, it was shown that the one-time-step-at-a-time EKF approach yielded good estimations for lower sampling rates, but the quality of these estimations deteriorated when increasing the sampling rate. This counter-intuitive behavior was explained via a rigorous error analysis in Appendix. The polynomial chaos truncation errors affect the solution at each filter step; more filter steps mean more information but also more errors. The truncation errors can accumulate at a fast rate, and over-ride the benefits of the additional information coming from more measurements. Sampling below the Nyquist frequency is usually a necessity.

To alleviate this effect, a version of the filter that uses all the information in a single batch was discussed, which was called the whole-set-of-data-at-once EKF approach. The filter formula is applied only once, on a vector containing all the observations .

The two EKF approaches are equivalent only for linear systems with Gaussian assumptions. Even in that case, they might not always be equivalent in practice, due to numerical issues. The

whole-set-of-data-at-once EKF approach yielded more accurate results than the ones obtained with the one-time-step-at-a-time EKF approach for the nonlinear four degree of freedom roll plane model of a vehicle used in this study. However, the results obtained with the whole-set-of-data-at-once EKF approach were still not always very accurate.

Therefore, the objective of this chapter is to use the Bayesian approach developed in Chapter 2 for the same roll plane model, and compare the results with the results obtained with the whole-set-of-data-at-once EKF approach.

## 5.2 Comparison of the Two Approaches Using the Roll Plane Model

The model used to compare the results of the two approaches is the same roll plane model of a vehicle which was already used in Chapter 3 and Chapter 4. It is based on the same four degree of freedom roll plane model of a vehicle used in [102] with the addition of a mass on the roll bar, as shown in Figure 3.16. The parameters still have the same values than in Chapter 3, and their values can be found in Table 3.1. The uncertain parameters are still the value of the added mass $M$, and the distance $d_{CG}$ between its center of gravity and the roll bar. It is still assumed that the probability density functions of the values of $M$ and $d_{CG}$ can be represented with Beta (2, 2) distributions, with uncertainties of +/- 50% and +/- 25%, respectively, as shown in Figure 3.17. Unless otherwise specified, the polynomial chaos expansions of all the variables affected by the uncertainties on $M$ and $d_{CG}$ are still modeled by polynomials chaos expansions using 15 terms, and 30 collocation points will be used to derive the coefficients associated to each of the 15 terms of the different polynomial chaos expansions. The set of collocation points is still the same one that was used in Chapter 3, which is shown in Figure 2.2(b).

The speed bump, the chirp input, and the harmonic inputs refer to the same inputs already used earlier. They were described in Sections 3.3.3, 3.3.4, and 3.3.5., respectively.

### 5.2.1. Speed Bump

The value of the cost function can be visualized, as shown in Figure 5.1. A simple Matlab code can estimate the values of $\xi_1$ and $\xi_2$ (and thus the values of $M$ and $d_{CG}$) corresponding to the minimum value of the cost function.

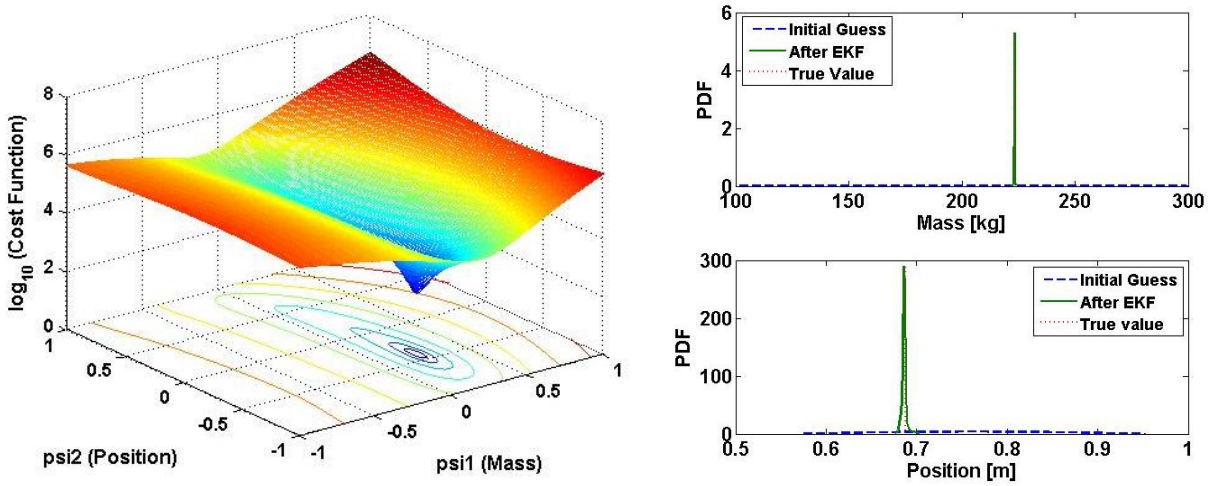


(a) (b)

Figure 5.1: Estimations for Speed Bump Input with 10 Time Points (Noise = 1%): (a) Cost Function Using the Bayesian Approach; (b) EKF Estimations (Whole-Set-of-Data-at-Once) in the Forms of PDFs

The estimated values of $\xi_1$ and $\xi_2$ obtained using the Bayesian approach are $\xi_1^{\ est} = 0.2236$ and $\xi_2^{\ est} = -0.4024$, i.e., $M^{\ est} = 222.36\,\text{kg}$ and $d_{CG}^{\ est} = 0.6853\,\text{m}$. The actual values were $\xi_1^{\ ref} = 0.2326$ and $\xi_2^{\ ref} = -0.3875$, i.e., $M^{\ ref} = 223.26\ \text{kg}$ and $d_{CG}^{\ ref} = 0.6882\,\text{m}$. It seems to be a good estimation since there is noise associated to the measurements. The estimated values of $\xi_1$ and $\xi_2$ obtained using the EKF approach are $\xi_1^{\ est} = 0.2321$ and $\xi_2^{\ est} = -0.3969$, i.e., $M^{\ est}\,223.21\,\text{kg}$ and $d_{CG}^{\ est} = 0.6864\,\text{m}$. The EKF approach therefore works better for this specific example.

Figure 5.2 shows the cost function that would be obtained if the motion variables could be measured with a sampling rate of 0.03 s, for a noise level of 1%. It can be observed that the extra measurement point do not change the shape of the cost function by much. The fact that the cost function had a well defined minimum value with 10 measurement points told us that we had enough information in order to obtain a precise estimation that can be trusted. Using 100 measurement points will add more accuracy, but not so much considering that the computing time will be 10 times greater.

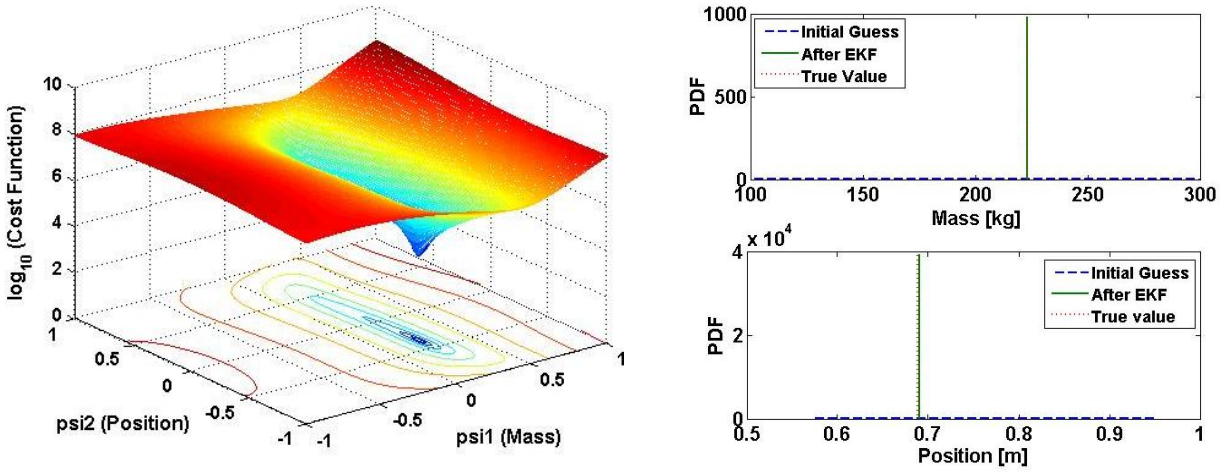


(a) (b)

Figure 5.2: Estimations for Speed Bump Input with 100 Time Points (Noise = 1%): (a) Cost Function Using the Bayesian Approach; (b) EKF Estimations (Whole-Set-of-Data-at-Once) in the Forms of PDFs

With 100 sample points and a noise level of 1%, which corresponds to the cost function shown in Figure 5.2, the estimated values of $\xi_1$ and $\xi_2$ obtained using the Bayesian approach are $\xi_1^{\,est} = 0.2339$ and $\xi_2^{\,est} = -0.3662$, i.e., $M^{\,est} = 223.39$ kg and $d_{CG}^{\,est} = 0.6922\,\text{m}$. The estimation of $\xi_1$ (i.e., of the added mass) is more accurate than with 10 measurement points, but the estimation of $\xi_2$ is not more accurate in this case. The estimated values of $\xi_1$ and $\xi_2$ obtained using the EKF approach are $\xi_1^{\,est} = 0.2305$ and $\xi_2^{\,est} = -0.3773$, i.e.,

$M^{est} = 223.05$ kg and $d_{CG}{}^{est} = 0.6901\,\mathrm{m}$. With the EKF approach, the estimation of the added mass is actually less accurate than it was with 10 measurement points, and the estimation of its position is not more accurate. One could think that the estimations would be more accurate with 100 measurement points after noticing that the aposteriori probability densities of the estimated parameters have a much smaller standard deviation, but the truncation errors can over-ride the benefits of the additional information coming from more measurements with the EKF approach that. This problem has been illustrated in Appendix via a rigorous error analysis for their one-time-step-at-a-time EKF approach. That problem has also been observed to a lesser extent for the whole-set-of-data-at-once EKF approach used here. This is an advantage of the Bayesian approach over the EKF approach. For both approaches, truncation errors in the polynomial chaos can affect the results. However, for the EKF approach, these errors can get larger when the number of measurement points is increased, which is never observed with the Bayesian approach when the cost function has a well defined minimum. With the Bayesian approach, adding measurement points to a set of points already yielding an estimation we know to be already quite accurate (i.e., the cost function has a very clear minimum) can randomly slightly change the estimates to slightly less accurate values due to truncations in the polynomial chaos expansions, but adding measurement points will not deteriorate the results in a very significant way unless there is at least a small region of minima (e.g., a valley), with each parameter value in the region being almost equally likely, as explained and illustrated in Chapter 3. In that case, any tiny change in the set of measurements will randomly yield another result somewhere in that valley of minima: the algorithm will be very sensitive to noise and approximations in that region.

Table 5.1 and Table 5.2 show the effect of the Polynomial Chaos approximation for the Bayesian approach and the EKF approach, respectively, with 10 measurement points. Table 5.1 and Table 5.2 show that the results of the estimation processes are affected by the number of terms used in the polynomial chaos approximation and by the number of collocation points. Adding more measurement points is desirable if the computational cost is not already high, which also depends on the complexity of the system. If the computational time is an issue and the cost function yields a clear minimum in the Bayesian case, or the standard deviation of the aposteriori probability densities of the estimated parameters are already small in the EKF case, not adding more measurements might be a good idea then.

Table 5.1: Effect of the Polynomial Chaos Approximation for the Bayesian Approach (with 10 Time Points and a Gaussian Measurement Noise with Zero Mean and 1% Variance)

| Number of Collocation Points | 10 terms | 15 terms | 21 terms |
|---|---|---|---|
| 10 | 0.2305, -0.3864 | | |
| 15 | 0.2249, -0.3793 | 0.2307, -0.3790 | |
| 21 | 0.2218, -0.3918 | 0.2307, -0.3885 | 0.2239, -0.5036 |
| 30 | 0.2224, -0.3869 | **0.2236, -0.4024** | 0.2279, -0.4012 |
| 40 | | | 0.2275, -0.4004 |
| 45 | | 0.2257, -0.4006 | |
| 60 | | | 0.2270, -0.3972 |
| Actual Values | 0.2326, -0.3875 | 0.2326, -0.3875 | 0.2326, -0.3875 |

Table 5.1 shows that the Bayesian estimations obtained with 15 terms become similar to the observations obtained with 21 terms as the number of collocation points gets larger. Therefore, working with 15 terms in the polynomial chaos expansions and with 30 collocation points seems to be a good comprise. Adding more terms and more collocation points would increase the precision of the estimation, but the extra precision would eventually become small compared with the effect of the noise, and would come at a great computational cost.

It can be noticed that when using the minimum number of collocation points required to perform the estimation, i.e., a number of collocation points equal to the number of terms, increasing the number of terms results in poorer estimations. This is something that has been observed on other test cases. For this case, it becomes very noticeable when using 21 terms and 21 collocation points. This makes sense since solving a system with more unknowns is more complicated, and adding extra information into a least squares algorithm becomes more valuable as the system becomes more complex.

The fact that the estimation performed with 10 collocations for 10 terms works so well in this particular case with the Bayesian approach seems to be due to a very favorable random choice of the collocation points. Using 10 terms in the polynomial chaos expressions results in approximations. Using only 10 collocation points also results in less precision. However, many approximations can still lead to an accurate result when they cancel out each other by chance.

Table 5.2: Effect of the Polynomial Chaos Approximation for the EFK Approach (with 10 Time Points and a Gaussian Measurement Noise with Zero Mean and 1% Variance)

| Number of Collocation Points | 10 terms | 15 terms | 21 terms |
|---|---|---|---|
| 10 | 0.2306, -0.3952 | | |
| 15 | 0.2295, -0.3990 | 0.2352, -0.3980 | |
| 21 | 0.2326, -0.4072 | 0.2335, -0.3849 | 0.2355, -0.3980 |
| 30 | 0.2319, -0.4092 | **0.2321, -0.3969** | 0.2335, -0.4000 |
| 40 | | | 0.2317, -0.3908 |
| 45 | | 0.2324, -0.3997 | |
| 60 | | | 0.2320, -0.3997 |
| Actual Values | 0.2326, -0.3875 | 0.2326, -0.3875 | 0.2326, -0.3875 |

Table 5.2 shows that the results using the EKF approach are less affected by the number of terms in the polynomial chaos expansions and the number of collocation points. The EKF approach is more affected by the number of measurement points. This is something that has been observed on other test cases. The estimated values of $\xi_1$ and $\xi_2$ obtained using the EKF approach with 15 terms and 30 collocation points but 100 measurement points were $\xi_1^{\,est} = 0.2305$ and $\xi_2^{\,est} = -0.3773$, which is quite different from all the results shown in Table 5.2.

## 5.2.2. Chirp Input

In this section, linear swept-frequency sine input signals are used from $t = 0$ to $t = 3\,\text{seconds}$ with frequencies ranging from 0 Hz at $t = 0$ to 2 Hz at $t = 3\,\text{seconds}$, as was shown in Figure 3.22. The amplitude of the input signals is 5 cm and the highest frequency of the chirp input used in this study was selected to be 2 Hz.

Parameters estimation is performed using the EKF approach the same way it was performed with the Bayesian approach in Chapter 3. In order to work with a realistic set of measurements, a Gaussian measurement noise with zero mean and 1% variance is added to the observed relative

displacements and velocities before performing parameter estimation. Figure 5.3 shows the cost function obtained with a sampling rate of 0.1 s, for a noise level of 1%. Since the maximum frequency in the chirp input is 2 Hz, using 30 measurement points is enough in order to respect the Nyquist criterion.

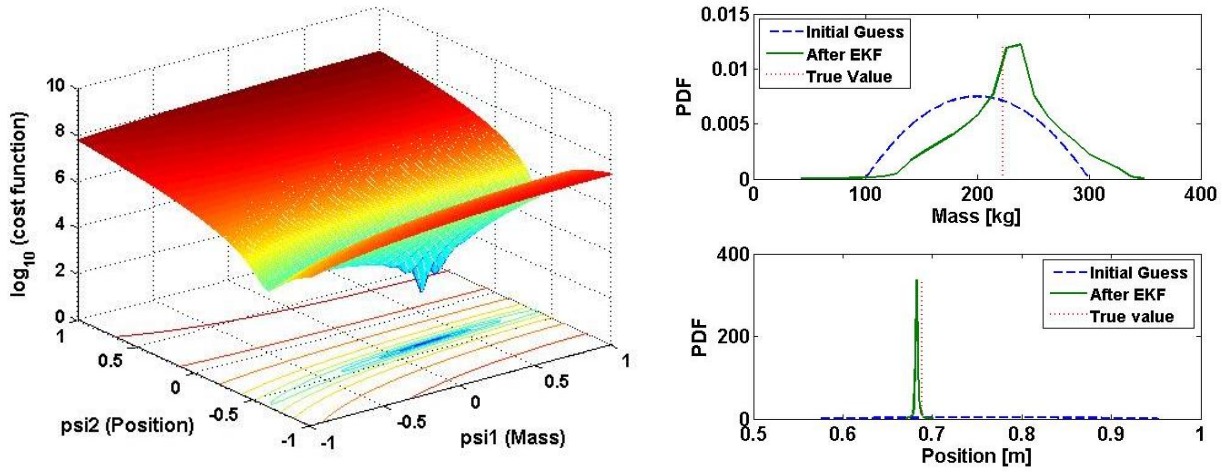


(a) (b)

Figure 5.3: Estimations for the Chirp Input with 30 Time Points and 1% Measurement Noise: (a) Cost Function Using the Bayesian Approach; (b) EKF Estimations (Whole-Set-of-Data-at-Once) in the Forms of PDFs

The estimated values of $\xi_1$ and $\xi_2$ obtained using the Bayesian approach are $\xi_1^{\,est} = 0.2364$ and $\xi_2^{\,est} = -0.3872$, i.e., $M^{\,est} = 223.64\,\text{kg}$ and $d_{CG}^{\,est} = 0.6882\,\text{m}$. The estimated values of $\xi_1$ and $\xi_2$ obtained using the EKF approach are $\xi_1^{\,est} = 0.3013$ and $\xi_2^{\,est} = -0.4181$, i.e., $M^{\,est} = 230.13\,\text{kg}$ and $d_{CG}^{\,est} = 0.6823\,\text{m}$. The actual values were $\xi_1^{\,ref} = 0.2326$ and $\xi_2^{\,ref} = -0.3875$, i.e., $M^{\,ref} = 223.26$ kg and $d_{CG}^{\,ref} = 0.6882\,\text{m}$. Using a chirp signal is therefore a good way to estimate the value of the mass and its position, as long as it does not contain frequencies where the dampers are in saturation mode most of the time, which actually starts being the case for frequencies above 1.5 Hz, as shown in Chapter 3 (Figure 3.32-3.34). This chirp input results in a case in which estimating our uncertain parameters is difficult, and

where it can be observed that the Bayesian approach is more reliable, which has been observed on other test cases too. The fact that the EKF approach yields a slightly inaccurate estimation of the mass is explained by the shape of the apriori PDF: it can be seen that the probability of the true value is not very different from the probability of the estimated mass. The fact that the EKF yields a poorer estimation of the position is more problematic since the PDF has a small standard deviation: it can lead the user into thinking that the estimate is quite accurate when it is not, whereas a having a Bayesian cost function with very clear minimum (which is not really the case for this latest cost function) is a very clear indication that the results can be trusted, as explained in Chapter 3. Another indication that the EKF approach cannot be trusted as much as the Bayesian approach is the fact that it yields values above 300 kg for the mass.

The cost function of the Bayesian approach has a clear minimum, but it can be seen that this minima is in a region of low values along the line. Adding higher frequency content in the input signal would start preventing us from obtaining a clear minimum along this line. This is illustrated in the next section.

### 5.2.3. Harmonic Inputs

In order to assess the efficiency of the polynomial chaos theory for parameter estimation, $M$ and $d_{CG}$ will be estimated using a plot of four motion variables: the displacements across the suspensions ($x_1 - x_{t1}$ and $x_2 - x_{t2}$), and their corresponding velocities ($\dot{x}_1 - \dot{x}_{t1}$ and $\dot{x}_2 - \dot{x}_{t2}$). The estimations will be performed for different harmonic inputs, ranging from 0.33 Hz to 25 Hz, with amplitudes of +/- 0.05 m for $y_1$ and $y_2$. The input signals are still supposed to be exactly known. The estimations are performed using 15 terms in the polynomial chaos expansions and 30 collocation points.

Figure 5.4 shows the estimated values of $M$ (psi1) and $d_{CG}$ (psi2), obtained using the Bayesian approach and the EKF approach for harmonic inputs with frequencies ranging from 0.33 Hz to 25 Hz. It is still assumed that measurements can only be obtained at a sampling rate of 0.3 s (i.e., we have 10 measurement points) and that the Gaussian measurement noise has a zero mean and 1% variance. It can be observed that good estimations are obtained for

frequencies lower than or equal to 1.33 Hz with the Bayesian approach, but the quality of the estimations is clearly poorer for frequencies higher than or equal to 1.66 Hz. With the EKF approach, only the estimation of the position is accurate at low frequencies.

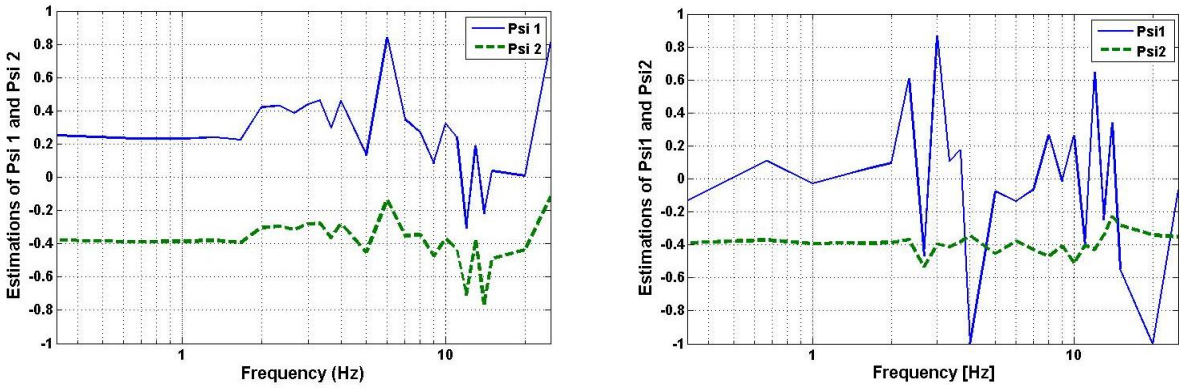


(a) (b)

Figure 5.4: Estimation of the Added Mass and the Position of the Mass at Different Frequencies Using 10 Time Points and a 1% Noise: (a) with Bayesian Approach; (b) with EKF Approach

Figure 5.5 shows the estimated values of $M$ and $d_{CG}$, obtained using the Bayesian approach and the EKF approach for harmonic inputs with frequencies ranging from 0.33 Hz to 25 Hz, but a sampling rate of 0.03 s (i.e., we have 10 measurement points). The main drawback of the EKF approach clearly appears: a higher sampling frequency can sometimes make the filter diverge, which can be observed at high frequencies for this test case.

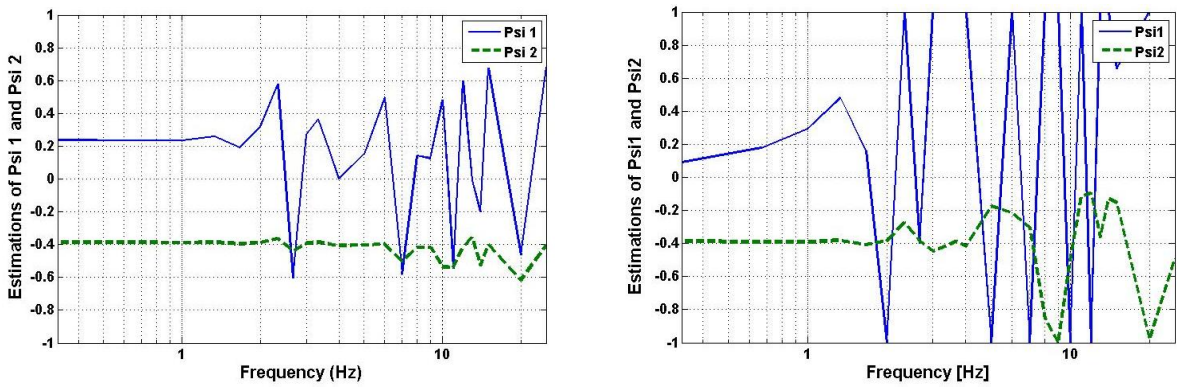


(a) (b)

Figure 5.5: Estimation of the Added Mass and the Position of the Mass at Different Frequencies Using 150 Time Points and a 1% Noise; (a) with Bayesian Approach; (b) with EKF Approach

Figure 5.5 also shows that adding extra measurements does not result in better estimations at frequencies higher than or equal to 1.66 Hz for the Bayesian approach, even though it slightly improves the estimates at lower frequencies. The problem is a non-identifiability problem (i.e., different parameters yield very similar time responses) at high frequencies, as illustrated later in this section. When different combinations ($M$ , $d_{CG}$) yield identical time responses, neither the Bayesian approach nor the EKF approach can yield accurate estimates. However, the Bayesian approach is more accurate than the EKF approach. There are cases where different parameters yield time responses that are very similar but not identical for which the Bayesian approach can still yield accurate estimates while the EKF fails to do so. This is what is observed for the estimation of the added mass at low frequencies. When the different combinations ($M$ , $d_{CG}$) yield almost identical time responses, both approaches fail to yield good estimates since there is not a single answer, but at least, the Bayesian approach yields estimates that would generate the same time responses for our measured parameters, while the EKF approach can have divergence problems and yield incoherent results. This is what is observed for the estimation of the added mass at high frequencies. This can be illustrated by looking at Bayesian cost functions and time responses, as shown below.

Figure 5.6 shows that with 10 time points, the Bayesian approach yields accurate results at 1 Hz, but that with a measurement noise of 1% added to the observations, a few other combinations ($M$ , $d_{CG}$) would yield very similar values of the cost function. If we were able to obtain measurement with no noise, the answer peak would be sharper and the answer would be clear. This is illustrated in Figure 5.6(b) for a Gaussian measurement noise with zero mean and 0.01% variance since our formulation does not allow for no noise since the inverse of the matrices $R_k$ 's need to computed in order to calculate the cost function, as shown in Equation (3.12).

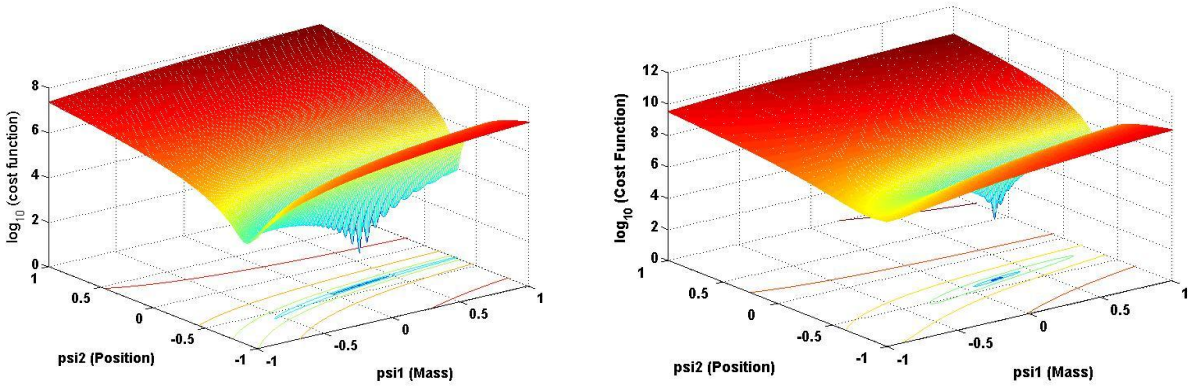


(a) (b)

Figure 5.6: Cost Function at 1 Hz with 10 Time Points: (a) Noise = 1%; (b) Noise = 0.01%

Figure 5.7 shows the effect of non-identifiability problem on the shape of the Bayesian cost function at 2 Hz and at 3 Hz. To make sure the measurement noise is not the problem and that it is indeed a non-identifiability problem, the Bayesian cost functions displayed in Figure 5.7 were computed with a Gaussian measurement noise with zero mean and 0.01% variance. It was shown in Chapter 3 that when the noise level is extremely low, adding extra measurement points does not yield better results for this example.

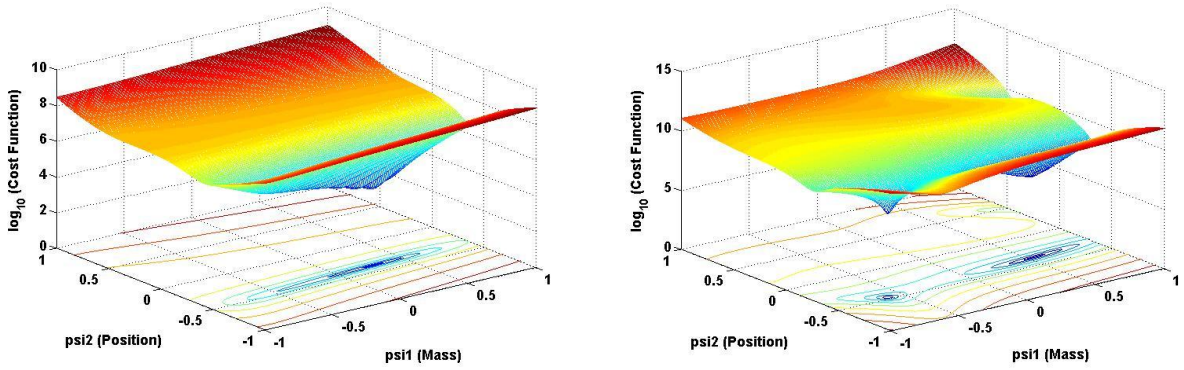


(a) (b)

Figure 5.7: Cost Function with 10 Time Points and 0.01% Measurement Noise: (a) at 2 Hz, (b) at 3 Hz

Figure 5.7 shows that at 2 Hz and at 3 Hz, the Bayesian cost functions have entire regions of minima (e.g., valleys), with each parameter value in the region being equally likely. This is because these different values of $(M, d_{CG})$ yields identical time responses, as illustrated in Figures 3.33-3.34. It can be observed that the value of $d_{CG}$ does not change much within these valleys, which is why the estimates of the position of the mass were somewhat accurate. The problem is that these valleys contain a wide range of values for $M$, which is why the Bayesian approach could not yield accurate estimates of $M$. However, it the estimated values of $(M, d_{CG})$ as well as the other combinations $M$ and $d_{CG}$ in the regions of minima yield identical time responses, whereas the EKF approach cannot yield coherent results when different combinations of uncertain parameters can yield identical time responses.

For a linearized system, i.e., with $F_{C_i}(v) = c_i v$ for the dampers and $k_{i,3} = 0$ for the suspension springs ($i$ = 1, 2), the system become identifiable for all frequencies from 0.33 Hz to 25 Hz, as shown in Figure 5.8: the Bayesian approach can estimate both uncertain parameters accurately for most frequencies. The estimation is still sensitive to numerical approximations (e.g., in running the ODE's, which yields larger errors at higher frequencies) and the polynomial chaos approximation, which explains why the estimation of the added mass is not always perfect. Figure 5.8 shows again that the Bayesian approach is more robust than the EKF approach.

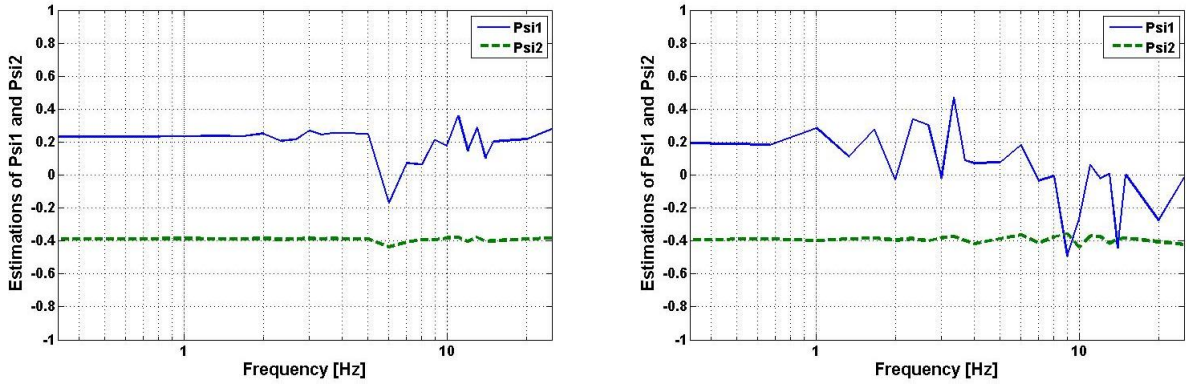


(a) (b)

Figure 5.8: Estimations for the Linearized System Using 150 time Points and a 1% Noise: (a) with Bayesian Approach; (b) with EKF Approach

## 5.3. Summary and Conclusions

The two new polynomial-chaos based computational approaches for parameter estimation developed in Chapter 3 and Chapter 4 are compared in this chapter. In the first approach, the maximum likelihood estimates are obtained by minimizing a cost function derived from the Bayesian theorem. The second approach uses an Extended Kalman Filter (EKF) to obtain the polynomial chaos representation of the uncertain states and the uncertain parameters. All the information was filtered in a single batch since it usually results in better estimates. In this chapter, the two computational approaches are applied to the same mechanical system. Parameter estimation is performed on a nonlinear four degree of freedom roll plane model of a vehicle, in which an uncertain mass with an uncertain position is added on the roll bar. Uncertainties on the values of the added mass and its position are assumed to have a Beta (2, 2) distribution. The value of the mass and its position are estimated from periodic observations of the displacements and velocities across the suspensions.

The accuracy of the estimations has been shown to be sensitive to the number of terms used in the polynomial expressions and to the number of collocation points, and thus it may become computationally expensive when a very high accuracy of the results is desired. However, the

noise level in the measurements affects the accuracy of the estimations as well. Therefore, it is usually not necessary to use a large number of terms in the polynomial expressions and a very large number of collocation points since the addition of extra precision eventually affects the results less than the effect of the measurement noise.

The proposed methods have several advantages. Simulations using Polynomial Chaos methods are much faster than Monte Carlo simulations. Both approaches can work with noisy measurements. One advantage of the Bayesian approach is that it is optimal; it can treat non-Gaussian uncertainties since the Bayesian approach is not tailored to any specific distribution. The EKF approach is suboptimal for non-Gaussian uncertainties, but has an advantage over the Bayesian approach: the estimation comes in form of a PDF.

Appropriate excitations are needed in order to obtain accurate results. When using appropriate excitations, the results obtained with both approaches are close to the actual values of the parameters. However, for some excitations, different combinations of uncertain parameters lead to essentially the same time responses, and no estimation method can work without additional information. With the Bayesian approach, regularization techniques can still yield most likely values among the possible combinations of uncertain parameters resulting in the same time responses than the ones observed. With the EKF approach, the aposteriori probability densities of the estimated parameters cannot be trusted as different combinations of uncertain parameters lead to essentially the same time response than the measured response. Using higher sampling frequencies makes the problem even worse. Therefore, the EKF approach provides valuable information, but should not be trusted blindly. If possible, the PDFs obtained with the EKF approach should be computed with different sampling frequencies, and when increasing the sampling frequency yields different estimates, the EKF estimates should not be trusted anymore. Also the EKF results should be compared with the Bayesian approach to check their coherence.

As a conclusion, the Bayesian approach is more robust: sampling at a higher frequency yields more accurate result except when non-identifiability issues exist, in which case sampling at a higher frequency does not hurt and regularization techniques can be used, whereas sampling at a higher frequency with the EKF approach can yield poorer estimations when dealing with non-identifiability issues.

# 6 Polynomial Chaos Theory Applied to Controller Analysis

The purpose of this chapter is to illustrate how to use the polynomial chaos theory on a simple example, a bicycle model with a $H_2$ controller designed to prevent 'spinout', or uncontrolled yawing, and explain why it can be applied to some control problems (Bode diagrams in this example) and not others (location of open-loop and closed loop poles): the polynomial chaos theory needs to be applied to variables which are $C^1$ (i.e., have continuous derivatives) with respect to the uncertain parameters. I would like to thank Brendan Chan for providing me a deterministic bicycle model, associated figures, as well as a Matlab code to perform $H_2$ control on that model for the deterministic case. A second example, an active suspension model, is used in Section 6.6 to illustrate that the polynomial chaos theory can also be applied to the analysis of transfer functions obtained using an $H_\infty$ controller.

## 6.1 Description of the Deterministic Example

The objective of the deterministic case was to use a $H_2$ controller in order to prevent 'spinout', or uncontrolled yawing, for a vehicle, which is modeled as a bicycle. Figure 6.1 shows the trajectory of two possible skidding scenarios. Over-steer is when the car turns too much and under-steer is when the car does not turn enough.

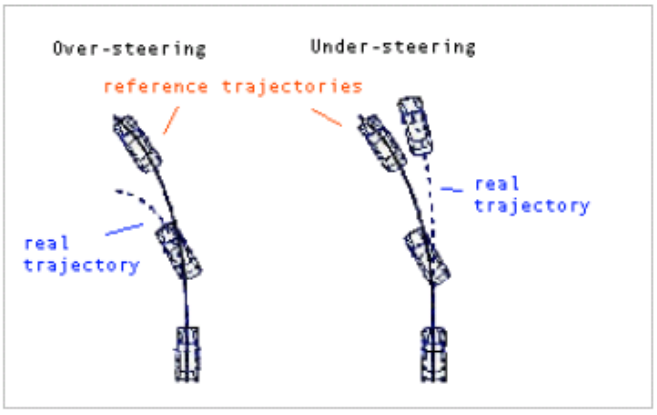


Figure 6.1: Trajectory of Two Possible Skidding Scenarios

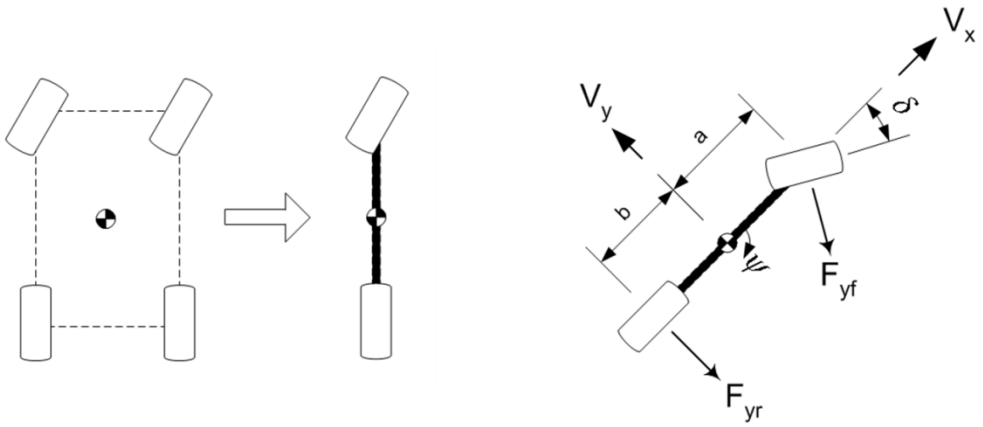


Figure 6.2: Modeling of the Vehicle as a 'Bicycle' Model

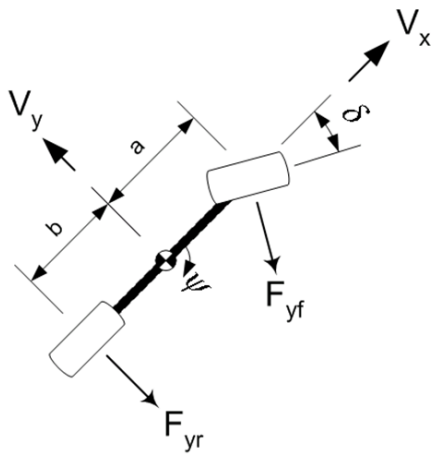


$a$ = Distance *from CG to the front axle*
$b$ = Distance *from CG to the rear axle*
$C_f$ = *Front cornering stiffness*
$C_r$ = *Rear cornering stiffness*
$V_x$ = *Longitudinal velocity*
$\delta$ = *Steering angle*
$V_y$ = *Lateral velocity*
$I_z$ = *Moment of inertia about the* $z-$*axis*
$\psi$ = *Yaw angle*
$m$ = *Mass of the vehicle*
$t_r$ = *Front vehicle width*
$t_f$ = Rear *vehicle width*
$\Delta F_{xf}$ = *Front differential braking force*
$\Delta F_{xr}$ = Rear *differential braking force*

$$\beta = \textit{Sideslip angle} \approx \tan(\beta) = \tan\left(\frac{V_y}{V_x}\right) \approx \frac{V_y}{V_x}$$

Figure 6.3: Bicycle Model, with the Quantities Used to Describe the Dynamics of the System

The objective is to use a $H_2$ controller to prevent the vehicle from over-steering or under-steering (vehicle speed: 70 mph), then introduce two uncertain parameters (front/rear cornering stiffness), and finally, use the polynomial chaos theory to study how the uncertainties affect our system and the Bode diagrams. The vehicle is modeled using a 'bicycle' model, as shown in Figure 6.2 and Figure 6.3.

The assumptions for this model are:

- The steer angles are small (0-5 degrees).
- The vehicle longitudinal velocity $V_x$ is near constant or varying very slowly.
- The model does not take into account roll dynamics and considers effect of the width of the vehicle negligible.
- The lateral forces on the tire is a linear product of a static cornering stiffness and the slip angle of the vehicle, which are considered small for our model as well (slip angle is defined as the angle between where the tire is pointed and where it is heading).
- The road friction coefficient is assumed to be high at all times.
- The vehicle is already in motion and hence is operating in quasi-steady state conditions.
- The speed of the vehicle is constant: 70 mph

The full linearized system of equations is:

$$\begin{pmatrix} \dot{\beta} \\ \ddot{\psi} \end{pmatrix} = \begin{bmatrix} -\frac{C_f + C_r}{m V_x} & -\frac{a C_f - b C_r}{m V_x^{\,2}} - 1 \\ -\frac{a C_f - b C_r}{I_z} & -\frac{a^2 C_f + b^2 C_r}{I_z V_x} \end{bmatrix} \begin{pmatrix} \beta \\ \dot{\psi} \end{pmatrix} + \begin{bmatrix} 0 & 0 \\ \frac{t_f}{2 I_z} & \frac{t_r}{2 I_z} \end{bmatrix} \begin{pmatrix} \Delta F_{yf} \\ \Delta F_{yr} \end{pmatrix} + \begin{bmatrix} \frac{C_f}{m} \\ \frac{a C_f}{I_z} \end{bmatrix} \delta \qquad (6.1)$$

where $\Delta F_{yf}$ and $\Delta F_{yr}$ are controller gains, which will be computed using $H_2$ synthesis.

The vehicle data used in this study was from [104] and is shown in Table 6.1.

Table 6.1: Vehicle Parameters

| Vehicle Parameters | Data |
|---|---|
| m | 2000 kg |
| $I_z$ | 2677.2 kg $m^2$ |
| a | 1.013 m |
| b | 1.5 m |
| $C_f$ | 19,750 N/rad |
| $C_r$ | 15,750 N/rad |
| $t_f$ | 1.554 m |
| $t_r$ | 1.554 |

## 6.2 Description of the Stochastic Example

Two parameters will be assumed to be uncertain: $C_f$ and $C_r$. It will be assumed that they have independent uniform distributions centered around the values they were given in the deterministic case (19,750 N/rad for $C_f$ and 15,750 N/rad for $C_r$). For uniform distribution, the basis functions are Legendre polynomials. An important property of the Legendre polynomials is that they are orthogonal with respect to the $L^2$ inner product on the interval $-1 \le x \le 1$:

$$\int_{-1}^{1} L_i(\xi)\, L_j(\xi)\, d\xi = \tfrac{2}{2i+1}\,\delta_{ij} \tag{6.2}$$

The first Legendre polynomials are given by:

$$\begin{cases} L_0(\xi) = 1 \\ L_1(\xi) = \xi \\ L_2(\xi) = \tfrac{1}{2}\left(3\,\xi^2 - 1\right) \\ L_3(\xi) = \tfrac{1}{2}\left(-3 + 5\,\xi^2\right) \end{cases} \tag{6.3}$$

For a two-dimensional uniform distribution, the basis functions are:

$$\begin{cases} \psi^1(\xi_1, \xi_2) = 1 \\ \psi^2(\xi_1, \xi_2) = \xi_1 \\ \psi^3(\xi_1, \xi_2) = \xi_2 \\ \psi^4(\xi_1, \xi_2) = \tfrac{1}{2}\left(3\,{\xi_1}^2 - 1\right) \\ \psi^5(\xi_1, \xi_2) = \tfrac{1}{2}\left(3\,{\xi_2}^2 - 1\right) \\ \psi^6(\xi_1, \xi_2) = \xi_1\,\xi_2 \\ \psi^7(\xi_1, \xi_2) = \tfrac{1}{2}\,\xi_1\,(-3 + 5\,{\xi_1}^2) \\ \psi^8(\xi_1, \xi_2) = \tfrac{1}{2}\,\xi_2\,(-1 + 3\,{\xi_1}^2) \\ \psi^9(\xi_1, \xi_2) = \tfrac{1}{2}\,\xi_1\,(-1 + 3\,{\xi_2}^2) \\ \psi^{10}(\xi_1, \xi_2) = \tfrac{1}{2}\,\xi_2\,(-3 + 5\,{\xi_2}^2) \end{cases} \tag{6.4}$$

The polynomial chaos expansions will use 10 terms. For a given pole, its PC expansion can be written as:

$$pole(\xi) = pole^{1}\ \psi^1(\xi) + pole^{2}\ \psi^2(\xi) + pole^{3}\,\psi^3(\xi) + \ldots + pole^{10}\,\psi^{10}(\xi), \quad \xi = (\xi_1, \xi_2) \tag{6.5}$$

The uncertain parameter $C_f$ and $C_r$ have independent uniform distributions centered around the values they were given in the deterministic case, Therefore, the polynomial chaos expansions of the uncertain parameters $C_f$ and $C_r$ are:

$$C_f(\xi) = C_f^1 + C_f^2\ \xi_1,\ \ \xi_1 \in [-1, 1] \tag{6.6}$$

$$C_r(\xi) = C_r^1 + C_r^3\ \xi_2,\ \ \xi_2 \in [-1, 1] \tag{6.7}$$

where $C_f^1$ and $C_r^1$ are the center of the distributions, i.e., $C_f^1 = 19{,}750$ N/rad and $C_r^1 = 15{,}750$ N/rad , and $C_f^2$ and $C_r^3$ represent the maximum deviations from the center of the distribution for $C_f$ and $C_r$, respectively.

The open-loop poles depend on two variables, $\xi_1$ and $\xi_2$ , and are given by:

$$\begin{aligned} \textit{Open Loop Poles}\ (\xi_1,\xi_2) &= \frac{1}{2}\left[a_{11}(\xi_1,\xi_2) + a_{22}(\xi_1,\xi_2)\right] \\ &\pm \frac{1}{2}\sqrt{(a_{11}(\xi_1,\xi_2))^2 + (a_{22}(\xi_1,\xi_2)^2) - 2\,a_{11}(\xi_1,\xi_2)\,a_{22}(\xi_1,\xi_2) + 4\,a_{12}(\xi_1,\xi_2)\,a_{21}(\xi_1,\xi_2)} \end{aligned} \tag{6.8}$$

where $a_{11}(\xi_1, \xi_2)$, $a_{12}(\xi_1, \xi_2)$, $a_{21}(\xi_1, \xi_2)$ and $a_{22}(\xi_1, \xi_2)$ are given by:

$$\begin{bmatrix} a_{11}(\xi_1, \xi_2) & a_{12}(\xi_1, \xi_2) \\ a_{21}(\xi_1, \xi_2) & a_{22}(\xi_1, \xi_2) \end{bmatrix} = \begin{bmatrix} -\dfrac{C_f(\xi_1, \xi_2) + C_r(\xi_1, \xi_2)}{m\,V_x} & -\dfrac{a\,C_f(\xi_1, \xi_2) - b\,C_r(\xi_1, \xi_2)}{m\,V_x^{\,2}} - 1 \\ \dfrac{a\,C_f(\xi_1, \xi_2) - b\,C_r(\xi_1, \xi_2)}{I_z\,V_x} & \dfrac{a^2\,C_f(\xi_1, \xi_2) + b^2\,C_r(\xi_1, \xi_2)}{I_z\,V_x} \end{bmatrix} \tag{6.9}$$

The collocation approach is used in this example. It is faster than Galerkin's approach, and much faster than Monte Carlo methods. It gives very similar results to the Galerkin approach, usually even slightly better (i.e. more similar to a Monte Carlo simulation using a huge number of points) for this example depending on the collocation points we choose

At least 10 collocation points are needed since 10 terms are used for the polynomial chaos expansions. However, using more than 10 collocation points is recommended. In that case, a least square algorithm will be used. This example uses 16 collocation points $\mu_1, \mu_2, \ldots, \mu_{16}$, which are shown in Figure 6.4.

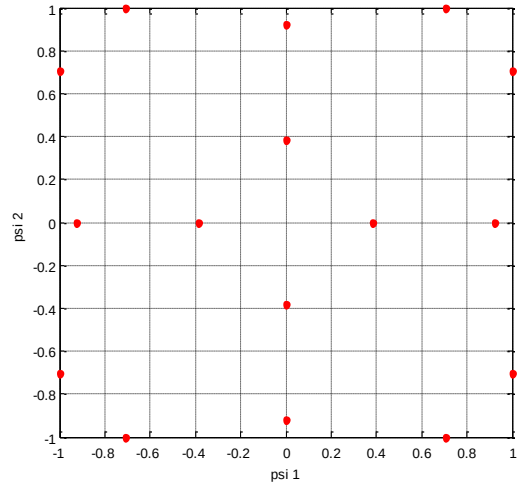


Figure 6.4: Collocation Points

A collocation matrix *Acolloc* can be defined using the basis function values at the collocation points

$$Acolloc = \begin{bmatrix} \psi^1(\mu_1) & \psi^2(\mu_1) & \dots & \psi^{10}(\mu_1) \\ \psi^1(\mu_2) & \psi^2(\mu_2) & \dots & \psi^{10}(\mu_2) \\ \dots & \dots & \dots & \\ \psi^1(\mu_{16}) & \psi^2(\mu_{16}) & \dots & \psi^{10}(\mu_{16}) \end{bmatrix} \tag{6.10}$$

The polynomial chaos expressions for the open loop poles at the 16 collocation points can be written as:

$$\begin{cases} pole1(\mu_1) = pole1^1\,\psi^1(\mu_1) + pole1^2\,\psi^2(\mu_1) + \dots + pole1^{10}\,\psi^{10}(\mu_1) \\ \qquad\qquad \dots\dots \\ pole1(\mu_{16}) = pole1^1\,\psi^1(\mu_{16}) + pole1^2\,\psi^2(\mu_{16}) + \dots + pole1^{10}\,\psi^{10}(\mu_{16}) \end{cases} \tag{6.11}$$

$$\begin{cases} pole2(\mu_1) = pole2^1\,\psi^1(\mu_1) + pole2^2\,\psi^2(\mu_1) + \dots + pole2^{10}\,\psi^{10}(\mu_1) \\ \qquad\qquad \dots\dots \\ pole2(\mu_{16}) = pole2^1\,\psi^1(\mu_{16}) + pole2^2\,\psi^2(\mu_{16}) + \dots + pole2^{10}\,\psi^{10}(\mu_{16}) \end{cases} \tag{6.12}$$

where $pole1(\mu_1), \dots, pole1(\mu_{16})$ and $pole2(\mu_1), \dots, pole2(\mu_{16})$ are known since they are simply the values open loop poles at the 16 collocation points. The unknown coefficients are $pole1^1, \dots, pole1^{10}$ and $pole2^1, \dots, pole2^{10}$. After being calculated, the polynomial chaos

expressions of the open loop poles will be available. A left matrix divide by the collocation matrix gives the polynomial chaos expressions for the open loop poles:

$$\begin{bmatrix} pole1^1 \\ pole1^2 \\ \dots \\ pole1^{10} \end{bmatrix} = Acolloc \setminus \begin{bmatrix} pole1(\mu_1) \\ pole1(\mu_2) \\ \dots \\ pole1(\mu_{16}) \end{bmatrix} \tag{6.13}$$

$$\begin{bmatrix} pole2^1 \\ pole2^2 \\ \dots \\ pole2^{10} \end{bmatrix} = Acolloc \setminus \begin{bmatrix} pole2(\mu_1) \\ pole2(\mu_2) \\ \dots \\ pole2(\mu_{16}) \end{bmatrix} \tag{6.14}$$

The location of the open loop poles in a stochastic from is given by:

$$pole1(\xi) = pole1^1\ \psi^1(\xi) + pole1^2\ \psi^2(\xi) + pole1^3\,\psi^3(\xi) + ... + pole1^{10}\,\psi^{10}(\xi) \tag{6.15}$$

$$pole2(\xi) = pole2^1\ \psi^1(\xi) + pole2^2\ \psi^2(\xi) + pole2^3\,\psi^3(\xi) + ... + pole2^{10}\,\psi^{10}(\xi) \tag{6.16}$$

## 6.3 Stochastic Results for the Open Loop Poles

Let's assume that the range of possible values for the uncertain parameters $C_f$ and $C_r$ are +/- 2% of their deterministic values, i.e. $C_f^2 = 0.02\,C_f^1$ and $C_f^2 = 0.02\,C_f^1$ in Equations (6.6) and (6.7) can be replaced by:

$$C_f^2 = 0.02\,C_f^1 \tag{6.17}$$

$$C_r^3 = 0.02\ \ C_r^1 \tag{6.18}$$

Figure 6.5 shows the possible location of the open loop poles with Monte Carlo (a) and Collocation (b). The pole denoted $pole1$ is represented in blue and the pole denoted $pole2$ is represented in green. Both plots show 500 points for each pole location. The vectors in red represent the second and third terms of the polynomial chaos and start at the mean values of the location of the open loop poles given by the first terms of the polynomial chaos expressions. This is to illustrate that for this case, using 10 terms in the Polynomial Chaos expansions was sufficient since using only the first three terms already gives a good idea of the location of the

poles in this case. In our case, the nonlinear terms (fourth to tenth terms) are extremely small. This is not a general conclusion since the relationship between the uncertain parameters and resulting stochastic variables of interest is usually more complex.

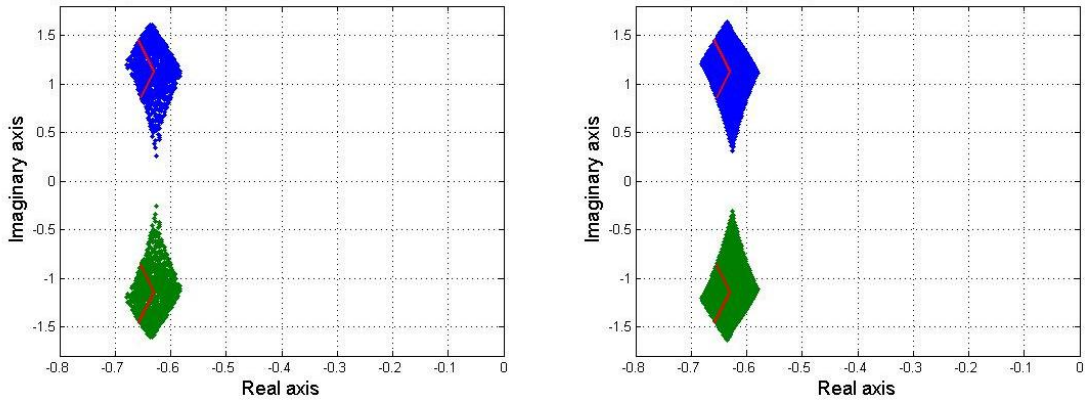


(a) (b)

Figure 6.5: Location of Open Loop Poles with 2% Uncertainties on the Values $C_f$ and $C_r$: (a) with Monte Carlo; (b) with Collocation

The fact that the Polynomial Chaos theory worked in this case was due to the fact location of the open loop poles in this case were a $C^1$ function with respect to the uncertain parameters $C_f$ and $C_r$.

Figure 6.6 shows the possible location of the open loop poles with 15% uncertainties on the values of the uncertain parameters $C_f$ and $C_r$ , instead of 2% in Figure 6.5. The location of the open loop poles has non-continuous derivatives when reaching the real axis and the Polynomial Chaos theory cannot yield accurate results anymore.

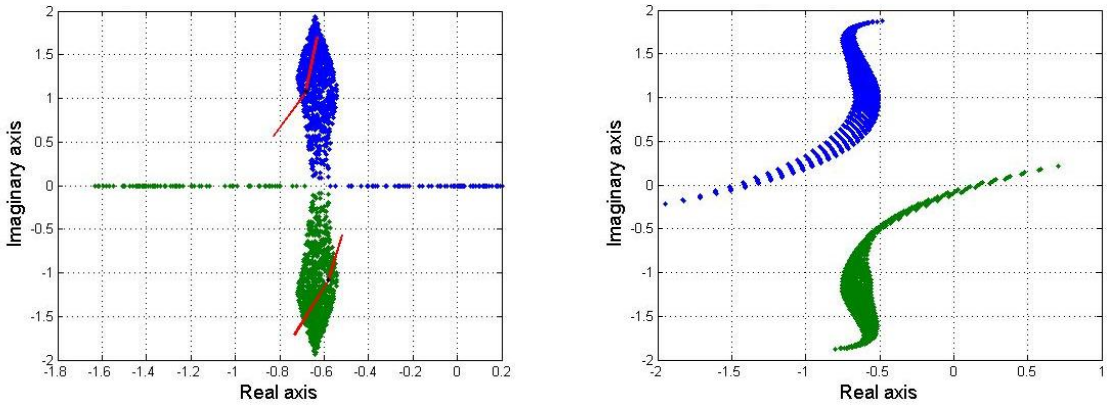


(a) (b)

Figure 6.6: Location of Open Loop Poles with 15% Uncertainties on the Values $C_f$ and $C_r$: (a) with Collocation; (b) with Monte Carlo

## 6.4 Stochastic Results for the Closed-Loop Poles

In order to illustrate that the function that needs to be $C^1$ in order to use the Polynomial Chaos theory is the function describing the specific parameter calculated at the collocation points with respect to the uncertain parameters $C_f$ and $C_r$, another example will be illustrated. This section uses Monte Carlo and Collocation in order to describe the location of the closed loop poles for our uncertain parameters $C_f$ and $C_r$ after computing gains with the deterministic system (i.e., using the nominal values of $C_f$ and $C_r$) using the $H_2$ control synthesis. The $H_2$ control is based on minimizing the $H_2$ norm of the state dependent cost function $J_2$, as shown in Figure 6.7.

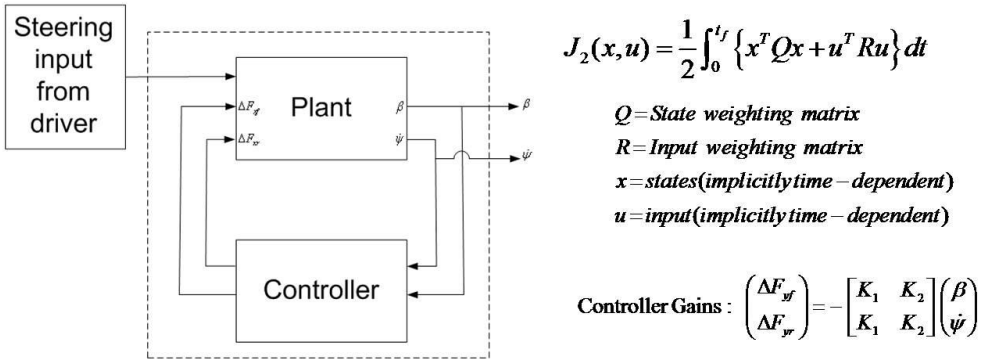


Figure 6.7: $H_2$ Control for the Bicycle Model

Optimal Gains are computed for the deterministic values for seven different input weighting matrices, which results in 7 pairs of gains. Figure 6.8 shows the locations of the closed loop poles with 2% uncertainties on the values $C_f$ and $C_r$ with Monte Carlo (a) and Collocation (b). It can be observed that if the closed loop poles reach the critical point where the derivatives of the position are not continuous, collocation does not work anymore. The values of the uncertainties are +/-2 %, which makes the collocation approach fail for 3 of the 7 pairs of gains. With uncertainties of +/-1 %, collocation and Monte Carlo give similar results since the closed loop poles do reach the critical point on the real axis where the derivatives of the position are not continuous, as shown in Figure 6.9.

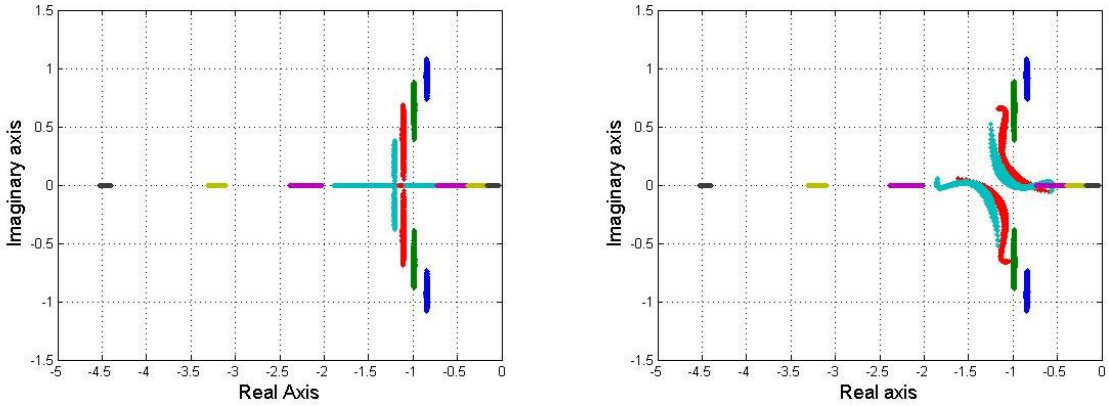


Figure 6.8: Location of Closed-Loop Poles with 2% Uncertainties on the Values $C_f$ and $C_r$ for Seven Different Pairs of Gains (a) with Monte Carlo; (b) with Collocation

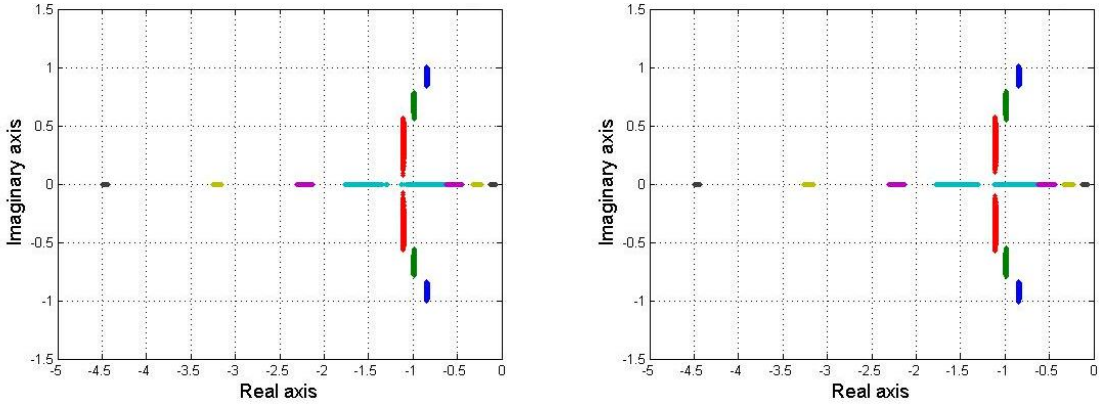


Figure 6.9: Location of Closed-Loop Poles with 1% Uncertainties on the Values $C_f$ and $C_r$ for Seven Different Pairs of Gains (a) with Monte Carlo; (b) with Collocation

Since the polynomial chaos theory cannot be used for very general applications related to pole placement methods, its use is limited, and many well-known methods for controller design, such as the root locus, cannot be applied in the general case. Controller analysis is still possible, but controller synthesis is a more difficult problem due to the need of using functions having continuous derivatives. Examples of Controller analysis using the polynomial chaos theory are shown in Section 6.5 below.

## 6.5 Bode Diagrams and Stability Margins

The polynomial chaos theory can be applied to the Bode plots. Figure 6.10 shows the Bode diagram for the yaw rate vs. the steering input (i.e. the magnitude corresponds to the transfer function $\dot{\beta}(s)/\delta(s)$), using the collocation method. The PDF of the magnitude and the phase of the TF can be obtained from their polynomial chaos expressions. In order to obtain larger PDFs which are easier to visualize for the reader, 20% uncertainties were assumed on the values $C_f$ and $C_r$. Obtaining the figure shown below takes a few minutes with the Collocation Approach. For the same resolution, it takes hours with Monte Carlo  However, for each frequency, the PDF of the Phase can be represented, as shown in Figure 6.11 for the collocation method. Therefore, the results obtained with the collocation method can be compared with Monte Carlo, as shown in Figure 6.12.

Figure 6.12 shows that the Polynomial Chaos expression with only 16 collocation points already gives very similar histograms to a Monte Carlo simulation using the same uncertainty points (two slight differences in the example below). Having more histogram points in order to represent a PDF is very expensive with Monte Carlo. The PDF obtained with the collocation approach can become more accurate if we take more collocation points, which is still much less expensive than using Monte Carlo.

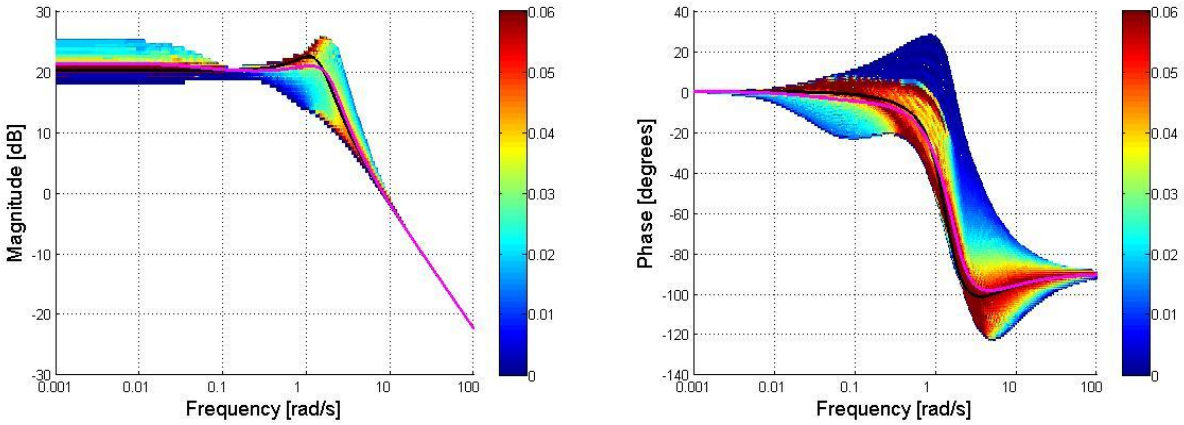


(a) (b)

Figure 6.10: Bode Diagram for Yaw Rate vs. Steering Input with 20% Uncertainties on the Values $C_f$ and $C_r$ for: (a) Magnitude; (b) Phase

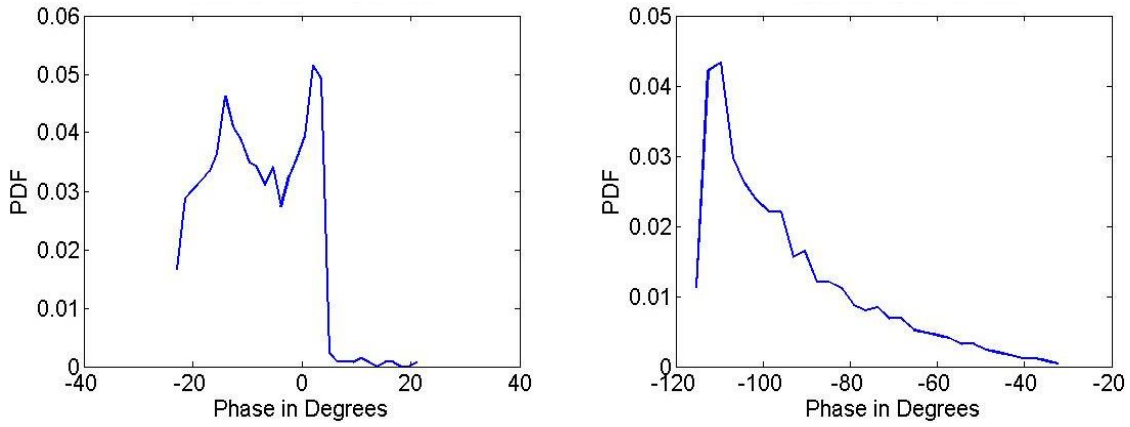


(a) (b)

Figure 6.11: Phase Histogram Obtained with the Collocation Approach: (a) at ω = 0.3 rad/s; (b) at ω = 3 rad/s

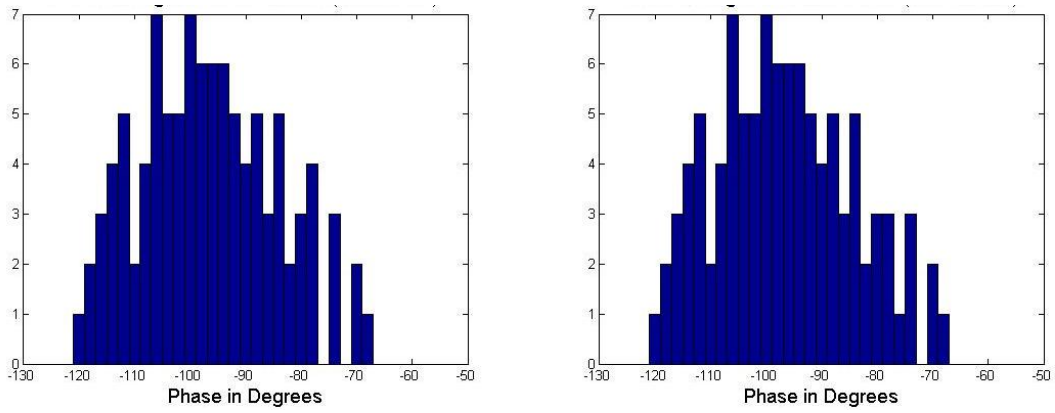


(a) (b)

Figure 6.12: Phase Histogram at ω = 8 rad/s: (a) with Collocation; (b) with Monte Carlo

Finally, the Polynomial Chaos expressions of the phase margin can be computed (the gain margin is always infinity in this example, so will not be computed).

$$PM(\xi) = PM^1\ \psi^1(\xi) + PM^2\ \psi^2(\xi) + PM^3\ \psi^3(\xi) + ... + PM^{10}\ \psi^{10}(\xi) \qquad (6.19)$$

The Phase Margin can be used as a measure of stability and its PDF using the collocation approach is shown in Figure 6.13, which also shows the stochastic Bode plot of the phase.

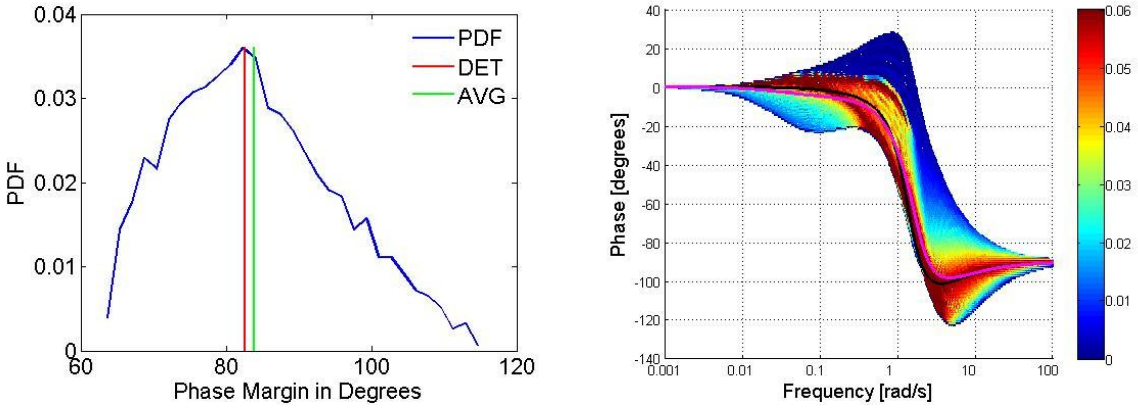


(a) (b)

Figure 6.13: Probability Density Functions: (a): Phase Margin; (b) Bode Diagram for the Phase

The mean value of the phase margin is $PM^1$ and its standard deviation is: $\sqrt{\int_{-1}^{1}\int_{-1}^{1}\left(PM(\xi_1,\xi_2)-PM^1\right)^2 d\xi_1 d\xi_2}$ . The mean value for the Phase Margin is: 83.879 degrees and its standard deviation for the Phase Margin is: 10.835 degree. The same way, the polynomial chaos expression of the frequency at which the phase margin is obtained (i.e. the frequency for which the gain is 0 dB) can be obtained. Its mean value is 8.006 rad/s and its standard deviation is 0.532 rad/s.

## 6.6 Transfer Functions Obtained Using an H-infinity Controller

The purpose of this section is to show that the polynomial chaos theory can also be applied to Bode diagrams obtained using state-space methods, or more generally, transfer functions obtained using state space methods. The deterministic example used in this section is the application of $H_\infty$ to active suspension control found in the Matlab Robust Control Toolbox help section [105]. The controllers are designed using linear $H_\infty$ synthesis, and are based on [106]. This example reproduces the first control design shown in [105]. For the sake of brevity, the controller design is not described here. It includes weighting functions to keep the car deflection and the suspension deflection small, to limit the magnitude and frequency content of the control force, to model the sensor noise, and to scale the magnitude of road disturbances. The feedback signal is the suspension deflection. The controller produces a force through an actuator based on that signal. A quarter-car model with an active suspension is shown in Figure 6.14. The actuator force $f_S$ can act in both directions.

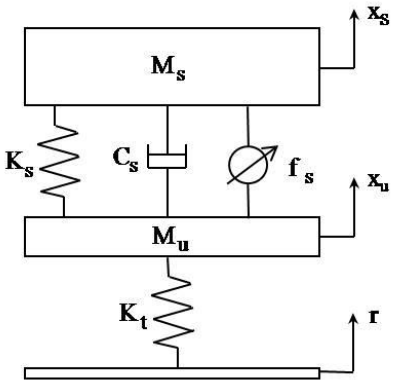


Figure 6.14: Quarter Car Model with Active Suspension

Transfer functions of many quantities can be obtained. They depend on the controller. Figure 6.15 shows the magnitude of the transfer function between the road input and the suspension deflection. The line in black corresponds to the deterministic case. The controller was designed using the deterministic value of the damper $C_S$. The PDF of the magnitude is obtained for a Beta (2, 2) distribution with uncertainties of +/- 20% on the value of $C_S$ (all other values are still assumed to be perfectly known). The PDF was obtained by using the magnitude of the transfer function for each frequency as a Polynomial Chaos expression, with 5 polynomial chaos terms and 15 collocation points. Therefore, at each frequency, the magnitude of the transfer function was evaluated for the 15 collocation points and then interpolated to a PDF.

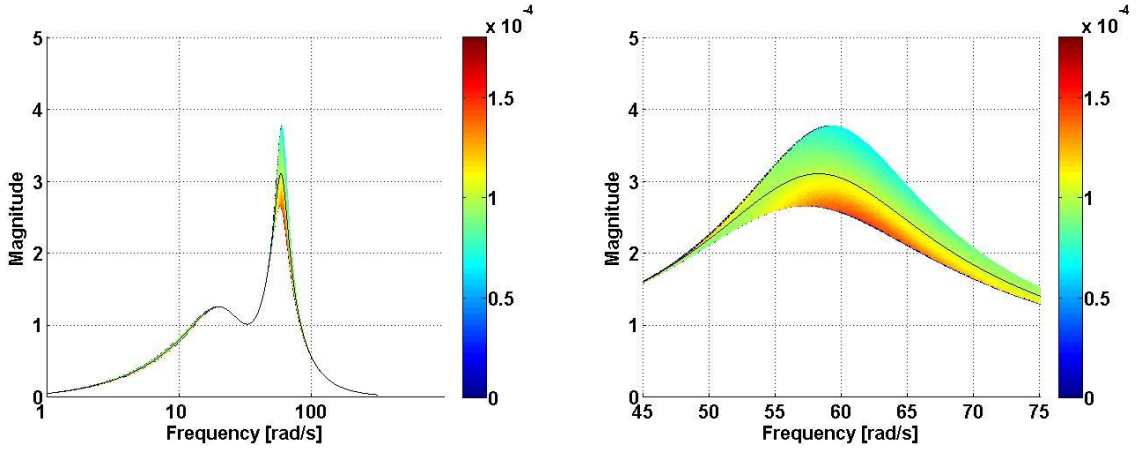


Figure 6.15: PDF of the Magnitude of the Transfer Function between the Road Input and the Suspension Deflection: (a) with Logarithmic Scale for the Frequency; (b) around the Peak Value and wit Linear Scale for the Frequency

Figure 6.16 shows the PDF and the CDF (Cumulative Distribution Function) of the peak magnitude of the transfer function between the road input and the suspension deflection. It is obtained by using the peak magnitude of the transfer function as a Polynomial Chaos expression and directly evaluating it at the 15 collocation points. The advantage of the CDF is that it directly yields the percentage of cases for which the peak magnitude stays below a given value.

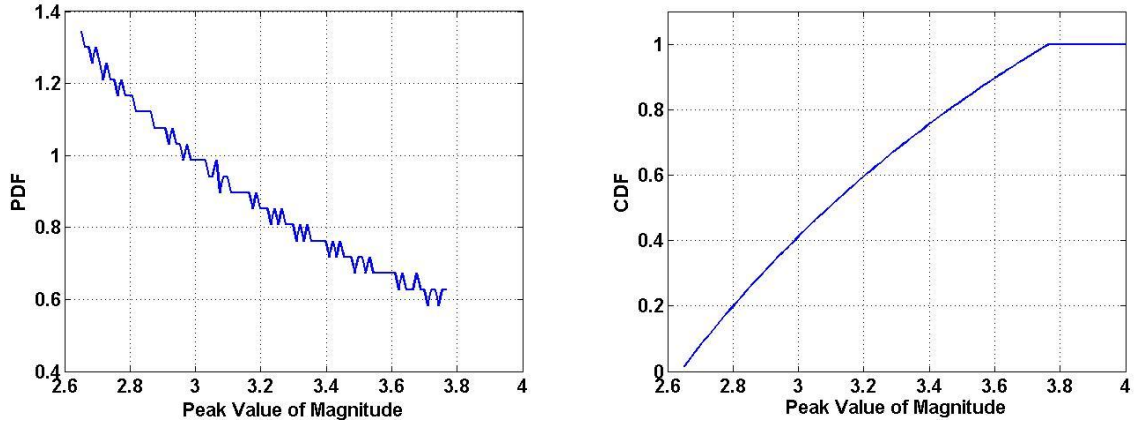


(a) (b)

Figure 6.16: PDF and CDF of the Peak Magnitude of the Transfer Function between the Road Input and the Suspension Deflection: (a) PDF; (b) CDF

It can be observed that the peak magnitude of the transfer function ranges from 2.65 to 3.77 depending on the value of Cs. When designing the $H_\infty$ controller, the magnitude of the transfer function was expected to reach a peak value of 3.10, but the effect of uncertainties on Cs were unknown.

## 6.7 Summary and Conclusions

It has been found that the Polynomial Chaos theory is not very well adapted to many control methods because it needs to be applied to variables which are $C^1$ (i.e., have continuous derivatives) with respect to the uncertain parameters in order to work. However, examples using a bicycle model with a $H_2$ controller designed to prevent 'spinout', or uncontrolled yawing have showed the efficiency of the polynomial chaos theory for control systems analysis when using control methods more adapted to the polynomial theory, such as Bode diagrams and stability margins. A second example, an active suspension model, illustrated that the polynomial chaos theory can also be applied to the analysis of transfer functions obtained using an $H_\infty$ controller.

Since the polynomial chaos theory cannot be used for very general applications related to pole placement methods, its use is limited, and many well-known methods for controller design,

such as the root locus, cannot be applied in the general case. Chapter 7 will therefore focus on a state-space method for controller design.

# 7 Polynomial-Chaos-Based Controller Design: the LQR Problem with Uncertain Parameters

This chapter proposes a polynomial chaos based numerical method providing an optimal controller for the linear- quadratic regulator (LQR) problem when the parameters in the formulation are uncertain, i.e., a controller minimizing the mean value of the LQR cost function obtained for a certain distribution of the uncertainties which is assumed to be known. The LQR problem is written as an optimality problem using Lagrange multipliers in an extended form associated with the polynomial chaos framework, and an iterative algorithm converges to the optimal answer. The algorithm is applied to a simple example for which the answer is already known. Polynomial chaos based methods have the advantage of being computationally much more efficient than Monte Carlo simulations.

The Linear-Quadratic Regulator controller is not very well adapted to robust design, and the optimal controller does not guarantee a minimum performance or even stability for the worst case scenario. Stability robustness and performance robustness in the presence of uncertainties are therefore not guaranteed. However, this is a first step aimed at designing more judicious controllers if combined with other techniques in the future. The next logical step would be to extend this numerical method to $H_2$ and then $H_\infty$ problems.

## 7.1 Introduction and Background

The solution to the $H_\infty$ problem as well as the $H_2$ problem are based on solutions of Riccati equations and can therefore be seen as extensions of the LQR problem [83]. Therefore, developing a new computationally efficient numerical method in order to solve the LQR problem in a framework taking parametric uncertainties into account might have the potential of leading to other computationally efficient methods solving $H_2$ and $H_\infty$ problems with parametric uncertainties. Fisher and Bhattacharya [97] presented a framework for LQR design with uncertain parameters in the formulation, using the polynomial chaos theory. However, their work yields a system of equations with no known answer for the specific problem described in this

chapter. Templeton [98] used the same framework than Fisher and Bhattacharya [97], which consists of extended matrices in a polynomial chaos framework, and developed a gradient descent optimization method finding optimal gains for $H_2$ and LQR design with parametric uncertainties.

We are not aware of any study trying to use the polynomial chaos framework to find a closed form solution for the LQR problem in this framework, i.e., a solution that would depend on the number of terms $S$ in the polynomial chaos expansions and that would numerically converge to the solution of the problem as $S \to \infty$. The original intent of the work presented in this chapter was to try deriving such a solution, but this proved to be extremely difficult, if not impossible, as briefly explained later in this chapter. However, an efficient numerical method to solve this problem could be derived instead. Polynomial chaos based methods have the advantage of computationally much more efficient than Monte Carlo simulations. The method presented in this chapter is different than the method used in [98], even though it also uses the same framework consisting of extended matrices in a polynomial chaos framework. It treats the LQR problem as an optimality problem using Lagrange multipliers in an extended form associated with the polynomial chaos framework, and uses an iterative algorithm which converges to the optimal answer. Therefore, it is based on the fundamental approach to solving the LQR problem, which is derived using Lagrange multipliers in the deterministic case [99], which leads to the well-known algebraic Riccati equations. Therefore, the method presented in this chapter might have the potential of being a first step towards the development of computationally efficient numerical methods for $H_\infty$ design with parametric uncertainties.

## 7.2 Overview of the Numerical Method

### 7.2.1 Description of the Problem Setting in the Polynomial Chaos Framework

The continuous LQR problem studied in this chapter consists of finding the feedback control law

$$u(t) = -K\ x(t) \tag{7.1}$$

that minimizes the value of the quadratic cost function

$$J = \int_0^\infty \left( x(t)^T \, Q \, x(t) + u(t)^T \, R u(t) \right) dt \tag{7.2}$$

subject to the dynamics

$$\dot{x}(t) = A \, x(t) + B \, u(t) \tag{7.3}$$

where $Q$ and $R$ are symmetric matrices, in order to match the structure of the equivalent standard LQR problem in the frequency domain used by Zhou *et. al* [83] as a basis for the $H_2$ and the $H_\infty$ theory.

It will also be assumed that there are $n$ states and $m$ control inputs, i.e. $x \in R^n$ and $u \in R^m$ i.e.,

The solution to this problem is given by

$$K = R^{-1} B^T \, P \tag{7.4}$$

where $P$ is the solution of the following continuous-time algebraic Riccati equation:

$$A^T P + P \, A - P \, B \, R^{-1} \, B^T \, P + Q = 0 \tag{7.5}$$

In the stochastic framework, the matrices $A$ and $B$ are uncertain and the system ODE can be written as

$$\dot{x}(\xi,t) = A(\xi) \, x(\xi,t) + B(\xi) \, u(\xi,t) \tag{7.6}$$

The stochastic LQR problem consists of finding the feedback control law

$$u(\xi,t) = -K \, x(\xi,t) \tag{7.7}$$

minimizing the expected value of the stochastic LQR cost function, i.e., minimizing

$$J_{stoch}(u) = E\left( \int_0^\infty (x(t,\xi)^T \, Q \, x(t,\xi) + u(t,\xi)^T \, R u(t,\xi)) \, dt \right) \tag{7.8}$$

where the distributions of $A(\xi)$ and $B(\xi)$ are supposed to be known and can be written algebraically.

The stochastic LQR cost function can be rewritten as

$$J_{stoch}(u) = \int_{\Omega} \left( \int_{0}^{\infty} (x(t,\xi)^T \, Q \, x(t,\xi) + u(t,\xi)^T \, R u(t,\xi)) \, dt \right) \rho(\xi) \, d\xi \tag{7.9}$$

where $\rho(\xi)$ is the joint probability density defined in Chapter 2.

For instance, if $\xi$ has only one component (which means every uncertainty in the system can be described using that 1-dimentional variable) and the distribution of $\xi$ is defined between -1 and 1, then

$$J_{stoch}(u) = \int_{\xi=-1}^{1} \left( \int_{0}^{\infty} (x(t,\xi)^T \, Q \, x(t,\xi) + u(t,\xi)^T \, R u(t,\xi)) \, dt \right) \rho(\xi) \, d\xi \tag{7.10}$$

To the best of our knowledge, there is no closed form solution to this problem available for the general case, which is part of a larger problem called random differential equations. However, we are not aware of any study trying to use the polynomial chaos framework to find a closed form solution in this framework, i.e., a solution that would depend on the number of terms $S$ in the polynomial chaos expansions and that would numerically converge to the solution of the problem as $S \to \infty$. The original intent of the work presented in this chapter was to try deriving such a solution, but this proved to be extremely difficult, if not impossible, as briefly explained later in this chapter. However, an efficient numerical method to solve this problem could be derived instead. Polynomial chaos based methods have the advantage of being computationally much more efficient than Monte Carlo simulations.

Physically, a controller $K$ controls the states $x(t,\xi)$ using the inputs $u(t,\xi)$ with the following relation

$$u(t,\xi) = -K \; x(t,\xi) \tag{7.11}$$

since it is assumed that $K$ is fixed once and for all, while the uncertainty $\xi$ can take different values.

Using the polynomial chaos expansions of $x(t,\xi)$ and $u(t,\xi)$ yields

$$\sum_{i=1}^{S} \left( u^i(t) \, \psi^l(\xi) \right) = -K \sum_{j=1}^{S} \left( x^i(t) \, \psi^l(\xi) \right) \tag{7.12}$$

i.e.

$$\sum_{i=1}^{S} u^i(t)\,\psi^l(\xi) = \sum_{i=1}^{S} -K\,x^i(t)\,\psi^l(\xi) \tag{7.13}$$

Therefore, in the polynomial chaos framework, it is necessary to use a controller such that $u^i = -K\,x^i$ with the same $K$ for each polynomial chaos mode $i$.

In the remainder of the chapter, superscripts denote a Polynomial Chaos index ($S$ is the number of PC terms), while subscripts denote a state index.

### 7.2.2 Equivalent Problem Using an Extended Framework

Let's calculate the expected value of $x(t,\xi)^T Q\,x(t,\xi)$, which will simply be written as $E\left(x^T Q\,x\right)$

$$E\left(x^T\,Q\,x\right) = E\left(\sum_{i,\,j=1}^{n} x_i(t,\xi)\,Q_{ij}\;x_j(t,\xi)\right) \tag{7.14}$$

$$E\left(x^T\,Q\,x\right) = \sum_{i,\,j=1}^{n} E\left(x_i(t,\xi)\,Q_{ij}\;x_j(t,\xi)\right) \tag{7.15}$$

$$E\left(x^T\,Q\,x\right) = \sum_{i,\,j=1}^{n} E\left(\sum_{l,\,r=1}^{S}\left(x_i^l(t)\,\psi^l(\xi)\,Q_{ij}\;x_j^r(t)\,\psi^r(\xi)\right)\right) \tag{7.16}$$

$$E\left(x^T\,Q\,x\right) = \sum_{i,\,j=1}^{n}\sum_{l,\,r=1}^{S} x_i^l(t)\;\;Q_{ij}\;x_j^r(t)\;\;E\left(\psi^l(\xi)\,\psi^r(\xi)\right) \tag{7.17}$$

It is preferable to choose an orthonormal base for the polynomial chaos expansions. In that case this expression is simplified to

$$E\left(x^T\,Q\,x\right) = \sum_{i,\,j=1}^{n}\sum_{l,\,r=1}^{S} x_i^l(t)\;\;Q_{ij}\;x_j^r(t)\;\delta_{lr} \tag{7.18}$$

With an orthonormal base, we obtain

$$E\left(x^T\,Q\,x\right) = \sum_{i,\,j=1}^{n}\sum_{l\,r=1}^{S} x_i^r(t)\;\;Q_{ij}\;x_j^r(t) \tag{7.19}$$

which is equivalent to

$$E\left(x^T\,Q\,x\right)=\begin{bmatrix} x^1 \\ \vdots \\ \vdots \\ x^S \end{bmatrix}^T \begin{bmatrix} R & 0 & \cdots & 0 \\ 0 & R & \ddots & \vdots \\ \vdots & \ddots & \ddots & 0 \\ 0 & \cdots & 0 & R \end{bmatrix} \begin{bmatrix} x^1 \\ \vdots \\ \vdots \\ x^S \end{bmatrix} \tag{7.20}$$

Similarly, with an orthonormal basis,

$$E\left(u^T\,R\,u\right)=\begin{bmatrix} u^1 \\ \vdots \\ \vdots \\ u^S \end{bmatrix}^T \begin{bmatrix} R & 0 & \cdots & 0 \\ 0 & R & \ddots & \vdots \\ \vdots & \ddots & \ddots & 0 \\ 0 & \cdots & 0 & R \end{bmatrix} \begin{bmatrix} u^1 \\ \vdots \\ \vdots \\ u^S \end{bmatrix} \tag{7.21}$$

Since, it is necessary to use a controller such that $u^i = -K\,x^i$ with the same $K$ for each polynomial chaos mode $i$, it yields

$$E\left(u^T\,R u\right)=\begin{bmatrix} x^1 \\ \vdots \\ \vdots \\ x^S \end{bmatrix}^T \begin{bmatrix} K^T\,R\,K & 0 & \cdots & 0 \\ 0 & K^T\,R\,K & \ddots & \vdots \\ \vdots & \ddots & \ddots & 0 \\ 0 & \cdots & 0 & K^T\,R\,K \end{bmatrix} \begin{bmatrix} x^1 \\ \vdots \\ \vdots \\ x^S \end{bmatrix} \tag{7.22}$$

And therefore,

$$E\left(x^T\,Q\,x+u^T\,R u\right)=\begin{bmatrix} x^1 \\ \vdots \\ x^S \end{bmatrix}^T \begin{bmatrix} Q+K^T\,R\,K & & (0) \\ & \ddots & \\ (0) & & Q+K^T\,R\,K \end{bmatrix} \begin{bmatrix} x^1 \\ \vdots \\ x^S \end{bmatrix} \tag{7.23}$$

Let's remind that the problem consists of minimizing the expected value of the LQR cost function, i.e., minimizing

$$J_{stoch}(u) = E\left(\int_0^\infty (x(t,\xi)^T\,Q\,x(t,\xi)+u(t,\xi)^T\,R u(t,\xi))\,dt\right) \tag{7.24}$$

Therefore, with orthonormal bases, the problem is equivalent to minimizing

$$J_{ext} = \int_0^{\infty} \begin{bmatrix} x^1 \\ \vdots \\ \vdots \\ x^S \end{bmatrix}^T \begin{pmatrix} Q + K^T\ R\ K & & (0) \\ & \ddots & \\ (0) & & Q + K^T\ R\ K \end{pmatrix} \begin{bmatrix} x^1 \\ \vdots \\ \vdots \\ x^S \end{bmatrix} \tag{7.25}$$

which we will write as

$$J_{ext} = \int_0^{\infty} x_{ext}{}^T\ \underset{S}{diag}\left(Q + K^T\ R\ K\right) x_{ext} \tag{7.26}$$

where

$$x_{ext} = \left[ x_1^1 \cdots x_n^1 \cdots x_1^S \cdots x_n^S \ \right]^T \tag{7.27}$$

$$u_{ext} = \left[ u_1^1 \cdots u_m^1 \cdots u_1^S \cdots u_m^S \ \right]^T \tag{7.28}$$

which can also be written as

$$x_{ext} = \left[ (x^1)^T \cdots (x^S)^T \right]^T \tag{7.29}$$

$$u_{ext} = \left[ (u^1)^T \cdots (u^S)^T \right]^T \tag{7.30}$$

where $x^i$ has *n* components and $u^i$ has *m* components (for $1 \le i \le S$)

Therefore, the problem consists of finding $K$ minimizing

$$J_{ext} = \int_0^{\infty} x_{ext}{}^T\ \underset{S}{diag}\left(Q + K^T\ R\ K\right) x_{ext} \tag{7.31}$$

In the extended framework, the controller will be

$$K_{ext} = \begin{bmatrix} K & 0 & \cdots & 0 \\ 0 & K & \ddots & \vdots \\ \vdots & \ddots & \ddots & 0 \\ 0 & \cdots & 0 & K \end{bmatrix} = \underset{S}{diag}(K) \tag{7.32}$$

and the control law will be

$$u_{ext}(t) = -K_{ext}\ x_{ext}(t) \tag{7.33}$$

In order to use a framework equivalent to the framework used in [97, 98], an uncertain matrix $A(\xi)$ with a well-defined distribution that can be translated in a polynomial-chaos expansion

$$A(\xi) = \sum_{i=1}^{S} A^i \psi^i(\xi) \tag{7.34}$$

will be associated to the corresponding extended matrix $A_{ext}$ defined as

$$A_{ext} = \sum_{i=1}^{S} kron\left(F^i, A^i\right) \tag{7.35}$$

where

$$F^i = \begin{bmatrix} \delta_{i11}/\delta_{11} & \delta_{i12}/\delta_{11} & \cdots & \delta_{i1S}/\delta_{11} \\ \delta_{i21}/\delta_{22} & \delta_{i22}/\delta_{22} & \cdots & \delta_{i2S}/\delta_{22} \\ \vdots & \vdots & \ddots & \vdots \\ \delta_{iS1}/\delta_{SS} & \delta_{iS2}/\delta_{SS} & \cdots & \delta_{iSS}/\delta_{SS} \end{bmatrix} \tag{7.36}$$

where $\delta_{ij}$ is the inner product of the *i*-th and *j*-th basis functions and $\delta_{ijk}$ is the inner product of the *i*-th, the *j*-th and *k*-th basis functions, i.e.

$$\begin{cases} \delta_{i\,j} = \int_{\Omega} \psi^i(\xi)\, \psi^j(\xi)\, \rho(\xi)\, d\xi \\ \delta_{i\,j\,k} = \int_{\Omega} \psi^i(\xi)\, \psi^j(\xi)\, \psi^k(\xi)\, \rho(\xi)\, d\xi \end{cases} \tag{7.37}$$

In this extended framework, the state – space equations can be written as [97, 98]

$$\dot{x}_{ext}(t) = A_{ext}\; x_{ext}(t) + B_{ext}\; u_{ext}(t) \tag{7.38}$$

with $A_{ext} \in R^{n\,S \times n\,S}$ and $B_{ext} \in R^{n\,S \times m\,S}$.

Equations (7.38) and (7.33) can be written as

$$\begin{bmatrix} \dot{x}^1 \\ \vdots \\ \dot{x}^i \\ \vdots \\ \dot{x}^S \end{bmatrix} = \begin{bmatrix} A_{ext}^{11} & & \cdots & & A_{ext}^{1S} \\ & \ddots & & & \\ \vdots & & A_{ext}^{ij} & & \vdots \\ & & & \ddots & \\ A_{ext}^{S1} & & \cdots & & A_{ext}^{SS} \end{bmatrix} \begin{bmatrix} x^1 \\ \vdots \\ x^j \\ \vdots \\ x^S \end{bmatrix} + \begin{bmatrix} B_{ext}^{11} & & \cdots & & B_{ext}^{1S} \\ & \ddots & & & \\ \vdots & & B_{ext}^{ij} & & \vdots \\ & & & \ddots & \\ B_{ext}^{S1} & & \cdots & & B_{ext}^{SS} \end{bmatrix} \begin{bmatrix} u^1 \\ \vdots \\ u^j \\ \vdots \\ u^S \end{bmatrix} \tag{7.39}$$

$$\begin{bmatrix} u^1 \\ \vdots \\ \vdots \\ u^S \end{bmatrix} = - \begin{bmatrix} K & 0 & \cdots & 0 \\ 0 & K & \ddots & \vdots \\ \vdots & \ddots & \ddots & 0 \\ 0 & \cdots & 0 & K \end{bmatrix} \begin{bmatrix} x^1 \\ \vdots \\ \vdots \\ x^S \end{bmatrix} \tag{7.40}$$

where $A_{ext}^{ij} \in R^{n \times n}$, $B_{ext}^{ij} \in R^{n \times m}$ $(1 \le i \le S)$.

### 7.2.3 Derivation of the Method

The vectors quantities and their components in this section still implicitly depend on $t$. When the vectors and matrices in the extended form need to appear with subscripts or superscripts, the notation "ext" will be dropped, the same way it's already been omitted for the components of $x_{ext} = \left[ x_1^1 \cdots x_n^1 \cdots x_1^S \cdots x_n^S \right]$ and $u_{ext} = \left[ u_1^1 \cdots u_m^1 \cdots u_1^S \cdots u_m^S \right]$. For instance, $(A_{ext})_{l\mu}^{ji}$ will simply be written as $A_{l\mu}^{ji}$: the fact that both superscripts and subscripts are present implies that the matrix is in its extended form. The vectors $\lambda_{ext}^i$ defined below will be written as $\lambda^i$ since superscripts imply an extended form.

The forward equations are

$$\dot{x}^i = \sum_{j=1}^{S} \left( A^{ij} - B^{ij} K \right) x^j, \; 1 \le i \le S \tag{7.41}$$

Therefore, the Lagrangian function is

$$L = \int_0^\infty \left( \begin{array}{c} \sum_{i=1}^{S} (x^i)^T (Q + K^T \; R \; K) \; x^i - \sum_{i=1}^{S} (\lambda^i)^T \; \dot{x}^i \\ + \sum_{i,\, j=1}^{S} (\lambda^i)^T \; (A^{ij} - B^{ij} \; K) \; x^j \end{array} \right) dt \tag{7.42}$$

where $\lambda^i$'s are the Lagrange multipliers. Let's note that each $\lambda^i$ has *n* components. All the Lagrange multipliers can be represented using an extended vector

$$\lambda_{ext} = \left[ (\lambda^1)^T \cdots (\lambda^S)^T \right]^T \in R^{n \times S} \tag{7.43}$$

Differentiating the Lagrangian yields

$$\delta L = \int_0^{\infty} \left( \begin{array}{l} \sum_{i=1}^{S} 2\,(\delta x^i)^T (Q + K^T\ R\ K)\ x^i - \sum_{i=1}^{S} (\lambda^i)^T\ (\delta \dot{x}^i) \\ + \sum_{i,j=1}^{S} (\delta x^j)^T\ (A^{ij} - B^{ij}\ K)^T\ \lambda^i \\ + \sum_{i=1}^{S} (x^i)^T\ (\delta K^T\ R\ K)\ x^i + \sum_{i=1}^{S} (x^i)^T\ (K^T\ R\ \delta K)\ x^i \\ - \sum_{i,j=1}^{S} (\lambda^i)^T\ B^{ij}\ \delta K\ x^j \end{array} \right) dt \qquad (7.44)$$

After integrating by part, this yields

$$\delta L = -\sum_{i=1}^{S} \left( (\lambda^i)^T\ \delta x^i \right)_0^{\infty} + \int_0^{\infty} \left( \begin{array}{l} \sum_{i=1}^{S} 2\,(\delta x^i)^T (Q + K^T\ R\ K)\ x^i - \sum_{i=1}^{S} (\delta x^i)^T\ (\dot{\lambda}^i) \\ + \sum_{i,j=1}^{S} (\delta x^j)^T\ (A^{ij} - B^{ij}\ K)^T\ \lambda^i + \sum_{i=1}^{S} (x^i)^T\ (\delta K^T\ R\ K)\ x^i \\ + \sum_{i=1}^{S} (x^i)^T\ (K^T\ R\ \delta K)\ x^i - \sum_{i,j=1}^{S} (\lambda^i)^T\ B^{ij}\ \delta K\ x^j \end{array} \right) dt \qquad (7.45)$$

Since $R$ is a symmetric matrix, this is equivalent to

$$\delta L = -\sum_{i=1}^{S} \left( (\lambda^i)^T\ \delta x^i \right)_0^{\infty} + \int_0^{\infty} \left( \begin{array}{l} \sum_{i=1}^{S} (\delta x^i)^T \left( 2\,(Q + K^T\ R\ K)\ x^i + \dot{\lambda}^i + \sum_{j=1}^{S} (A^{ij} - B^{ij}\ K)^T\ \lambda^j \right) \\ + \sum_{i,j=1}^{S} \left( 2\,(x^j)^T\ K^T\ R - (\lambda^i)^T\ B^{ij} \right) \delta K\ x^j \end{array} \right) dt \qquad (7.46)$$

and finally

$$\delta L = -\sum_{i=1}^{S} \left( (\lambda^i)^T\ \delta x^i \right)_0^{\infty} + \int_0^{\infty} \left( \begin{array}{l} \sum_{i=1}^{S} (\delta x^i)^T \left( 2\,(Q + K^T\ R\ K)\ x^i + \dot{\lambda}^i + \sum_{j=1}^{S} (A^{ij} - B^{ij}\ K)^T\ \lambda^j \right) \\ + \sum_{i,j=1}^{S} \left( 2\,R\ K\ x^j - (B^{ij})^T\ \lambda^i \right)^T\ \delta K\ x^j \end{array} \right) dt \qquad (7.47)$$

Assuming the initial conditions are not uncertain, the boundary conditions yield $\sum_{i=1}^{S} \left( (\lambda^i)^T\ \delta x^i \right)_0^{\infty} = 0$, and it can be rewritten as

$$\delta L = \int_0^\infty \left( \begin{array}{l} \sum_{i=1}^{S} (\delta x^i)^T \left( 2\,(Q + K^T\ R\ K)\ x^i + \dot{\lambda}^i + \sum_{j=1}^{S} (A^{ij} - B^{ij}\ K)^T\ \lambda^j \right) \\ + \sum_{i,\,j=1}^{S} \left( 2\ R\ K\ x^j - (B^{ij})^T\ \lambda^i \right)^T\ \delta K\ x^j \end{array} \right) dt \tag{7.48}$$

The term in $\delta x^i$ should be zero, which yields the adjoint equations:

$$\dot{\lambda}^i = -\left( \sum_{j=1}^{S} (A^{ij} - B^{ij}\ K)^T\ \lambda^j \right) - 2\,(Q + K^T\ R\ K)\ x^i, \quad (i = 1, \ldots, S) \tag{7.49}$$

The optimality condition is given by

$$\int_0^\infty \left( \sum_{j=1}^{S} \left( 2\ R\ K\ x^j - (B^{ij})^T\ \lambda^i \right)^T\ \delta K\ x^j \right) dt = 0 \quad \text{for } 1 \le i \le S \tag{7.50}$$

which is equivalent to

$$\sum_{j=1}^{S} \int_0^\infty \left( 2\ R\ K\ x^j \right)^T \delta K\ x^i\ dt = \sum_{j=1}^{S} \int_0^\infty \left( (B^{ij})^T\ \lambda^i \right)^T \delta K\ x^j\ dt \tag{7.51}$$

Written one by one, the optimality equations are

$$\int_0^\infty \sum_{l=1}^{S} \left( \left( 2\ R\ K \right)_{\mu l}\ x_l^j - \sum_{i=1}^{S} B_{l\mu}^{ji}\ \lambda_l^i \right) x_\nu^j\ dt = 0,\ 1 \le \mu \le m,\ 1 \le \nu \le n \tag{7.52}$$

Therefore, the optimality equations can be written as

$$\int_0^\infty \left( \begin{array}{l} 2\ R\ K \sum_{j=1}^{S} \left[ x^j\ x_1^j, x^j\ x_2^j, \ldots, x^j\ x_n^j \right] \\ - \sum_{j=1}^{S} \sum_{i=1}^{S} \left[ (B^{ij})^T \lambda^i\ x_1^j, (B^{ij})^T \lambda^i\ x_2^j, \ldots, (B^{ij})^T \lambda^i\ x_n^j \right] \end{array} \right) dt = 0 \tag{7.53}$$

which can also be written as

$$2\ R\ K \int_0^\infty XX(t)\ dt = \int_0^\infty XL(t)\ dt \tag{7.54}$$

with

$$\begin{cases} XX(t) = \sum_{j=1}^{S} x^j(t) \left(x^j(t)\right)^T \\ XL(t) = \sum_{j=1}^{S} \sum_{i=1}^{S} \left(B^{ij}\right)^T \lambda^i(t) \left(x^j(t)\right)^T \end{cases} \tag{7.55}$$

The quantity $XX(t)$ can also be written as

$$XX(t) = \begin{bmatrix} \sum_{j=1}^{S} x_1^j(t)\, x_1^j(t) & \cdots & \sum_{j=1}^{S} x_1^j(t)\, x_n^j(t) \\ \sum_{j=1}^{S} x_2^j(t)\, x_1^j(t) & \cdots & \sum_{j=1}^{S} x_2^j(t)\, x_n^j(t) \\ \vdots & & \vdots \\ \sum_{j=1}^{S} x_n^j(t)\, x_1^j(t) & \cdots & \sum_{j=1}^{S} x_1^j(t)\, x_n^j(t) \end{bmatrix} \tag{7.56}$$

Let's note that $R$ was defined as a positive definite matrix and is therefore invertible. Assuming that $\int_0^\infty XX(t)\, dt$ is invertible, the optimal controller $K$ is given by

$$K = \frac{1}{2} R^{-1} \int_0^\infty XL(t)\, dt \left( \int_0^\infty XX(t)\, dt \right)^{-1} \tag{7.57}$$

with $XX(t)$ and $XL(t)$ defined in Equation (7.55).

Equation (7.57) is not a usable closed form solution. The main problem is that the coefficients $x^i$ 's cannot be used individually in the real world. Since $K$ is fixed once and for all while the uncertainty $\xi$ can take different values that are not measured, a usable closed-form solution would have to come in the form of polynomial chaos expansions for which no coefficient can be taken off the weighted sum. Indeed, the values that can physically be used by the controller are

$$x_k(t, \xi) = \sum_{i=1}^{S} x_k^i(t)\, \psi^i(\xi), \quad 1 \le k \le n \tag{7.58}$$

Many approximations related to the polynomial framework have been tried before developing a numerical method, but none of them gave very satisfactory results when applied to basic examples. Therefore, a numerical method was needed.

### 7.2.4 Proposed Method

The proposed algorithm consists of performing the following iterations until $K$ converges, starting with a best guess $K_0$. By default, it is advised to start with a best guess $K_0$ corresponding to the optimal controller for the deterministic case, which can be calculated using equations (7.4) and (7.5).

Each iteration corresponds to the following three steps:

1. Use the forward equations $\dot{x}_{ext}(t) = \left( A_{ext} - B_{ext} \underset{S}{diag}(K) \right) x_{ext}(t)$ to obtain the states $x_\nu^j(t)$ $(\forall j\,,\ \forall \nu\,,\ \forall t)$
2. Then use the adjoint equations displayed in (7.49), i.e.

$$\dot{\lambda}_{ext}(t) = -\left( A_{ext}^T - \underset{S}{diag}\left(K^T\right) B_{ext}^T \right) \lambda_{ext}(t) - 2 \underset{S}{diag}\left(Q + K^T R K\right) x_{ext}(t)$$

   to obtain the Lagrange multipliers $\lambda_\mu^j(t)$ $(\forall j\,,\ \forall \mu\,,\ \forall t)$
3. Compute the new iterative value of $K$ using Equation (7.57)

The problem with the algorithm is that practically, it is not possible to numerically calculate all expression from $t = 0$ to $t = \infty$. Therefore, it is advised to use a large final time value $t_f$ and check that an even larger value $t_f$ still yields the same results. The algorithm can also be used for the finite time LQR problem, as illustrated below.

The forward equations are integrated starting with $x_{ext}(0)$. The adjoint equations need to be integrated backwards starting with $\lambda_{ext}(t_f) = 0$.

## 7.3 Application to a Simple System

### 7.3.1 Description of the System

The test case used for this study consists of a system for which the equations of motion can be described by

$$\dot{x}(\xi,t) = A(\xi)\, x(\xi,t) + B(\xi)\, u(\xi,t) \tag{7.59}$$

with

$$\begin{cases} A(\xi) = -1 - 0.5\,\xi \\ B(\xi) = 1 - 0.5\,\xi \end{cases} \tag{7.60}$$

and with a known initial condition $x(0) = 1$

For the sake of simplicity, the distribution of $\xi$ is assumed to be uniform, i.e.:

$$\rho(\xi) = \frac{1}{2}, \quad \xi \in [-1,1] \tag{7.61}$$

The problem consists of finding $K$ minimizing the following LQR function

$$J = \int_{\xi=-1}^{1} \left( \int_{0}^{\infty} x(t,\xi)^T\, Q\, x(t,\xi) + u(t,\xi)^T\, R u(t,\xi)\, dt \right) \rho(\xi)\, d\xi \tag{7.62}$$

with

$$\begin{cases} Q = 1 \\ R = 1 \end{cases} \tag{7.63}$$

This example has been chosen because the LQR cost function can be calculated analytically and is equal to

$$J = \left( \frac{1 + K^2}{2} \right) \left( \frac{\log_n[3 + K] - \log_n[1 + 3\,K]}{1 - K} \right) \tag{7.64}$$

which is minimized for the following $K$:

$$K_{stoch} = 0.4518 \tag{7.65}$$

Since $t = \infty$ cannot be used in the formulation for this method, a final time yielding the same answer than with $t = \infty$ must be found. Solving the finite time problem consists of finding $K$ minimizing

$$J = E\left(\int_0^{t_f} (x(t,\xi)^T Q\, x(t,\xi) + u(t,\xi)^T R u(t,\xi))\, dt\right) \tag{7.66}$$

The final time $t_f = 20$ is chosen because it is large enough to also yields $K_{stoch} = 0.4518$, which can be calculated by numerically evaluating the corresponding cost function, which is shown in Figure 7.1. This cost function is very similar to the cost function (7.64) for the infinite-time problem. If the answer was not already provided by a cost function that is already evaluated, we would need to see the answer converging as $t_f$ increases. Therefore, future work will need to include a more rigorous formulation and an efficient numerical method to estimate what final time can be considered good enough.

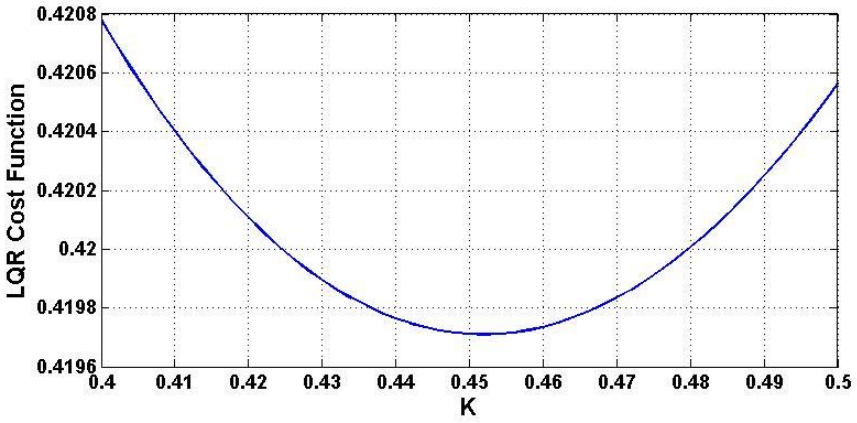


Figure 7.1: Expected Value of the LQR Cost Function with $t_f = 20$

### 7.3.2 Results Obtained with the Polynomial Chaos Based Numerical Method

The results displayed in Table 7.1 are obtained by starting the algorithm with $K_0$ corresponding to the optimal controller for the deterministic case, i.e. $K_0 = 0.4142$. The algorithm was run with a final time $t_f = 20$

The results do not converge exactly to 0.4518, which is the solution for the finite time problem with $t_f = 20$. For instance, with 8 polynomial chaos terms and 15 iterations, the result is still 0.4516 (and 15 significant digits have converged after 14 iterations). This is due to the fact that the cost function is extremely flat in an area containing our estimate (0.4516) and the real answer (0.4518), as shown in Figure 7.2. In a way, the LQR function is minimized: the value of the LQR function obtained with $K_{est} = 0.4516$ is basically the same than the value obtained with $K_{stoch} = 0.4518$. Both cases yields a LQR function equal to 0.419736. The slightest numerical errors (in the ODEs for instance) can result in a slightly different estimate for the controller.

Table 7.1: Estimation Results with K0 = 0.4142

| *Number of PC terms* | *Iteration 1* | *Iteration 2* | *Iteration 3* | *Iteration 4* | *Iteration 5* |
|---|---|---|---|---|---|
| 3 | 0.4559 | 0.4511 | 0.4516 | 0.4516 | 0.4515 |
| 4 | 0.4559 | 0.4511 | 0.4516 | 0.4516 | 0.4516 |
| 6 | 0.4559 | 0.4511 | 0.4516 | 0.4516 | 0.4516 |

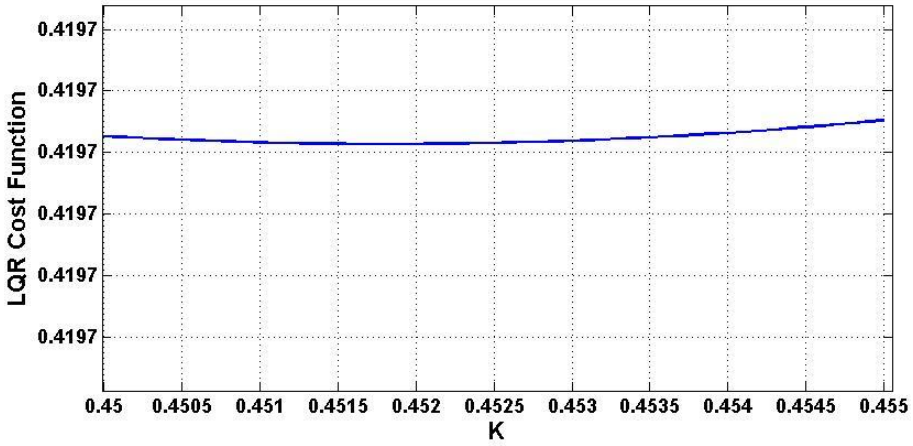


Figure 7.2: Expected Value of the LQR Cost Function Around the Solution

The results displayed in Table 7.2 are obtained by starting the algorithm with $K_0 = 0$ (i.e., uncontrolled system) in order to show that the algorithm would converge to the same value than with $K_0 = 0.4142$. It can be observed that after the fourth iteration, the same results are obtained than with $K_0 = 0.4142$ for each different number of polynomial chaos terms that were used (using 4 significant digits). After a certain number of iteration, the algorithm's precision was indeed expected to depend only on the number of polynomial chaos terms that are used, and not the initial guess. Negative values for $K_0$ (which would never actually be used) have also been tried, and the algorithm still converges, but with much larger errors for the first few iterations, which means a few extra iterations are needed.

Table 7.2: Estimation Results with K0 = 0

| *Number of PC terms* | *Iteration 1* | *Iteration 2* | *Iteration 3* | *Iteration 4* | *Iteration 5* |
|---|---|---|---|---|---|
| 3 | 0.7091 | 0.4542 | 0.4513 | 0.4516 | 0.4515 |
| 4 | 0.7123 | 0.4545 | 0.4513 | 0.4516 | 0.4516 |
| 6 | 0.7126 | 0.4545 | 0.4513 | 0.4516 | 0.4516 |

### 7.3.3 Controller Analysis after Designing the Controller

As mentioned earlier, the optimal LQR controller does not guarantee a minimum performance or even stability for the worst case scenario. However, using the optimal LQR controller for the stochastic problem will very often result in a better overall controller compared with the controller consisting of the gains obtained for the deterministic case. Though there is no guarantee it will be the case, it can be easily be checked by performing controller analysis, which is much easier task than controller design. Figure 7.3 shows a general framework for the analysis and for compensator design for linear systems

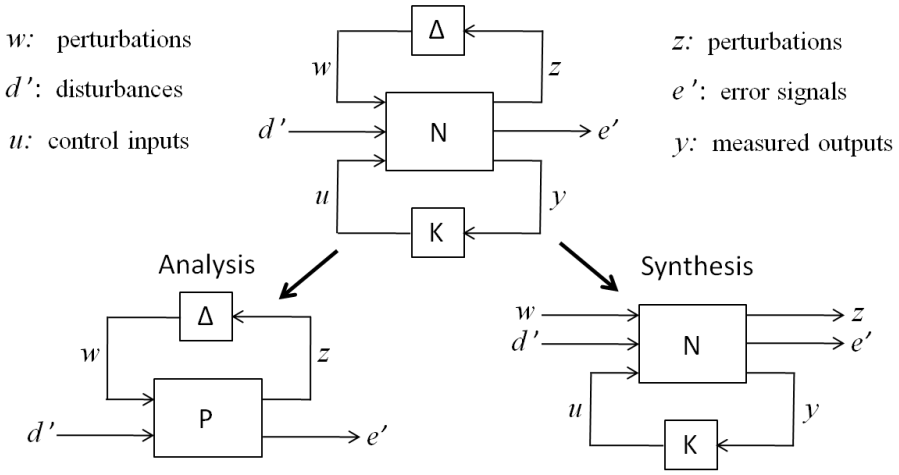


Figure 7.3: A General Framework for the Analysis and for Compensator Design for Linear Systems (adapted from [84])

The classical approach consists of guaranteeing $\| e'(s)/d'(s) \| < \gamma$ where $\gamma$ is a constant. The best controllers correspond to the smallest possible values of $\gamma$. For instance, an $H_\infty$ controller would guarantee $\left\| \frac{e'(s)}{d'(s)} \right\|_\infty < \gamma$. A judicious probabilistic approach would consist of finding the probability $P\left( \left\| \frac{e'(s)}{d'(s)} \right\| \right) < \gamma$ for different value of $\gamma$ and the cost associated to it.

In the LQR case, for a given controller, the percentage of cases staying below a certain cost is directly obtained by simply looking at the Cumulative Distribution Function of the LQR cost function. Figure 7.4 displays the PDF and the CDF of the LQR cost function for the simple system presented in this section, for the deterministic controller (i.e., K = 0.4142) and for the controller minimizing the expected value of the LQR cost function (i.e., K = 0.4518). The red lines in Figure 7.4 correspond to the LQR cost function obtained with the deterministic controller. The stochastic controller yields a better worst case scenario. It yields a maximum cost function equal to 0.5112 while the deterministic controller yields a maximum cost function equal to 0.5224. However, the best case scenario is obtained with the deterministic controller, which can yield a LQR cost function equal to 0.3432 (while the smallest LQR cost function obtained

with the stochastic controller is 0.3489). On average, the stochastic controller yields the smallest LQR function: that is what it has been designed for.

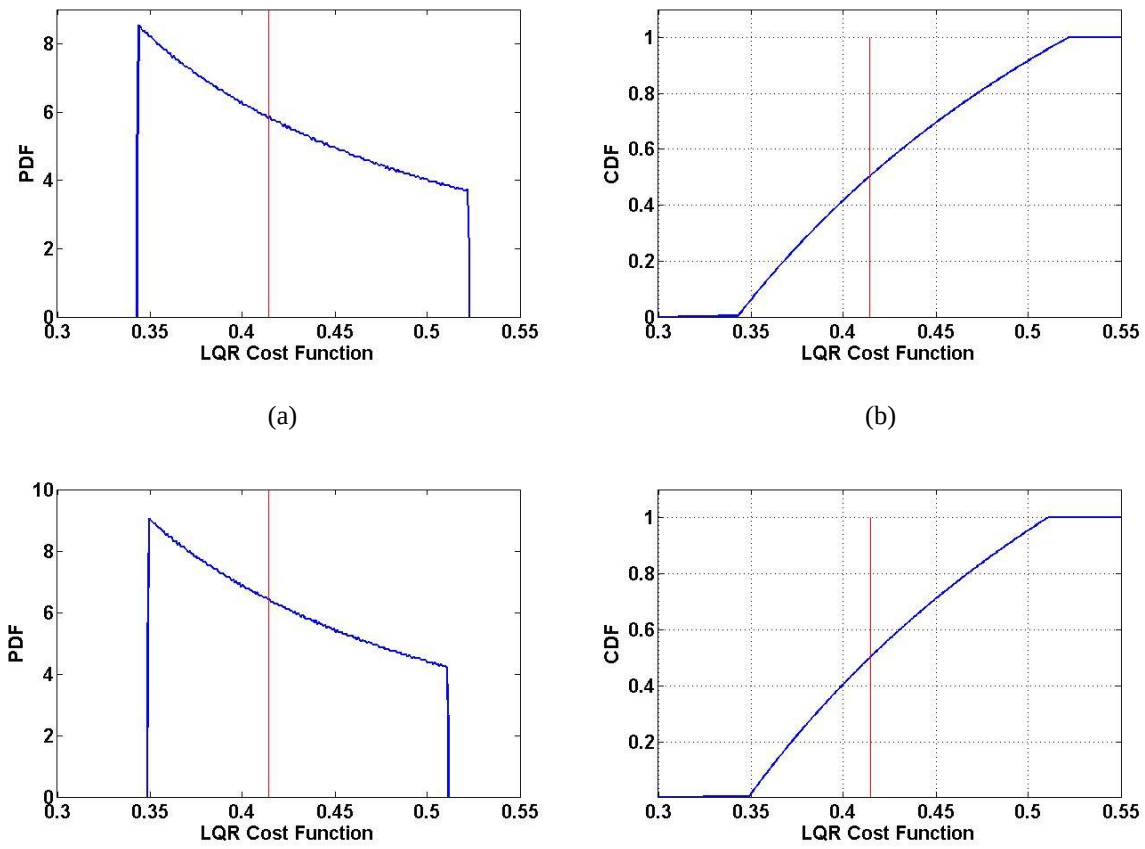


Figure 7.4: PDF and CDF of the LQR Cost Function: (a) PDF Obtained with the Optimal Deterministic Controller (K = 0.4142); (b) CDF Obtained with the Optimal Deterministic Controller (K = 0.4142); (c) PDF Obtained with the Optimal Stochastic Controller (K = 0.4518); (d) CDF Obtained with the Optimal Stochastic Controller (K = 0.4518)

## 7.4. Summary and Conclusions

This chapter applies the polynomial chaos theory to the LQR problem when the parameters in the formulation are uncertain. The numerical method described in this chapter provides a

controller minimizing the mean value of the LQR cost function obtained for a certain distribution of the uncertainties which is assumed to be known.

The original attempt was to find a closed form solution, hoping that the polynomial chaos framework might provide a solution that would depend on the number of terms used in the polynomial chaos expansions but would converge to the solution of the problem as the number of terms increases. The LQR problem was written as an optimality problem using Lagrange multipliers in an extended form associated with the polynomial chaos framework. The formulas obtained for that problem were then used in order to develop a numerical method solving that problem. This is a polynomial chaos based method, which therefore has the advantage of being computationally more efficient than Monte Carlo simulations. The algorithm has been applied to a simple example for which the answer was already known, and it yielded correct results within a few iterations for that case study.

The Linear-Quadratic Regulator controller is not very well adapted to robust design, and the optimal controller does not guarantee a minimum performance or even stability for the worst case scenario. Stability robustness and performance robustness in the presence of uncertainties are therefore not guaranteed. However, the answer provided by this algorithm might still prove to yield a judicious controller in certain cases. The method presented in this chapter might also have the potential of being a first step towards the development of computationally efficient numerical methods for $H_\infty$ design with parametric uncertainties.

Possible extensions of this work would be a more rigorous formulation for the infinite time LQR problem, adding uncertainties on Q and R and therefore introducing matrices $Q_{ext}$ and $R_{ext}$ , and applying this method to more complex dynamic systems, such as vehicle suspensions. The longer term objective would be to extend this method to $H_2$ and $H_\infty$ problems. After designing LQR, $H_2$ and $H_\infty$ controllers for more complex systems, controller analysis should be performed as well

# 8 Conclusion and Future Research Directions

This chapter provides a summary of the research presented in the previous chapters and the significant results that have been obtained. It further includes several directions for future work that should be pursued in this area of research. Each section is divided into two parts corresponding to the two main areas of this study: parameter estimation and controls.

## 8.1 Summary of Research Accomplishments

### 8.1.1 Polynomial Chaos Theory and Parameter Estimation

Mechanical systems operate under parametric and external excitation uncertainties. The polynomial chaos approach has been shown to be more efficient than Monte Carlo approaches for quantifying the effects of such uncertainties on the system response. We applied it to parameter estimation, which is a computationally expensive problem. Parameter estimation is an important problem, because in many applications parameters cannot be directly measured with sufficient accuracy; this is the case, for example, in real time applications. Rather, parameter values must be inferred from available measurements of different aspects of the system response. Information about the poorly known parameters is obtained via parameter estimation techniques. In this dissertation, two new computational approaches for parameter estimation based on the polynomial chaos theory have been developed. Both methods have been illustrated on a nonlinear four-degree-of-freedom roll plane model of a vehicle in which the parameters of interest to be estimated were an uncertain mass and its uncertain position at which the mass is added on the roll bar.

The first approach is a polynomial-chaos based Bayesian approach in which maximum likelihood estimates are obtained by minimizing a cost function derived from the Bayesian theorem. It has been shown that the quality of the maximum likelihood estimate is related to the shape of the Bayesian cost function, with a sharp minimum indicating an accurate estimate. The parameters are non-identifiable when different parameter values lead to identical system outputs. In this case the Bayesian cost function has an entire region of minima (e.g., a valley), with each

parameter value in the region being equally likely. Regularization techniques can still yield most likely values among the possible combinations of uncertain parameters resulting in the same time responses than the ones observed. For identifiable and observable systems accurate estimates can be obtained in most cases even if the output signal is sampled below the Nyquist frequency. In the worst case, however, sampling below the Nyquist rate cannot guarantee that sufficient information is extracted from the output. In this worst case the apriori information becomes important and the estimate is biased toward the apriori most likely value.

The second approach is based on the Extended Kalman Filter (EKF). The error covariances needed for the EKF approach are computed from polynomial chaos expansions, and the EKF is used to update the polynomial chaos representation of the uncertain states and the uncertain parameters. This EKF approach benefits from the computational efficiency of the polynomial chaos approach in the simulation of systems with a small number of uncertain parameters. The filter formula based on the EKF is also computationally inexpensive. Polynomial chaoses offer an accurate representation of uncertainties and can accommodate non-Gaussian probability distributions. The EKF approach gives more information about the parameters of interest than a single value: the estimation comes in the form of a polynomial chaos expansion from which the aposteriori probability density of the estimated parameters can be retrieved. The EKF approach deteriorates with increased sampling rates. A rigorous error analysis was performed in order to explain this counter-intuitive behavior, and a new version of the EKF approach was developed to alleviate this problem. However, the Bayesian approach is still more robust than the new version of the EKF approach when dealing with non-identifiable systems.

As a conclusion, the new methods developed in this study have several advantages. Simulations using Polynomial Chaos methods are much faster than Monte Carlo simulations for the same accuracy, and both approaches can accommodate noisy measurements. One advantage of the Bayesian approach is that it is optimal; it can treat non-Gaussian uncertainties since the Bayesian approach is not tailored to any specific distribution. The EKF approach is suboptimal for non-Gaussian uncertainties, but has an advantage over the Bayesian approach: the estimation comes in form of a PDF. Finally, the Bayesian approach is more robust: sampling at a higher frequency yields more accurate result except when non-identifiability issues exist, in which case sampling at a higher frequency does not hurt and regularization techniques can be used, whereas

sampling at a higher frequency with the EKF approach can yield poorer estimations when dealing with non-identifiability issues.

### 8.1.2 Polynomial Chaos Theory and Control Methods

The polynomial chaos theory has been applied to a simple example, a bicycle model with a controller designed to prevent 'spinout', or uncontrolled yawing, in order to explain why it can $H_2$ be applied to some control problems (Bode diagrams and stability margins in this example) and not others (location of open-loop and closed loop poles): the polynomial chaos theory needs to be applied to variables which are $C^1$ (i.e., have continuous derivatives) with respect to the uncertain parameters. Since the polynomial chaos theory cannot be used for very general applications related to pole placement methods, its use is limited, and many well-known classical methods for controller design, such as the root locus, cannot be applied in the general case. Controller analysis is still possible, but controller synthesis is a much more difficult problem due to the need of using functions having continuous derivatives. The efficiency of the polynomial chaos theory for controller analysis has been showed for several examples using the bicycle model: Bode diagrams and PDFs of the stability margins. It has also been illustrated for the analysis of a transfer function obtained using an $H_\infty$ controller for an active suspension model.

The controller synthesis part of the research has focused on the development of a new computational approach for the Linear-Quadratic Regulator (LQR) problem with uncertain parameters in the formulation. The problem consist of finding a controller minimizing the mean value of the LQR cost function obtained for a certain distribution of the uncertainties which is assumed to be known. Brian Templeton, who was also working under VIPER, already developed an efficient polynomial-chaos based gradient descent optimization method finding optimal gains for $H_2$ and LQR design with parametric uncertainties. However, extending his method to $H_\infty$ design would seem difficult to achieve. The original intent of the work presented in this study was to try deriving a closed-form solution of the LQR problem in the polynomial chaos framework because the $H_\infty$ problem can be seen as extension of the LQR problem. This proved to be extremely difficult, if not impossible. However, this work led to the development of a new numerical method based on the fundamental approach to solving the LQR problem, which is derived using Lagrange multipliers in the deterministic case and leads to the well-known

algebraic Riccati equations. In this new method, the LQR problem is written as an optimality problem using Lagrange multipliers in an extended form associated with the polynomial chaos framework, and an iterative algorithm converges to the optimal answer. The algorithm has been applied to a simple example for which the answer was already known.

The Linear-Quadratic Regulator controller is not very well adapted to robust design, and the optimal controller does not guarantee a minimum performance or even stability for the worst case scenario. Stability robustness and performance robustness in the presence of uncertainties are therefore not guaranteed. However, this is a first step aimed at designing more judicious controllers if combined with other techniques in the future. The solution to the $H_\infty$ problem as well as the $H_2$ problem can be seen as extensions of the LQR problem. This new method might therefore have the potential of being a first step towards the development of computationally efficient numerical methods for $H_\infty$ design with parametric uncertainties.

## 8.2 Recommendations for Future Research

### 8.2.1 Polynomial Chaos Theory and Parameter Estimation

Future work should include the automation of the polynomial chaos based parameter estimation methods presented in this study, as well as real time implementation. For the Bayesian approach, an improvement would consist of automatically choosing a number of polynomial chaos terms and collocation points for a certain desired level of precision. The current approach consists of simply checking that adding extra terms an extra collocation points does not change the results significantly. The EKF approach can yield poor estimations when dealing with non-identifiability issues, and would therefore need an extra improvement, which would consist of having an algorithm automatically deciding whether the results can be trusted or not. An even better improvement would consist of calculating a coefficient indicating how much trust we have in the results. One idea would be to compute the PDFs obtained with different subsets of measurements and find a correlation index between them. This would especially be useful when using high sampling frequency is possible, since a very low correlation with high frequency samples would indicate divergence problems in the filter and not a lack of samples. After achieving this, the methods should be validated using real data instead of synthetic measurements.

Dr. Corina Sandu, Joe Hays and I are currently working in collaboration with the University of Michigan on implementing the methods presented in this study to mass estimators for on-road vehicles. One objective is to estimate the vehicle mass without previewing the road. Another objective will be estimating C.G. heights for on-road vehicles. If successful, real-time estimation would be the next objective.

### 8.2.2 Polynomial Chaos Theory and Control Methods

Possible extensions of this work would be a more rigorous formulation for the infinite time LQR problem, adding uncertainties on Q and R and therefore introducing matrices $Q_{ext}$ and $R_{ext}$ , and applying this method to more complex dynamic systems, such as vehicle suspensions. The longer term objective would be to extend this method to $H_2$ and $H_\infty$ problems. After designing LQR, $H_2$ and $H_\infty$ controllers for more complex systems, controller analysis should be performed as well. Future work should also include theoretical analysis of conditions under which performance (e.g., stability) is guaranteed in the worst case.

## Appendix: EKF Error Analysis

The objective of this analysis is to show that the truncations in the polynomial chaos expansions can prevent the convergence of the covariance of the assimilated state and that the error can decrease with the length of the time step when there is no model error (which was the case for this study: the EKF approach assumes that the equations of motion of the system are perfectly known). This analysis will also show that when model errors are present, a nonzero optimal time step can exist.

### A1. Framework

Consider the scalar system $y' = a\,y$ with $a < 0$, which is considered to be the true system, with initial condition $y_0^{true}$. It has a well-known analytical solution: $y(t) = y_0\, e^{a\,t}$. After $k$ time steps $\Delta t$ which are assumed to be constant, the "true" value of the state variable $y$ is:

$$y_k^{true} = e^{a\,\Delta t}\; y_{k-1}^{true} = e^{k\,a\,\Delta t}\; y_0^{true} \tag{A1.1}$$

Using the notation $b = e^{a\,\Delta t}$, it can also be written as:

$$y_k^{true} = b\; y_{k-1}^{true} = b^k\; y_0^{true} \tag{A1.2}$$

Let's notice that $a < 0$ is equivalent to $0 < b < 1$.

A perturbed model will be used:

$$y' = a\,y + \varepsilon, \quad y(0) = y_0^a \tag{A1.3}$$

It is also assumed that the error model $\varepsilon(t)$ is independent Gaussian with mean $B$ ($B$ is the bias) and covariance $Q$. For the sake of simplicity, it will also be assumed that $\varepsilon(t)$ is fixed during each time interval $\Delta t$, i.e., that it takes the fixed value $\varepsilon_{k+1}$ between time $t_k$ and $t_{k+1}$.

**A2. Recurrence Relationships – Error and Covariance**

The state $y$ is propagated using the model equations:

$$y_{k+1}^f = e^{a\,\Delta t} y_k^a + \varepsilon_{k+1}\left(\frac{e^{a\,\Delta t}-1}{a}\right) \tag{A2.1}$$

where the superscript *f* stands for forecast and the superscript *a* stands for assimilated.

The assimilated state at step $k$, $y_k^a$, is given by:

$$y_k^a = (1-K_k)\, y_k^f + K_k\; y_k^{obs}, \tag{A2.2}$$

where $K_k$ is the Kalman gain at step $k$, given by

$$K_k = P_k^f\, H_k{}^T \left(R_k + H_k P_k^f\, H_k{}^T\right)^{-1} \tag{A2.3}$$

In the 1-dimentional case, each matrix becomes a scalar. Here, it will be assumed that all the $R_k$ 's can be replaced by $R$ ( where $R_k$ is the covariance matrix of the observational error $\mu_k$ defined in Equation (4.3)), which means that the noise level associated with the measurements is assumed to be constant. It will also be assumed that $H_k = 1$, i.e., we can directly measure $y$. Therefore, the Kalman gain at step $k$ is

$$K_k = \frac{P_k^f}{R + P_k^f} \tag{A2.4}$$

where $P_k^f$ is the forecast covariance matrix defined in Equation (4.4)

and the assimilated state at step $k$, $y_k^a$, is given by:

$$y_k^a = \frac{R}{R + P_k^f}\, y_k^f + \frac{P_k^f}{R + P_k^f}\; y_k^{obs} \tag{A2.5}$$

Using the notation $c = \dfrac{e^{a\,\Delta t}-1}{a} = \dfrac{b-1}{a}$, the model equation can be rewritten as

$$y_{k+1}^f = b\, y_k^a + c\, \varepsilon_{k+1} \tag{A2.6}$$

Let $E_k^a$ be the error at step $k$ after assimilation,

$$E_k^a = y_k^a - y_k^{true} \tag{A2.7}$$

Then, the "forecast" error at step $k+1$ (before assimilation) is given by:

$$E_{k+1}^f = b\, E_k^a + c\, \varepsilon_{k+1} \tag{A2.8}$$

Therefore,

$$< E_{k+1}^f >= b\ < E_k^a > + c\ B \tag{A2.9}$$

$$E_{k+1}^f - < E_{k+1}^f >= b\left(E_k^a - < E_k^a >\right) + c\ (\varepsilon_k - B) \tag{A2.10}$$

$$\left\langle \left(E_{k+1}^f - < E_{k+1}^f >\right)^2 \right\rangle = b^2 \left\langle \left(E_k^a - < E_k^a >\right)^2 \right\rangle + c^2 <\varepsilon_k - B>^2 + \underbrace{\left\langle b < \left(E_k^a - < E_k^a >\right), c <\varepsilon_k - B> \right\rangle}_{=0\ (uncorrelated)} \tag{A2.11}$$

which can also be written as

$$P_{k+1}^f = b^2\ P_k^a + c^2\ Q \tag{A2.12}$$

where $P_{k+1}^f$ is the forecast variance at step $k+1$.

The objective of this analysis is to study the effect of the polynomial chaos approximation. Therefore, a term $\mu$ due to the truncation in the polynomial chaos expansion will be added to the forecast covariance:

$$P_{k+1}^f = b^2\ P_k^a + c^2\ Q + \mu \tag{A2.13}$$

For the sake of simplicity, $\mu$ will be assumed to be a constant. The assumption about the error being constant can be regarded as a lower bound on the error since the term $\mu$ due to the truncation always has the same sign ($\mu < 0$), which means that the covariance is underestimated. Therefore, the error will always be at least that number. Indeed, the average value of a quantity $y = \sum_{i=1}^{\infty} y^i\ \psi^j(\xi)$ is

$$\langle y \rangle = y^1, \tag{A2.14}$$

which means that its covariance can be expressed as

$$\mathrm{cov}(y) = \sum_{i=2}^{\infty} \left(y^i\right)^2 \tag{A2.15}$$

while the covariance of its truncated polynomial chaos expression is

$$\mathrm{cov}(y^{PC}) = \sum_{i=2}^{S} \left(y^i\right)^2 \tag{A2.16}$$

Therefore, the term $\mu$ due to the truncation in the polynomial chaos expansion is

$$\mu = \mathrm{cov}(y^{PC}) - \mathrm{cov}(y) = -\sum_{i=S+1}^{\infty} \left(y^i\right)^2 < 0 \tag{A2.17}$$

Thus, the effect of the truncation will be to underestimate the covariance. It will be shown later in Equation (A3.7) that overestimating the covariance is not a problem, but underestimating it too much prevents the convergence of the covariance. Therefore, the assumption about the truncation error of the covariance being constant can be regarded as a lower bound on the error.

Using the notation $\zeta = c^2\, Q + \mu$ yields

$$P_{k+1}^f = b^2\, P_k^a + \zeta \tag{A2.18}$$

Let's note that $\zeta$ is a constant for a constant time interval $\Delta t$. An independent Gaussian noise $\eta$ with mean zero and covariance $R$ is added to the observations:

$$y_{k+1}^{obs} = y_{k+1}^{true} + \eta_{k+1} = b\, y_k^{true} + \eta_{k+1} = b^{k+1}\, y_0^{true} + \eta_{k+1} \tag{A2.19}$$

The assimilated state at step $k+1$, $y_{k+1}^a$, is given by

$$y_{k+1}^a = (1 - K_{k+1})\, y_{k+1}^f + K_{k+1}\, y_{k+1}^{obs} \tag{A2.20}$$

Using the notation $E_k = E_k^a$ (i.e., $E_k$ is the error after assimilation at step $k$), the error after assimilation at step $k+1$ is:

$$E_{k+1} = y_{k+1}^a - y_{k+1}^{true} = y_{k+1}^a - b\, y_k^{true} \tag{A2.21}$$

$$E_{k+1} = (1 - K_{k+1})\, b\, y_k^a + K_{k+1}\, b\, y_k^{true} - b\, y_k^{true} + (1 - K_{k+1})\, c\, \varepsilon_{k+1} + K_{k+1}\, y_{k+1} \tag{A2.22}$$

$$E_{k+1} = (1 - K_{k+1})\, b\, y_k^a - (1 - K_{k+1})\, b\, y_k^{true} + (1 - K_{k+1})\, c\, \varepsilon_{k+1} + K_{k+1}\, \eta_{k+1} \tag{A2.23}$$

$$E_{k+1} = (1 - K_{k+1})\, b\, (y_k^a - y_k^{true}) + (1 - K_{k+1})\, c\, \varepsilon_{k+1} + K_{k+1}\, \eta_{k+1} \tag{A2.24}$$

$$E_{k+1} = (1 - K_{k+1})\, b\, E_k + (1 - K_{k+1})\, c\, \varepsilon_{k+1} + K_{k+1}\, \eta_{k+1} \tag{A2.25}$$

For our 1-dimentional example the Kalman gain at step $k+1$ is

$$K_{k+1} = \frac{P_{k+1}^f}{R + P_{k+1}^f} \tag{A2.26}$$

which yields

$$E_{k+1} = \frac{R\,b\,E_k + R\,c\,\varepsilon_{k+1} + P_{k+1}^f\,\eta_{k+1}}{R + P_{k+1}^f} \tag{A2.27}$$

Replacing $P_{k+1}^f$ by its expression given in Equation (A2.18) yields:

$$E_{k+1} = \frac{R\,b\,E_k + R\,c\,\varepsilon_{k+1} + (b^2\,P_k^a + \zeta)\,\eta_{k+1}}{R + b^2\,P_k^a + \zeta} \tag{A2.28}$$

The assimilated covariance at step $k+1$, $P_{k+1}^a$, is given by:

$$P_{k+1}^a = P_{k+1}^f - K_{k+1}\,H_{k+1}\,P_{k+1}^f \tag{A2.29}$$

For our 1-dimentional case, it is assumed that $H_k = 1$, and $K_{k+1}$ is given in Equation (A2.26), which yields

$$P_{k+1}^a = \frac{R\,P_{k+1}^f}{R + P_{k+1}^f} \tag{A2.30}$$

Replacing $P_{k+1}^f$ by it expression given in Equation (A2.18) yields:

$$P_{k+1}^a = \frac{R\,(b^2\,P_k^a + \zeta)}{R + b^2\,P_k^a + \zeta} \tag{A2.31}$$

## A3. Convergence of the Covariance of the Assimilated State

Using the recurrence for the error and the covariance after assimilation yields the following Jacobian matrix:

$$\begin{pmatrix} \frac{dE_{k+1}}{dE_k} & \frac{dE_{k+1}}{dP_k^a} \\ \frac{dP_{k+1}^a}{dE_k} & \frac{dP_{k+1}^a}{dP_k^a} \end{pmatrix} = \begin{pmatrix} \frac{b\,R}{b^2\,P_k^a + R + \zeta} & \frac{b^2\,R\,(-b\,E_{k+1} - c\,\varepsilon_{k+1} + \eta_{k+1})}{\left(b^2\,P_k^a + R + \zeta\right)^2} \\ 0 & \left(\frac{b\,R}{b^2\,P_k^a + R + \zeta}\right)^2 \end{pmatrix} \tag{A3.1}$$

which yields the conditions for linear stability:

$$-1 < \frac{b\,R}{b^2\,P_k^a + R + \zeta} < 1 \tag{A3.2}$$

which is equivalent to the following two conditions

$$\frac{b^2\,P_k^a + R + \zeta}{b\,R} > 1 \quad \text{or} \quad \frac{b^2\,P_k^a + R + \zeta}{b\,R} < -1 \tag{A3.3}$$

i.e..

$$\zeta > -b^2\,P_k^a - (1-b)\,R \quad \text{and} \quad \zeta > -b^2\,P_k^a - (1+b)\,R \tag{A3.4}$$

The second case, $\zeta < -b^2\,P_k^a - (b+1)\,R$, cannot result in the convergence of $P_k^a$ because it is impossible to have $\zeta < -b^2\,P_{conv} - (b+1)\,R$ with $P_{conv} \geq 0$. This has been proved with Mathematica, as shown below.

```
P_conv = (-(1 - b^2) R - ζ + Sqrt[4 b^2 R ζ + ((1 - b^2) R + ζ)^2]) / (2 b^2) ;
Reduce[P_conv ≥ 0 && Q > 0 && R > 0 && 0 < b < 1 && ζ < -b^2 P_conv - (b + 1) R, ζ, Reals]
False
```

It means that the only case for which the covariance converges is when:

$$\zeta > -b^2\,P_k^a - (1-b)\,R \tag{A3.5}$$

or equivalently, when

$$\mu > -b^2\ P_k^a - (1-b)\,R - \left(\frac{1-b}{a}\right)^2 Q, \quad b = e^{a\,\Delta t} \tag{A3.6}$$

which also forces the following condition to be true,

$$\zeta \geq 0 \text{ , i.e. } \mu \geq -\left(\frac{1-b}{a}\right)^2 Q \tag{A3.7}$$

which can be proved by using Mathematica, as shown below.

```
P_conv = (-(1 - b^2) R - ζ + Sqrt[4 b^2 R ζ + ((1 - b^2) R + ζ)^2]) / (2 b^2) ;
Reduce[P_conv ≥ 0 && Q > 0 && R > 0 && 0 < b < 1 && ζ > -b^2 P_conv - (1 - b) R, ζ, Reals]
R > 0 && Q > 0 && 0 < b < 1 && ζ ≥ 0
```

It has just been shown that the convergence of $P_k^a$, i.e., the convergence of the covariance of $y_k^a$, is affected by the truncations in the polynomial chaos expansions. Let's remind that $P_{k+1}^f = b^2\ P_k^a + \zeta$. It means that overestimating the covariance is not a problem, but underestimating it too much prevents the convergence of the covariance. It can be explained by looking at Equation (A2.4) and seeing that a very large forecast covariance results in a Kalman gain close to 1, which means that the assimilated value of the state $y$ will be very similar to the observation and the impact of the previous error will be gone, which can be seen by looking at Equation (A2.20). When the forecast covariance is very small, the Kalman gain will be close to 0, and the assimilated value of the state $y$ will be very similar to its forecast value, which means that the convergence of the covariance will be slow.

Let us find the value $P_{conv}$ towards which the covariance $P_k^a$ converges to when is converges. The assimilated covariance at step $k+1$, $P_{k+1}^a$, is given by:

$$P_{k+1}^a = P_{k+1}^f - K_{k+1}\,H_{k+1}\,P_{k+1}^f \tag{A3.8}$$

which yields

$$P_{k+1}^a = \frac{R\,(b^2\ P_k^a + \zeta)}{R + b^2\ P_k^a + \zeta} \tag{A3.9}$$

Therefore, if the covariance convergences, it converges to

$$P_{conv} = \frac{-(1-b^2)\ R - \zeta + \sqrt{4\,b^2\ R\,\zeta + ((1-b^2)\ R + \zeta)^2}}{2\,b^2} \tag{A3.10}$$

**A4. Error after the Covariance of the Assimilated State has Converged**

The recurrence relationship for the error after assimilation is:

$$E_{k+1} = \frac{R\,b\,E_k + R\,c\,\varepsilon_{k+1} + (b^2\ P_k^a + \zeta)\,\eta_{k+1}}{R + b^2\ P_k^a + \zeta} \tag{A4.1}$$

Therefore, after convergence, the recurrence relationship for the error after assimilation becomes:

$$E_{k+1} = \frac{R\,b\,E_k + R\,c\,\varepsilon_{k+1} + (b^2\ P_{conv} + \zeta)\,\eta_{k+1}}{R + b^2\ P_{conv} + \zeta} \tag{A4.2}$$

The EKF error recurrence after $P_k^a$ convergences to $P_{conv}$ becomes:

$$E_{k+1} = M\ E_k + \alpha\,\varepsilon_{k+1} + \beta\,\eta_{k+1} \tag{A4.3}$$

with

$$M = \frac{b\,R}{R + b^2\ P_{conv} + \zeta},\quad \alpha = \frac{c\,R}{R + b^2\ P_{conv} + \zeta},\quad \beta = \frac{(b^2\ P_{conv} + \zeta)}{R + b^2\ P_{conv} + \zeta} \tag{A4.4}$$

If we rename the steps so that the step $k = 0$ is the first step, the error $E_N$ ($N$ steps after $P_k^a$ convergences to $P_{conv}$, after assimilation) can be written as:

$$E_N = M^N\ E_0 + \alpha \sum_{i=1}^{N-1} M^i\ \varepsilon_{N-i} + \beta \sum_{i=1}^{N-1} M^i\ \eta_{N-i} \tag{A4.5}$$

The fact that $E_0$ is the error at a new step and therefore has a different value does not matter when studying the convergence of Equation (A4.5) since $M^N = \left( \frac{b\,R}{R + b^2\,P_{conv} + \zeta} \right)^N \to 0$ as $N \to \infty$ .

Therefore, for large values of $N$, i.e., long after the covariance has converged.

$$E_N = \alpha \sum_{i=1}^{N-1} M^i\, \varepsilon_{N-i} + \beta \sum_{i=1}^{N-1} M^i\, \eta_{N-i} \tag{A4.6}$$

For $\varepsilon_i$'s independent Gaussian with mean $B$ and covariance $Q$, the term $\alpha \sum_{i=1}^{N-1} M^i\, \varepsilon_{N-i}$ is Gaussian with mean

$$\alpha \sum_{i=1}^{N-1} M^i\, B = B\,\alpha\, \frac{1 - M^N}{1 - M} \approx \frac{B\,\alpha}{1 - M} \tag{A4.7}$$

and covariance

$$\alpha^2\, Q \sum_{i=1}^{N-1} M^{2i} \approx \frac{\alpha^2\, Q}{1 - M^2} \tag{A4.8}$$

When $N \to \infty$, the term $\alpha \sum_{i=1}^{N-1} M^i\, \varepsilon_{N-i}$ is Gaussian with mean $\frac{B\,\alpha}{1 - M}$ and covariance $\frac{\alpha^2\, Q}{1 - M^2}$.

Similarly, for $\eta_i$'s independent Gaussian with mean zero and covariance $R$, the expression $\beta \sum_{i=1}^{N-1} M^i\, \eta_{N-i}$ is Gaussian with mean zero and covariance $\beta^2\, R \sum_{i=1}^{N-1} M^{2i} = \beta^2\, R\, \frac{1 - M^{2N}}{1 - M^2}$.

When $N \to \infty$, the term $\beta \sum_{i=1}^{N-1} M^i\, \eta_{N-i}$ is Gaussian with mean zero and covariance $\frac{\beta^2\, R}{1 - M^2}$.

Since the error model and the measurement noise are not correlated, the covariance of $E_N$ is the sum of the covariance of $\alpha \sum_{i=1}^{N-1} M^i\, \varepsilon_{N-i}$ and the covariance of $\beta \sum_{i=1}^{N-1} M^i\, \eta_{N-i}$. The mean value of $E_N$ is also the sum of the mean values of the different terms in the sum. Therefore, when $N \to \infty$, the mean value of $E_N$ is $\frac{B\,\alpha}{1 - M}$ and the covariance of $E_N$ is

$\frac{\alpha^2\ Q+\beta^2\ R}{1-M^2}$, with $\alpha$, $\beta$ and $M$ defined in Equation (A4.4). These expressions can expressed in terms of $b$, $R$, $Q$, $B$, $a$ and $\mu$, which is implicitly in terms of $\Delta t$, $R$, $Q$, $B$, $a$ and $\mu$ since $b=e^{a\,\Delta t}$.

**Summary - Error after the covariance of the assimilated state has converged:**

For large values of $N$, the error after assimilation $N$ steps after the covariance has converged, $E_N$, has a mean value $\frac{B\,\alpha}{1-M}$ with a covariance $\frac{\alpha^2\ Q+\beta^2\ R}{1-M^2}$ with:

$$M=\frac{b\ R}{R+b^2\ P_{conv}+\zeta},\quad \alpha=\frac{c\ R}{R+b^2\ P_{conv}+\zeta},\quad \beta=\frac{(b^2\ P_{conv}+\zeta)}{R+b^2\ P_{conv}+\zeta}$$

$$P_{conv}=\frac{-(1-b^2)\ R-\zeta+\sqrt{4\ b^2\ R\ \zeta+((1-b^2)\ R+\zeta)^2}}{2\ b^2},\ \zeta=c^2\ Q+\mu,\ c=\left(\frac{b-1}{a}\right),\ b=e^{a\,\Delta t}$$

**A5. Possible Optimal Time Steps**

Finding a simple analytical expression of the time step $\Delta t$ that minimizes the expression of the mean or the covariance of $E_N$, or even simply the covariance of $\alpha\ \sum_{i=1}^{N-1} M^i\ \varepsilon_{N-i}$ or the covariance of $\beta\ \sum_{i=1}^{N-1} M^i\ \eta_{N-i}$, is not possible in the general case, as illustrated by Appendix A6. With Mathematica, we cannot find analytical expressions for the $b$'s that set the derivatives of these expressions with respect to $b$ to 0, which would yield an optimal time step $\Delta t_{opt}=\frac{1}{a}Log_n(b_{opt})$ when the second derivative with respect to $b$ is positive.

However, in the case where there is no model error ($B=0$, $Q=0$), it can be shown analytically that the derivative of the total covariance of $E_N$ (which is also equal to the covariance of

$\beta \sum_{i=1}^{N-1} M^i \eta_{N-i}$ in that case) with respect to $b$ is positive, which means that the covariance increases with $b = e^{a\Delta t}$, so decreases with $\Delta t$ since $a < 0$. The derivation is shown in Appendix A6 with Mathematica.

A numerical example is shown in Figure A1, where the covariance of $E_N$ is plotted for different time steps, assuming a perfect model ($B = 0$, $Q = 0$). The scalar system used for this example is $y' = -y$, i.e., $a = -1$.

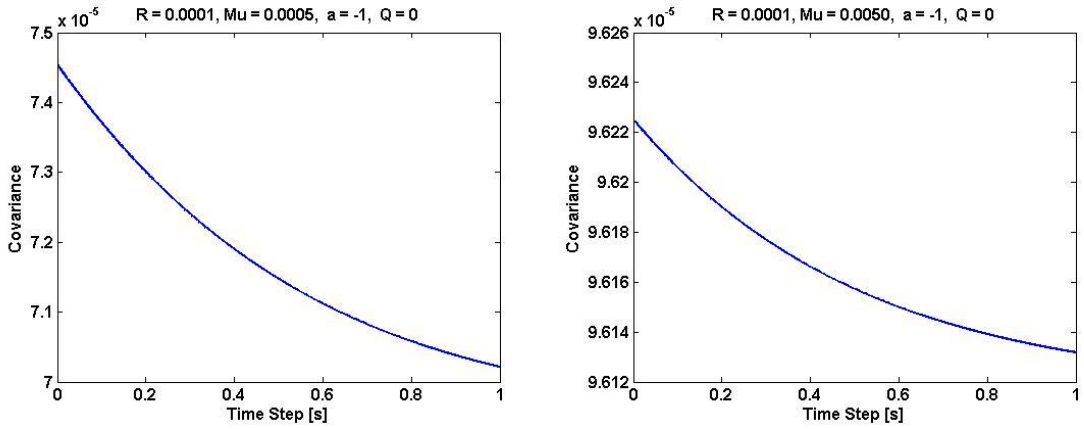


(a) (b)

Figure A1: Covariance after Convergence of the Covariance with no Model Error (Q = 0, B = 0): (a) R = 0.0001, Mu = 0.0005, a = -1; (b) R = 0.0001, Mu = 0.0050, a = -1

Therefore, when there is no model error, it can be shown analytically that the error decreases with $\Delta t$, which means a larger $\Delta t$ results in a smaller error. Figure 4.4 showed the absolute error for our two estimated parameters, i.e., $\left| \xi_{1,est} - \xi_{1,ref} \right|$ and $\left| \xi_{2,est} - \xi_{2,ref} \right|$, with the nonlinear half-car model for the speed bump with respect to the different corresponding time steps. It is reproduced in Figure A2. There was no model error and a Gaussian measurement noise of mean 0 and variance 1% was added to the observation. It could be observed that for this case study with a perfect model, the error gets worse for small time steps $\Delta t$. The fact that the error can get larger as the time step is increase too much was due to the fact that with very few observations, the covariance had not converged yet. For instance, with a time step of 1.5 seconds, only two

significant measurements were available. The error for the case study $y' = -y$, which was plotted in Figure A1, was calculated assuming the covariance had already converged.

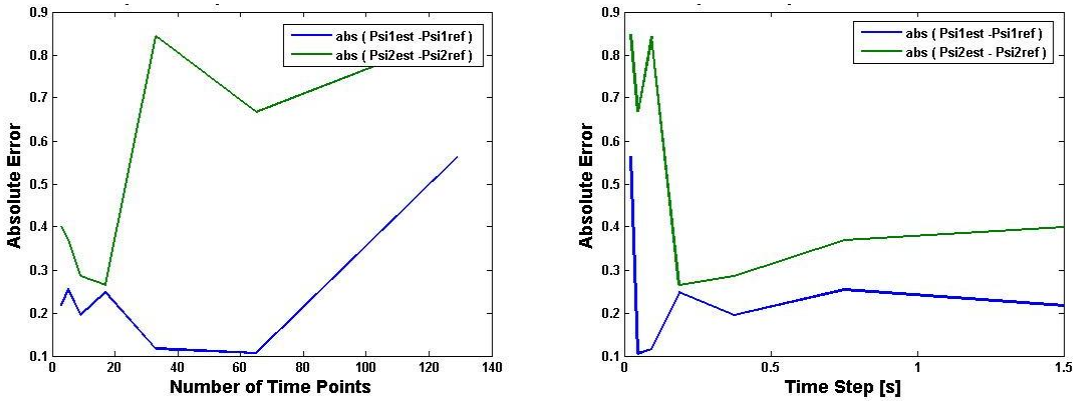


(a) (b)

Figure A2: Absolute Error for the Estimated Parameters $\xi_1$ and $\xi_2$ with the Nonlinear Half-Car Model for the Speed Bump with Respect to: (a) the Number of Time Points; (b) the Length of the Time Step

With numerical examples, it can be shown that a nonzero optimal time step can exist when $Q \neq 0$, i.e., when there is a model error. Figure A3 shows an example where the model error has no bias, i.e., with $B = 0$. The covariance of $E_N$ is the sum of the covariance of $\alpha \sum_{i=1}^{N-1} M^i \varepsilon_{N-i}$, shown in Figure A3(a), and the covariance of $\beta \sum_{i=1}^{N-1} M^i \eta_{N-i}$, shown in Figure A3(b). For the example shown in Figure A3, the covariance of $E_N$ is approximately equal to the covariance of $\beta \sum_{i=1}^{N-1} M^i \eta_{N-i}$, so it is not displayed in Figure A3 since it would be impossible to notice any difference with the covariance of $E_N$. For the example shown in Figure A3, there is a nonzero optimal time step that minimizes the covariance of the estimation error. Even though the covariance of $\alpha \sum_{i=1}^{N-1} M^i \varepsilon_{N-i}$ is very small compared with the covariance $\beta \sum_{i=1}^{N-1} M^i \eta_{N-i}$, the fact that $Q \neq 0$ completely changes the shape of the covariance $\beta \sum_{i=1}^{N-1} M^i \eta_{N-i}$, and therefore the shape of the covariance of $E_N$: there is a nonzero optimal time step that minimizes the covariance of the estimation error (0.015 s in this case).

Figure A4 shows an example where the model error has a bias, i.e., with $B \neq 0$. With a large bias, it can be observed that the error increases with the length of the time step.

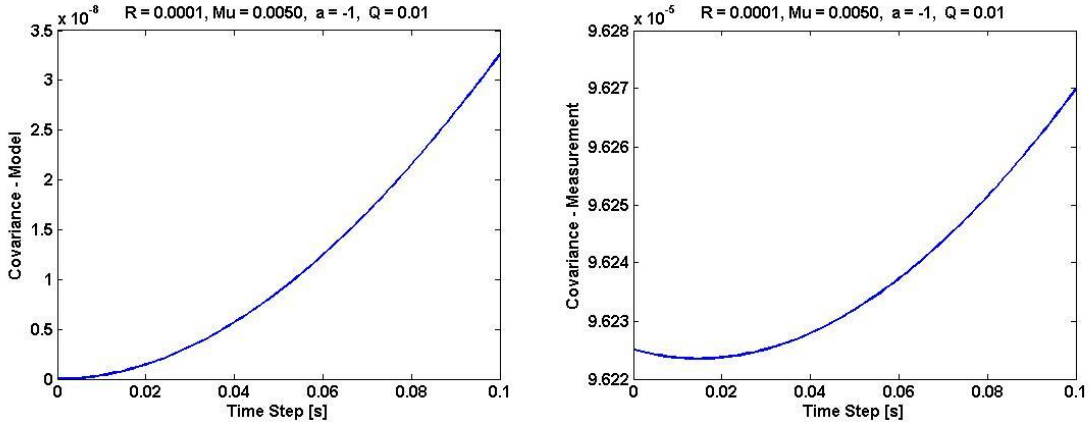


(a) (b)

Figure A3: Covariance of $E_N$ after Convergence for R = 0.0001, Mu = 0.0050, a = -1, Q = 0.01, B = 0 (i.e., Model Error, but with no Bias): (a) Covariance Due to Model Errors; (b) Covariance Due to Measurement Noise

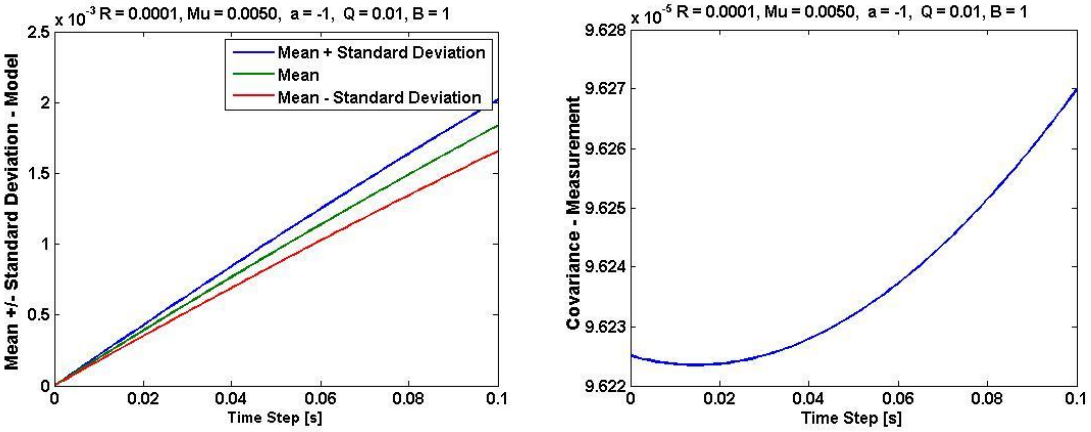


(a) (b)

Figure A4: Covariance of $E_N$ after Convergence for R = 0.0001, Mu = 0.0050, a = -1, Q = 0.01, B = 1; (i.e., Model Error, but with Bias): (a) Error Due to Model Errors; (b) Covariance of Error Due to Measurement Noise

## A6. Detailed Expressions of the Mean Errors and the Covariances - Possible Optimal Time Steps

The mean of $E_N$, which is also the mean of $\alpha \sum_{i=1}^{N-1} M^i \varepsilon_{N-i}$ is:

$$\text{MeanModel} = \frac{2\,B\,c\,R}{(-1+b)^2 R + \zeta + \sqrt{4\,b^2 R\,\zeta + (R - b^2 R + \zeta)^2}}$$

The covariance of $\alpha \sum_{i=1}^{N-1} M^i \varepsilon_{N-i}$ is:

$$\text{CovModel} = \frac{2\,c^2 Q R^2}{(-1+b^2)^2 R^2 + \zeta\left(\zeta + \sqrt{(-1+b^2)^2 R^2 + 2(1+b^2) R\,\zeta + \zeta^2}\right) + (1+b^2) R\left(2\zeta + \sqrt{(-1+b^2)^2 R^2 + 2(1+b^2) R\,\zeta + \zeta^2}\right)}$$

The covariance of $\beta \sum_{i=1}^{N-1} M^i \eta_{N-i}$ is:

$$\text{CovMeas} = \frac{R\left(-R + b^2 R + \zeta + \sqrt{4\,b^2 R\,\zeta + (R - b^2 R + \zeta)^2}\right)^2}{2\left((-1+b^2)^2 R^2 + \zeta\left(\zeta + \sqrt{(-1+b^2)^2 R^2 + 2(1+b^2) R\,\zeta + \zeta^2}\right) + (1+b^2) R\left(2\zeta + \sqrt{(-1+b^2)^2 R^2 + 2(1+b^2) R\,\zeta + \zeta^2}\right)\right)}$$

The covariance of $E_N$ is:

$$\text{CovTotal} = \frac{R\left(R\left(2c^2 Q + (-1+b^2)^2 R + 2b^2\zeta\right) + \zeta^2 - R\sqrt{4b^2 R\,\zeta + (R - b^2 R + \zeta)^2} + b^2 R\sqrt{4b^2 R\,\zeta + (R - b^2 R + \zeta)^2} + \zeta\sqrt{4b^2 R\,\zeta + (R - b^2 R + \zeta)^2}\right)}{(-1+b^2)^2 R^2 + \zeta\left(\zeta + \sqrt{(-1+b^2)^2 R^2 + 2(1+b^2) R\,\zeta + \zeta^2}\right) + (1+b^2) R\left(2\zeta + \sqrt{(-1+b^2)^2 R^2 + 2(1+b^2) R\,\zeta + \zeta^2}\right)}$$

In order to study the error and the covariances vs. the time step $\Delta t$, we need to replace $c$ by $\left(\frac{b-1}{a}\right)$ and $\zeta$ by $\mu + \left(\frac{b-1}{a}\right)^2 Q$ in order to have only one variable that depends on $\Delta t$: $b = e^{a\,\Delta t}$.

Then we can take the derivative of the error and the covariances vs. $b = e^{a\,\Delta t}$ and try to find an optimal value of $b_{opt}$ minimizing the expression we're trying to minimize by finding a $b_{opt}$

resulting in the derivative equal to zero and by checking that the second derivative is positive at that point.

If an optimal time step exists, it will be $\Delta t_{opt} = \frac{1}{a} Log_n(b_{opt})$

Replacing $c$ by $\left(\frac{b-1}{a}\right)$ and $\zeta$ by $\mu + \left(\frac{b-1}{a}\right)^2 Q$ yields the following expressions:

$$\text{MeanModel} = \frac{2\,(-1+b)\,B\,R}{a\left(\frac{(-1+b)^2 Q}{a^2} + (-1+b)^2 R + \mu + \sqrt{4\,b^2\,R\left(\frac{(-1+b)^2 Q}{a^2} + \mu\right) + \left(\frac{(-1+b)^2 Q}{a^2} + R - b^2 R + \mu\right)^2}\right)}$$

$$\text{CovModel} = \left(2\,(-1+b)^2\,Q\,R^2\right) \Big/ \left(a^2\left(\left(-1+b^2\right)^2 R^2 + \left(\frac{(-1+b)^2 Q}{a^2} + \mu\right)\left(\frac{(-1+b)^2 Q}{a^2} + \mu + \sqrt{\left(-1+b^2\right)^2 R^2 + 2\left(1+b^2\right) R\left(\frac{(-1+b)^2 Q}{a^2} + \mu\right) + \left(\frac{(-1+b)^2 Q}{a^2} + \mu\right)^2}\right) + \left(1+b^2\right) R\left(2\left(\frac{(-1+b)^2 Q}{a^2} + \mu\right) + \sqrt{\left(-1+b^2\right)^2 R^2 + 2\left(1+b^2\right) R\left(\frac{(-1+b)^2 Q}{a^2} + \mu\right) + \left(\frac{(-1+b)^2 Q}{a^2} + \mu\right)^2}\right)\right)\right)$$

$$\text{CovMeas} = \left(R\left(\frac{(-1+b)^2 Q}{a^2} - R + b^2 R + \mu + \sqrt{4\,b^2\,R\left(\frac{(-1+b)^2 Q}{a^2} + \mu\right) + \left(\frac{(-1+b)^2 Q}{a^2} + R - b^2 R + \mu\right)^2}\right)^2\right) \Big/ \left(2\left(\left(-1+b^2\right)^2 R^2 + \left(\frac{(-1+b)^2 Q}{a^2} + \mu\right)\left(\frac{(-1+b)^2 Q}{a^2} + \mu + \sqrt{\left(-1+b^2\right)^2 R^2 + 2\left(1+b^2\right) R\left(\frac{(-1+b)^2 Q}{a^2} + \mu\right) + \left(\frac{(-1+b)^2 Q}{a^2} + \mu\right)^2}\right) + \left(1+b^2\right) R\left(2\left(\frac{(-1+b)^2 Q}{a^2} + \mu\right) + \sqrt{\left(-1+b^2\right)^2 R^2 + 2\left(1+b^2\right) R\left(\frac{(-1+b)^2 Q}{a^2} + \mu\right) + \left(\frac{(-1+b)^2 Q}{a^2} + \mu\right)^2}\right)\right)\right)$$

$$\text{CovTotal} = \left(R\left(\frac{4\,(-1+b)^2\,Q\,R}{a^2} + \left(\frac{(-1+b)^2 Q}{a^2} - R + b^2 R + \mu + \sqrt{4\,b^2\,R\left(\frac{(-1+b)^2 Q}{a^2} + \mu\right) + \left(\frac{(-1+b)^2 Q}{a^2} + R - b^2 R + \mu\right)^2}\right)^2\right)\right) \Big/ \left(2\left(\left(-1+b^2\right)^2 R^2 + \left(\frac{(-1+b)^2 Q}{a^2} + \mu\right)\left(\frac{(-1+b)^2 Q}{a^2} + \mu + \sqrt{4\,b^2\,R\left(\frac{(-1+b)^2 Q}{a^2} + \mu\right) + \left(\frac{(-1+b)^2 Q}{a^2} + R - b^2 R + \mu\right)^2}\right) + \left(1+b^2\right) R\left(2\left(\frac{(-1+b)^2 Q}{a^2} + \mu\right) + \sqrt{4\,b^2\,R\left(\frac{(-1+b)^2 Q}{a^2} + \mu\right) + \left(\frac{(-1+b)^2 Q}{a^2} + R - b^2 R + \mu\right)^2}\right)\right)\right)$$

In the general case, we cannot find analytical expressions for the $b$'s that set the derivatives of these expressions to 0, even though we can show an optimal time step $\Delta t_{opt} = \frac{1}{a} Log_n(b_{opt})$ can exist with numerical examples. For instance, if we're trying to set the derivative of the mean of $E_N$ to 0, which is the simplest case, we obtain:

```
Solve[D[MeanModel, b] == 0, b]
```

$$\{\{b \to \text{Root}[Q^3 + 2a^2Q^2R + a^4QR^2 + a^2Q^2\mu - a^6R^2\mu - a^4Q\mu^2 - 2a^6R\mu^2 - a^6\mu^3 + Q(-6Q^2 - 12a^2QR - 6a^4R^2 - 4a^2Q\mu - 4a^4R\mu + 2a^4\mu^2)\#1 + (15Q^3 + 30a^2Q^2R + 15a^4QR^2 + 6a^2Q^2\mu + 12a^4QR\mu + 6a^6R^2\mu - a^4Q\mu^2 - 2a^6R\mu^2)\#1^2 + (-20Q^3 - 40a^2Q^2R - 20a^4QR^2 - 4a^2Q^2\mu - 12a^4QR\mu - 8a^6R^2\mu)\#1^3 + (15Q^3 + 30a^2Q^2R + 15a^4QR^2 + a^2Q^2\mu + 4a^4QR\mu + 3a^6R^2\mu)\#1^4 + Q(-6Q^2 - 12a^2QR - 6a^4R^2)\#1^5 + Q(Q^2 + 2a^2QR + a^4R^2)\#1^6 \&, 1]\},$$
$$\{b \to \text{Root}[Q^3 + 2a^2Q^2R + a^4QR^2 + a^2Q^2\mu - a^6R^2\mu - a^4Q\mu^2 - 2a^6R\mu^2 - a^6\mu^3 + Q(-6Q^2 - 12a^2QR - 6a^4R^2 - 4a^2Q\mu - 4a^4R\mu + 2a^4\mu^2)\#1 + (15Q^3 + 30a^2Q^2R + 15a^4QR^2 + 6a^2Q^2\mu + 12a^4QR\mu + 6a^6R^2\mu - a^4Q\mu^2 - 2a^6R\mu^2)\#1^2 + (-20Q^3 - 40a^2Q^2R - 20a^4QR^2 - 4a^2Q^2\mu - 12a^4QR\mu - 8a^6R^2\mu)\#1^3 + (15Q^3 + 30a^2Q^2R + 15a^4QR^2 + a^2Q^2\mu + 4a^4QR\mu + 3a^6R^2\mu)\#1^4 + Q(-6Q^2 - 12a^2QR - 6a^4R^2)\#1^5 + Q(Q^2 + 2a^2QR + a^4R^2)\#1^6 \&, 2]\},$$
$$\{b \to \text{Root}[Q^3 + 2a^2Q^2R + a^4QR^2 + a^2Q^2\mu - a^6R^2\mu - a^4Q\mu^2 - 2a^6R\mu^2 - a^6\mu^3 + Q(-6Q^2 - 12a^2QR - 6a^4R^2 - 4a^2Q\mu - 4a^4R\mu + 2a^4\mu^2)\#1 + (15Q^3 + 30a^2Q^2R + 15a^4QR^2 + 6a^2Q^2\mu + 12a^4QR\mu + 6a^6R^2\mu - a^4Q\mu^2 - 2a^6R\mu^2)\#1^2 + (-20Q^3 - 40a^2Q^2R - 20a^4QR^2 - 4a^2Q^2\mu - 12a^4QR\mu - 8a^6R^2\mu)\#1^3 + (15Q^3 + 30a^2Q^2R + 15a^4QR^2 + a^2Q^2\mu + 4a^4QR\mu + 3a^6R^2\mu)\#1^4 + Q(-6Q^2 - 12a^2QR - 6a^4R^2)\#1^5 + Q(Q^2 + 2a^2QR + a^4R^2)\#1^6 \&, 3]\},$$
$$\{b \to \text{Root}[Q^3 + 2a^2Q^2R + a^4QR^2 + a^2Q^2\mu - a^6R^2\mu - a^4Q\mu^2 - 2a^6R\mu^2 - a^6\mu^3 + Q(-6Q^2 - 12a^2QR - 6a^4R^2 - 4a^2Q\mu - 4a^4R\mu + 2a^4\mu^2)\#1 + (15Q^3 + 30a^2Q^2R + 15a^4QR^2 + 6a^2Q^2\mu + 12a^4QR\mu + 6a^6R^2\mu - a^4Q\mu^2 - 2a^6R\mu^2)\#1^2 + (-20Q^3 - 40a^2Q^2R - 20a^4QR^2 - 4a^2Q^2\mu - 12a^4QR\mu - 8a^6R^2\mu)\#1^3 + (15Q^3 + 30a^2Q^2R + 15a^4QR^2 + a^2Q^2\mu + 4a^4QR\mu + 3a^6R^2\mu)\#1^4 + Q(-6Q^2 - 12a^2QR - 6a^4R^2)\#1^5 + Q(Q^2 + 2a^2QR + a^4R^2)\#1^6 \&, 4]\},$$
$$\{b \to \text{Root}[Q^3 + 2a^2Q^2R + a^4QR^2 + a^2Q^2\mu - a^6R^2\mu - a^4Q\mu^2 - 2a^6R\mu^2 - a^6\mu^3 + Q(-6Q^2 - 12a^2QR - 6a^4R^2 - 4a^2Q\mu - 4a^4R\mu + 2a^4\mu^2)\#1 + (15Q^3 + 30a^2Q^2R + 15a^4QR^2 + 6a^2Q^2\mu + 12a^4QR\mu + 6a^6R^2\mu - a^4Q\mu^2 - 2a^6R\mu^2)\#1^2 + (-20Q^3 - 40a^2Q^2R - 20a^4QR^2 - 4a^2Q^2\mu - 12a^4QR\mu - 8a^6R^2\mu)\#1^3 + (15Q^3 + 30a^2Q^2R + 15a^4QR^2 + a^2Q^2\mu + 4a^4QR\mu + 3a^6R^2\mu)\#1^4 + Q(-6Q^2 - 12a^2QR - 6a^4R^2)\#1^5 + Q(Q^2 + 2a^2QR + a^4R^2)\#1^6 \&, 5]\},$$
$$\{b \to \text{Root}[Q^3 + 2a^2Q^2R + a^4QR^2 + a^2Q^2\mu - a^6R^2\mu - a^4Q\mu^2 - 2a^6R\mu^2 - a^6\mu^3 + Q(-6Q^2 - 12a^2QR - 6a^4R^2 - 4a^2Q\mu - 4a^4R\mu + 2a^4\mu^2)\#1 + (15Q^3 + 30a^2Q^2R + 15a^4QR^2 + 6a^2Q^2\mu + 12a^4QR\mu + 6a^6R^2\mu - a^4Q\mu^2 - 2a^6R\mu^2)\#1^2 + (-20Q^3 - 40a^2Q^2R - 20a^4QR^2 - 4a^2Q^2\mu - 12a^4QR\mu - 8a^6R^2\mu)\#1^3 + (15Q^3 + 30a^2Q^2R + 15a^4QR^2 + a^2Q^2\mu + 4a^4QR\mu + 3a^6R^2\mu)\#1^4 + Q(-6Q^2 - 12a^2QR - 6a^4R^2)\#1^5 + Q(Q^2 + 2a^2QR + a^4R^2)\#1^6 \&, 6]\}\}$$

However, in the case where there is no model error ($Q = 0$, $B = 0$), it can be shown analytically that the derivative of the total covariance of $E_N$ (which is also equal to the covariance of $\beta \sum_{i=1}^{N-1} M^i \eta_{N-i}$ in that case) with respect to $b$ is positive, which means that the covariance increases with $b = e^{a\Delta t}$, so decreases with $\Delta t$ since $a < 0$. The derivation with Mathematica is shown below. The expression calculated for the covariance of the error was defined only after $P_k^a$ converges to $P_{conv}$, which means that Equation (A3.7), i.e., $\zeta \geq 0$, has to be verified. In the

case where there is no model error Equation (A3.7) becomes equivalent to $\mu \geq 0$, which will therefore be used in the Mathematica code shown below.

```
CovTotalnoQ = Simplify[ CovTotal /. {Q→ 0}]
```

$$\frac{R\left(-R+b^2 R+\mu+\sqrt{4 b^2 R \mu+\left(R-b^2 R+\mu\right)^2}\right)^2}{2\left(\left(-1+b^2\right)^2 R^2+\mu\left(\mu+\sqrt{4 b^2 R \mu+\left(R-b^2 R+\mu\right)^2}\right)+\left(1+b^2\right) R\left(2 \mu+\sqrt{4 b^2 R \mu+\left(R-b^2 R+\mu\right)^2}\right)\right)}$$

```
DerivCovTotalnoQ = D[CovTotalnoQ, b];
Reduce[DerivCovTotalnoQ < 0 && R > 0 && (μ ≥ 0  && (0 < b < 1)), Reals]
Reduce[DerivCovTotalnoQ == 0 && R > 0 && (μ ≥ 0  && (0 < b < 1)), Reals]
Reduce[DerivCovTotalnoQ > 0 && R > 0 && (μ ≥ 0  && (0 < b < 1)), Reals]
```

```
False
```

```
μ == 0 && 0 < b < 1 && R > 0
```

```
μ > 0 && 0 < b < 1 && R > 0
```

## A7. Extension to the Case where the Truncation Error is Proportional to the Covariance of the Model Forecast

For the sake of simplicity, $\mu$ was assumed to be a constant. The assumption about the error being constant could be regarded as a lower bound on the error since the term $\mu$ due to the truncation always has the same sign ($\mu < 0$). The purpose of this section is to show that in the case where the truncation error is proportional to the covariance of the model forecast, which is more realistic, taking time steps which are too small can also result in numerical errors increasing at each time step.

This new assumption can be written as

$$P_{k+1}^f = b^2 P_k^a + c^2 Q + \mu_k \quad \text{with} \quad \mu_k = \beta_{trunc} P_{k+1}^f \tag{A7.1}$$

which is equivalent to

$$P_{k+1}^f = b^2\ P_k^a + \zeta_k \quad \text{with } \zeta_k = c^2\ Q + \beta_{trunc}\ P_{k+1}^f \tag{A7.2}$$

It can be noted that $\beta_{trunc} < 0$ since $\mu_k < 0$. Also, using a recurrence relationship, it can be shown that

$$\zeta_k = c^2\ Q + (b^2\ P_k^a + c^2\ Q) \sum_{k=1}^{\infty} \beta_{trunc}^k \tag{A7.3}$$

It can be shown that this still yields

$$E_{k+1} = \frac{R\,b\,E_k + R\,c\,\varepsilon_{k+1} + (b^2\ P_k^a + \zeta_k)\,\eta_{k+1}}{R + b^2\ P_k^a + \zeta_k}, \quad P_{k+1}^a = \frac{R\,(b^2\ P_k^a + \zeta_k)}{R + b^2\ P_k^a + \zeta_k} \tag{A7.4}$$

and that the error $E_k$ increases with $k$ when $\zeta_k > 0$.

Assuming $\beta_{trunc}^2 << 1$, which is true when a significant number of polynomial chaos terms is used,

$$\zeta_k \approx c^2\ Q + \beta_{trunc}\,(b^2\ P_k^a + c^2\ Q) \tag{A7.5}$$

Using this approximation, the error $E_k$ increases with $k$ when

$$c^2\ Q + \beta_{trunc}\,(b^2\ P_k^a + c^2\ Q) > 0 \tag{A7.6}$$

which is equivalent to

$$-\beta_{trunc} > \frac{c^2\ Q}{c^2\ Q + b^2\ P_k^a} \quad \text{with } b = e^{a\,\Delta t}\ ,\ c = \left(\frac{1 - e^{a\,\Delta t}}{a}\right) \tag{A7.7}$$

Using the approximations $b \approx 1 + a\,\Delta t$ and $c \approx -\Delta t$ for small $\Delta t$'s , it can be noticed that the error $E_k$ increases with $k$ when

$$-\beta_{trunc} > \frac{\Delta t^2\ Q}{P_k^a + \Delta t\ (2\ a\ P_k^a) + \Delta t^2\ (Q + a^2\ P_k^a)} \approx \frac{\Delta t^2\ Q}{P_k^a} \tag{A7.8}$$

For any nonzero truncation error (i.e., for $-\beta_{trunc} > 0$), it is possible to find a time step $\Delta t$ small enough to result in an increase of the error $E_k$.

# References


1. Blanchard, E., Sandu, C., Sandu, A., *A Polynomial-Chaos-based Bayesian Approach for Estimating Uncertain Parameters of Mechanical Systems* in *Proceedings of the ASME 2007 International Design Engineering Technical Conferences & Computers and Information in Engineering Conference IDETC/CIE 2007, 9th International Conference on Advanced Vehicle and Tire Technologies (AVTT)*. 2007. Las Vegas, Nevada.

2. Blanchard, E., Sandu, A., Sandu, C., *Parameter Estimation Method Using an Extended Kalman Filter*. in *Proceedings of the Joint North America, Asia-Pacific ISTVS Conference and Annual Meeting of Japanese Society for Terramechanics*. 2007. Fairbanks, Alaska.

3. Blanchard, E., Sandu, C., Sandu, A., *Comparison Between a Polynomial-Chaos Based Bayesian Approach and a Polynomial-Chaos Based EKF Approach for Parameter Estimation with Application to Vehicle Dynamics* in *Proceedings of the ASME 2009 International Design Engineering Technical Conferences & Computers and Information in Engineering Conference IDETC/CIE 2009, 11th International Conference on Advanced Vehicle and Tire Technologies (AVTT)*. 2009. San Diego, California.

4. Blanchard, E., Sandu, A., Sandu, C., *Parameter Estimation for Mechanical Systems via an Explicit Representation of Uncertainty.* Engineering Computations - International Journal for Computer-Aided Engineering and Software, 2009. **26**(5): p. 541-569.

5. Blanchard, E., Sandu, A., Sandu, C., *Polynomial Chaos-Based Parameter Estimation Methods Applied to Vehicle System.* Proceedings of the Institution of Mechanical Engineers, Part K: Journal of Multi-body Dynamics, 2010. **224**(1): p. 59-81

6. Blanchard, E., Sandu, A., Sandu, C., *A Polynomial Chaos-Based Kalman Filter Approach for Parameter Estimation of Mechanical Systems.* accepted by the ASME Journal of Dynamic Systems, Measurement and Control - Special Issue of Physical System Modeling (should be in press soon) 2010.

7. Cheng, H., Sandu, A., *Uncertainty Quantification and Apportionment in Air Quality Models using the Polynomial Chaos Method"* 2007, Computer Science Department of Virginia Tech.

8. Ghanem, R.G., Spanos, P.D., *Stochastic Finite Elements* 2003: Dover Publications Inc, Mineola, NY.

9. Wiener, N., *The Homogeneous Chaos.* American Journal of Mathematics, 1938. **60**: p. 897–936.

10. Askey, R., Wilson, J. , *Some Basic Hypergeometric Polynomials that Generalize Jacobi Polynomials.* Memoirs of the American Mathematical Society, 1985. **319**: p. 1-55.

11. Xiu, D., Karniadakis, G.E., *The Wiener-Askey Polynomial Chaos for Stochastic Differential Equations.* Journal on Scientific Computing, 2002. **24**(2): p. 619-644.

12. Xiu, D., Karniadakis, G.E., *Modeling Uncertainty in Flow Simulations via Generalized Polynomial Chao.* Journal of Computational Physics, 2003. **187**: p. 137-167.

13. Cheng, H., Sandu, A. *Numerical Study of Uncertainty Quantification Techniques for Implicit Stiff Systems*. in *Proceedings of the 45th Annual Southeast Regional Conference*. 2007.

14. Hammersley, J.M., *Monte Carlo Methods for Solving Multivariables Problems.* Annals of the New York Academy of Sciences, 1960. **86**: p. 844–874.

15. Halton, J.H., Smith, G. B., *Radical-inverse Quasi-random Point Sequence.* Communications of the ACM, 1964. **7**(12): p. 701–702.

16. Smolyak, S., *Quadrature and Interpolation Formulas for Tensor Products of Certain Classes of Functions.* Soviet Math. Dokl., 1963. **4**: p. 240–243.

17. Nobile, F., Tempone, R., Webster, C.G., *A Sparse Grid Stochastic Collocation Method for Elliptic Partial Differential Equations with Random Input Data, Technical Report MOX 85*. 2006, Politecnico di Milano.

18. Webster, C.G., *Sparse Grid Stochastic Collocation Techniques for the Numerical Solution of Partial Differential Equations with Random Input Data*. 2007, Ph.D. dissertation, Florida State University.

19. Sandu, A., Sandu, C., Ahmadian, M., *Modeling Multibody Dynamic Systems with Uncertainties. Part I: Theoretical and Computational Aspects.* Multibody System Dynamics, Publisher: Springer Netherlands, ISSN: 1384-5640 (Paper) 1573-272X (Online), DOI 10.1007/s11044-006-9007-5, pp. 1-23 (23), 2006.

20. Tarantola, A., *Inverse Problem Theory and Methods for Model Parameter Estimation*. 2004: Society for Industrial and Applied Mathematics, Philadelphia, PA.

21. Bishwal, J.P.N., *Parameter Estimation in Stochastic Differential Equations*. 2008: Springer, Berlin, Germany. .

22. Aster, R.C., Borchers, B., Thurber, C.H. , *Parameter Estimation and Inverse Problems*. 2005, Elsevier Academic Press, Amsterdam, The Netherlands; Boston, MA.

23. Liu, C.S., *Identifying Time-dependent Damping and Stiffness Functions by a Simple and Yet Accurate Method.* Journal of Sound and Vibration, 2008. **318**: p. 148–165.

24. Araújo, A.L., Mota Soares, C.M., Herskovits, J., Pedersen, P., *Estimation of Piezoelastic and Viscoelastic Properties in Laminated Structures.* Composite Structures, 2009. **87**(2): p. 168-174.

25. Pradlwarter, H.J., Pellissetti, M.F., Schenk, C.A., Schuëller, G.I., Kreis, A., Fransen, S., Calvi, A., Klein, M., *Realistic and Efficient Reliability Estimation for Aerospace Structures.* Computer Methods in Applied Mechanics and Engineering, Special Issue on Computational Methods in Stochastic Mechanics and Reliability Analysis, 2005. **194**(12-16): p. 1597-1617.

26. Catania, F., Paladino, O., *Optimal Sampling for the Estimation of Dispersion Parameters in Soil Columns Using an Iterative Genetic Algorithm.* Environmental Modelling & Software, 2009. **24**(1): p. 115-123.

27. Varziri, M.S., Poyton, A.A., McAuley, K.B., McLellan, P.J., Ramsay, J.O., *Selecting Optimal Weighting Factors in iPDA for Parameter Estimation in Continuous-Time Dynamic Models.* Computers & Chemical Engineering, 2008. **32**(12): p. 3011-3022.

28. Fathy, H.K., Kang, D., Stein, J.L. *Online Vehicle Mass Estimation Using Recursive Least Squares and Supervisory Data Extraction*. in *Proceedings of the 2008 American Control Conference*. 2008.

29. Liang , J.W., *Damping Estimation via Energy-dissipation Method.* Journal of Sound and Vibration, 2007. **307**: p. 349–364.

30. Oliveto, N.D., Scalia, G., Oliveto, G., *Dynamic Identification of Structural Systems with Viscous and Friction Damping.* Journal of Sound and Vibration, 2008. **318**: p. 911–926.

31. Raïssi, T., Ramdani, N., Candau, Y., *Set Membership State and Parameter Estimation for Systems Described by Nonlinear Differential Equations.* Automatica, 2004. **40**: p. 1771–1777.

32. Mockus, J., Eddy, W., Mockus, A., Mockus, L., Reklaitis, G., *Bayesian Heuristic Approach to Discrete and Global Optimization: Algorithms, Vizualization, Software and Applications*. 1997: Kluwer Academic Publishers, Dordrecht, The Netherlands.

33. Thompson, B., Vladimirov, I., *Bayesian Parameter Estimation and Prediction in Mean Reverting Stochastic Diffusion Models.* Nonlinear Analysis, 2005. **63**: p. e2367 – e2375.

34. Wang, J., Zabaras, N., *Using Bayesian Statistics in the Estimation of Heat Source in Radiation.* International Journal of Heat and Mass Transfer, 2005. **48**: p. 15-29.

35. Khan, T., Ramuhalli, P., *A Recursive Bayesian Estimation Method for Solving Electromagnetic Nondestructive Evaluation Inverse Problems.* IEEE Transactions on Magnetics, 2008. **44**(7): p. 1845-1855.

36. Nocedal, J., Wright, S.J., *Numerical Optimization*. 2 ed. 2006: Springer, New York. .

37. Horst, R., Pardalos, P. M., Thoai, N. V., *Introduction to Global Optimization*. 2 ed. 2000: Kluwer Academic Publishers, Dordrecht, The Netherlands.

38. Floudas, C.A., *Deterministic Global Optimization: Theory, Methods, and Applications* 2000: Kluwer Academic Publishers, Dordrecht, The Netherlands.

39. Horst, R., Pardalos, P.M., editors, *Handbook of Global Optimization*. Vol. 1. 1995: Kluwer Academic Publishers, Dordrecht, The Netherlands.

40. Pardalos, P.M., Romeijn, H.E., editors, *Handbook of Global Optimization*. 2002: Kluwer Academic Publishers Dordrecht, The Netherlands. .

41. Liberti, L., Maculan, N., *Optimization: From Theory to Implementation*. 2006: Springer, Berlin, Germany.

42. Davis, L., *Handbook of Genetic Algorithms*. 1991: Van Nostrand Reinhold, New York.

43. Zhang, B.T., *A Bayesian Framework for Evolutionary Computation.* Proceedings of the 1999 Congress on Evolutionary Computation, 1999. **1**: p. 722-728.

44. Sun, J., Zhang, Q., Tsang, E.P.K., *DE/EDA: A New Evolutionary Algorithm for Global Optimization.* Information Sciences, 2005. **169**(3-4): p. 249-262.

45. Zhang, Q., Sun, J., Tsang, E., Ford, J., *Hybrid Estimation of Distribution Algorithm for Global Optimization.* Engineering Computations - International Journal for Computer-Aided Engineering and Software, 2004. **21**(1): p. 91-107.

46. Zhang, Q., Sun, J., Tsang, E. P. K., *An Evolutionary Algorithm with Guided Mutation for the Maximum Clique Problem.* IEEE Transactions on Evolutionary Computation, 2005. **9**(2): p. 192-200.

47. Kalman, R.E., *A New Approach to Linear Filtering and Prediction Problems.* Transaction of the ASME- Journal of Basic Engineering, 1960. **82**: p. 35-45.

48. Evensen, G., *Using the Extended Kalman Filter with a Multi-layer Quasi-geostrophic Ocean Model.* Journal of Geophysical Research, 1992. **97**(C11): p. 17905-17924.

49. Evensen, G., *Open Boundary Conditions for the Extended Kalman Filter with a Quasi-geostrophic Mode.* Journal of Geophysical Research, 1993. **98**(C19): p. 16529-16546.

50. Evensen, G., *Sequential Data Assimilation with a Non-linear Quasi-geostrophic Model using Monte Carlo Methods to Forecast Error Statistics.* Journal of Geophysical Research, 1994. **99**(C5): p. 10143–10162.

51. Saad, G., Ghanem, R.G., Masri, S., *Robust system identification of strongly non-linear dynamics using a polynomial chaos based sequential data assimilation technique,* in *Collection of Technical Papers - 48th AIAA/ASME/ASCE/AHS/ASC Structures, Structural Dynamics and Materials Conference*. 2007: Honolulu, Hawaii. p. 6005-6013.

52. Snyder, C., Bengtsson, T., Bickel, P., Anderson, J., *Obstacles to High-dimensional Particle Filtering.* Monthly Weather Review, 2008. **136**(12): p. 4629-4640.

53. Sohns, B., Allison, J., Fathy, H.K., Stein, J.L. *Efficient Parameterization of Large-Scale Dynamic Models Through the Use of Activity Analysis*. in *Proceedings of the ASME IMECE 2006*. 2006. Chicago, Illinois.

54. Zhang, D., Lu, Z., *An Efficient, High-order Perturbation Approach for Flow in Random Porous Media via Karhunen–Loeve and Polynomial Expansions.* Journal of Computational Physics, 2004. **194**(2): p. 773–794.

55. Ghanem, R.G., Spanos, P.D., *Polynomial Chaos in Stochastic Finite Element.* Journal of Applied Mechanics, 1990. **57**: p. 197-202.

56. Ghanem, R.G., Spanos, P.D., *Spectral Stochastic Finite-Element Formulation for Reliability Analysis.* ASCE Journal of Engineering Mechanics, 1991. **117**(10): p. 2351-2372.

57. Ghanem, R.G., Spanos, P.D., *A Stochastic Galerkin Expansion for Nonlinear Random Vibration Analysis.* Probabilistic Engineering Mechanics, 1993. **8**(3): p. 255-264.

58. Xiu, D., Lucor, D., Su, C.H., Karniadakis, G.E., *Stochastic Modeling of Flow-Structure Interactions using Generalized Polynomial Chaos.* Journal of Fluids Engineering, 2002. **124**: p. 51-59.

59. Xiu, D., Karniadakis, G.E., *Modeling Uncertainty in Steady-state Diffusion Problems via Generalized Polynomial Chaos.* Modeling Uncertainty in Steady-state Diffusion Problems via Generalized Polynomial Chaos, 2002. **191**: p. 4927-4948.

60. Sandu, C., Sandu, A., Chan, B.J., Ahmadian, M. *Treating Uncertainties in Multibody Dynamic Systems using a Polynomial Chaos Spectral Decomposition*. in *Proceedings of the ASME IMECE 2004, 6th Annual Symposium on "Advanced Vehicle Technology"*. 2004. Paper number IMECE2004-60482, Anaheim, California.

61. Sandu, C., Sandu, A., Chan, B.J., Ahmadian, M. *Treatment of Constrained Multibody Dynamic Systems with Uncertainties*. in *Proceedings of the SAE Congress 2005* 2005. Paper number 2005-01-0936, Detroit, Michigan.

62. Sandu, C., Sandu, A., Ahmadian, M., *Modeling Multibody Dynamic Systems with Uncertainties. Part II: Numerical Applications.* Multibody System Dynamics, Publisher: Springer Netherlands, ISSN: 1384-5640 (Paper) 1573-272X (Online), DOI: 10.1007/s11044-006-9008-4, Vol. 15, No. 3, pp. 241 - 262 (22), April 2006., 2006.

63. Li, L., Sandu, C., Sandu, A. *Modeling and Simulation of a Full Vehicle with Parametric and External Uncertainties*. in *Proceedings of the 2005 ASME Int. Mechanical Engineering Congress and Exposition, 7th VDC Annual Symposium on "Advanced Vehicle Technologies", Session 4: Advances in Vehicle Systems Modeling and Simulation, Paper number IMECE2005-82101* 2005. Orlando, Florida.

64. Sandu, C., Sandu, A., Li, L., *Stochastic Modeling of Terrain Profiles and Soil Parameters.* SAE 2005 Transactions Journal of Commercial Vehicles, 2006. **114**(2): p. 211-220.

65. Soize, C., Ghanem, R., *Physical Systems with Random Uncertainties: Chaos Representations with Arbitrary Probability Measure.* SIAM Journal on Scientific Computing, 2005. **26**(2): p. 395-410.

66. Desceliers, C., Ghanem, R., Soize, C., *Maximum Likelihood Estimation of Stochastic Chaos Representations from Experimental Data.* International Journal for Numerical Methods in Engineering,, 2006. **66**(6): p. 978-1001.

67. Desceliers, C., Soize, C., Ghanem, R., *Identification of Chaos Representations of Elastic Properties of Random Media Using Experimental Vibration Tests.* Computational Mechanics, 2007. **39**(6): p. 831-838.

68. Li, J., Xiu, D., *A Generalized Polynomial Chaos Based Ensemble Kalman Filter with High Accuracy.* Journal of Computational Physics, 2009. **228**: p. 5454-5694.

69. Evensen, G., *The Ensemble Kalman Filter: Theoretical Formulation and Practical Implementation.* Ocean Dynamics, 2003. **53**: p. 343–367.

70. Lenartz, F., Raick, C., Soetaert, K., and Grégoire M., *Application of an Ensemble Kalman Filter to a 1-D Coupled Hydrodynamic-Ecosystem Model of the Ligurian Sea.* Journal of Marine Systems, 2007. **68**: p. 327–348.

71. Smith, A.H.C., Monti, A., Ponci, F., *Indirect Measurements via a Polynomial Chaos Observer.* IEEE Transactions on Instrumentation and Measurement, 2007. **56**(3): p. 743 – 752.

72. Wan, X., Karniadakis, G.E., *Multi-Element Generalized Polynomial Chaos for Arbitrary Probability Measures.* SIAM Journal on Scientific Computing, 2006. **28**(3): p. 901–928.

73. Cheng, H., Sandu, A., *Uncertainty Quantification and Apportionment in Air Quality Models.* 2009. **24**: p. 917–925.

74. Cheng, H., Sandu, A., *Efficient Uncertainty Quantification with the Polynomial chaos Method for Stiff Systems.* Mathematics and Computers in Simulation, 2009. **79**(11): p. 3278-3295.

75. Skogestad, S., Postlethwaite, I., *Multivariable Feedback Control: Analysis and Design*. 2 ed. 2005: Wiley-Interscience.

76. Dorf, R.C., Bishop. R.F., *Modern Control Systems*. 9 ed. 2000: Prentice-Hall.

77. Astrom, K.J., *Model Uncertainty and Robust Control Design*. Lecture Notes, COSY Valencia Workshop, 1999. http://www.control.lth.se/~kja/modunoh.pdf

78. Doyle, J.C., *Guaranteed Margins for LQG Regulators.* IEEE Transactions on Automatic Control, 1978. **23**: p. 756–757.

79. Doyle, J.C., Glover, K., Khargonekar, P., Francis, B., *State Space Solutions to Standard $H_2$ and H-infinity Control Problems.* IEEE Transactions on Automatic Control, 1989. **34**: p. 831–847.

80. Doyle, J.C., Stein, G., *Multivariable Feedback Design: Concepts for a Classical/Modern Synthesis.* IEEE Transactions on Automatic Control, 1981. **AC-26**: p. 4–16.

81. Zames, G., *Feedback and Optimal Sensitivity: Model Reference Transformation, Multiplicative Semi-norms and Approximate Inverses.* IEEE Transactions on Automatic Control, 1981. **26**: p. 301–320.

82. Green, M., Limebeer, D. J. N., *Linear Robust Control*. 1995: Prentice Hall, Englewood Cliffs, N.J.

83. Zhou, K., Doyle, J.C., Glover, K., *Robust and Optimal Control*. 1996: Prentice Hall, New Jersey.

84. Tøffner-Clausen, S., Andersen, P. and Stoustrup, J., *Robust Control* 2001: Fourth Edition, Lecture Notes, Aalborg Univeristy, Aalborg, Denmark.

85. Balas, G.J., *Robust Control of Flexible Structures: Theory and Experiments*. 1990, California Institute of Technology: Pasadena, CA.

86. Safonov, M.G., Laub, A.J., Hartmann, G., *Feedback Properties of Multivariable Systems: The Role and Use of Return Difference Matrix.* IEEE Transactions on Automatic Control, 1981. **AC-26**(1): p. 47-65.

87. Packard, A.K., Doyle, J.C., Balas, G.J., *Linear, Multivariable Robust Control with a μ Perspective.* ASME Journal of Dynamics, Measurements and Control: Special Edition on Control, 1993. **115**(2b): p. 426-438.

88. Stein, G., Doyle, J.C., *Beyond Singular Values and Loopshapes.* AIAA Journal of Guidance and Control, 1991. **14**(1): p. 5-16.

89. VanAntwerp, J.G., Braatz, R. D., Sahinidis, N. V., *Globally Optimal Robust Process Control.* Journal of Process Control, 1999. **9**: p. 375-383.

90. Boyd, S., El Ghaoui, L., Feron, E., Balakrishnan, V., *Linear Matrix Inequalities in System and Control Theory*. 1994: SIAM.

91. Iwasaki, T., Skelton, R.E., *All Controllers for the General H Control Problem: LMI Existence Conditions and State-Space Formulas.* Automatica, 1994. **30**: p. 1307-1317.

92. Asami, T., Nishihara, O., Baz, M., *Analytical Solutions to H-infinity and $H_2$ Optimization of Dynamic Vibration Absorbers Attached to Damped Linear Systems.* Journal of Vibration and Acoustics, 2002. **124**: p. 284- 294.

93. Sammier, D., Sename, O., Dugard, L., *Skyhook and $H_\infty$ Control of Semi-active Suspensions: Some Practical Aspects.* Vehicle System Dynamics, 2003. **39**(4): p. 279–308.

94. Du, H., Sze, K.Y, Lam, J., *Semi-active $H_\infty$ Control of Vehicle Suspension with Magneto-Rheological Dampers.* Journal of Sound and Vibration, 2005. **283**: p. 981–996.

95. Du, H., Zhang, N., *$H_\infty$ Control of Active Vehicle Suspensions with Actuator Time Delay.* Journal of Sound and Vibration, 2007. **301**: p. 236–252.

96. Du, H., Lam, J., Sze, K.Y., *Non-fragile Output Feedback $H_\infty$ Vehicle Suspension Control Using Genetic Algorithm.* Engineering Applications of Artificial Intelligence, 2003. **16**: p. 667–680.

97. Fisher, J., Bhattacharya, R. *On Stochastic LQR Design and Polynomial Chaos*. in *Proceedings of the 2008 American Control Conference*. 2008. Seattle, Washington.

98. Templeton, B.A., *A Polynomial Chaos Approach to Control Design*. 2009, Virginia Tech: Ph.D. dissertation, Blacksburg, Virginia.

99. Bryson, A.E., Ho, Y.-C., *Applied Optimal Control: Optimization, Estimation, and Control*. 1975, Washington, D.C. : Hemisphere.

100. Cohn, S.E., *An Introduction to Estimation Theory*. Journal of the Meteorological Society of Japan, 1997. **75**(B): p. 257-288.

101. Inman, D.J., *Engineering Vibration*. 2 ed. 2001: Prentice Hall, Inc., Upper Saddle River, N.J.

102. Simon, D.E., *An Investigation of the Effectiveness of Skyhook Suspensions for Controlling Roll Dynamics of Sport Utility Vehicles Using Magneto-Rheological Dampers*. 2001, Virginia Tech: Ph.D. dissertation, Blacksburg, Virginia.

103. Fisher, M., *Assimilation Techniques(5): Approximate Kalman Filters and singular vectors.* 2001. http://www.ecmwf.int/newsevents/training/rcourse_notes/pdf_files/Assim_techniques_RRKF.pdf

104. Dixon, J.C., *Tires, Suspension and Handling: Second Edition*. 1996: Society of Automotive Engineers

105. Matlab Robust Control Toolbox helpdesk, http://www.mathworks.com/access/helpdesk/help/toolbox/robust/gs/f6-44171.html

106. Fialho, I., Balas, G.J., *Design of Nonlinear Controllers for Active Vehicle Suspensions Using Parameter-Varying Control Synthesis.* Vehicle System Dynamics, 2000. **33**: p. 351–370.